

FAUX RICCATI EQUATION TECHNIQUES FOR FEEDBACK CONTROL OF
NONLINEAR AND TIME-VARYING SYSTEMS

A THESIS SUBMITTED TO
THE GRADUATE SCHOOL OF NATURAL AND APPLIED SCIENCES
OF
MIDDLE EAST TECHNICAL UNIVERSITY

BY

ANNA PRACH

IN PARTIAL FULFILLMENT OF THE REQUIREMENTS
FOR
THE DEGREE OF DOCTOR OF PHILOSOPHY
IN
AEROSPACE ENGINEERING

MAY 2015

Approval of the thesis:

**FAUX RICCATI EQUATION TECHNIQUES FOR FEEDBACK CONTROL OF
NONLINEAR AND TIME-VARYING SYSTEMS**

submitted by **ANNA PRACH** in partial fulfillment of the requirements for the degree
of **Doctor of Philosophy in Aerospace Engineering Department, Middle East
Technical University** by,

Prof. Dr. Gülbin Dural Ünver
Dean, Graduate School of **Natural and Applied Sciences** _____

Prof. Dr. Ozan Tekinalp
Head of Department, **Aerospace Engineering** _____

Prof. Dr. Ozan Tekinalp
Supervisor, **Aerospace Engineering Department, METU** _____

Prof. Dr. Dennis S. Bernstein
Co-supervisor, **Aerospace Eng. Dept., Univ. of Michigan** _____

Examining Committee Members:

Assoc. Prof. Dr. Ali Türker Kutay
Mechanical Engineering Department, METU _____

Prof. Dr. Ozan Tekinalp
Aerospace Engineering Department, METU _____

Prof. Dr. Kemal Özgoren
Aerospace Engineering Department, METU _____

Prof. Dr. Metin U. Salamci
Mechanical Engineering Department, Gazi University _____

Prof. Dr. Mehmet Önder Efe
Computer Engineering Department, Hacettepe University _____

Date: _____

I hereby declare that all information in this document has been obtained and presented in accordance with academic rules and ethical conduct. I also declare that, as required by these rules and conduct, I have fully cited and referenced all material and results that are not original to this work.

Name, Last Name: ANNA PRACH

Signature :

ABSTRACT

FAUX RICCATI EQUATION TECHNIQUES FOR FEEDBACK CONTROL OF NONLINEAR AND TIME-VARYING SYSTEMS

Prach, Anna

Ph.D., Department of Aerospace Engineering

Supervisor : Prof. Dr. Ozan Tekinalp

Co-Supervisor : Prof. Dr. Dennis S. Bernstein

May 2015, 150 pages

Rapid development of nonlinear control theory for application to challenging and complex problems is motivated by the fast technological development and demand for highly accurate control systems. In infinite-horizon nonlinear optimal control the essential difficulty is that no efficient analytical or numerical algorithm is available to derive exact expressions for optimal controls.

This work concerns the numerical investigation of faux Riccati equation methods for control of nonlinear and linear time-varying (LTV) systems. These methods are attractive due to their simplicity and potentially wide applicability. Considered methods include state-dependent Riccati equation (SDRE) control and forward-propagating Riccati equation (FPRE) control. In SDRE control the instantaneous dynamics matrix is used within an algebraic Riccati equation solved at each time step. FPRE control solves the differential algebraic Riccati equation forward in time rather than backward in time as in classical optimal control.

While applications and theoretical developments of the SDRE technique are widely reflected in the literature, FPRE is a newly developed approach, which is heuristic and suboptimal in the sense that neither stability nor optimal performance is guaranteed. This approach requires development of a theoretical framework that addresses practical aspects of FPRE design, and provides conditions and guidelines for im-

plementation. This work presents the basic properties of the solution of the FPRE for LTI plants in comparison with the solution of the backward-propagating Riccati equation (BPRE), shows the duality between FPRE and BPRE, and investigates stabilizing properties of FPRE. Pareto performance tradeoff curves are used to illustrate the suboptimality of the FPRE as well as the dependence on the initial condition of the Riccati equation.

When applied to nonlinear systems, faux Riccati equation techniques entail pseudo-linear models of nonlinear plants that use either a state-dependent coefficient (SDC) or the Jacobian of the vector field. To investigate the strengths and weaknesses of SDRE and FPRE methods, this work presents a numerical study of various nonlinear plants under full-state-feedback and output-feedback control.

Within the scope of FPRE, an internal model principle is used for command following and disturbance rejection problems for LTV and nonlinear systems. The performance of this approach is investigated numerically by considering the effect of performance weightings, the initial conditions of the difference Riccati equations, plant initial conditions and domain of attraction, and the choice of SDC. Numerical studies include an inverted pendulum, a two-mass system, Mathieu equation, Van der Pol oscillator, ball and beam, rotational- translational actuator, and a fixed-wing aircraft.

Keywords: Optimal control, Riccati equation, nonlinear systems, linear time-varying systems, pseudo-linear model, output feedback, internal-model control.

ÖZ

DOĞRUSAL OLMAYAN VE ZAMAN BAĞLI SİSTEMLER İÇİN FAUX RİCCATİ DENKLEMİ TEKNİKLERİ

Prach, Anna

Doktora, Bölümü

Tez Yöneticisi : Prof. Dr. Ozan Tekinalp

Ortak Tez Yöneticisi : Prof. Dr. Dennis S. Bernstein

Mayıs 2015 , 150 sayfa

Doğrusal olmayan kontrol teorisinin hızlı gelişimini, zor ve karmaşık problemlere uygulanmasını teknolojinin hızlı gelişimi ve hassas kontrol sistemlerine olan ihtiyaçlar motive etmektedir. Sonsuz ufuk doğrusal olmayan optimal kontrol probleminde, çözümü kesin ve verimli analitik ve numerik çözüm algoritmalarının eksik olmaması bir problem olarak karşımıza çıkmaktadır.

Bu çalışmanın konusu, faux Riccati denklemi metodlarının doğrusal olmayan ve doğrusal LTV sistemlere uygulmasıdır. Bu metodların avantajı kolay uygulanabilirlikleri ve basit olmalarıdır. Kullanılan yöntemler, SDRE kontrol ve FPRE kontrol yöntemleridir. SDRE kontrolde anlık dinamik matrisler her zaman adımında Riccati denkleminin çözümünde kullanılır. FPRE kontrolü ise dinamik Riccati denklemini, optimal kontrol probleminde olduğu gibi zamanda geriye doğru değil, ileriye doğru çözer.

SDRE tekniği teorisi ve uygulamaları literatüre yansımıştır. Oysa FPRE daha yeni geliştirilmekte olup, hem heuristik hem de suboptimaldir, çünkü halen ne stabilite ne de optimal performans garanti edilmektedir. FPRE yönteminin teorisinin, pratik uygulaması kullanım yöntem ve şartlarının geliştirilmesi gerekmektedir. Bu çalışma, FPRE yönteminin LTI sistemlere uygulanmasındaki çözümlerin özelliklerini, BPRE ile karşılaştırılmasını, ve stabilite özelliklerinin belirlenmesini konu almaktadır. Pareto performans eğrileri kullanılarak FPREin suboptimalitesi ve başlangıç noktasına

bağımlılığı gösterilmiştir.

Doğrusal olmayan sistemlere uygulandığında faux Riccati denklemi teknikleri pseudo-doğrusal modeller oluşturur, ve SDC veya vector alanının Jacobianını kullanır. SDRE ve FPRE yöntemlerinin kuvvetli ve zayıf yönlerini görmek için bu çalışma, doğrusal olmayan sistemlerde tam durum ve çıktı durum geri beslemesini numerik olarak inceler.

FPRE yönteminde, doğrusal olmayan ve LTV sistemlerde emir takibi ve bozan sinyal reddi için bir internal model kullanılmıştır. Kontrolcü performansı numerik olarak incelenmiş, bunun için performans ağırlıklarına, Riccati denkleminin çözümündeki başlangıç noktasına, etki alanına ve SDC seçimine bakılmıştır. Numerik çalışmalar, ters sarkaç, iki kütleli bir sistem, Mathieu denklemi, Van der Pol osilatörü, top ve tah-terevalli problemi, döner ve ilerleyen aktuatör problemi ve sabit kanat uçak modelleri kullanılarak yapılmıştır.

Anahtar Kelimeler: Optimal Kontrol, Riccati denklemi, doğrusal olmayan sistemler, doğrusal zamana göre değişken sistemler, pseudo-doğrusal model, çıktı beslemeli kontrol, internal-model kontrolü.

To my loving family...

ACKNOWLEDGMENTS

I would like to express my special appreciation and thanks to my supervisor Professor Dr. Ozan Tekinalp. I would like to thank you for encouraging my research and for giving me freedom to work in the area that was exciting for me. I consider it as a great opportunity to do my PhD under your guidance and to learn from your research expertise.

My special thanks go to my co-supervisor, Professor Dennis S. Bernstein, who helped me come up with the thesis topic and guided me over almost two years of development. I would like to thank you for your patience and support that helped me to finish this work.

I would like to acknowledge all the instructors and professors at Middle East Technical University and National Technical University of Ukraine "Kiev Polytechnic Institute". I am thankful for the opportunity to learn from their knowledge and experience.

I also have to thank the members of my PhD committee for their helpful advices and suggestions.

I would like to thank Dr. Ilkay Yavrucuk for his valuable feedback. Additionally, I am very grateful to all great people at Aerotim Engineering, especially Gönenç Gürsoy, who was always very helpful and supportive.

I would also like to thank to all my friends in Ukraine and Turkey.

Most importantly, I would like to express my gratitude to my father and mother, Alexander and Larisa, who encouraged and helped me at every stage of my personal and academic life. I want to thank to my sisters Tanya, Marina, Oksana, and my best friend Anya. I love you so much, and I would not have made it this far without all of you.

This work is supported by the Scientific and Technological Research Council of Turkey (TÜBİTAK) within 2215-Ph.D. Fellowship Program.

TABLE OF CONTENTS

ABSTRACT	v
ÖZ	vii
ACKNOWLEDGMENTS	x
TABLE OF CONTENTS	xi
LIST OF TABLES	xvi
LIST OF FIGURES	xvii
LIST OF ABBREVIATIONS	xxiii
CHAPTERS	
1 INTRODUCTION	1
1.1 Faux Riccati Techniques	2
1.1.1 SDRE Control	3
1.1.2 FPRE Control	4
1.2 Output Feedback for Nonlinear and LTV Systems	5
1.3 Internal Model Principle	8
1.4 Tracking Problem	9
1.5 Numerical Investigation	10

1.6	Original Contribution and Organization	12
2	INFINITE-HORIZON LINEAR-QUADRATIC CONTROL BY FORWARD PROPAGATION OF THE DIFFERENTIAL RICCATI EQUATION	13
2.1	Backward-propagating Riccati equation control	14
2.2	Forward-propagating Riccati equation control	25
2.2.1	Lyapunov Analysis of the Forward-Propagating Riccati Equation	33
2.3	How Suboptimal Is FPRE?	36
2.3.1	Transient Responses of BPRE and FPRE	39
3	COMMAND FOLLOWING AND DISTURBANCE REJECTION CONTROL FOR LTI SYSTEMS	43
3.1	Review of Linear Quadratic Optimal Control	43
3.1.1	Linear Quadratic Tracking and Disturbance Rejection: Finite-Time Case	43
3.1.2	Linear Quadratic Tracking and Disturbance Rejection: Infinite-Time Case	46
3.2	Internal-Model-Based Command Following and Disturbance Rejection for LTI SISO Systems	47
3.2.1	Full-State-Feedback	47
3.2.1.1	ARE Control Law	49
3.2.1.2	FPRE Control Law	49
3.2.2	Convergence Analysis	49
3.2.3	Internal Models	51
3.2.4	Discrete-Time Models	52

	3.2.5	Output-Feedback	54
	3.2.5.1	ARE Observer-Based Compensator	56
	3.2.5.2	FPRE Observer-Based Compensator	56
	3.2.6	Convergence Analysis	57
4		FPRE CONTROL FOR LTV SYSTEMS	61
	4.1	FPRE Control for Stabilization of LTV Systems	61
	4.1.1	Full-State-Feedback	62
	4.1.2	Output-Feedback	65
	4.2	FPRE Control for Command Following and Disturbance Re- jection	71
	4.2.1	Tracking FPRE Control	72
	4.2.2	Internal-Model-Based FPRE Control	73
5		REVIEW OF SDRE CONTROL FOR NONLINEAR SYSTEMS	77
	5.1	The SDRE Nonlinear Regulator	77
	5.1.1	State-Dependent-Coefficient Parameterization	78
	5.1.2	Pseudo-Linear Model	79
	5.1.3	Full-State-Feedback	79
	5.1.4	Output-Feedback	80
	5.2	Discrete-Time SDRE Control Formulation	81
	5.2.1	Discrete-Time Full-State-Feedback	81
	5.2.2	Discrete-Time Output-Feedback	86
	5.3	Tracking SDRE Control	89

6	FPRE CONTROL FOR NONLINEAR SYSTEMS	93
6.1	FPRE Control for Stabilization of Nonlinear Systems	93
6.1.1	Full-State-Feedback	93
6.1.2	Output-Feedback	96
6.2	FPRE for Command Following and Disturbance Rejection	99
6.2.1	Tracking FPRE Control	99
6.2.2	Internal-Model-Based FPRE Control	100
6.2.2.1	Full-State Feedback	102
6.2.2.2	Output Feedback	102
6.2.2.3	Numerical Investigation of Performance and Robustness	103
6.2.2.4	Effect of initial condition $P_{a,0}$ for the Ball and Beam	111
6.2.2.5	Numerical Investigation of the Domain of Attraction for the Van der Pol Os- cillator	113
6.2.2.6	Numerical Investigation of the Domain of Attraction for the Ball and Beam	113
7	APPLICATION OF FPRE AND SDRE FOR AN AIRCRAFT	117
7.1	Aircraft Platform	117
7.2	Dual-Loop Controller Structure	117
7.3	State-Dependent Model for a Fixed-Wing Aircraft	119
7.3.1	Inner-Loop Model	121
7.3.2	Outer-Loop Model	123

7.4	SDRE Controller	124
7.4.1	Numerical Simulation Results	125
7.4.1.1	Case 1: Uniform Atmosphere	126
7.4.1.2	Case 2: Light Turbulence	127
7.5	FPRE Controller	128
7.5.1	Initial Conditions for FPRE	130
7.5.2	Numerical Simulation Results	130
7.5.2.1	Case 1: Uniform Atmosphere	131
7.5.2.2	Case 2: Light Turbulence	132
8	CONCLUSIONS	135
	REFERENCES	139
	CURRICULUM VITAE	149

LIST OF TABLES

TABLES

Table 2.1	Inverted Pendulum Model Parameters	37
Table 5.1	RTAC Parameters	84
Table 6.1	Ball and Beam Parameters	109
Table 7.1	UAV Specification	118
Table 7.2	UAV Mass and Inertia Parameters	118
Table 7.3	Non-dimensional Aerodynamic Derivatives	121

LIST OF FIGURES

FIGURES

Figure 2.1 Example 2.1. Illustrative results for Theorem 1.	22
Figure 2.2 Example 2.2. Illustrative results for Proposition 2.	24
Figure 2.3 Example 3.2. Illustrative results for Theorem 2.	29
Figure 2.4 Example 2.4. Illustrative results for Proposition 4.	32
Figure 2.5 Example 2.5. State trajectories for BPRE for the inverted pendulum on a cart.	38
Figure 2.6 Example 2.5. State trajectories for FPRE for the inverted pendulum on a cart.	39
Figure 2.7 Example 2.5. The convergence of $P(t)$ to \bar{P} for BPRE and FPRE.	39
Figure 2.8 Example 2.5. Pareto performance tradeoff curves.	40
Figure 2.9 Example 2.5. Lyapunov-function candidate and its derivative.	40
Figure 2.10 Example 2.6. State trajectories, maximum singular value of $P(t) - \bar{P}$, and spectral abscissa of $A_{cl}(t)$ for BPRE.	41
Figure 2.11 Example 2.6. State trajectories, maximum singular value of $P(t) - \bar{P}$ and spectral abscissa of $A_{cl}(t)$ for FPRE.	42
Figure 3.1 Internal-model-based, full-state-feedback controller.	48
Figure 3.2 Reformulation of Fig. 3.1 for final value theorem analysis.	50
Figure 3.3 Example 3.1. Two-mass system.	53
Figure 3.4 Example 3.1. Closed-loop responses.	54
Figure 3.5 Example 3.1. Convergence of $P_{a,k}$ of FPRE to \bar{P}_a	54
Figure 3.6 Internal-model-based output-feedback controller.	55

Figure 3.7	Augmented plant.	56
Figure 3.8	Reformulation of Fig. 3.6 for final value theorem analysis.	58
Figure 3.9	Example 3.2. Closed-loop responses.	60
Figure 4.1	Example 4.1. Open-loop phase portrait of Mathieu equation.	63
Figure 4.2	Example 4.1. Full-state feedback for Mathieu equation: closed-loop responses.	64
Figure 4.3	Example 4.1. Full-state feedback for Mathieu equation: Pareto performance tradeoff curves.	64
Figure 4.4	Example 4.2. Full-state feedback for the rotating disc: closed-loop responses.	65
Figure 4.5	Example 4.2. Full-state feedback for the rotating disc: Pareto performance tradeoff curves.	66
Figure 4.6	Example 4.3. Output feedback for Mathieu equation: closed-loop responses.	67
Figure 4.7	Example 4.3. Output feedback for Mathieu equation: Pareto performance tradeoff curves.	67
Figure 4.8	Example 4.4. Output feedback for the rotating disc: closed-loop responses.	68
Figure 4.9	Example 4.4. Output feedback for the rotating disc: Pareto performance tradeoff curves.	68
Figure 4.10	Example 4.5. Simply supported beam.	69
Figure 4.11	Example 4.5. Open-loop response.	70
Figure 4.12	Example 4.5. Output feedback for the flexible beam: closed-loop responses.	71
Figure 4.13	Example 4.5. Output feedback for the flexible beam: Pareto performance tradeoff curves.	71
Figure 4.14	Example 4.6. Tracking FPRE control of the Mathieu equation: closed-loop responses.	73
Figure 4.15	Example 4.6. Tracking FPRE control of the Mathieu equation: closed-loop responses.	74

Figure 4.16 Example 4.7. Internal-model-based, full-state-feedback and output-feedback control of the Mathieu equation: closed-loop responses.	75
Figure 4.17 Example 4.7. Internal-model-based, full-state-feedback and output-feedback control of the Mathieu equation: closed-loop responses.	76
Figure 4.18 Example 4.7. Internal-model-based, full-state-feedback and output-feedback control of the Mathieu equation: closed-loop responses.	76
Figure 5.1 Example 5.1. Full-state-feedback SDRE control of the Van der Pol oscillator.	83
Figure 5.2 Example 5.1. Pareto performance tradeoff curves for full-state-feedback SDRE control of the Van der Pol oscillator.	83
Figure 5.3 Rotational-translational actuator.	84
Figure 5.4 Example 5.2. Full-state-feedback SDRE control of the RTAC. . . .	87
Figure 5.5 Example 5.3. Output-feedback SDRE control of the Van der Pol oscillator.	88
Figure 5.6 Example 5.3. Pareto performance tradeoff curves for output-feedback SDRE control of the Van der Pol oscillator.	88
Figure 5.7 Example 5.4. Output-feedback SDRE control of the RTAC with arm angle measurements.	89
Figure 5.8 Example 5.4. Output-feedback SDRE control of the RTAC with cart position and arm angle measurements.	90
Figure 5.9 Example 5.5. SDRE control of the Van der Pol oscillator with a step command and step disturbance.	92
Figure 5.10 Example 5.5. SDRE control of the Van der Pol oscillator with a harmonic command and harmonic disturbance.	92
Figure 6.1 Example 6.1. Full-state-feedback FPRE control of the Van der Pol oscillator.	94
Figure 6.2 Example 6.1. Pareto performance tradeoff curves for full-state-feedback FPRE control of the Van der Pol oscillator.	95
Figure 6.3 Example 6.1. Full-state-feedback FPRE control of the RTAC. . . .	95
Figure 6.4 Example 6.3. Output-feedback FPRE control of the Van der Pol oscillator.	97

Figure 6.5 Example 6.3. Pareto performance tradeoff curves for output-feedback FPRE control of the Van der Pol oscillator.	97
Figure 6.6 Example 6.4. Output-feedback FPRE control of the RTAC with cart position measurements.	98
Figure 6.7 Example 6.4. Output-feedback FPRE control of the RTAC with arm angle measurements.	98
Figure 6.8 Example 6.4. Output-feedback FPRE control of the RTAC with cart position and arm angle measurements.	99
Figure 6.9 Example 6.5. FPRE control of the Van der Pol oscillator with a step command and step disturbance.	101
Figure 6.10 Example 6.5. FPRE control of the Van der Pol oscillator with a harmonic command and harmonic disturbance.	101
Figure 6.11 Example 6.6. Internal-model-based, full-state-feedback FPRE control of the Van der Pol oscillator.	104
Figure 6.12 Example 6.6. Internal-model-based, output-feedback FPRE control of the Van der Pol oscillator.	104
Figure 6.13 Example 6.7. Internal-model-based, full-state-feedback control of the RTAC.	105
Figure 6.14 Example 6.7. Internal-model-based, output-feedback control of the RTAC.	106
Figure 6.15 Example 6. Amplitude vs frequency for internal-model-based, output-feedback control of the RTAC.	106
Figure 6.16 Ball and beam system.	107
Figure 6.17 Example 6.8. Internal-model-based, full-state-feedback FPRE control of the ball and beam.	109
Figure 6.18 Example 6.8. Internal-model-based, output-feedback FPRE control of the ball and beam.	110
Figure 6.19 Example 6.8. Internal-model-based, full-state-feedback FPRE control of the ball and beam.	110
Figure 6.20 Example 6.8. Internal-model-based, output-feedback FPRE control of the ball and beam.	110

Figure 6.21 Example 6.8. Internal-model-based, output-feedback FPRE control of the ball and beam.	111
Figure 6.22 Example 6.8. Internal-model-based, output-feedback FPRE control of the ball and beam.	111
Figure 6.23 Example 6.9. Internal-model-based, output-feedback control of the ball and beam.	112
Figure 6.24 Example 6.9. Internal-model-based, output-feedback control of the ball and beam.	112
Figure 6.25 Example 6.10. Numerical investigation of the domain of attraction of the Van der Pol oscillator under output-feedback control.	113
Figure 6.26 Example 6.10. Numerical investigation of the domain of attraction for nonzero $x_{1,0}$ and $x_{2,0}$ for the ball and beam.	114
Figure 6.27 Example 6.10. Numerical investigation of the domain of attraction for full-state-feedback control of the ball and beam using.	115
Figure 6.28 Example 6.10. Numerical investigation of the domain of attraction for output-feedback control of the ball and beam using measurements of ball position and beam angle.	115
Figure 6.29 Example 6.10. Numerical investigation of the domain of attraction for output-feedback control of the ball and beam using measurements of ball position only.	116
Figure 7.1 Fixed-wing UAV platform	117
Figure 7.2 Dual-loop controller structure	118
Figure 7.3 SDRE control of the aircraft, case 1: altitude and XY -position. . .	126
Figure 7.4 SDRE control of the aircraft, case 1: Euler angles, angle of attack and sideslip angle.	126
Figure 7.5 SDRE control of the aircraft, case 1: linear and angular velocities. . .	127
Figure 7.6 SDRE control of the aircraft, case 1: control-surfaces deflections and thrust.	127
Figure 7.7 Wind profile.	128
Figure 7.8 SDRE control of the aircraft, case 2: altitude and XY -position. . .	128

Figure 7.9 SDRE control of the aircraft, case 2: Euler angles, angle of attack and sideslip angle.	128
Figure 7.10 SDRE control of the aircraft, case 2: linear and angular velocities.	129
Figure 7.11 SDRE control of the aircraft, case 2: control-surfaces deflections and thrust.	129
Figure 7.12 FPRE control of the aircraft, case 1: altitude and XY -position.	131
Figure 7.13 FPRE control of the aircraft, case 1: Euler angles, angle of attack and sideslip angle.	131
Figure 7.14 FPRE control of the aircraft, case 1: linear and angular velocities.	132
Figure 7.15 FPRE control of the aircraft, case 1: control-surfaces deflections and thrust.	132
Figure 7.16 FPRE control of the aircraft, case 2: altitude and XY -position.	133
Figure 7.17 FPRE control of the aircraft, case 2: Euler angles, angle of attack and sideslip angle.	133
Figure 7.18 FPRE control of the aircraft, case 2: linear and angular velocities.	133
Figure 7.19 FPRE control of the aircraft, case 2: control-surfaces deflections and thrust.	134

LIST OF ABBREVIATIONS

Symbols

A	System matrix
B	Input matrix
C	Output matrix
D_1	Disturbance matrix
I	Identity matrix
F	Observer gain matrix
G	Transfer function
J	Performance index
J	Moment of inertia
H	Hamiltonian
K	Full-state-feedback controller gain matrix
P	Positive-semidefinite solution of control differential Riccati equation
\bar{P}	Positive-semidefinite solution of control algebraic Riccati equation
R_1, R_2	State and input weighting matrices
Q	Positive-semidefinite solution of observer differential Riccati equation
\bar{Q}	Positive-semidefinite solution of observer algebraic Riccati equation
V	Lyapunov function candidate
V_1, V_2	Disturbance and sensor weighting matrices
d	Disturbance
\det	Determinant
$f(t), g(t)$	Vector field
g	Gravitational acceleration
k	Discrete time index
p, q, r	resp. roll, pitch, yaw angular rate about body axis

r	Command
t	Time
u	Control vector
u, v, w	Aircraft velocity components in body axis
x	State vector
\hat{x}	State estimate vector
y	Output vector
z	Command-following error
\mathbf{z}	\mathbf{z} -transform variable
$\alpha(z), \beta(z), \gamma(z)$	Class \mathcal{K} functions
α	Angle of attack
β	Sideslip angle
$\delta_a, \delta_e, \delta_r$	resp. aileron, elevator, rudder deflection
δ_T	Throttle control
λ	Lagrange multiplier
ϕ, θ, ψ	Euler angles of an aircraft

Abbreviations

BPRE	Backward-Propagating Riccati Equation
FPRE	Forward-Propagating Riccati Equation
IMP	Internal Model Principle
LTV	Linear Time Varying
OBC	Observer-Based Compensator
RTAC	Rotational-translational actuator
SDRE	State-Dependent Riccati Equation
UAV	Unmanned Aerial Vehicle

CHAPTER 1

INTRODUCTION

One of the foundational principles of optimal control theory is that optimal control laws must be propagated backwards in time. For linear-quadratic control, this means that the solution of the Riccati equation must be obtained from backward integration from a final-time condition [69, 81]. These features are a direct consequence of the transversality conditions of optimal control, which imply that a free final state implies a fixed final adjoint state [110, 89]. In addition, the principle of dynamic programming and associated Hamilton-Jacobi-Bellman equation is an inherently backward-propagating methodology [6].

The need for backward propagation means that, in practice, the control law must be computed in advance, stored, and then implemented forward in time. The control law may be either open-loop or closed-loop (as in the linear-quadratic case), but, in both cases, must be computed in advance. Fortunately, the dual case of optimal observers, such as the Kalman filter, is based on forward propagation of the error covariance and thus is more amenable to practical implementation.

For linear time-invariant (LTI) plants, a practical suboptimal solution is to implement the asymptotic control law based on the algebraic Riccati equation (ARE). For plants with linear time-varying (LTV) dynamics, perhaps arising from linearization of a non-linear plant about a specified trajectory, the main drawback of backward propagation is the fact that the future dynamics of the plant must be known. To circumvent this requirement, at least partially, various forward-propagating control laws have been developed, such as receding horizon control and model predictive control [86], [99], [85], [72]. Although these techniques require that the future dynamics of the plant

be known, the control law is determined over a limited horizon, and thus the user can tailor the control law based on the available modeling information. Of course, all such control laws are suboptimal over the entire horizon.

An alternative approach to linear-quadratic control is to modify the sign of the Riccati equation and integrate forward, in analogy with the Kalman filter. This approach, which is described in [28, 27, 121], requires knowledge of the dynamics at only the present time. As shown in [121], stability is guaranteed for plants with symmetric closed-loop dynamics as well as for plants with sufficiently fast dynamics. However, a proof of stability for larger classes of plants remains open. Finally, the reinforcement learning approach of [83] is also based on forward integration, as is the "cost-to-come" technique in [119].

The basic features and convergence properties of the solution of the backward-propagating Riccati equation (BPRE) are given in [81, 19, 20, 21]. However, properties of the solution of the forward-propagating Riccati equation (FPRE), are not covered in the literature. This work presents analytical expressions for the solution of the FPRE, examines its basic features, and uses Lyapunov methods for time-varying systems to prove convergence of the FPRE control law for LTI systems.

1.1 Faux Riccati Techniques

Nonlinear control has seen extensive progress during the last several decades through the development of a wide range of techniques, such as HJB methods [1], backstepping [79], sliding mode [22, 118], nested saturations [115, 117, 23], and feedback linearization [78, 25, 26, 62]. The HJB equation provides the solution to the optimal control problem for nonlinear systems; however, solving the HJB equation is challenging due to its nonlinear and spatially distributed nature. Approximate HJB solutions are given in [55, 4, 77, 1].

While these techniques are generally confined to full-state feedback, under some conditions, such as passivity, output feedback control of nonlinear systems is feasible. In many applications, however, control of nonlinear systems without benefit of the full state remains a serious challenge. In particular, difficulties arise in constructing non-

linear observers that can be used in conjunction with a nonlinear separation principle.

This work considers nonlinear full-state-feedback and output-feedback compensation for nonlinear and time-varying systems by taking advantage of the confluence of several ideas and techniques, all of which are, to varying degrees, heuristic.

The focus is on nonlinear dynamics $\dot{x} = f(x) + B(x)u$ that can be factorized into the product of a *state-dependent coefficient* (SDC) matrix function and the state vector, which results in the pseudo-linear dynamics $\dot{x} = A(x)x + B(x)u$. This factorization allows the use of linear control techniques while capturing the nonlinearities of the system. These systems have been widely studied using the *state-dependent Riccati equation* (SDRE) formulation, where an algebraic Riccati equation (ARE) is solved at each time instant [33, 36, 106, 87, 30, 48].

1.1.1 SDRE Control

SDRE is a nonlinear control technique that exploits the SDC formulation. Introduced in [93, 122, 53, 34, 35], the effectiveness of SDRE control is demonstrated by numerous applications for designing nonlinear controllers, observers, and filters [88, 87, 24, 125]. SDRE is also widely used in aerospace applications [92, 37, 111, 10, 12, 98].

With the nonlinear dynamics given in SDC form, SDRE minimizes a performance index with a quadratic-like structure. A suboptimal full-state-feedback control law is obtained by solving an algebraic state-dependent Riccati equation. The SDRE nonlinear regulator has the same structure as the infinite-horizon linear quadratic regulator (LQR). The non-uniqueness of the SDC parameterization creates extra degrees of freedom that can be used to enhance controller performance [30]. One of the main advantages of SDRE control is that the user can adjust the tradeoffs between control effort and state errors by tuning the penalty (weighting) matrices, which, in general, can be state-dependent.

Reference [29] presents theory on the existence of solutions as well as stability and optimality properties associated with SDRE controllers for the nonlinear regulation problem. Estimation of stability regions of SDRE is discussed in [47], whereas global stability for second-order systems under SDRE control is given in [46]. The most

complete survey [31] summarizes theoretical developments on SDRE nonlinear regulation; provides an extensive literature survey on the results, proofs of all theorems concerning SDRE nonlinear regulator theory; covers systematic design tools, successful applications of SDRE to various platforms; presents practical aspects of SDRE design and real-time implementation, and discusses issues that are open for investigation.

Implementation of SDRE requires that stabilizability and detectability conditions be satisfied at each time instant, and global guarantees of stability and performance are not available. The dual case of estimation for nonlinear systems can also be addressed [88, 24, 8]. If A and B are also time varying, that is, $A(x, t)$ and $B(x, t)$, then ARE can also be solved at each time step, leading to a frozen-time Riccati equation (FTRE) formulation [95].

1.1.2 FPRE Control

An alternative approach to SDRE, a *forward-propagating Riccati equation* (FPRE) technique, is proposed in [28, 121]. The idea behind this approach is to remove the minus sign in the backward-propagating regulator Riccati equation and propagate it forward as in the case of the differential estimator Riccati equation. FPRES is a natural dual to the Kalman filter error-covariance update, which also propagates forward in time. This approach is not guaranteed to be optimal or even stabilizing. In [121] it is shown that symmetry of the closed-loop dynamics is a sufficient condition for closed-loop stability. In addition, [121] shows that, for FPRES, stabilizability is achieved for some plants with sufficiently fast time-varying dynamics, and that stability for output-feedback FPRES holds for LTV systems. Unlike SDRE, for FPRES, stabilizability and detectability conditions need not be satisfied at each instant of time.

While state-dependent coefficient parameterizations provide a heuristic technique that can be used to apply linear control techniques to nonlinear control problems, there is another approach that is more established, at least within the context of estimation. Referring to the extended Kalman filter (EKF), which uses the Jacobian (linearization along the trajectory) of the vector field for the error covariance update [39, 56]. While

the Jacobian is routinely used for the EKF, it apparently has not been used for control, although there is nothing that prevents its use within the context of either SDRE or FPRE. By the same token, although SDC has been used for SDRE-based estimation [58, 5], SDC does not appear to have been studied within the context of the Kalman filter with differential error-covariance update. Of course, the Jacobian cannot be used if the vector field is not differentiable, just as the SDC cannot be used if the vector field cannot be factored. Together, SDRE and FPRE with either SDC or Jacobian pseudo-linear models constitute “faux Riccati” techniques.

Whether the SDC or Jacobian is used for control and estimation within either the FPRE or SDRE, the resulting regulator and estimator can be combined to form an observer-based compensator. This “forced separation” is, of course, ad hoc, and there is no guarantee that the resulting closed-loop system is asymptotically stable, either locally or globally. Note that, within the context of output feedback, the SDC and Jacobian must be evaluated at the state estimate, which introduces additional error.

Having laid out the various elements of faux Riccati control techniques, the goal is to illustrate several variations of this technique for full-state-feedback and output-feedback compensation, and provide numerical experiments that are intended to motivate further investigation of this approach. One of the basic questions that these numerical experiments are aimed at concerns the relative accuracy of SDRE and FPRE. In addition, comparing the accuracy of the SDC and Jacobian for both SDRE and FPRE is of interest of this work.

1.2 Output Feedback for Nonlinear and LTV Systems

Output-feedback control of LTV and nonlinear systems is a problem of fundamental importance. In many applications, the assumption of linearity and the ability to measure all states can be satisfied to a sufficient extent that both aspects need not be dealt with simultaneously. In some applications, however, plant nonlinearity cannot be ignored, and the available measurements are a strictly proper subset of the dominant states. In reality, all systems are nonlinear, and the inevitable presence of unmodeled dynamics means that full-state feedback is an idealization confined to textbooks.

From a theoretical point of view, output-feedback control of nonlinear systems remains a challenging and largely unsolved problem. The source of at least some of the difficulty stems from the lack of observer-regulator separation in the nonlinear case; in special cases, however, these difficulties can be overcome [3, 73]. Separation aside, constructing nonlinear observers and state estimators for nonlinear systems is itself a challenging problem that continues to attract considerable attention [66, 91].

Among the available techniques for output-feedback control of nonlinear systems are passivity-based methods [18]. Flatness-based techniques are also applicable assuming that multiple derivatives of the measurement can be obtained [120]. Model predictive control techniques implemented with nonlinear observers provide another option [50, 84, 38].

In view of the practical need for output-feedback control of nonlinear systems, the paucity of rigorous techniques has motivated interest in heuristic methods. Traditionally, gain-scheduling techniques based on local linearizations are widely used in practice [105]. A closely related technique consists of parameterized linearizations in the form of linear parameter-varying (LPV) models [103].

Another heuristic class of nonlinear controllers is based on reformulating the nonlinear dynamics $\dot{x} = f(x, u)$ in the “faux linearization” form $\dot{x} = A(x)x + B(x)u$, where $A(x)$ and $B(x)$ are state-dependent coefficients. The regulator gain can then be used in a separation structure by solving the dual estimator algebraic Riccati equation with the state x in the state-dependent coefficients $A(x)$ and $B(x)$ replaced by the state estimate \hat{x} [88, 24].

A variation of SDRE is to replace the algebraic Riccati equations with differential Riccati equations. For the estimator, this presents no difficulty since the Kalman filter propagates forward in time. The only distinction is thus the use of the state-dependent coefficient $A(\hat{x})$ in place of the Jacobian used in the extended Kalman filter. For the regulator, however, the optimal gain is obtained by propagating the differential Riccati equation backward in time [21]. Unfortunately, this is not feasible for nonlinear systems due to the fact that the future state estimate is not known.

To overcome the problem of backward propagation of the differential regulator Ric-

cati equation and the need to know the future state estimate, FPRE technique is considered. When combined with the dual estimator with estimate-dependent coefficients, FPRE provides a heuristic technique for output-feedback control of nonlinear systems [96].

A related application of FPRE is control of linear time-varying (LTV) plants without future knowledge of the time-varying plant matrices [121, 95]. If $A(t)$ and $B(t)$ are known in advance, then classical optimal control methods can be used over a finite horizon. If $A(t)$ and $B(t)$ are known over a limited future interval but the objective is stabilization, then receding horizon techniques can be used [112]. For periodically time-varying systems, stabilization and control for all time is considered in [11]. However, in some applications, knowledge of the future dynamics is not available. This is the case for LPV models, where $A(\rho(t))$ and $B(\rho(t))$ depend on a time-varying parameter $\rho(t)$ whose future time variation is not known.

For LTV plants, the heuristic nature of FPRE stems from the fact that the differential regulator Riccati equation is not guaranteed to be stabilizing. For the case of the differential estimator Riccati equation, a quadratic Lyapunov function can be used to prove stability, and this provides the foundation for the stability of the Kalman filter when used as an observer for LTV plants. In the differential regulator Riccati equation, the analogous technique does not yield stability due to the fact that the time-varying matrices $A(t)$ and $C(t)$ are replaced by $A^T(t)$ and $B^T(t)$, respectively. In the LTI case, this replacement makes no difference since the spectra of $A - FC$ and $(A - FC)^T$ are identical. As shown in [121], however, asymptotic stability of the state transition matrix of $A(t) - F(t)C(t)$ does not imply asymptotic stability of the state transition matrix of $(A(t) - F(t)C(t))^T$. Consequently, for LTV plants, there is no guarantee of stability through a duality argument. For nonlinear plants, the use of the state-dependent coefficient $A(\hat{x}(t))$ compounds the heuristic nature of the technique.

1.3 Internal Model Principle

To achieve simultaneous command following and disturbance rejection for a given class of signals, the classical internal model principle (IMP) is applied. IMP of control theory states that asymptotic command following and disturbance rejection require a model of the exogenous signal in the feedback loop. In [63], the controller contains both an embedded internal model that tracks the reference trajectory and a stabilizing component that drives the tracking error to zero, and an internal model approach assumes that the uncertainty and disturbance belong to a family of trajectories generated by a dynamical system. In [63], necessary and sufficient conditions, which comprise the regulator equations that characterize the internal model property, are derived for the existence of a solution of the robust asymptotic tracking problem.

The most basic example of IMP in linear feedback control is the fact that an integrator in the controller suffices to reject step disturbances, whereas an integrator in either the plant or controller suffices to follow step commands. Both statements are consequences of the final value theorem, while analogous statements apply to ramp and harmonic disturbances and commands. The fundamental nature of IMP is reflected by its extensive application to linear controller synthesis [65, 44, 124, 40, 41, 43, 42, 51, 52, 123, 7]. Within the context of nonlinear feedback control, IMP is developed in [17, 62].

This work revisits IMP-based control within the context of output feedback control of nonlinear systems. In particular, to circumvent the difficulties associated with output feedback, where the vector field $f(x)$ is assumed to be factorizable as $A(x)x$. Due to the fact that SDRE is based on a pointwise-in-time solution of the algebraic Riccati equation, only the FPRE technique is used for IMP-based control since it does not require pointwise stabilizability and detectability.

This work takes advantage of IMP within the context of full-state-feedback and output-feedback control of nonlinear systems. In order to do this, firstly the nonlinear plant is cascaded with an internal model of the reference command. Then regulator and observer FPRE's are solved in order to construct an observer-based compensator (OBC) for the cascaded plant. The implemented controller is thus an output-feedback OBC

whose order is $n + 2n_{\text{im}}$, where n is the order of the plant and n_{im} is the order of the internal model. In this work the methodology for IMP-based FPRE control is presented for discrete-time systems.

This approach to IMP-based control of nonlinear systems with output feedback is heuristic in several respects. First, there is no guarantee that a stabilizing IMP-based controller for a nonlinear plant will drive the command-following error to zero. Next, there is no guarantee that the FPRE has a solution for all time, much less a stabilizing solution. Finally, the separation structure of the output-feedback OBC, which is copied from output-feedback, observer-based compensation of linear plants, is not guaranteed to asymptotically stabilize the nonlinear plant even if the regulator and observer dynamics are both asymptotically stable.

Despite these obstacles, this work takes an experimental approach motivated by the fact that output-feedback control of nonlinear systems remains a challenging and largely open problem. The performance of FPRE is investigated under various choices of controller tuning parameters. These parameters include the state and control weights, the initial conditions of the forward-propagating Riccati equations, and the choice of the state-dependent coefficient matrices. Also the initial conditions of the plant are varied in order to estimate the domain of attraction of FPRE and its dependence on the convergence of the state of the observer-based compensator.

1.4 Tracking Problem

The last problem considered is a tracking control for nonlinear systems. Many controllers developed for trajectory tracking of nonlinear systems rely on approximations or linearizations [89, 107, 102]. In [32], a recursive approximation theory is applied to solve the nonlinear optimal tracking control problem. [70] presents an approximate dynamic-programming-based approach for approximate solution of the infinite horizon optimal tracking problem for control affine nonlinear systems with quadratic cost. An optimal tracking technique for regulation and tracking for nonlinear stochastic systems based on the SDRE for finite-horizon control of nonlinear systems is given in [74], and is implemented with an observer in [76, 75],

The classical finite-horizon optimal tracking problem for LTV systems [89, 2] involves solving two differential equations, a matrix differential Riccati equation for $P(t)$, and a non-homogeneous vector differential equation for $g(t)$, which are propagated backward-in-time with given final-time conditions, and require prior knowledge of the system dynamics and the command input. With a focus on a classical tracking problem formulation, SDRE and FPRE methods are utilized for a tracking problem for nonlinear systems. In addition to tracking, a disturbance rejection problem with known disturbance is considered, and leads to additional terms in the vector differential equation.

For SDRE and FPRE control, the classical finite-horizon optimal tracking control law is extended to nonlinear systems given in SDC form. For SDRE method, the matrix differential Riccati equation is replaced by the ARE with state-dependent coefficients, and the non-homogeneous vector differential equation is replaced by an algebraic vector equation with state-dependent coefficients, which is done under the assumptions of slow command inputs and setting $\dot{g}(t) = 0$. For FPRE control, the backward-propagating matrix differential Riccati equation and the vector differential equation are replaced by corresponding forward-in-time equations with state-dependent coefficients. This involves introducing initial conditions $P(0)$ and $g(0)$ for $P(t)$ and $g(t)$, respectively.

Despite the heuristic nature of these methods, the advantages of SDRE and FPRE tracking controllers reside in their simple structure and the possibility of real-time implementation. Additional degrees of freedom come from the non-uniqueness of SDC parameterization of nonlinear system, and weighting matrices.

1.5 Numerical Investigation

A collection of plants, which have been considered in the literature for alternative control methods, is used for numerical investigation. These plants include the two-mass system, Mathieu equation, Van der Pol oscillator, ball and beam, and rotational-translational actuator. For the ball-and-beam system, full-state-feedback control laws are derived in [59, 104, 114], while output-feedback control laws are considered in

[116]. Likewise, for the rotational-translational actuator (RTAC), full-state-feedback control laws are derived in [16, 64, 113], and an observer-based controller using dissipativity techniques is given in [113].

In some examples, a discrete-time setting is adopted in order to avoid clouding the numerics with issues of integration accuracy. The main numerical issue that using discrete-time allows to avoid is the finite escape time. For the continuous-time cases, it appeared that the solution of FPRE using numerical integration techniques, could blow up in finite time, and this caused sensitivity to the integration methods. Use of discrete-time setting is for convenience only since all of the techniques are valid for continuous-time systems. To do this, continuous-time examples are discretized at a fixed step size. The resulting discrete-time model is adopted as the truth model for the purposes of the subsequent investigation. The accuracy of the discrete-time model relative to the underlying continuous-time system does not concern us here since that aspect is irrelevant to the objective of the investigation.

Application of tracking SDRE and FPRE control is illustrated by designing a flight controller for a fixed-wing aircraft. Linear control systems for an aircraft usually require linearization of the aircraft nonlinear dynamics for each flight condition, and then use gain scheduling [90, 61]. However, this approach is often not desirable for highly maneuverable flight. One of the benefits of a nonlinear controller for an aircraft is that a single controller can be used for the entire flight envelope. Nonlinear dynamic inversion control laws for aircraft flight control are demonstrated in [71, 82, 15, 108]. Disadvantages of model inversion control are that the input matrix must be square and invertible, the control gains may be large, and the dynamics may be uncertain.

A tracking controller for a fixed-wing unmanned aerial vehicle (UAV) uses an SDC model, which reflects the nonlinearities of a fixed-wing aircraft dynamics and thus allows the use of a single controller throughout the flight envelope. Another advantage of SDRE and FPRE controllers is that the weighting matrices can be used to adjust the tradeoff between the control effort (actuator deflections and thrust) and the state error. The goal of this controller is to control the attitude and altitude of an aircraft by giving the corresponding commands. A dual-loop structure for the controller allows reduction in the dimensions of the SDC matrices, which minimizes the computational

effort. SDC models for the inner and outer loops capture the nonlinearities in the actual aircraft model, whereas the inner-loop controller handles the modeling mismatch present in the inner-loop SDC model. The performance of these controllers is validated through simulation using a nonlinear UAV model. Two simulation cases are considered, namely, uniform atmosphere and light turbulence.

1.6 Original Contribution and Organization

Original contribution of this thesis contains derivation of analytical expressions for the solution of FPRE for LTI systems and prove its convergence, which places FPRE on rigorous foundation for LTI plants. Numerically investigation of capabilities of FPRE for nonlinear and LTV systems is performed for full-state feedback and output feedback. For output feedback, attainable frequencies and amplitudes for RTAC with two measurements, and the domain of attraction for ball and beam with two measurements are explored. SDRE and FPRE techniques are extended to classical feedforward control law for tracking and disturbance rejection for nonlinear systems. Also, FPRE is extended to command following and disturbance rejection using internal-model-control principle.

This work is organized as follows. Chapter 2 reviews main results associated with the properties of the BPRE and FPRE solutions, and provides proof on the exponential convergence of FPRE solution using Lyapunov methods. Chapter 3 reviews the problem of command following and disturbance rejection for LTI systems, focusing on the linear-quadratic control and IMP-based control for SISO systems. In Chapter 4 application of FPRE control for stabilization, command following and disturbance rejection for LTV systems is given. Chapter 5 gives a review of SDRE control for nonlinear systems, which includes SDRE regulation and tracking SDRE control. Chapter 6 covers application of FPRE control for nonlinear systems with numerical investigation of performance, robustness and domain of attraction. Application of tracking SDRE and FPRE controls for a fixed-wing aircraft is given in Chapter 7. Finally, Chapter 8 contains the concluding remarks.

CHAPTER 2

INFINITE-HORIZON LINEAR-QUADRATIC CONTROL BY FORWARD PROPAGATION OF THE DIFFERENTIAL RICCATI EQUATION

In view of the need for forward-integration techniques for control that depend only on the present dynamics, this chapter revisits linear-quadratic control for LTI plants. The chapter starts with a review of the basic features of the backward-propagating Riccati equation (BPRE), including the convergence of the Riccati solution to the ARE solution as the final time approaches infinity. These results are based on [81, 19, 20, 21]. Stronger assumptions on the plant and cost weightings are adopted in order to simplify the analysis. In particular, it is assumed that (A, B) is controllable and (A, C) is observable, whereas in [19, 20, 21, 80] the weaker assumptions that (A, B) is stabilizable and (A, C) is detectable are invoked.

Next, the forward-propagating Riccati equation (FPRE) is introduced. FPRE is analogous to BPRE but different due to the absence of the minus sign along with an initial condition rather than a final condition. It is shown that the results for BPRE have a dual form for the case of FPRE. In order to emphasize the similarities and differences relative to the case of BPRE, this section is written in a parallel fashion.

Although BPRE and FPRE can be viewed as dual equations, a crucial difference is the fact that BPRE is meaningful over only a finite horizon, whereas FPRE can be extended to infinity. This fact raises the question as to whether the FPRE control law is stabilizing. Since the solution of FPRE converges exponentially to the solution of ARE, it seems reasonable to conjecture that this is true. The main contribution is

thus to prove this fact. Since the control laws and Lyapunov function are both time-varying, Lyapunov methods for time-varying systems are used. The required results can be found in [57].

2.1 Backward-propagating Riccati equation control

For $t \in [0, t_f]$, consider the LTI plant

$$\dot{x}(t) = Ax(t) + Bu(t), \quad x(0) = x_0, \quad (2.1)$$

where $A \in \mathbb{R}^{n \times n}$, $B \in \mathbb{R}^{n \times m}$, and (A, B) is stabilizable, with the finite-horizon quadratic cost function

$$\mathbf{J}(u) = x^T(t_f)P_f x(t_f) + \int_0^{t_f} [x^T(t)R_1 x(t) + u^T(t)R_2 u(t)] dt, \quad (2.2)$$

where $R_1, P_f \in \mathbb{R}^{n \times n}$ are positive semidefinite and $R_2 \in \mathbb{R}^{m \times m}$ is positive definite. If (A, R_1) is observable, then the control $u : [0, t_f] \rightarrow \mathbb{R}^m$ that minimizes (2.2) is given by [89].

$$u(t) = K(t)x(t), \quad (2.3)$$

where

$$K(t) \triangleq -R_2^{-1}B^T P(t) \quad (2.4)$$

and $P : [0, t_f] \rightarrow \mathbb{R}^{n \times n}$ satisfies the backwards-in-time differential Riccati equation

$$-\dot{P}(t) = A^T P(t) + P(t)A - P(t)SP(t) + R_1, \quad P(t_f) = P_f, \quad (2.5)$$

where $S \triangleq BR_2^{-1}B^T$. For $t \in [0, t_f]$, the closed-loop dynamics are given by

$$\dot{x}(t) = A_{cl}(t)x(t), \quad (2.6)$$

where $A_{cl}(t) \triangleq A + BK(t) = A - SP(t)$. Note that (2.5) can be written as

$$-\dot{P}(t) = A_{cl}^T(t)P(t) + P(t)A_{cl}(t) + P(t)SP(t) + R_1, \quad P(t_f) = P_f. \quad (2.7)$$

For $t_f = \infty$, the infinite horizon cost is

$$\mathbf{J}(u) = \int_0^{\infty} [x^T(t)R_1 x(t) + u^T(t)R_2 u(t)] dt, \quad (2.8)$$

and the optimal feedback law $u : [0, \infty) \rightarrow \mathbb{R}^m$ is given by

$$u(t) = \bar{K}x(t), \quad (2.9)$$

where $\bar{K} \triangleq -R_2^{-1}B^T\bar{P}$ and, assuming that (A, R_1) has no unobservable eigenvalues on the imaginary axis, \bar{P} is the unique positive-semidefinite stabilizing solution of the algebraic Riccati equation

$$A^T\bar{P} + \bar{P}A - \bar{P}S\bar{P} + R_1 = 0. \quad (2.10)$$

For $t \in [0, \infty)$, the asymptotically stable closed-loop dynamics are given by

$$\dot{x}(t) = \bar{A}x(t), \quad (2.11)$$

where $\bar{A} \triangleq A + B\bar{K} = A - S\bar{P}$. Note that (2.10) can be written as

$$\bar{A}^T\bar{P} + \bar{P}\bar{A} + \bar{P}S\bar{P} + R_1 = 0. \quad (2.12)$$

Under stronger assumptions on A, B , and R_1 the following result is obtained.

Proposition 1. Assume that (A, B) is controllable and (A, R_1) is observable. Then \bar{P} is positive definite and, for all $t > 0$,

$$W(t) \triangleq \int_0^t e^{\bar{A}s} S e^{\bar{A}^T s} ds \quad (2.13)$$

is positive definite. Furthermore, for all $t_2 > t_1 > 0$,

$$\bar{P} \leq \bar{W}^{-1} < W^{-1}(t_2) < W^{-1}(t_1), \quad (2.14)$$

where

$$\bar{W} \triangleq \lim_{t \rightarrow \infty} W(t) = \int_0^\infty e^{\bar{A}s} S e^{\bar{A}^T s} ds \quad (2.15)$$

is positive definite and satisfies

$$\bar{A}\bar{W} + \bar{W}\bar{A}^T + S = 0. \quad (2.16)$$

Proof. Corollary 12.19.2 of [9] implies that \bar{P} is positive definite. Multiplying (2.12) on both sides by \bar{P}^{-1} yields

$$\bar{A}\bar{P}^{-1} + \bar{P}^{-1}\bar{A}^T + \bar{P}^{-1}R_1\bar{P}^{-1} + S = 0. \quad (2.17)$$

Subtracting (2.16) from (2.17) yields

$$\bar{A}(\bar{P}^{-1} - \bar{W}) + (\bar{P}^{-1} - \bar{W})\bar{A}^T + \bar{P}^{-1}R_1\bar{P}^{-1} = 0.$$

Since \bar{A} is asymptotically stable, it follows that

$$\bar{P}^{-1} - \bar{W} = \int_0^\infty e^{\bar{A}s} \bar{P}^{-1} R_1 \bar{P}^{-1} e^{\bar{A}^T s} ds \geq 0.$$

Hence,

$$\bar{W} \leq \bar{P}^{-1}. \quad (2.18)$$

Now, let $t_2 > t_1 > 0$. Then

$$\begin{aligned} W(t_2) - W(t_1) &= \int_0^{t_2} e^{\bar{A}s} S e^{\bar{A}^T s} ds - \int_0^{t_1} e^{\bar{A}s} S e^{\bar{A}^T s} ds \\ &= \int_{t_1}^{t_2} e^{\bar{A}s} S e^{\bar{A}^T s} ds \\ &= e^{\bar{A}t_1} \int_{t_1}^{t_2} e^{\bar{A}(s-t_1)} S e^{\bar{A}^T(s-t_1)} ds e^{\bar{A}^T t_1} \\ &= e^{\bar{A}t_1} \int_0^{t_2-t_1} e^{\bar{A}s} S e^{\bar{A}^T s} ds e^{\bar{A}^T t_1} \\ &= e^{\bar{A}t_1} W(t_2 - t_1) e^{\bar{A}^T t_1}. \end{aligned} \quad (2.19)$$

Since (A, B) is controllable, it follows that (\bar{A}, B) is controllable, and thus $W(t) > 0$ for all $t > 0$. Therefore, $W(t_2 - t_1) > 0$, and thus (2.19) implies that $W(t_1) < W(t_2)$. Hence, $W^{-1}(t_2) < W^{-1}(t_1)$. Furthermore, $W(t_2) < \bar{W}$, and thus \bar{W} is positive definite. Hence, (2.18) implies that $\bar{P} \leq \bar{W}^{-1} < W^{-1}(t_2)$. \square

Theorem 1. Assume that (A, B) is controllable and (A, R_1) is observable. Then, for all $t \in [0, t_f]$, the solution $P(t)$ of (2.5) is given by

$$P(t) = \bar{P} + e^{\bar{A}^T(t_f-t)} (P_f - \bar{P}) [I + W(t_f - t)(P_f - \bar{P})]^{-1} e^{\bar{A}(t_f-t)}, \quad (2.20)$$

where $W(t_f - t)$ is given by (2.13). Furthermore, for all $t \in [0, t_f]$, $P(t)$ is positive semidefinite, and, for all $t \geq 0$,

$$\lim_{t_f \rightarrow \infty} P(t) = \bar{P}. \quad (2.21)$$

Now assume that $P_f - \bar{P}$ is nonsingular. Then, for all $t \in [0, t_f]$,

$$P(t) = \bar{P} + e^{\bar{A}^T(t_f-t)} [(P_f - \bar{P})^{-1} + W(t_f - t)]^{-1} e^{\bar{A}(t_f-t)}, \quad (2.22)$$

and

$$P(t) = \bar{P} + Z^{-1}(t), \quad (2.23)$$

where $Z : [0, t_f] \rightarrow \mathbb{R}^{n \times n}$ defined by

$$Z(t) \triangleq e^{\bar{A}(t-t_f)} [(P_f - \bar{P})^{-1} + \bar{W}] e^{\bar{A}^T(t-t_f)} - \bar{W} \quad (2.24)$$

is nonsingular and satisfies

$$\dot{Z}(t) = \bar{A}Z(t) + Z(t)\bar{A}^T - S. \quad (2.25)$$

Proof. For all $0 \leq t < t_f$, Proposition 1 implies that $\bar{P} < W^{-1}(t_f - t)$. Therefore, for all $t \in [0, t_f)$,

$$\det [I + W(t_f - t)(P_f - \bar{P})] = (\det W(t_f - t)) \det [W^{-1}(t_f - t) - \bar{P} + P_f] > 0,$$

and thus $I + W(t_f - t)(P_f - \bar{P})$ is nonsingular. In fact, $I + W(t_f - t)(P_f - \bar{P})$ is nonsingular for all $t \in [0, t_f]$.

To show that (2.20) is symmetric, note that, for all $t \in [0, t_f]$,

$$[I + (P_f - \bar{P})W(t_f - t)] (P_f - \bar{P}) = (P_f - \bar{P}) [I + W(t_f - t)(P_f - \bar{P})],$$

and thus

$$\begin{aligned} (P_f - \bar{P}) [I + W(t_f - t)(P_f - \bar{P})]^{-1} &= [I + (P_f - \bar{P})W(t_f - t)]^{-1} (P_f - \bar{P}) \\ &= [I + W(t_f - t)(P_f - \bar{P})]^{-T} (P_f - \bar{P}) \\ &= \left[(P_f - \bar{P}) [I + W(t_f - t)(P_f - \bar{P})]^{-1} \right]^T. \end{aligned}$$

To show that, for all $t \in [0, t_f]$, $P(t)$ is positive semidefinite, rewrite (2.5) as

$$\dot{P}(t) = -A_{cl}^T(t)P(t) - P(t)A_{cl}(t) - P(t)SP(t) - R_1. \quad (2.26)$$

Then, for all $t \in [0, t_f]$, $P(t)$ satisfies

$$P(t) = \Phi(t, t_f)P_f\Phi^T(t, t_f) + \int_t^{t_f} \Phi(t, s) [P(s)SP(s) + R_1] \Phi^T(t, s) ds, \quad (2.27)$$

which is positive semidefinite, where, for all $t, s \in [0, t_f]$, the state transition matrix $\Phi(t, s)$ of the dual closed-loop system satisfies $\frac{\partial}{\partial t}\Phi(t, s) = -A_{cl}^T(t)\Phi(t, s)$, $\Phi(t, t) = I$. To show that (2.27) is the solution of (2.26), note that, by Leibniz's rule,

$$\begin{aligned}
\dot{P}(t) &= \frac{\partial}{\partial t}\Phi(t, t_f)P_f\Phi^T(t, t_f) + \Phi(t, t_f)P_f\frac{\partial}{\partial t}\Phi^T(t, t_f) \\
&\quad + \int_t^{t_f} \frac{\partial}{\partial t}\Phi(t, s)(P(s)SP(s) + R_1)\Phi^T(t, s) ds \\
&\quad + \int_t^{t_f} \Phi(t, s)(P(s)SP(s) + R_1)\frac{\partial}{\partial t}\Phi^T(t, s) ds \\
&\quad - \Phi(t, t)(P(t)SP(t) + R_1)\Phi^T(t, t) \\
&= -A_{cl}^T(t)\Phi(t, t_f)P_f\Phi^T(t, t_f) - \Phi(t, t_f)P_f\Phi^T(t, t_f)A_{cl}(t) \\
&\quad - \int_t^{t_f} A_{cl}^T(t)\Phi(t, s)(P(s)SP(s) + R_1)\Phi^T(t, s) ds \\
&\quad - \int_t^{t_f} \Phi(t, s)(P(s)SP(s) + R_1)\Phi^T(t, s)A_{cl}(t) ds \\
&\quad - P(t)SP(t) - R_1 \\
&= -A_{cl}^T(t) \left(\Phi(t, t_f)P_f\Phi^T(t, t_f) + \int_t^{t_f} \Phi(t, s)(P(s)SP(s) + R_1)\Phi^T(t, s) ds \right) \\
&\quad - \left(\Phi(t, t_f)P_f\Phi^T(t, t_f) + \int_t^{t_f} \Phi(t, s)(P(s)SP(s) + R_1)\Phi^T(t, s) ds \right) A_{cl}(t) \\
&\quad - P(t)SP(t) - R_1 \\
&= -A_{cl}^T(t)P(t) - P(t)A_{cl}(t) - P(t)SP(t) - R_1.
\end{aligned}$$

To show that (2.20) satisfies (2.5), note that $\frac{d}{dt}W(t_f - t) = -e^{\bar{A}(t_f-t)}Se^{\bar{A}^T(t_f-t)}$, and

thus

$$\begin{aligned}
\dot{P}(t) &= -\bar{A}^T e^{\bar{A}^T(t_f-t)}(P_f - \bar{P}) [I + W(t_f - t)(P_f - \bar{P})]^{-1} e^{\bar{A}(t_f-t)} \\
&\quad - e^{\bar{A}^T(t_f-t)}(P_f - \bar{P}) [I + W(t_f - t)(P_f - \bar{P})]^{-1} e^{\bar{A}(t_f-t)} \bar{A} \\
&\quad - e^{\bar{A}^T(t_f-t)}(P_f - \bar{P}) [I + W(t_f - t)(P_f - \bar{P})]^{-1} \\
&\quad \cdot \left[\frac{d}{dt} W(t_f - t) \right] (P_f - \bar{P}) [I + W(t_f - t)(P_f - \bar{P})]^{-1} e^{\bar{A}(t_f-t)} \\
&= -\bar{A}^T(P(t) - \bar{P}) - (P(t) - \bar{P})\bar{A} \\
&\quad + e^{\bar{A}^T(t_f-t)}(P_f - \bar{P}) [I + W(t_f - t)(P_f - \bar{P})]^{-1} e^{\bar{A}(t_f-t)} S \\
&\quad \cdot e^{\bar{A}^T(t_f-t)}(P_f - \bar{P}) [I + W(t_f - t)(P_f - \bar{P})]^{-1} e^{\bar{A}(t_f-t)} \\
&= -\bar{A}^T(P(t) - \bar{P}) - (P(t) - \bar{P})\bar{A} + (P(t) - \bar{P})S(P(t) - \bar{P}) \\
&= -\bar{A}^T P(t) - P(t)\bar{A} + P(t)SP(t) - P(t)S\bar{P} - \bar{P}SP(t) - R_1 \\
&\quad + \bar{A}^T \bar{P} + \bar{P}\bar{A} + \bar{P}S\bar{P} + R_1 \\
&= -\bar{A}^T P(t) - P(t)\bar{A} + P(t)SP(t) - P(t)S\bar{P} - \bar{P}SP(t) - R_1 \\
&= -A^T P(t) - P(t)A + P(t)SP(t) - R_1.
\end{aligned}$$

Since, for all $t \geq 0$, $e^{\bar{A}^T(t_f-t)} \rightarrow 0$ as $t_f \rightarrow \infty$, it follows from (2.20) that, for all $t \geq 0$,

$$\begin{aligned}
\lim_{t_f \rightarrow \infty} P(t) &= \bar{P} + \lim_{t_f \rightarrow \infty} \left[e^{\bar{A}^T(t_f-t)}(P_f - \bar{P}) [I + W(t_f - t)(P_f - \bar{P})]^{-1} e^{\bar{A}(t_f-t)} \right] \\
&= \bar{P} + \lim_{t_f \rightarrow \infty} e^{\bar{A}^T(t_f-t)} \left(\lim_{t_f \rightarrow \infty} \left[(P_f - \bar{P}) [I + W(t_f - t)(P_f - \bar{P})]^{-1} \right] \right) \\
&\quad \cdot \lim_{t_f \rightarrow \infty} e^{\bar{A}(t_f-t)} = \bar{P}.
\end{aligned}$$

Now assume that $P_f - \bar{P}$ is nonsingular. Then (2.20) implies (2.22). To show that

(2.23) is equivalent to (2.22), note that

$$\begin{aligned}
& \left[e^{\bar{A}^T(t_f-t)} \left[(P_f - \bar{P})^{-1} + W(t_f - t) \right]^{-1} e^{\bar{A}(t_f-t)} \right]^{-1} \\
&= e^{-\bar{A}(t_f-t)} \left[(P_f - \bar{P})^{-1} + \int_0^{t_f-t} e^{\bar{A}s} S e^{\bar{A}^T s} ds \right] e^{-\bar{A}^T(t_f-t)} \\
&= e^{\bar{A}(t-t_f)} \left[(P_f - \bar{P})^{-1} + \int_0^\infty e^{\bar{A}s} S e^{\bar{A}^T s} ds \right] e^{\bar{A}^T(t-t_f)} \\
&\quad - e^{-\bar{A}(t_f-t)} \int_{t_f-t}^\infty e^{\bar{A}s} S e^{\bar{A}^T s} ds e^{-\bar{A}^T(t_f-t)} \\
&= e^{\bar{A}(t-t_f)} \left[(P_f - \bar{P})^{-1} + \bar{W} \right] e^{\bar{A}^T(t-t_f)} \\
&\quad - \int_{t_f-t}^\infty e^{\bar{A}(s-t_f+t)} S e^{\bar{A}^T(s-t_f+t)} ds \\
&= e^{\bar{A}(t-t_f)} \left[(P_f - \bar{P})^{-1} + \bar{W} \right] e^{\bar{A}^T(t-t_f)} - \bar{W} \\
&= Z(t).
\end{aligned}$$

Therefore, $Z(t)$ is nonsingular, and

$$Z^{-1}(t) = e^{\bar{A}^T(t_f-t)} \left[(P_f - \bar{P})^{-1} + W(t_f - t) \right]^{-1} e^{\bar{A}(t_f-t)},$$

which shows that (2.22) and (2.23) are equivalent.

To show that (2.24) satisfies (2.25), note that (2.16) implies that

$$\begin{aligned}
\dot{Z}(t) &= \bar{A} e^{\bar{A}(t-t_f)} \left[(P_f - \bar{P})^{-1} + \bar{W} \right] e^{\bar{A}^T(t-t_f)} + e^{\bar{A}(t-t_f)} \left[(P_f - \bar{P})^{-1} + \bar{W} \right] e^{\bar{A}^T(t-t_f)} \bar{A}^T \\
&= \bar{A} (Z(t) + \bar{W}) + (Z(t) + \bar{W}) \bar{A}^T \\
&= \bar{A} Z(t) + Z(t) \bar{A}^T + \bar{A} \bar{W} + \bar{W} \bar{A}^T \\
&= \bar{A} Z(t) + Z(t) \bar{A}^T - S. \quad \square
\end{aligned}$$

Note that (2.20) implies that

$$P(0) = \bar{P} + e^{\bar{A}^T t_f} (P_f - \bar{P}) \left[I + W(t_f) (P_f - \bar{P}) \right]^{-1} e^{\bar{A} t_f} \quad (2.28)$$

and

$$\begin{aligned}
P(t_f) &= \bar{P} + e^{\bar{A}^T(t_f-t_f)} (P_f - \bar{P}) \left[I + W(t_f - t_f) (P_f - \bar{P}) \right]^{-1} e^{\bar{A}(t_f-t_f)} \\
&= \bar{P} + P_f - \bar{P} = P_f. \quad (2.29)
\end{aligned}$$

The expression for $P(t)$ given by (2.23) - (2.25) is based on [67], pages 418–419.

The expression for $P(t)$ given by (2.20) can be viewed as a superposition formula.

For details, see [109].

Example 2.1. Consider the asymptotically stable plant

$$A = \begin{bmatrix} 0 & 1 \\ -0.5 & -1.5 \end{bmatrix}, B = \begin{bmatrix} 0 \\ 1 \end{bmatrix} \quad (2.30)$$

and the unstable plant

$$A = \begin{bmatrix} 0 & 1 \\ -8 & 6 \end{bmatrix}, B = \begin{bmatrix} 0 \\ 1 \end{bmatrix}, \quad (2.31)$$

with $R_1 = I$ and $R_2 = 1$ for both plants. For (2.30), \bar{P} is given by

$$\bar{P} = \begin{bmatrix} 1.6 & 0.6 \\ 0.6 & 0.6 \end{bmatrix}, \quad (2.32)$$

and for (2.31), \bar{P} is given by

$$\bar{P} = \begin{bmatrix} 97.1 & 0.06 \\ 0.06 & 12.1 \end{bmatrix}. \quad (2.33)$$

For both plants consider P_f given by

$$P_f = \begin{bmatrix} 5 & 0 \\ 0 & 5 \end{bmatrix}. \quad (2.34)$$

Figure 2.1 illustrates Theorem 1 for the plants (2.30), (2.31), with P_f given by (2.34) and t_f equal to 5 sec, 10 sec, and 15 sec. Norm denotes the largest singular value. For the asymptotically stable plant (2.30), (a) shows the convergence of $P(t)$ to \bar{P} for each fixed t as t_f approaches infinity, whereas (b) shows the convergence of $P(t)$ to \bar{P} for the unstable plant (2.31) for each fixed t as t_f approaches infinity. ■

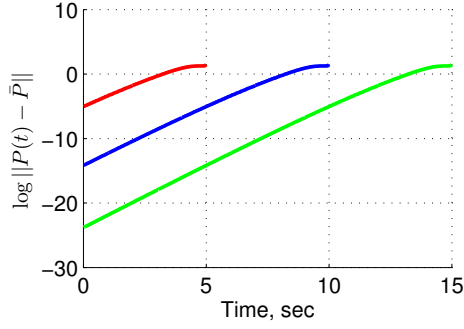
Proposition 2. Assume that $P_f < \bar{P}$. Then, for all $t \in [0, t_f)$, $(P_f - \bar{P})^{-1} + W(t_f - t) < 0$ and $P(t) < \bar{P}$. If, in addition, P_f satisfies

$$A^T P_f + P_f A - P_f S P_f + R_1 \geq 0, \quad (2.35)$$

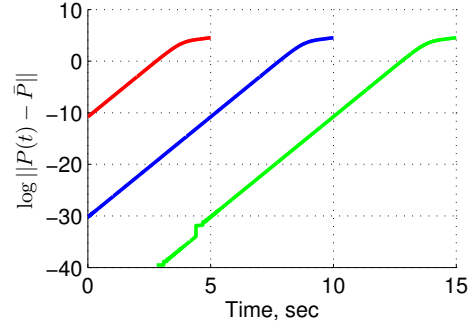
then, for all $t \in [0, t_f)$, $P_f \leq P(t)$.

Proof. It follows from (2.14) and the fact that $P_f \geq 0$ that, for all $t \in [0, t_f)$,

$$\bar{P} - P_f \leq \bar{P} < W^{-1}(t_f - t).$$



(a) Plant (2.30)



(b) Plant (2.31)

Figure 2.1: Example 2.1. Illustrative results for Theorem 1.

Therefore, since $\bar{P} - P_f > 0$, it follows that, for all $t \in [0, t_f)$,

$$W(t_f - t) < (\bar{P} - P_f)^{-1} = -(P_f - \bar{P})^{-1}.$$

Therefore, for all $t \in [0, t_f)$, $(P_f - \bar{P})^{-1} + W(t_f - t)$ is negative definite, and thus (2.22) implies that, for all $t \in [0, t_f)$, $P(t) < \bar{P}$.

Next, note that (2.35) can be written as

$$\begin{aligned} & (\bar{A} + S\bar{P})^T P_f + P_f(\bar{A} + S\bar{P}) - P_f S P_f + R_1 \\ & = -\bar{A}^T(\bar{P} - P_f) - (\bar{P} - P_f)\bar{A} - (\bar{P} - P_f)S(\bar{P} - P_f) \geq 0, \end{aligned}$$

which implies

$$(\bar{P} - P_f)S(\bar{P} - P_f) \leq -\bar{A}^T(\bar{P} - P_f) - (\bar{P} - P_f)\bar{A}. \quad (2.36)$$

Multiplying (2.36) on the left and right by $e^{\bar{A}s}(\bar{P} - P_f)^{-1}$ and $(\bar{P} - P_f)^{-1}e^{\bar{A}^T s}$, respectively, yields

$$\begin{aligned} e^{\bar{A}s} S e^{\bar{A}^T s} & \leq -e^{\bar{A}s} \bar{A} (\bar{P} - P_f)^{-1} e^{\bar{A}^T s} - e^{\bar{A}s} (\bar{P} - P_f)^{-1} \bar{A}^T e^{\bar{A}^T s}, \\ & = -\frac{d}{ds} e^{\bar{A}s} (\bar{P} - P_f)^{-1} e^{\bar{A}^T s}. \end{aligned}$$

Hence,

$$\begin{aligned} W(t_f - t) & = \int_0^{t_f - t} e^{\bar{A}s} S e^{\bar{A}^T s} ds \\ & \leq -\int_0^{t_f - t} \frac{d}{ds} e^{\bar{A}s} (\bar{P} - P_f)^{-1} e^{\bar{A}^T s} ds \\ & = (\bar{P} - P_f)^{-1} - e^{\bar{A}(t_f - t)} (\bar{P} - P_f)^{-1} e^{\bar{A}^T(t_f - t)}. \end{aligned}$$

Thus,

$$(\bar{P} - P_f)^{-1} \leq e^{-\bar{A}(t_f-t)}[(\bar{P} - P_f)^{-1} - W(t_f - t)]e^{-\bar{A}^T(t_f-t)}. \quad (2.37)$$

Since, for all $t \in [0, t_f]$, $(\bar{P} - P_f)^{-1} - W(t_f - t)$ is positive definite, (2.37) implies

$$e^{\bar{A}^T(t_f-t)}[(\bar{P} - P_f)^{-1} - W(t_f - t)]^{-1}e^{\bar{A}(t_f-t)} \leq \bar{P} - P_f,$$

which is equivalent to

$$P_f \leq \bar{P} + e^{\bar{A}^T(t_f-t)}[(P_f - \bar{P})^{-1} + W(t_f - t)]^{-1}e^{\bar{A}(t_f-t)} = P(t). \quad \square$$

For $n = 1$, now it is shown that $P_f < \bar{P}$ implies that (2.35) holds. Therefore, in the scalar case, (2.35) need not be invoked as an assumption in Proposition 2. Define $a \triangleq A$, $b \triangleq B$, $p_f \triangleq P_f$, $\bar{p} \triangleq \bar{P}$, $r_1 \triangleq R_1$, and $s \triangleq S$, and assume $R_2 = 1$. Then $s = b^2$, and the left hand side of (2.35) can be written as

$$\begin{aligned} -b^2 p_f^2 + 2ap_f + r_1 &= -b^2 \bar{p}^2 + 2a\bar{p} + r_1 - (-b^2 \bar{p}^2 + 2a\bar{p} + r_1) \\ &= b^2(\bar{p}^2 - p_f^2) - 2a(\bar{p} - p_f) \\ &= b^2(\bar{p} - p_f)(\bar{p} + p_f) - 2a(\bar{p} - p_f). \end{aligned} \quad (2.38)$$

Furthermore, the solution \bar{p} of (2.10) is given by

$$\bar{p} = \frac{1}{b^2}(a + \sqrt{a^2 + b^2 r_1}). \quad (2.39)$$

Since $\bar{p} - p_f > 0$, dividing (2.38) by $\bar{p} - p_f$ and using (2.39) yields

$$\begin{aligned} b^2(\bar{p} + p_f) - 2a &= b^2 p_f + a + \sqrt{a^2 + b^2 r_1} - 2a \\ &= b^2 p_f + \sqrt{a^2 + b^2 r_1} - a \\ &> 0, \end{aligned} \quad (2.40)$$

which implies (2.35). The following example shows that, for $n \geq 2$, $P_f < \bar{P}$ does not imply (2.35).

Example 2.2. Consider the unstable plant

$$A = \begin{bmatrix} 0 & 1 \\ -0.34 & 1.2 \end{bmatrix}, \quad B = \begin{bmatrix} 0 \\ 1 \end{bmatrix} \quad (2.41)$$

with $R_1 = I$ and $R_2 = 1$. For this plant, \bar{P} is given by

$$\bar{P} = \begin{bmatrix} 2.48 & 0.71 \\ 0.71 & 3.17 \end{bmatrix}. \quad (2.42)$$

Consider two choices of P_f , namely,

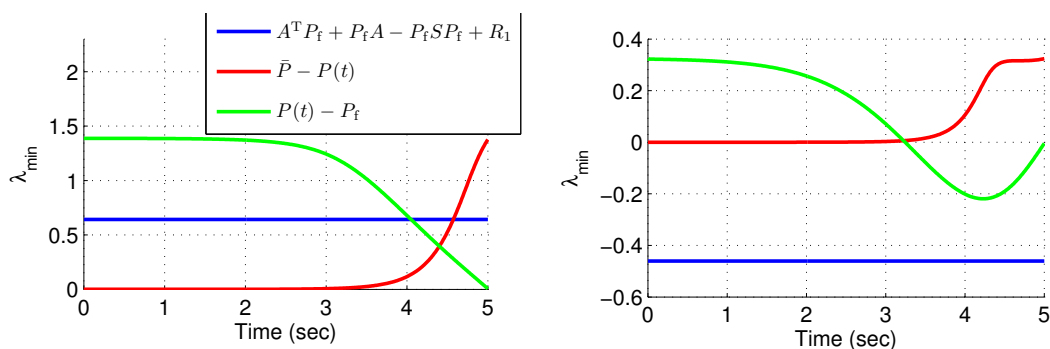
$$P_f = \begin{bmatrix} 0.8 & 0.3 \\ 0.3 & 1.2 \end{bmatrix} \quad (2.43)$$

and

$$P_f = \begin{bmatrix} 2 & 0.1 \\ 0.1 & 0.5 \end{bmatrix}. \quad (2.44)$$

For P_f given by (2.43), condition (2.35) is satisfied, whereas, for P_f given by (2.44), condition (2.35) is not satisfied. Figure 2.2 illustrates Proposition 2 for the unstable plant (2.41) with P_f given by (2.43) and (2.44), and $t_f = 5$ sec. λ_{\min} denotes the minimum eigenvalue. For P_f given by (2.43), (a) shows that (2.35) is satisfied, and, for all $t \in [0, 5]$ sec, $P_f \leq P(t) < \bar{P}$, whereas, for P_f given by (2.44), (b) shows that (2.35) is not satisfied, for all $t \in [0, 5]$ sec, $P(t) < \bar{P}$, and, for all $t \in [3.2, 5]$ sec, $P_f \leq P(t)$ does not hold.

■



(a) (2.35) holds

(b) (2.35) does not hold

Figure 2.2: Example 2.2. Illustrative results for Proposition 2.

Numerical examples suggest that (2.35) is a necessary condition for $P_f \leq P(t)$ on $[0, t_f)$. Proof of this conjecture is open.

The following result complements Proposition 2.

Proposition 3. Assume that $\bar{P} < P_f$. Then, for all $t \in [0, t_f)$, $(P_f - \bar{P})^{-1} + W(t_f - t) > 0$ and $\bar{P} < P(t)$. If, in addition, P_f satisfies

$$A^T P_f + P_f A - P_f S P_f + R_1 \leq 0, \quad (2.45)$$

then, for all $t \in [0, t_f)$, $P(t) \leq P_f$.

If $P_f > \bar{P}$, then (2.22) implies that, for all $t \in [0, t_f]$, $P(t)$ is positive semidefinite, and thus (2.27) is not needed. In fact, if $P_f > \bar{P}$, then it follows from (2.22) that, for all $t \in [0, t_f)$, $P(t)$ is positive definite. Unfortunately, it does not seem to be possible to avoid using (2.27) for arbitrary positive-semidefinite P_f .

2.2 Forward-propagating Riccati equation control

The FPRE control law replaces (2.5) with the forward-in-time differential Riccati equation [121]

$$\dot{P}(t) = A^T P(t) + P(t) A - P(t) S P(t) + R_1, \quad P(0) = P_0, \quad (2.46)$$

where P_0 is positive semidefinite. Note that (2.46) can be written as

$$\dot{P}(t) = A_{cl}^T(t) P(t) + P(t) A_{cl}(t) + P(t) S P(t) + R_1, \quad P(0) = P_0, \quad (2.47)$$

which differs from (2.5) due to the minus sign and the initial condition. Otherwise, (2.3) and (2.6) remain unchanged. However, the FPRE control law is not guaranteed to minimize (2.2).

Theorem 2. Assume that (A, B) is controllable and (A, R_1) is observable. Then, for all $t \geq 0$, $I + W(t)(P_0 - \bar{P})$ is nonsingular, and the positive-semidefinite solution $P(t)$ of (2.46) is given by

$$P(t) = \bar{P} + e^{\bar{A}^T t} (P_0 - \bar{P}) [I + W(t)(P_0 - \bar{P})]^{-1} e^{\bar{A} t}, \quad (2.48)$$

where $W(t)$ is given by (2.13) and, for all $t \geq 0$,

$$\lim_{t \rightarrow \infty} P(t) = \bar{P}. \quad (2.49)$$

If $P_0 - \bar{P}$ is nonsingular, then, for all $t \geq 0$,

$$P(t) = \bar{P} + e^{\bar{A}^T t} [(P_0 - \bar{P})^{-1} + W(t)]^{-1} e^{\bar{A} t} \quad (2.50)$$

and

$$P(t) = \bar{P} + Z^{-1}(t), \quad (2.51)$$

where, $Z : [0, \infty) \rightarrow \mathbb{R}^{n \times n}$ defined by

$$Z(t) \triangleq e^{-\bar{A}t} [(P_0 - \bar{P})^{-1} + \bar{W}] e^{-\bar{A}^T t} - \bar{W} \quad (2.52)$$

is nonsingular and satisfies

$$\dot{Z}(t) = -\bar{A}Z(t) - Z(t)\bar{A}^T + S. \quad (2.53)$$

Proof. To show that, for all $t > 0$, $I + W(t)(P_0 - \bar{P})$ is nonsingular, note that, from Proposition 1, $\bar{P} < W^{-1}(t)$. Therefore, for all $t > 0$,

$$\det [I + W(t)(P_0 - \bar{P})] = (\det W(t)) \det [W^{-1}(t) - \bar{P} + P_0] > 0.$$

Thus, for all $t > 0$, $I + W(t)(P_0 - \bar{P})$ is nonsingular. In fact, for all $t \geq 0$, $I + W(t)(P_0 - \bar{P})$ is nonsingular.

To show that (2.48) is symmetric, note that, for all $t \geq 0$,

$$[I + (P_0 - \bar{P})W(t)] (P_0 - \bar{P}) = (P_0 - \bar{P}) [I + W(t)(P_0 - \bar{P})].$$

Thus

$$\begin{aligned} (P_0 - \bar{P}) [I + W(t)(P_0 - \bar{P})]^{-1} &= [I + (P_0 - \bar{P})W(t)]^{-1} (P_0 - \bar{P}) \\ &= [I + W(t)(P_0 - \bar{P})]^{-T} (P_0 - \bar{P}) \\ &= \left[(P_0 - \bar{P}) [I + W(t)(P_0 - \bar{P})]^{-1} \right]^T. \end{aligned}$$

To show that, for all $t \geq 0$, $P(t)$ is positive semidefinite, note that it follows from (2.47) that

$$P(t) = \Phi(t, 0)P_0\Phi^T(t, 0) + \int_0^t \Phi(t, s) [P(s)SP(s) + R_1] \Phi^T(t, s) ds \quad (2.54)$$

is positive semidefinite, where, for all $t, s \in [0, \infty)$, the state transition matrix $\Phi(t, s)$ of the closed-loop system satisfies $\frac{\partial}{\partial t} \Phi(t, s) = A_{cl}^T(t)\Phi(t, s)$, $\Phi(t, t) = I$. To show

that (2.54) satisfies (2.47), note that, by Leibniz's rule

$$\begin{aligned}
\dot{P}(t) &= \frac{\partial}{\partial t} \Phi(t, 0) P_0 \Phi^T(t, 0) + \Phi(t, 0) P_0 \frac{\partial}{\partial t} \Phi^T(t, 0) \\
&\quad + \int_0^t \frac{\partial}{\partial t} \Phi(t, s) [P(s)SP(s) + R_1] \Phi^T(t, s) ds \\
&\quad + \int_0^t \Phi(t, s) [P(s)SP(s) + R_1] \frac{\partial}{\partial t} \Phi^T(t, s) ds + P(t)SP(t) + R_1 \\
&= A_{cl}^T(t) \Phi(t, 0) P_0 \Phi^T(t, 0) + \Phi(t, 0) P_0 \Phi^T(t, 0) A_{cl}(t) \\
&\quad + \int_0^t A_{cl}^T(t) \Phi(t, s) [P(s)SP(s) + R_1] \Phi^T(t, s) ds \\
&\quad + \int_0^t \Phi(t, s) [P(s)SP(s) + R_1] \Phi^T(t, s) A_{cl}(t) ds + P(t)SP(t) + R_1 \\
&= A_{cl}^T(t) \left[\Phi(t, 0) P_0 \Phi^T(t, 0) + \int_0^t \Phi(t, s) [P(s)SP(s) + R_1] \Phi^T(t, s) ds \right] \\
&\quad + \left[\Phi(t, 0) P_0 \Phi^T(t, 0) + \int_0^t \Phi(t, s) [P(s)SP(s) + R_1] \Phi^T(t, s) ds \right] A_{cl}(t) \\
&\quad + P(t)SP(t) + R_1 \\
&= A_{cl}^T(t)P(t) + P(t)A_{cl}(t) + P(t)SP(t) + R_1. \tag{2.55}
\end{aligned}$$

Next to be shown is that (2.48) satisfies (2.46). Note that $\frac{d}{dt}W(t) = e^{\bar{A}t} S e^{\bar{A}^T t}$, and thus

$$\begin{aligned}
\dot{P}(t) &= \bar{A}^T e^{\bar{A}^T t} (P_0 - \bar{P}) [I + W(t)(P_0 - \bar{P})]^{-1} e^{\bar{A}t} \\
&\quad + e^{\bar{A}^T t} (P_0 - \bar{P}) [I + W(t)(P_0 - \bar{P})]^{-1} e^{\bar{A}t} \bar{A} \\
&\quad - e^{\bar{A}^T t} (P_0 - \bar{P}) [I + W(t)(P_0 - \bar{P})]^{-1} \frac{d}{dt} W(t) (P_0 - \bar{P}) \\
&\quad \cdot [I + W(t)(P_0 - \bar{P})]^{-1} e^{\bar{A}t} \\
&= \bar{A}^T (P(t) - \bar{P}) + (P(t) - \bar{P}) \bar{A} - (P(t) - \bar{P}) S (P(t) - \bar{P}) \\
&= \bar{A}^T P(t) + P(t) \bar{A} - P(t) S P(t) + P(t) S \bar{P} + \bar{P} S P(t) + R_1 \\
&\quad - (\bar{A}^T \bar{P} + \bar{P} \bar{A} + \bar{P} S \bar{P} + R_1) \\
&= \bar{A}^T P(t) + P(t) \bar{A} - P(t) S P(t) + P(t) S \bar{P} + \bar{P} S P(t) + R_1 \\
&= A^T P(t) + P(t) A - P(t) S P(t) + R_1.
\end{aligned}$$

Since $e^{\bar{A}^T t} \rightarrow 0$ as $t \rightarrow \infty$, it follows from (2.48) that

$$\begin{aligned}\lim_{t \rightarrow \infty} P(t) &= \bar{P} + \lim_{t \rightarrow \infty} \left[e^{\bar{A}^T t} (P_0 - \bar{P}) [I + W(t) (P_0 - \bar{P})]^{-1} e^{\bar{A} t} \right] \\ &= \bar{P} + \left(\lim_{t \rightarrow \infty} e^{\bar{A}^T t} \right) \left(\lim_{t \rightarrow \infty} \left[(P_0 - \bar{P}) [I + W(t) (P_0 - \bar{P})]^{-1} \right] \right) \lim_{t \rightarrow \infty} e^{\bar{A} t} \\ &= \bar{P}.\end{aligned}$$

Now, assume that $P_0 - \bar{P}$ is nonsingular. Then (2.50) follows from (2.48). To show that (2.51) is equivalent to (2.50), note that

$$\begin{aligned}\left[e^{\bar{A}^T t} [(P_0 - \bar{P})^{-1} + W(t)]^{-1} e^{\bar{A} t} \right]^{-1} &= e^{-\bar{A} t} \left[(P_0 - \bar{P})^{-1} + \int_0^t e^{\bar{A} s} S e^{\bar{A}^T s} ds \right] e^{-\bar{A}^T t} \\ &= e^{-\bar{A} t} \left[(P_0 - \bar{P})^{-1} + \int_0^\infty e^{\bar{A} s} S e^{\bar{A}^T s} ds \right] e^{-\bar{A}^T t} \\ &\quad - e^{-\bar{A} t} \int_t^\infty e^{\bar{A} s} S e^{\bar{A}^T s} ds e^{-\bar{A}^T t} \\ &= e^{-\bar{A} t} [(P_0 - \bar{P})^{-1} + \bar{W}] e^{-\bar{A}^T t} \\ &\quad - \int_t^\infty e^{\bar{A}(s-t)} S e^{\bar{A}^T(s-t)} ds \\ &= e^{-\bar{A} t} [(P_0 - \bar{P})^{-1} + \bar{W}] e^{-\bar{A}^T t} - \bar{W} \\ &= Z(t).\end{aligned}$$

Therefore, for all $t > 0$, $Z(t)$ is nonsingular, and

$$Z^{-1}(t) = e^{\bar{A}^T t} [(P_0 - \bar{P})^{-1} + W(t)]^{-1} e^{\bar{A} t},$$

which implies that (2.50) and (2.51) are equivalent.

To show that (2.52) satisfies (2.53), note that (2.16) implies that

$$\begin{aligned}\dot{Z}(t) &= -\bar{A} e^{-\bar{A} t} [(P_0 - \bar{P})^{-1} + \bar{W}] e^{-\bar{A}^T t} - e^{-\bar{A} t} [(P_0 - \bar{P})^{-1} + \bar{W}] e^{-\bar{A}^T t} \bar{A}^T \\ &= -\bar{A}(Z(t) + \bar{W}) - (Z(t) + \bar{W}) \bar{A}^T \\ &= -\bar{A} Z(t) - Z(t) \bar{A}^T - \bar{A} \bar{W} - \bar{W} \bar{A}^T \\ &= -\bar{A} Z(t) - Z(t) \bar{A}^T + S.\end{aligned} \quad \square$$

Note that (2.48) implies that

$$\begin{aligned}P(0) &= \bar{P} + e^{\bar{A}^T 0} (P_0 - \bar{P}) [I + W(0) (P_0 - \bar{P})]^{-1} e^{\bar{A} 0} \\ &= \bar{P} + P_0 - \bar{P} = P_0\end{aligned} \quad (2.56)$$

and

$$P(t_f) = \bar{P} + e^{\bar{A}^T t_f} (P_0 - \bar{P}) [I + W(t_f) (P_0 - \bar{P})]^{-1} e^{\bar{A} t_f}. \quad (2.57)$$

Example 2.3. Consider the plants given by (2.30) and (2.31), with $R_1 = I$ and $R_2 = 1$, where \bar{P} is given by (2.32) and (2.33), respectively, and P_0 is equal to P_f given by (2.34). Figure 2.3 illustrates Theorem 2 for the plants (2.30), (2.31) with P_0 equal to P_f given by (2.34). The norm is the largest singular value. The solutions are valid on $[0, \infty)$. For the asymptotically stable plant (2.30), (a) shows the convergence of $P(t)$ to \bar{P} as t goes to infinity, whereas (b) shows the convergence of $P(t)$ to \bar{P} for the unstable plant (2.31) as t goes to infinity. Note that the FPRE solutions $P(t)$ given in Figure 2.3 (a) and (b) on the interval $[0, 10]$ are the mirror image of the corresponding BPRES solutions $P(t)$ in Figure 2.1 (a) and (b) on the same interval. However, unlike the BPRES solution, the FPRES solution can be extended to $[0, \infty)$. ■

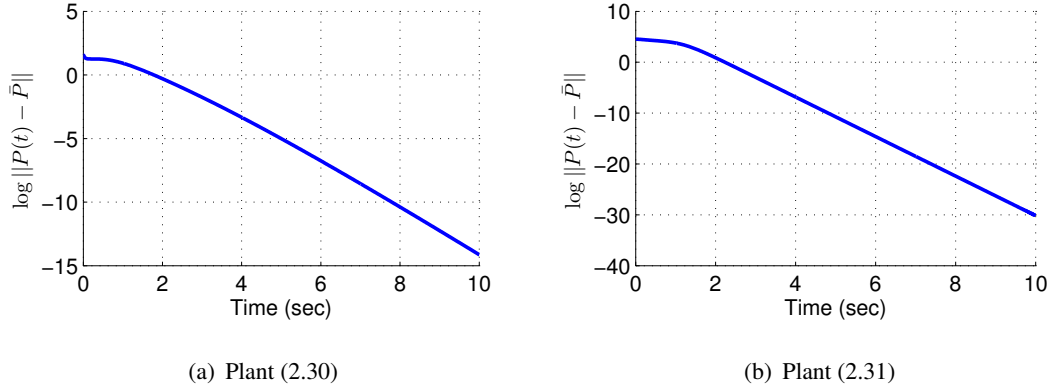


Figure 2.3: Example 3.2. Illustrative results for Theorem 2.

The following result is the FPRES version of Proposition 2.

Proposition 4. Assume that $P_0 < \bar{P}$. Then, for all $t \in [0, \infty)$, $(P_0 - \bar{P})^{-1} + W(t) < 0$ and $P(t) < \bar{P}$. If, in addition, P_0 satisfies

$$A^T P_0 + P_0 A - P_0 S P_0 + R_1 \geq 0, \quad (2.58)$$

then, for all $t \in [0, \infty)$, $P_0 \leq P(t)$.

Proof. From (2.14) and the fact that $P_0 \geq 0$, it follows that, for all $t \in [0, \infty)$,

$$\bar{P} - P_0 \leq \bar{P} < W^{-1}(t).$$

Therefore, since $\bar{P} - P_0$ is positive definite, it follows that, for all $t \in [0, \infty)$,

$$W(t) < (\bar{P} - P_0)^{-1} = -(P_0 - \bar{P})^{-1}.$$

Therefore, for all $t \in [0, \infty)$, $(P_0 - \bar{P})^{-1} + W(t)$ is negative definite, and thus (2.50) implies that, for all $t \in [0, \infty)$, $P(t) < \bar{P}$.

Next, note that (2.58) can be written as

$$\begin{aligned} & (\bar{A} + S\bar{P})^T P_0 + P_0(\bar{A} + S\bar{P}) - P_0 S P_0 + R_1 \\ & = -\bar{A}^T(\bar{P} - P_0) - (\bar{P} - P_0)\bar{A} - (\bar{P} - P_0)S(\bar{P} - P_0) \geq 0, \end{aligned}$$

which implies

$$(\bar{P} - P_0)S(\bar{P} - P_0) \leq -\bar{A}^T(\bar{P} - P_0) - (\bar{P} - P_0)\bar{A}. \quad (2.59)$$

Multiplying (2.59) on the left and right by $e^{\bar{A}s}(\bar{P} - P_0)^{-1}$ and $(\bar{P} - P_0)^{-1}e^{\bar{A}^T s}$, respectively, yields

$$\begin{aligned} e^{\bar{A}s} S e^{\bar{A}^T s} & \leq -e^{\bar{A}s} \bar{A} (\bar{P} - P_0)^{-1} e^{\bar{A}^T s} - e^{\bar{A}s} (\bar{P} - P_0)^{-1} \bar{A}^T e^{\bar{A}^T s}, \\ & = -\frac{d}{ds} e^{\bar{A}s} (\bar{P} - P_0)^{-1} e^{\bar{A}^T s}. \end{aligned}$$

Hence,

$$\begin{aligned} W(t) & = \int_0^t e^{\bar{A}s} S e^{\bar{A}^T s} ds \\ & \leq -\int_0^t \frac{d}{ds} e^{\bar{A}s} (\bar{P} - P_0)^{-1} e^{\bar{A}^T s} ds, \\ & = (\bar{P} - P_0)^{-1} - e^{\bar{A}t} (\bar{P} - P_0)^{-1} e^{\bar{A}^T t}. \end{aligned}$$

Thus,

$$(\bar{P} - P_0)^{-1} \leq e^{-\bar{A}t} [(\bar{P} - P_0)^{-1} - W(t)] e^{-\bar{A}^T t}. \quad (2.60)$$

Since, for all $t \in [0, \infty)$, $(\bar{P} - P_0)^{-1} - W(t)$ is positive definite, (2.60) can be written as

$$e^{\bar{A}^T t} [(\bar{P} - P_0)^{-1} - W(t)]^{-1} e^{\bar{A}t} \leq \bar{P} - P_0,$$

which is equivalent to

$$P_0 \leq \bar{P} + e^{\bar{A}^T t} [(P_0 - \bar{P})^{-1} + W(t)]^{-1} e^{\bar{A} t} = P(t). \quad \square$$

For $n = 1$, now it is to be show that $P_0 < \bar{P}$ implies that (2.58) holds. Therefore, in the scalar case, (2.58) need not be invoked as an assumption in Proposition 4. Define $a \triangleq A$, $b \triangleq B$, $p_0 \triangleq P_0$, $\bar{p} \triangleq \bar{P}$, $r_1 \triangleq R_1$, and $s \triangleq S$, and assume $R_2 = 1$. Then $s = b^2$, and the left hand side of (2.58) can be written as

$$\begin{aligned} -b^2 p_0^2 + 2ap_0 + r_1 &= -b^2 p_0^2 + 2ap_0 + r_1 - (-b^2 \bar{p}^2 + 2a\bar{p} + r_1) \\ &= b^2(\bar{p}^2 - p_0^2) - 2a(\bar{p} - p_0) \\ &= b^2(\bar{p} - p_0)(\bar{p} + p_0) - 2a(\bar{p} - p_0). \end{aligned} \quad (2.61)$$

Since $\bar{p} - p_0 > 0$, dividing (2.61) by $\bar{p} - p_0$ and using (2.39) yields

$$\begin{aligned} b^2(\bar{p} + p_0) - 2a &= b^2 p_0 + a + \sqrt{a^2 + b^2 r_1} - 2a \\ &= b^2 p_0 + \sqrt{a^2 + b^2 r_1} - a \\ &> 0, \end{aligned} \quad (2.62)$$

which implies (2.58).

The following example shows that, for $n \geq 2$, $P_0 < \bar{P}$ does not imply (2.58).

Example 2.4. Consider the unstable plant

$$A = \begin{bmatrix} 0 & 1 \\ -1.5 & 2.5 \end{bmatrix}, \quad B = \begin{bmatrix} 0 \\ 1 \end{bmatrix} \quad (2.63)$$

with $R_1 = I$ and $R_2 = 1$, where \bar{P} is given by

$$\bar{P} = \begin{bmatrix} 8.8 & 0.3 \\ 0.3 & 5.3 \end{bmatrix}. \quad (2.64)$$

Consider two choices of P_0 , namely,

$$P_0 = \begin{bmatrix} 0.6 & -0.5 \\ -0.5 & 1.4 \end{bmatrix} \quad (2.65)$$

and

$$P_0 = \begin{bmatrix} 2 & 1.8 \\ 1.8 & 4 \end{bmatrix}. \quad (2.66)$$

For P_0 given by (2.65), condition (2.58) is satisfied, whereas, for P_0 given by (2.66), condition (2.58) is not satisfied. Figure 2.4 illustrates Proposition 4 for the plant (2.63) with P_0 given by (2.65) and (2.66). The solutions are shown for the time interval $[0, 5]$ sec and are valid on $[0, \infty)$. λ_{\min} denotes the minimum eigenvalue. For P_0 given by (2.65), (a) shows that (2.58) is satisfied, and, for all $t \in [0, 5]$, $P_0 \leq P(t) < \bar{P}$, whereas, for P_0 given by (2.66), (b) shows that (2.58) is not satisfied, and, for all $t \in [0, 5]$, $P(t) < \bar{P}$, and, for all $t \in [0, 2.4]$ sec, $P_0 \leq P(t)$ does not hold. ■

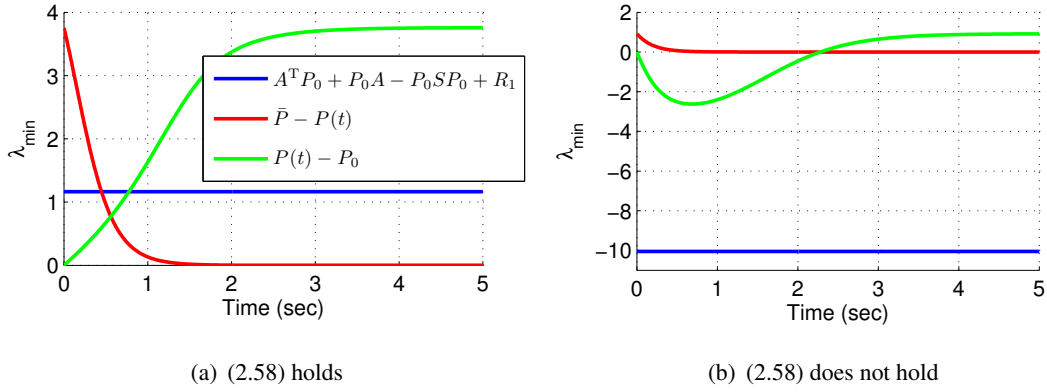


Figure 2.4: Example 2.4. Illustrative results for Proposition 4.

Numerical examples suggest that (2.58) is a necessary condition for $P_0 \leq P(t)$ on $[0, \infty)$. Proof of this conjecture is open.

The following result, which complements Proposition 4, is the FPRE version of Proposition 3.

Proposition 5. Assume that $\bar{P} < P_0$. Then, for all $t \in [0, \infty)$, $(P_0 - \bar{P})^{-1} + W(t) > 0$ and $\bar{P} < P(t)$. If, in addition, P_0 satisfies

$$A^T P_0 + P_0 A - P_0 S P_0 + R_1 \leq 0, \quad (2.67)$$

then, for all $t \in [0, \infty)$, $P(t) \leq P_0$.

If $P_0 > \bar{P}$, then (2.50) implies that $P(t)$ is positive semidefinite for all $t \in [0, \infty)$, and thus (2.54) is not needed. In fact, if $P_0 > \bar{P}$, then it follows from (2.50) that, for all $t \in [0, \infty)$, $P(t)$ is positive definite. Unfortunately, it does not seem to be possible to avoid using (2.54) for arbitrary positive-semidefinite P_0 .

2.2.1 Lyapunov Analysis of the Forward-Propagating Riccati Equation

Several definitions and a result from [57], which are to be used, are stated below.

Definition 1. Let $a > 0$ and $\gamma : [0, a) \rightarrow [0, \infty)$. Then γ is of class \mathcal{K} if $\gamma(0) = 0$ and γ is continuous and strictly increasing.

Definition 2. Let $f : [0, \infty) \times \mathbb{R}^n \rightarrow \mathbb{R}^n$. The solution $x(t) \equiv 0$ of the system $\dot{x}(t) = f(t, x(t))$ is *Lyapunov stable* if, for all $\varepsilon > 0$, there exists $\delta = \delta(\varepsilon) > 0$ such that, if $\|x(0)\| < \delta$, then, for all $t \geq 0$, $\|x(t)\| < \varepsilon$.

Definition 3. Let $f : [0, \infty) \times \mathbb{R}^n \rightarrow \mathbb{R}^n$. The solution $x(t) \equiv 0$ of the system $\dot{x}(t) = f(t, x(t))$ is *asymptotically stable* if it is Lyapunov stable and there exists $\delta > 0$ such that, if $\|x(0)\| < \delta$, then $\lim_{t \rightarrow \infty} x(t) = 0$.

Theorem 3. Let $f : [0, \infty) \times \mathbb{R}^n \rightarrow \mathbb{R}^n$ and assume that, for all $t \geq 0$ $x_0 \in \mathbb{R}^n$,

$$\dot{x}(t) = f(t, x(t)), \quad x(0) = x_0 \quad (2.68)$$

has a unique continuously differentiable solution. Furthermore, assume that there exist continuously differentiable functions $V : [0, \infty) \times \mathbb{R}^n \rightarrow \mathbb{R}$ and $W : [0, \infty) \times \mathbb{R}^n \rightarrow \mathbb{R}$, and class \mathcal{K} functions α, β , and γ such that $\dot{W}(t, x)$ is bounded from above, and

$$V(t, 0) = 0, \quad t \in [0, \infty), \quad (2.69)$$

$$\alpha(\|x\|) \leq V(t, x), \quad t \in [0, \infty) \times \mathbb{R}^n, \quad (2.70)$$

$$W(t, 0) = 0, \quad t \in [0, \infty), \quad (2.71)$$

$$\beta(\|x\|) \leq W(t, x), \quad t \in [0, \infty) \times \mathbb{R}^n, \quad (2.72)$$

$$\dot{V}(t, x) \leq -\gamma(W(t, x)), \quad t \in [0, \infty) \times \mathbb{R}^n, \quad (2.73)$$

where

$$\dot{V}(t, x) \triangleq \frac{\partial V}{\partial t}(t, x) + \frac{\partial V}{\partial x}(t, x)f(t, x) \quad (2.74)$$

and

$$\dot{W}(t, x) \triangleq \frac{\partial W}{\partial t}(t, x) + \frac{\partial W}{\partial x}(t, x)f(t, x). \quad (2.75)$$

Then the zero solution $x(t) \equiv 0$ to (2.68) is asymptotically stable.

Theorem 4. Assume that (A, B) is controllable, R_1 is positive definite, and consider the plant (2.1) with the control law (2.3) and feedback gain (2.4), where, for all $t \in [0, \infty)$, $P(t)$ is the positive-semidefinite solution of the forward propagating Riccati equation (2.46). Then $\lim_{t \rightarrow \infty} x(t) = 0$.

Proof. Consider the Lyapunov function candidate

$$V(t, x) \triangleq x^T P(t)x, \quad (2.76)$$

which satisfies (2.69). Since $P(t)$ converges to \bar{P} as $t \rightarrow \infty$ and \bar{P} is positive definite, there exist $T_1 > 0$ and $\alpha_1 > 0$ such that, for all $t > T_1$, $\lambda_{\min}(P(t)) > \alpha_1$. Therefore, for all $t > T_1$ and $x \in \mathbb{R}^n$,

$$V(t, x) \geq \alpha(\|x\|), \quad (2.77)$$

where $\alpha : [0, \infty) \rightarrow [0, \infty)$ defined by

$$\alpha(z) \triangleq \alpha_1 z^2 \quad (2.78)$$

is of class \mathcal{K} . Hence, $V(t, x)$ satisfies (2.70) with $[0, \infty)$ replaced by $[T_1, \infty)$.

Define

$$E(t) \triangleq P(t) - \bar{P} = e^{\bar{A}^T t} (P_0 - \bar{P}) [I + W(t) (P_0 - \bar{P})]^{-1} e^{\bar{A} t} \quad (2.79)$$

and

$$f(t, x) \triangleq (A - SP(t))x. \quad (2.80)$$

Then, for all $t \geq 0$ and $x \in \mathbb{R}^n$, (2.74) implies that

$$\begin{aligned} \dot{V}(t, x) &= x^T \dot{P}(t)x + x^T (A - SP(t))^T P(t)x + x^T P(t) (A - SP(t))x \\ &= x^T [2A^T P(t) + 2P(t)A - 3P(t)SP(t) + R_1]x \\ &= x^T [2(A^T \bar{P} + \bar{P}A - \bar{P}S\bar{P} + R_1) - \bar{P}S\bar{P} - R_1 \\ &\quad + 2A^T E(t) + 2E(t)A - 3\bar{P}SE(t) - 3E(t)S\bar{P} - 3E(t)SE(t)]x \\ &= -x^T [\bar{P}S\bar{P} + R_1 - Q(t)]x \\ &\leq -x^T [R_1 - Q(t)]x, \end{aligned} \quad (2.81)$$

where

$$Q(t) \triangleq 2[A^T E(t) + E(t)A] - 3[\bar{P}SE(t) + E(t)S\bar{P} + E(t)SE(t)] \quad (2.82)$$

is symmetric. Since $E(t) \rightarrow 0$ as $t \rightarrow \infty$, it follows that $Q(t) \rightarrow 0$ as $t \rightarrow \infty$. Since R_1 is positive definite, there exist $T_2 > T_1$ and $\alpha_2 > 0$ such that, for all $t > T_2$, $R_1 - Q(t) > \alpha_2 I$. Therefore, for all $t > T_2$ and $x \in \mathbb{R}^n$,

$$\dot{V}(t, x) \leq -W(t, x), \quad (2.83)$$

where

$$W(t, x) \triangleq \alpha_2 x^T \bar{P} x, \quad (2.84)$$

which satisfies (2.71). Furthermore, for all $t > T_2$ and $x \in \mathbb{R}^n$,

$$W(t, x) \geq \beta(\|x\|), \quad (2.85)$$

where $\beta : [0, \infty) \rightarrow [0, \infty)$ defined by

$$\beta(z) \triangleq \alpha_2 \lambda_{\min}(\bar{P}) z^2 \quad (2.86)$$

is of class \mathcal{K} . Hence, $W(t, x)$ satisfies (2.72) with $[0, \infty)$ replaced by $[T_2, \infty)$.

To show that, for all $t \in [0, \infty)$ and $x \in \mathbb{R}^n$, $\dot{W}(t, x)$ is bounded from above, note that (2.75) implies that

$$\begin{aligned} \dot{W}(t, x) &= \alpha_2 [x^T (A - SP(t))^T \bar{P} x + x^T \bar{P} (A - SP(t)) x] \\ &= \alpha_2 x^T (A_{\text{cl}}^T(t) \bar{P} + \bar{P} A_{\text{cl}}(t)) x. \end{aligned} \quad (2.87)$$

Since $P(t)$ converges to \bar{P} as $t \rightarrow \infty$, it follows that

$$\lim_{t \rightarrow \infty} (A_{\text{cl}}^T(t) \bar{P} + \bar{P} A_{\text{cl}}(t)) = \bar{A}^T \bar{P} + \bar{P} \bar{A}. \quad (2.88)$$

Note that, from (2.12),

$$\bar{A}^T \bar{P} + \bar{P} \bar{A} = -(\bar{P} S \bar{P} + R_1) < 0. \quad (2.89)$$

Hence, there exists $T_4 > T_3$ such that, for all $t > T_4$, $A_{\text{cl}}(t) \bar{P} + \bar{P} A_{\text{cl}}(t) < 0$, and thus (2.87) implies that, for all $t > T_4$ and $x \in \mathbb{R}^n$, $\dot{W}(t, x) \leq 0$. Therefore, for all $t > T_4$ and $x \in \mathbb{R}^n$, $\dot{W}(t, x)$ is bounded from above.

To show that $V(t, x)$ satisfies (2.73) note that (2.83) implies that

$$\dot{V}(t, x) \leq -\gamma(W(t, x)), \quad (2.90)$$

where $\gamma : [0, \infty) \rightarrow [0, \infty)$ defined by

$$\gamma(z) \triangleq z \quad (2.91)$$

is of class \mathcal{K} .

As a result, (2.69) – (2.73) hold with $[0, \infty)$ replaced by $[T_4, \infty)$. Then, Theorem 3 implies that, for all $t \in [T_4, \infty)$, $x(t) \rightarrow 0$ as $t \rightarrow \infty$. \square

Note that Theorem 4 does not provide Lyapunov stability since the conditions for Lyapunov stability of Theorem 3 are stated for $[0, \infty)$, whereas the proof of Theorem 4 shows that (2.69) – (2.73) hold with $[0, \infty)$ replaced by $[T_4, \infty)$.

2.3 How Suboptimal Is FPRE?

Example 2.5. Consider a linearized model of an inverted pendulum mounted on a moving cart. The objective is to bring the pendulum to the upward vertical position. Control is performed by applying a force to the cart. For this system, the state vector is defined as $x = [x \ \dot{x} \ \theta \ \dot{\theta}]^T$, where x, \dot{x} are the horizontal position and velocity of the cart, respectively, and $\theta, \dot{\theta}$ are the angular position and angular velocity of the pendulum, respectively. The upward vertical position of the pendulum corresponds to $\theta = 0$ rad. The linearized dynamics of this plant are given by

$$A = \begin{bmatrix} 0 & 1 & 0 & 0 \\ 0 & \frac{-(J+ml^2)b}{J(M+m)+Mml^2} & \frac{m^2gl^2}{J(M+m)+Mml^2} & 0 \\ 0 & 0 & 0 & 1 \\ 0 & \frac{-mlb}{J(M+m)+Mml^2} & \frac{mgl}{J(M+m)+Mml^2} & 0 \end{bmatrix}, B = \begin{bmatrix} 0 \\ \frac{J+ml^2}{J(M+m)+Mml^2} \\ 0 \\ \frac{ml}{J(M+m)+Mml^2} \end{bmatrix}. \quad (2.92)$$

Values of the parameters are given in Table 2.1.

Initial conditions for the state vector are given as $x(0) = 0.1$ m, $\dot{x}(0) = 0$ m/sec, $\theta(0) = 0.2618$ rad, and $\dot{\theta}(0) = 0$ rad/sec. Thus, the initial state vector is $x(0) = [0.1 \ 0 \ 0.2618 \ 0]^T$. For BPFE consider the final state weightings $P_f = 0$ and $P_f = I$. For FPFE consider two initial conditions, namely, $P_0 = \bar{P} + I$ and $P_0 = I$,

where the solution \bar{P} of ARE (2.10) is given by

$$\bar{P} = \begin{bmatrix} 1.94 & 1.37 & -3.93 & -0.77 \\ 1.37 & 2.20 & -6.85 & -1.33 \\ -3.93 & -6.85 & 40.04 & 7.22 \\ -0.77 & -1.33 & 7.22 & 1.39 \end{bmatrix}. \quad (2.93)$$

Table 2.1: Inverted Pendulum Model Parameters

Parameter	Value	Units
Mass of the cart (M)	0.5	kg
Mass of the pendulum (m)	0.2	kg
Friction coefficient of the cart (b)	0.1	$N/(m\text{-sec})$
Mass moment of inertia of the pendulum (J)	0.006	$\text{kg}\cdot\text{m}^2$
Length to pendulum center of mass (l)	0.3	m
Gravitational acceleration (g)	9.8	m/sec^2

Let $R_1 = I$, and $R_2 = 1$. Figures 2.5 shows the state responses for the BPRE controller for the plant (2.92) with $t_f = 15$ sec and the final state weightings $P_f = I$ and $P_f = 0$.

Figure 2.6 (a), (b), (c) show the state responses for the FPRE controller for (2.92) with the initial conditions $P_0 = I$, $P_0 = 0$, and $P_0 = \bar{P} + I$, respectively. Results are valid for $t \in [0, \infty)$. Note that $P_0 = \bar{P} + I$ provides better response than $P_0 = I$ and $P_0 = 0$. The convergence of $P(t)$ to \bar{P} for BPRE and FPRE is shown in terms of $\|P(t) - \bar{P}\|$ in Figure 2.7. Norm denotes the maximum singular value. (a) shows the convergence of $P(t)$ to \bar{P} for BPRE for each fixed t as t_f approaches infinity with $P_f = I$ and $P_f = 0$, whereas (b) shows that for results for FPRE with $P_0 = I$, $P_0 = 0$, and $P_0 = \bar{P} + I$. For BPRE the solutions are shown for t_f equal to 5, 10, and 15 sec, whereas for FPRE the solutions are valid on $[0, \infty)$.

To compare the performance of FPRE and BPRE, Pareto performance tradeoff curves are used to illustrate the efficiency of each control technique in terms of the state and

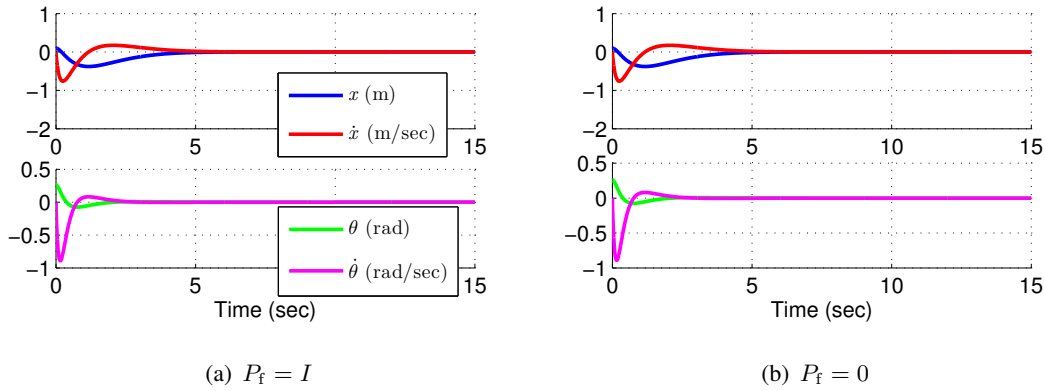


Figure 2.5: Example 2.5. State trajectories for BPRE for the inverted pendulum on a cart.

control costs

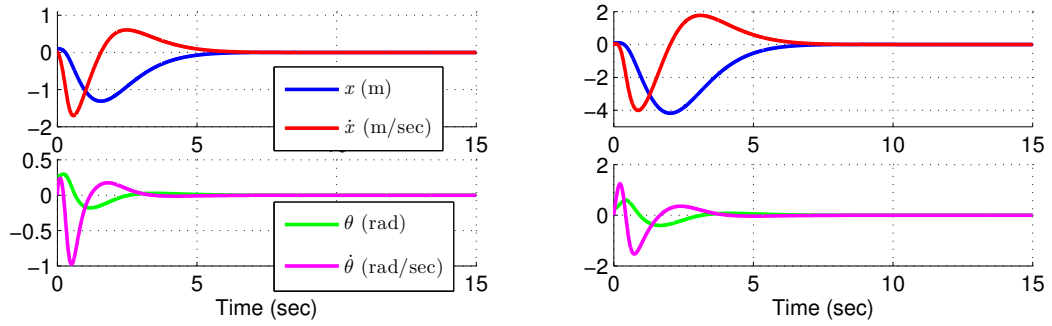
$$J_s(x_0, u) \triangleq \int_0^{t_f} x^T(t) R_1 x(t) dt + x^T P_f x \quad (2.94)$$

and

$$J_c(x_0, u) \triangleq \int_0^{t_f} u^T(t) u(t) dt. \quad (2.95)$$

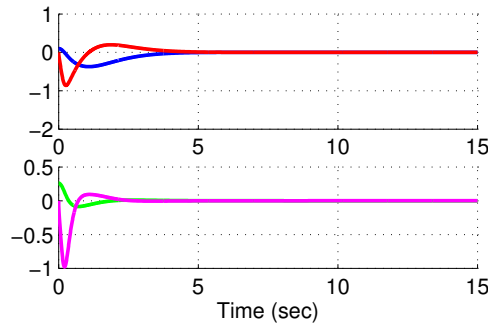
For the Pareto plot, let R_2 range from 0.1 to 10. For comparison, the Pareto performance curve of the linear-quadratic controller (LQ) is also illustrated. Figure 2.8 (a) and (b) show the Pareto curves for LQ, BPRE, and FPRE with final state weightings $P_f = I$ and $P_f = 0$, respectively. The initial conditions for FPRE are $P_0 = I$, $P_0 = 0$, and $P_0 = \bar{P} + I$. BPRE provides more efficient performance tradeoff curves than FPRE. For FPRE, the initial condition $P_0 = \bar{P} + I$ yields a better Pareto curve than $P_0 = I$ and $P_0 = 0$.

Next, consider the Lyapunov function candidate and its derivative given by (2.76) and (2.74), respectively. Figure 2.9 (a) and (b) show the Lyapunov function candidate $V(t, x)$ and its derivative $\dot{V}(t, x)$ for FPRE for (2.92) with initial time conditions $P_0 = I$, $P_0 = 0$, and $P_0 = \bar{P} + I$. (b) shows that $\dot{V}(x, t)$ is positive in an initial time interval, which illustrates the fact that FPRE does not guarantee Lyapunov stability.



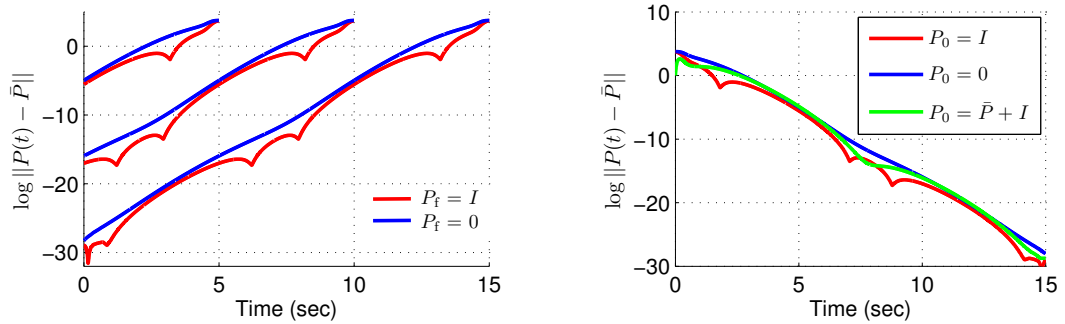
(a) $P_0 = I$

(b) $P_0 = 0$



(c) $P_0 = \bar{P} + I$

Figure 2.6: Example 2.5. State trajectories for FPRE for the inverted pendulum on a cart.



(a) BPRE

(b) FPRE

Figure 2.7: Example 2.5. The convergence of $P(t)$ to \bar{P} for BPRE and FPRE.

2.3.1 Transient Responses of BPRE and FPRE

In this section, the effect of the final time weighting P_f and the initial condition P_0 on the transient response of the closed-loop system for BPRE and FPRE, respectively, is shown. In particular, the focus is on the case of unstable plants for which the closed-loop dynamics are unstable during the latter part of the time interval for BPRE and

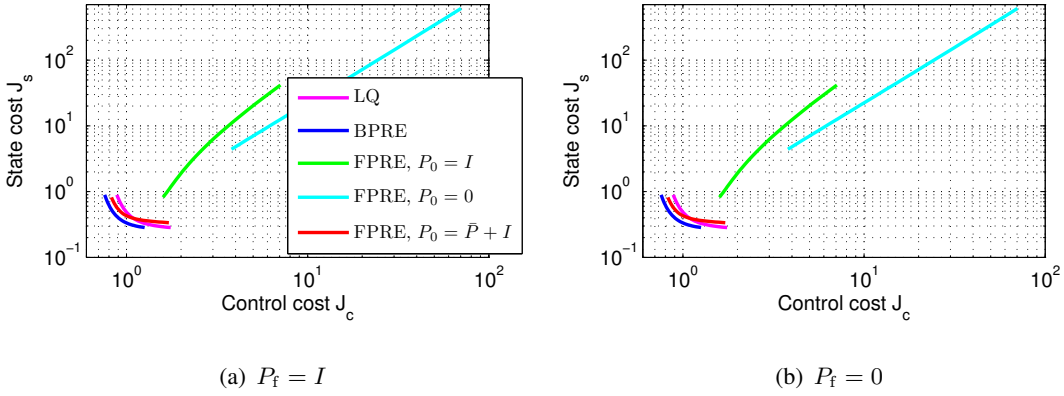


Figure 2.8: Example 2.5. Pareto performance tradeoff curves.

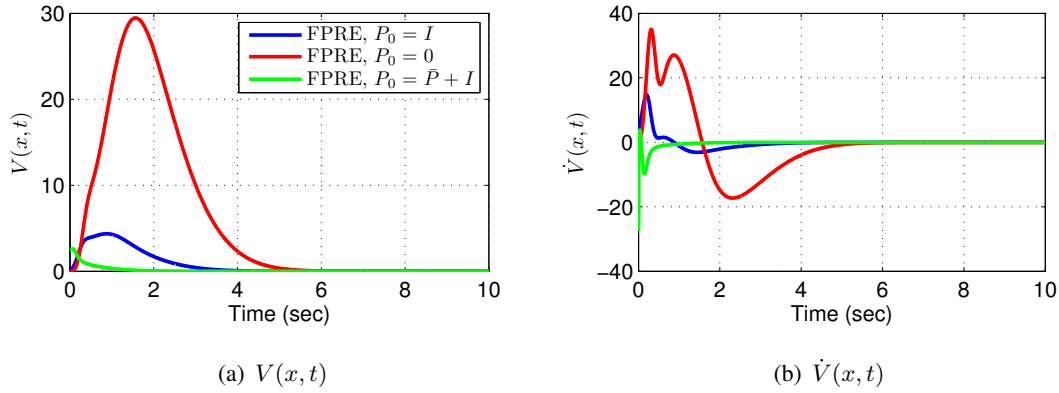


Figure 2.9: Example 2.5. Lyapunov-function candidate and its derivative.

the early part for FPRE.

Example 2.6. Consider the unstable plant

$$A = \begin{bmatrix} 0 & 1 \\ -10 & 7 \end{bmatrix}, B = \begin{bmatrix} 0 \\ 1 \end{bmatrix}, \quad (2.96)$$

with $R_1 = I$, $R_2 = 1$, and $x(0) = [3 \ 2]^T$. For BPRE, let $P_f = 0$, which implies that $A_{cl}(t_f) = A$ is unstable. Consider $t_f = 3$ sec and $t_f = 10$ sec. For FPRE, let $P_0 = 0$, which implies that $A_{cl}(0) = A$ is unstable. The state trajectories, the norm of $P(t) - \bar{P}$, and the spectral abscissa of $A_{cl}(t)$ for BPRE BPRE for the unstable plant (2.96) with $P_f = 0$ are shown in Fig. 2.10. (a) shows that, for $t_f = 3$ sec, the state trajectories diverge at t_f due to the fact that the closed-loop dynamics are unstable for $t \in [1.4, 3]$ sec, as shown by the spectral abscissa of the closed-loop system in (e). For $t_f = 10$ sec, (b) shows that the state trajectories asymptotically approach the origin due to the initially stable dynamics for $t \in [0, 8]$ sec, as shown by the spectral

abscissa of the closed-loop system in (f). (c) shows that, for $t_f = 3$ sec, $P(t)$ is not close to \bar{P} , whereas (d) shows that, for $t_f = 10$ sec, $P(t)$ is close to \bar{P} . The state trajectories, the norm of $P(t) - \bar{P}$, and the spectral abscissa of $A_{cl}(t)$ for FPRE for the unstable plant (2.96) with $P_0 = 0$ are shown in Fig. 2.11. Results are given for $t \in [0, 10]$ sec, and are valid for $t \rightarrow \infty$. (a) shows that the state trajectory has a large transient due to the initially unstable closed-loop dynamics for $t \in [0, 2]$, as shown by the spectral abscissa of the closed-loop system in (c). (b) shows that $P(t)$ approaches \bar{P} as $t \rightarrow \infty$.

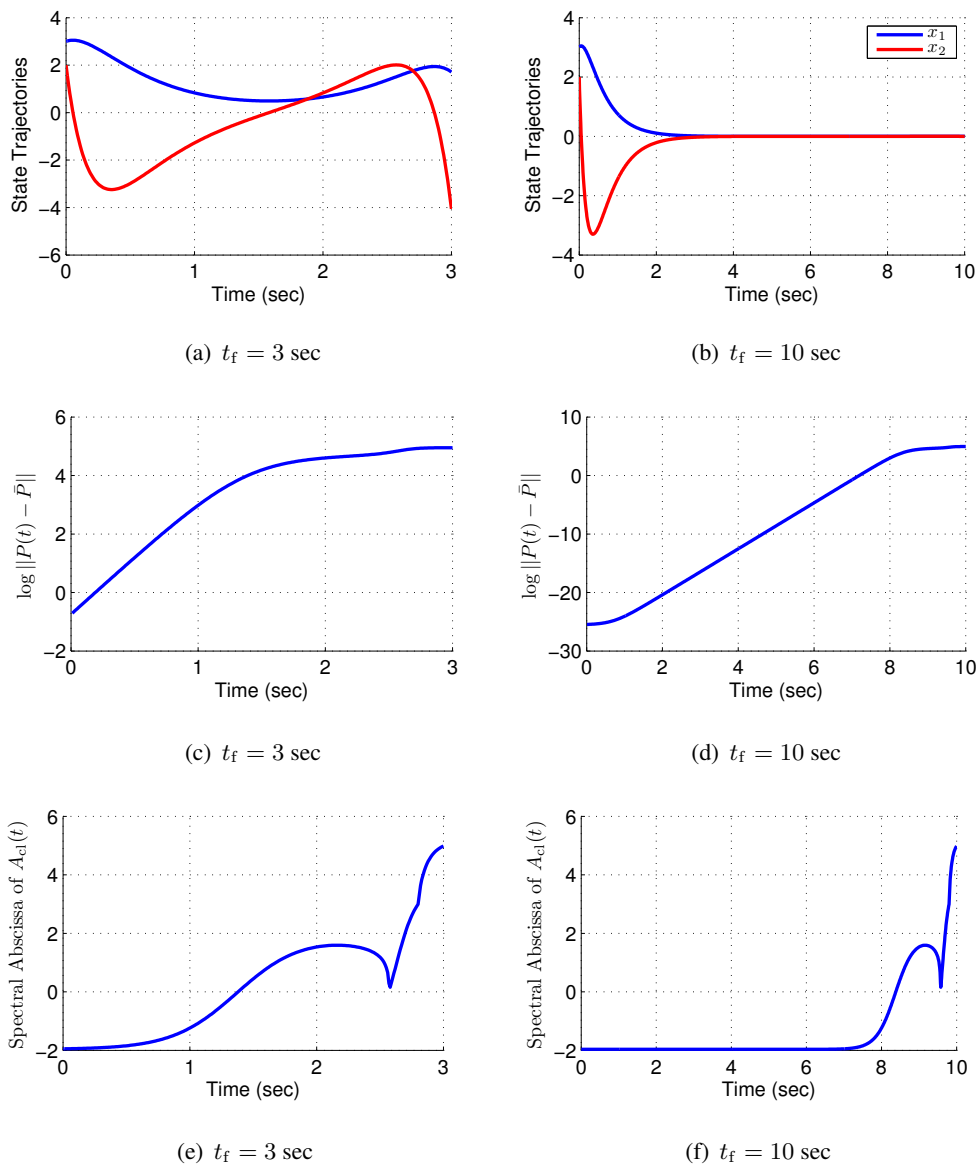
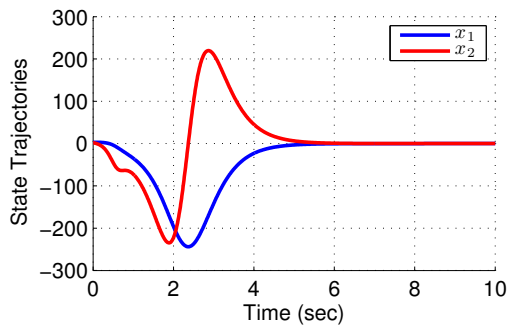
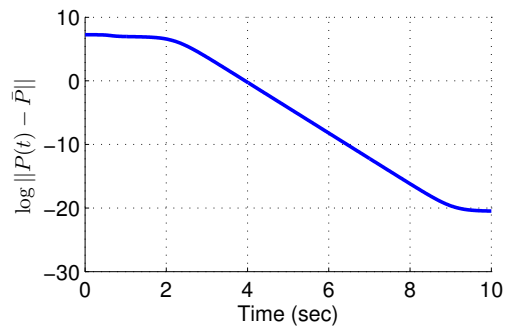


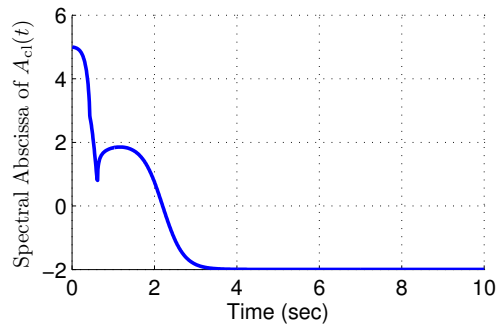
Figure 2.10: Example 2.6. State trajectories, maximum singular value of $P(t) - \bar{P}$, and spectral abscissa of $A_{cl}(t)$ for BPFE.



(a)



(b)



(c)

Figure 2.11: Example 2.6. State trajectories, maximum singular value of $P(t) - \bar{P}$ and spectral abscissa of $A_{cl}(t)$ for FPRE.

CHAPTER 3

COMMAND FOLLOWING AND DISTURBANCE REJECTION CONTROL FOR LTI SYSTEMS

3.1 Review of Linear Quadratic Optimal Control

The tracking problem arises when it is desired that the output of the closed-loop system tracks a given reference command. Linear quadratic regulation theory for a tracking problem is given in [89, 2]. In addition to a tracking control, a disturbance rejection problem is considered in this work.

3.1.1 Linear Quadratic Tracking and Disturbance Rejection: Finite-Time Case

Consider the LTI plant

$$\dot{x}(t) = Ax(t) + Bu(t) + D_1d(t), \quad x(0) = x_0, \quad (3.1)$$

$$y_r(t) = Hx(t), \quad (3.2)$$

where $x(t) \in \mathbb{R}^n$, $u(t) \in \mathbb{R}^m$, $d(t) \in \mathbb{R}^p$, $y_r(t) \in \mathbb{R}^l$, $A \in \mathbb{R}^{n \times n}$, $B \in \mathbb{R}^{n \times m}$, $D_1 \in \mathbb{R}^{n \times p}$, and $H \in \mathbb{R}^{l \times n}$. Assume that (A, B) is stabilizable. Let $r(t) \in \mathbb{R}^l$ be a command signal, and the control objective is to make the output $y_r(t)$ to track the command signal $r(t)$ and reject a disturbance $d(t)$, that is, $\|r(t) - y_r(t)\| \rightarrow 0$ as $t \rightarrow t_f$. It is assumed that the state $x(t)$ is measurable, and the command signal $r(t)$ and disturbance $d(t)$ are known over the interval $[0, t_f]$. Define the tracking error as

$$z(t) = r(t) - y_r(t) = r(t) - Hx(t), \quad (3.3)$$

and consider a finite-horizon quadratic cost function

$$\mathbf{J}(u) \triangleq \frac{1}{2} z^T(t_f) P_f z(t_f) + \frac{1}{2} \int_0^{t_f} [z^T(t) R_1 z(t) + u^T(t) R_2 u(t)] dt, \quad (3.4)$$

where $R_1, P_f \in \mathbb{R}^{l \times l}$ are positive semidefinite and $R_2 \in \mathbb{R}^{m \times m}$ is positive definite.

Let the Hamiltonian defined by

$$\begin{aligned} \mathcal{H}(x, u, t, \lambda) \triangleq & \frac{1}{2} [r(t) - Hx(t)]^T R_1 [r(t) - Hx(t)] \\ & + \frac{1}{2} u^T(t) R_2 u(t) + \lambda^T(t) [Ax(t) + Bu(t) + D_1 d(t)]. \end{aligned} \quad (3.5)$$

The optimal control is obtained from $\frac{\partial \mathcal{H}}{\partial u} = 0$, and results in

$$u(t) = -R_2^{-1} B^T \lambda(t). \quad (3.6)$$

In terms of Hamiltonian, the state equation is obtained from $\frac{\partial \mathcal{H}}{\partial \lambda}$, and with the optimal control (3.6), is given by

$$\dot{x}(t) = \frac{\partial \mathcal{H}}{\partial \lambda} = Ax(t) - R_2^{-1} B^T \lambda(t) + D_1 d(t). \quad (3.7)$$

The costate equation is given by

$$\dot{\lambda}(t) = -\frac{\partial \mathcal{H}}{\partial x} = -H^T R_1 H x(t) - A^T \lambda(t) + H^T R_1 r(t). \quad (3.8)$$

Define

$$S \triangleq B R_2^{-1} B^T \in \mathbb{R}^{n \times n}, \quad (3.9)$$

$$W \triangleq H^T R_1 \in \mathbb{R}^{n \times l}, \quad (3.10)$$

$$V \triangleq H^T R_1 H \in \mathbb{R}^{n \times n}, \quad (3.11)$$

$$(3.12)$$

then combining (3.7) and (3.8), results in

$$\begin{bmatrix} \dot{x}(t) \\ \dot{\lambda}(t) \end{bmatrix} = \begin{bmatrix} A & -S \\ -V & -A^T \end{bmatrix} \begin{bmatrix} x(t) \\ \lambda(t) \end{bmatrix} + \begin{bmatrix} 0_{n \times l} \\ W \end{bmatrix} z(t) + \begin{bmatrix} D_1 \\ 0_{n \times n} \end{bmatrix} d(t) \quad (3.13)$$

with the boundary conditions

$$x(0) = x_0, \quad (3.14)$$

and

$$\begin{aligned}
\lambda(t_f) &= \frac{\partial}{\partial x(t_f)} \left[\frac{1}{2} z^T(t) P_f z(t) \right] \\
&= \frac{\partial}{\partial x(t_f)} \left[\frac{1}{2} (r(t_f) - Hx(t_f))^T (t) P_f (r(t_f) - Hx(t_f)) \right] \\
&= H^T P_f H x(t_f) - H^T P_f r(t_f).
\end{aligned} \tag{3.15}$$

Let $\lambda(t)$ be given by

$$\lambda(t) = P(t)x(t) - g(t), \tag{3.16}$$

where $P(t) \in \mathbb{R}^{n \times n}$ and $g(t) \in \mathbb{R}^n$ that satisfy (3.13) are to be determined. Differentiating (3.16) yields

$$\dot{\lambda}(t) = \dot{P}(t)x(t) + P(t)\dot{x}(t) - \dot{g}(t), \tag{3.17}$$

and using (3.13), (3.17) can be written as

$$\begin{aligned}
&-Vx(t) - A^T [P(t)x(t) - g(t)] + Wr(t) \\
&= \dot{P}(t)x(t) + P(t)[Ax(t) - S(P(t)x(t) - g(t)) + D_1 d(t)] - \dot{g}(t).
\end{aligned} \tag{3.18}$$

Rearranging (3.18) results in

$$\begin{aligned}
&\left[\dot{P}(t) + P(t)A + A^T P(t) - P(t)SP(t) + V \right] x(t) \\
&- \left[\dot{g}(t) + A^T g(t) - P(t)Sg(t) + Wr(t) - P(t)D_1 d(t) \right] = 0.
\end{aligned} \tag{3.19}$$

From (3.19) it follows that, for all $t \in [0, t_f]$, $P(t)$ must satisfy the matrix differential Riccati equation

$$-\dot{P}(t) = P(t)A + A^T P(t) - P(t)SP(t) + V, \tag{3.20}$$

and, for all $t \in [0, t_f]$, $g(t)$ must satisfy the vector differential equation

$$-\dot{g}(t) = (A^T - P(t)S)g(t) + Wr(t) - P(t)D_1 d(t). \tag{3.21}$$

The boundary condition $P(t_f)$ for (3.20) and $g(t_f)$ for (3.21), are obtained using (3.15) and (3.16), and given by

$$P(t_f) = H^T P_f H, \tag{3.22}$$

$$g(t_f) = H^T P_f r(t_f). \tag{3.23}$$

Next, using (3.16), the optimal control (3.6) can be written as

$$u(t) = -R_2^{-1}B^T (P(t)x(t) - g(t)) = K(t)x(t) + R_2^{-1}B^T g(t), \quad (3.24)$$

where $K(t) = -R_2^{-1}B^T P(t)$, and $P(t)$ and $g(t)$ satisfy (3.20) and (3.21), respectively.

3.1.2 Linear Quadratic Tracking and Disturbance Rejection: Infinite-Time Case

The results obtained in the section above are extended to the case of infinite time. For an LTI plant (3.1), and a tracking error (3.3), let the performance index given by

$$\mathbf{J}(u) \triangleq \frac{1}{2} \int_0^\infty [z^T(t)R_1z(t) + u^T(t)R_2u(t)]dt, \quad (3.25)$$

Next, the results obtained for the finite-time case with $t_f \rightarrow \infty$ are used. As $t_f \rightarrow \infty$, the solution $P(t)$ of (3.20) converges to \bar{P} , which is a unique solution of the algebraic Riccati equation

$$\bar{P}A + A^T\bar{P} - \bar{P}S\bar{P} + V = 0, \quad (3.26)$$

and solution $g(t)$ of (3.21) converges to $\bar{g}(t)$, which is a solution of the following algebraic equation

$$-\dot{\bar{g}}(t) = (A^T - \bar{P}S)\bar{g}(t) + Wr(t) - \bar{P}D_1d(t). \quad (3.27)$$

Under assumption $P_f = 0$, the boundary condition is $\bar{g}(t_f) = 0$. More details about (3.27) are given in [2].

Approximately Optimal Tracking. Assuming that $r(t)$ and $d(t)$ in (3.27) are slow varying, and using approximation $\dot{\bar{g}}(t) = 0$ [2], yields

$$(A^T - \bar{P}S)\bar{g}(t) + Wr(t) - \bar{P}D_1d(t) = 0, \quad (3.28)$$

from which $\bar{g}(t)$ is found as

$$\bar{g}(t) = - (A^T - \bar{P}S)^{-1} Wr(t) + (A^T - \bar{P}S)^{-1} \bar{P}D_1d(t). \quad (3.29)$$

Using (3.26) and (3.29), the control law (3.24) becomes

$$u(t) = Kx(t) + K_r r(t) + K_d d(t), \quad (3.30)$$

where

$$K = -R_2^{-1} B^T \bar{P}, \quad (3.31)$$

$$K_r = -R_2^{-1} B^T (A^T - \bar{P}S)^{-1} W, \quad (3.32)$$

$$K_d = R_2^{-1} B^T (A^T - \bar{P}S)^{-1} \bar{P}D_1. \quad (3.33)$$

The results above depend on the full-state feedback assumption, namely, that the state x is directly measurable. If the full-state is not available, then a state estimator need to be constructed using an output y . More details on the observer design are given in [2]. Linear quadratic optimal control involves backward-in-time integration of (3.21) and, therefore, the command signal $r(t)$ and disturbance $d(t)$ must be known over the interval $[0, t_f]$. If this knowledge is not available, then the control cannot be achieved.

Next, an Internal-model-based command following and disturbance rejection control is introduced. This control does not require advance knowledge of neither the command $r(t)$ nor disturbance $d(t)$.

3.2 Internal-Model-Based Command Following and Disturbance Rejection for LTI SISO Systems

In this section the internal model principle is applied for the command following and disturbance rejection problem. The control formulation is given in discrete time.

3.2.1 Full-State-Feedback

Consider the discrete-time LTI plant

$$x_{k+1} = Ax_k + Bu_k + D_1d_k, \quad (3.34)$$

$$y_{r,k} = Hx_k, \quad (3.35)$$

where $x_k \in \mathbb{R}^n$, $u_k \in \mathbb{R}$, $d_k \in \mathbb{R}$, $y_{r,k} \in \mathbb{R}$, $A \in \mathbb{R}^{n \times n}$, $B \in \mathbb{R}^n$, $D_1 \in \mathbb{R}^n$, and $H \in \mathbb{R}^{1 \times n}$. For full-state-feedback control, it is assumed that x_k is measured. Let

$r_k \in \mathbb{R}$ be the command, and define the command-following error

$$z \triangleq r - y_r. \quad (3.36)$$

The signals r and d are assumed to be linear combinations of steps, ramps, and sinusoids. The goal is to have the command-following error z converge to zero in the presence of the disturbance d . This goal is facilitated by an internal model of the command r and disturbance d of the form

$$x_{\text{im},k+1} = A_{\text{im}} x_{\text{im},k} + B_{\text{im}} z_k, \quad (3.37)$$

where $x_{\text{im},k} \in \mathbb{R}^{n_{\text{im}}}$ is the state of the internal model.

Figure 3.1 shows the internal-model-based full-state-feedback control architecture, where G is the transfer function of the plant (3.34), G_{im} is the transfer function of the internal model (3.37), and K_{im} and K are full-state-feedback gains. These components are described in more detail below. Augmenting (3.34), (3.35) with (3.37)

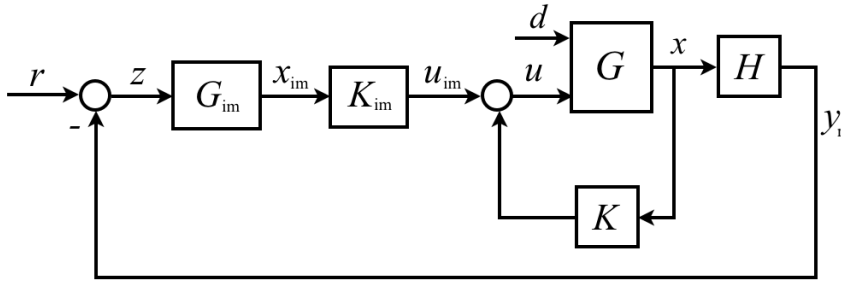


Figure 3.1: Internal-model-based, full-state-feedback controller.

yields

$$x_{\text{a},k+1} = A_{\text{a}} x_{\text{a},k} + B_{\text{a}} u_k + \begin{bmatrix} 0_{n \times 1} \\ B_{\text{im}} \end{bmatrix} r_k + \begin{bmatrix} D_1 \\ 0_{n_{\text{im}} \times 1} \end{bmatrix} d_k, \quad (3.38)$$

where

$$x_{\text{a},k} \triangleq \begin{bmatrix} x_k \\ x_{\text{im},k} \end{bmatrix}, A_{\text{a}} \triangleq \begin{bmatrix} A & 0_{n \times n_{\text{im}}} \\ -B_{\text{im}} H & A_{\text{im}} \end{bmatrix}, B_{\text{a}} \triangleq \begin{bmatrix} B \\ 0_{n_{\text{im}} \times 1} \end{bmatrix}. \quad (3.39)$$

Defining $u_{\text{im}} \triangleq K_{\text{im}} x_{\text{im}}$, the control u is given by

$$u_k = K_{\text{a}} x_{\text{a},k} = K x_k + K_{\text{im}} x_{\text{im},k} = K x_k + u_{\text{im},k}, \quad (3.40)$$

where $K_{\text{a}} = [K \ K_{\text{im}}] \in \mathbb{R}^{m \times (n+n_{\text{im}})}$ is the full-state-feedback gain.

3.2.1.1 ARE Control Law

For algebraic Riccati Equation (ARE) control, consider the cost

$$\mathbf{J}(u) = \sum_{k=0}^{\infty} (x_{a,k}^T R_1 x_{a,k} + u_k^T R_2 u_k), \quad (3.41)$$

where $R_1 \in \mathbb{R}^{(n+n_{im}) \times (n+n_{im})}$ is positive semidefinite and R_2 is a positive number.

The optimal constant feedback gain K_a is given by

$$K_a = -(B_a^T \bar{P}_a B_a + R_2)^{-1} B_a^T \bar{P}_a A_a, \quad (3.42)$$

where $\bar{P}_a \in \mathbb{R}^{(n+n_{im}) \times (n+n_{im})}$ satisfies the ARE

$$\bar{P}_a = A_a^T \bar{P}_a A_a - A_a^T \bar{P}_a B_a (B_a^T \bar{P}_a B_a + R_2)^{-1} B_a^T \bar{P}_a A_a + R_1. \quad (3.43)$$

3.2.1.2 FPRE Control Law

For forward Propagating Riccati Equation (FPRE) control, the constant feedback gain (3.42) is replaced by the time-varying feedback gain

$$K_{a,k} = -(B_a^T P_{a,k} B_a + R_2)^{-1} B_a^T P_{a,k} A_a, \quad (3.44)$$

where $P_{a,k} \in \mathbb{R}^{(n+n_{im}) \times (n+n_{im})}$ satisfies the difference Riccati equation

$$P_{a,k+1} = A_a^T P_{a,k} A_a - A_a^T P_{a,k} B_a (B_a^T P_{a,k} B_a + R_2)^{-1} B_a^T P_{a,k} A_a + R_1 \quad (3.45)$$

with the positive-semidefinite initial condition $P_{a,0}$, where $R_1 \in \mathbb{R}^{(n+n_{im}) \times (n+n_{im})}$ is positive semidefinite and R_2 is a positive number.

The solution $P_{a,k}$ of (3.45) converges exponentially to \bar{P}_a . This is demonstrated numerically in subsection 2.6 and proved in [97] for the continuous-time case. Because knowledge of the future dynamics is not needed, FPRE control will be used in later sections for LTV and nonlinear plants.

3.2.2 Convergence Analysis

The final value theorem is used to analyze the convergence of the error z for the internal-model-based full-state-feedback controller in the case where K_a is constant.

Although this treatment is classical, the goal is to set the stage for the later application to LTV and nonlinear plants. Consider the reformulation of Fig. 3.1 shown in Fig. 3.2, where G_c is the transfer function of the internal model with the feedback gain K_{im} , that is,

$$G_c(\mathbf{z}) \triangleq K_{im}(\mathbf{z}I - A_{im})^{-1}B_{im}, \quad (3.46)$$

and $\tilde{G} \triangleq [G_u \ G_d]$ is the transfer function of the plant (3.34), (3.35) from $[u \ d]^T$ to y_r with the feedback gain K , where

$$G_u(\mathbf{z}) \triangleq H(\mathbf{z}I - (A + BK))^{-1}B, \quad (3.47)$$

$$G_d(\mathbf{z}) \triangleq H(\mathbf{z}I - (A + BK))^{-1}D_1. \quad (3.48)$$

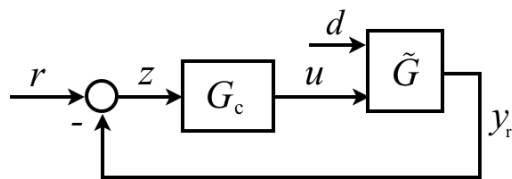


Figure 3.2: Reformulation of Fig. 3.1 for final value theorem analysis.

Let \hat{r} denote the \mathbf{z} -transform of r , and similarly for other signals. Then,

$$\hat{z} = \hat{r} - \hat{y}_r, \quad \hat{y}_r = \tilde{G} \begin{bmatrix} \hat{u} \\ \hat{d} \end{bmatrix} = G_u \hat{u} + G_d \hat{d}. \quad (3.49)$$

Thus,

$$\hat{z} = \hat{r} - G_u \hat{u} - G_d \hat{d} = \hat{r} - G_u G_c \hat{z} - G_d \hat{d}, \quad (3.50)$$

and (3.50) can be written as

$$\hat{z} = \frac{1}{1 + G_u G_c} \hat{r} - \frac{G_d}{1 + G_u G_c} \hat{d}. \quad (3.51)$$

Let $G_u = \frac{N_u}{D_u}$ and $G_c = \frac{N_c}{D_c}$, note that $G_d = \frac{N_d}{D_u}$, and let $\hat{r} = \frac{n_r}{d_r}$ and $\hat{d} = \frac{n_d}{d_d}$. Then,

$$\hat{z} = \frac{D_u D_c}{D_u D_c + N_u N_c} \frac{n_r}{d_r} - \frac{D_c N_d}{D_u D_c + N_u N_c} \frac{n_d}{d_d}. \quad (3.52)$$

Next, since (3.37) is an internal model of r and d , it follows that internal models of the command r and disturbance d are present in the dynamics D_c of G_c . Therefore,

$D_c = \tilde{d}_r d_r = \tilde{d}_d d_d$, where \tilde{d}_r and \tilde{d}_d are polynomials, and thus

$$\hat{z} = \frac{D_u \tilde{d}_r n_r}{D_u D_c + N_u N_c} - \frac{\tilde{d}_d N_d n_d}{D_u D_c + N_u N_c}. \quad (3.53)$$

Assuming that $D_u D_c + N_u N_c$ is asymptotically stable, the final value theorem yields

$$\lim_{k \rightarrow \infty} z_k = \lim_{\mathbf{z} \rightarrow 1} (\mathbf{z} - 1) \hat{z} = \lim_{\mathbf{z} \rightarrow 1} \left[\frac{(\mathbf{z} - 1) D_u \tilde{d}_r n_r}{D_u D_c + N_u N_c} - \frac{(\mathbf{z} - 1) \tilde{d}_d N_d n_d}{D_u D_c + N_u N_c} \right] = 0. \quad (3.54)$$

3.2.3 Internal Models

For the case where the command and disturbance are steps, the internal model is an integrator given by

$$A_{\text{im}} = 1, \quad B_{\text{im}} = 1, \quad C_{\text{im}} = 1. \quad (3.55)$$

For the case where the command and disturbance are ramps, the internal model is a double integrator given by

$$A_{\text{im}} = \begin{bmatrix} 0 & 1 \\ -1 & 2 \end{bmatrix}, \quad B_{\text{im}} = \begin{bmatrix} 0 \\ 1 \end{bmatrix}, \quad C_{\text{im}} = \begin{bmatrix} 1 & 0 \end{bmatrix}. \quad (3.56)$$

For the case where the command and disturbance are harmonic with the same frequency Ω , the internal model is an undamped oscillator with frequency Ω given by

$$A_{\text{im}} = \begin{bmatrix} 0 & 1 \\ -1 & 2 \cos(\Omega) \end{bmatrix}, \quad B_{\text{im}} = \begin{bmatrix} 0 \\ 1 \end{bmatrix}, \quad C_{\text{im}} = \begin{bmatrix} 1 & 0 \end{bmatrix}. \quad (3.57)$$

The matrix C_{im} is used for output feedback, but is not needed for full-state feedback.

If the command and disturbance are harmonic with frequencies Ω_1 and Ω_2 , respectively, then the internal model is 4th order and consists of the cascade of two undamped oscillators with frequencies Ω_1 and Ω_2 . Likewise, if the command is a step and the disturbance is harmonic with frequency Ω (or vice versa), then the internal model is 3rd order and consists of the cascade of an integrator and an undamped oscillator with frequency Ω .

In internal-model-based control, neither the height of a step command or disturbance nor the amplitude or phase shift of a harmonic command or disturbance need to be known. However, the frequencies of a harmonic command and a harmonic disturbance must be known.

3.2.4 Discrete-Time Models

Each example in this thesis is based on a continuous-time model. In order to obtain discrete-time models for feedback control, Euler integration is applied to the continuous-time system. For each example, T_s is chosen sufficiently small that the open-loop unit step response of the Euler-discretized model is numerically close to the open-loop step response of the continuous-time model computed by the Matlab ODE45 routine. In order to remove the issue of integration accuracy from the numerical investigation, the Euler-discretized model is then viewed as the truth model for control, and the performance of each control law is considered only within the context of the discretized model. Evaluation of the performance of the control laws on the underlying continuous-time system is outside the scope of the thesis.

Consider the continuous-time system

$$\dot{x}(t) = A_{\text{cont}}x(t) + B_{\text{cont}}u(t) + D_{1,\text{cont}}d(t), \quad (3.58)$$

$$y(t) = C_{\text{cont}}x(t). \quad (3.59)$$

Using Euler integration, the discrete-time version of (3.58), (3.59) is given by

$$x_{k+1} = x_k + T_s A_{\text{cont}}x_k + T_s B_{\text{cont}}u_k + T_s D_{1,\text{cont}}d_k, \quad (3.60)$$

$$y_k = C_{\text{cont}}x_k, \quad (3.61)$$

where T_s is the sample time, $x_k \triangleq x(kT_s)$, $u_k \triangleq u(kT_s)$, $d_k \triangleq d(kT_s)$, and $y_k \triangleq y(kT_s)$. Then, the discrete-time matrices A , B , C , D_1 are given by

$$A = I + T_s A_{\text{cont}}, \quad B = T_s B_{\text{cont}}, \quad C = C_{\text{cont}}, \quad D_1 = T_s D_{1,\text{cont}}. \quad (3.62)$$

Example 3.1. Full-State-Feedback Control of the Two-Mass System with Harmonic Command and Harmonic Disturbance

Consider the continuous-time LTI system in Fig. 3.3, which represents masses m_1 and m_2 connected by a spring with stiffness k and dashpot with damping b . The control force f is applied to m_2 , and the goal is to control the position q_1 of m_1 . Consider the case of an unmatched disturbance, where the disturbance d is applied to m_1 as shown

in Fig. 3.3. The equations of motion are given by

$$m_1 \ddot{q}_1 + b(\dot{q}_1 - \dot{q}_2) + k(q_1 - q_2) = d, \quad (3.63)$$

$$m_2 \ddot{q}_2 + b(\dot{q}_2 - \dot{q}_1) + k(q_2 - q_1) = f. \quad (3.64)$$

For the state vector $x \triangleq [q_1 \ \dot{q}_1 \ q_2 \ \dot{q}_2]^T$, the continuous-time matrices in (3.58) are given by

$$A_{\text{cont}} = \begin{bmatrix} 0 & 1 & 0 & 0 \\ -\frac{k}{m_1} & -\frac{b}{m_1} & \frac{k}{m_1} & \frac{b}{m_1} \\ 0 & 0 & 0 & 1 \\ \frac{k}{m_2} & \frac{b}{m_2} & -\frac{k}{m_2} & -\frac{b}{m_2} \end{bmatrix}, \quad B_{\text{cont}} = \begin{bmatrix} 0 \\ 0 \\ 0 \\ 1 \end{bmatrix}, \quad D_{1,\text{cont}} = \begin{bmatrix} 0 \\ 1 \\ 0 \\ 0 \end{bmatrix}. \quad (3.65)$$

Let $T_s = 0.1$ sec, and use (3.62) to obtain discrete-time matrices A, B, D_1 .

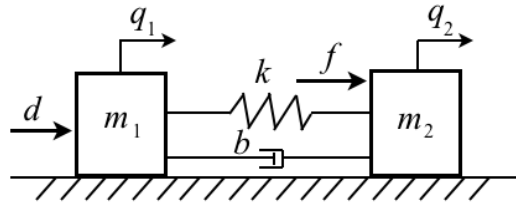


Figure 3.3: Example 3.1. Two-mass system.

To command the position q_1 of mass m_1 , let $y_r = q_1$. Let $m_1 = 1$ kg, $m_2 = 0.5$ kg, $k = 2$ N/m, $b = 0.3$ N-s/m, and $x_0 = [0.2 \text{ m}, 0 \text{ m/sec}, -0.1 \text{ m}, 0 \text{ m/sec}]^T$. For these parameters, the damped natural frequency is 2.45 rad/sec, and the damping ratio is 7.5%.

Consider the harmonic command $r_k = 0.5 \sin(\Omega_1 k)$ m and the harmonic disturbance $d_k = \cos(\Omega_2 k)$ N, with $\Omega_1 = 0.1$ rad/sample and $\Omega_2 = 0.5$ rad/sample. For $T_s = 0.1$ sec, these discrete-time frequencies correspond to the continuous-time frequencies 1 rad/sec and 5 rad/sec, respectively. The internal model is given by the cascade of two undamped oscillators (3.57) whose frequencies are equal to the frequencies of the command and disturbance.

Let $R_1 = I_{n+n_{\text{im}}}$, $R_2 = 1$, and $P_{a,0} = I_{n+n_{\text{im}}}$. Figure 3.4 shows the closed-loop response for the internal-model-based, full-state-feedback control of the two-mass

system, and Fig. 3.5 shows the exponential convergence of $P_{a,k}$ of FPRE to \bar{P}_a of ARE. The norm is the maximum singular value

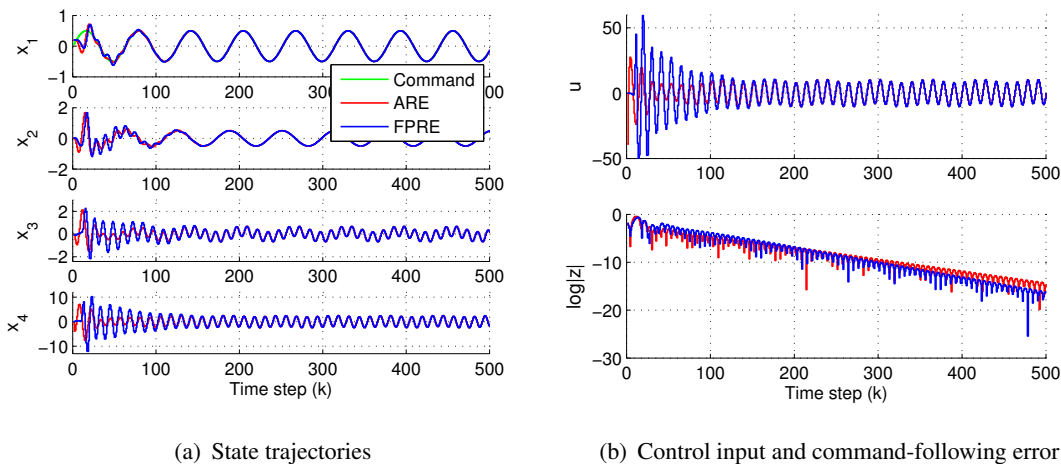


Figure 3.4: Example 3.1. Closed-loop responses.

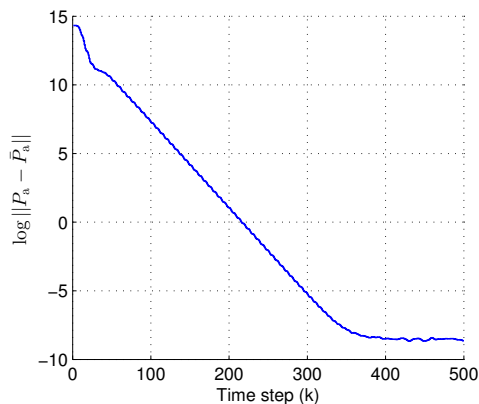


Figure 3.5: Example 3.1. Convergence of $P_{a,k}$ of FPRE to \bar{P}_a .

3.2.5 Output-Feedback

Consider the LTI system (3.34). Let $y_{r,k} \triangleq Hx_k$ and $y_k \triangleq Cx_k$, and define the measurement vector

$$y_{\text{meas},k} = \begin{bmatrix} y_{r,k} \\ y_k \end{bmatrix} = \begin{bmatrix} Hx_k \\ Cx_k \end{bmatrix} = C_{\text{meas}}x_k, \quad (3.66)$$

where $C_{\text{meas}} \in \mathbb{R}^{m \times n}$, $H \in \mathbb{R}^{1 \times n}$, and $C \in \mathbb{R}^{(m-1) \times n}$. If only one measurement is available, then $y_{\text{meas}} = y_r$ and C is absent. The command-following error is defined by (3.36).

Figure 3.6 shows the internal-model-based output-feedback control architecture, where G is the transfer function of the plant (3.34), (3.66), G_{im} is the transfer function of the internal model, G_{OBC} is the transfer function of the observer-based compensator, and G_{c} is the transfer function of the augmented compensator. These components are described below.

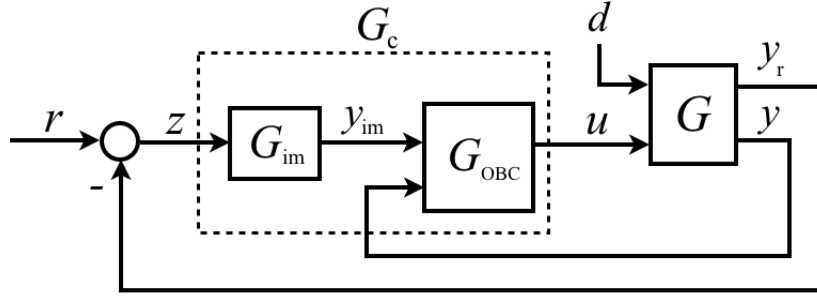


Figure 3.6: Internal-model-based output-feedback controller.

Augmenting (3.34), (3.66) with the SISO internal model yields

$$x_{\text{im},k+1} = A_{\text{im}} x_{\text{im},k} + B_{\text{im}} z_k, \quad (3.67)$$

$$y_{\text{im},k} = C_{\text{im}} x_{\text{im},k}, \quad (3.68)$$

where $x_{\text{im}} \in \mathbb{R}^{n_{\text{im}}}$. The augmented plant is thus given by

$$x_{\text{a},k+1} = A_{\text{a}} x_{\text{a},k} + B_{\text{a}} u_k + \begin{bmatrix} 0_{n \times 1} \\ B_{\text{im}} \end{bmatrix} r_k + \begin{bmatrix} D_1 \\ 0_{n_{\text{im}} \times 1} \end{bmatrix} d_k, \quad (3.69)$$

$$y_{\text{a},k} = C_{\text{a}} x_{\text{a},k}, \quad (3.70)$$

where

$$x_{\text{a},k} \triangleq \begin{bmatrix} x_k \\ x_{\text{im},k} \end{bmatrix} \in \mathbb{R}^{n+n_{\text{im}}}, \quad y_{\text{a},k} \triangleq \begin{bmatrix} y_k \\ y_{\text{im},k} \end{bmatrix} \in \mathbb{R}^{m-1+n_{\text{im}}},$$

$$A_{\text{a}} \triangleq \begin{bmatrix} A & 0_{n \times n_{\text{im}}} \\ -B_{\text{im}}H & A_{\text{im}} \end{bmatrix}, \quad B_{\text{a}} \triangleq \begin{bmatrix} B \\ 0_{n_{\text{im}} \times 1} \end{bmatrix}, \quad C_{\text{a}} \triangleq \begin{bmatrix} C & 0_{(m-1) \times n_{\text{im}}} \\ 0_{1 \times n} & C_{\text{im}} \end{bmatrix}. \quad (3.71)$$

A block diagram of the augmented plant (3.69), (3.70) is shown in Fig. 3.7.

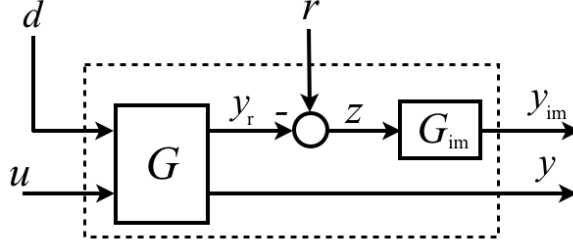


Figure 3.7: Augmented plant.

Next, for the augmented plant (3.69), (3.70), the observer-based compensator is used

$$\hat{x}_{a,k+1} = (A_a + B_a K_a - F_a C_a) \hat{x}_{a,k} + F_a y_{a,k}, \quad (3.72)$$

$$u_k = K_a \hat{x}_{a,k}, \quad (3.73)$$

where $\hat{x}_{a,k} \in \mathbb{R}^{n+n_{im}}$ and $F_a \in \mathbb{R}^{(n+n_{im}) \times m}$. For ARE control, the constant regulator feedback gain K_a is given by (3.42), whereas, for FPRE control, the time-varying regulator feedback gain $K_{a,k}$ is given by (3.44). The constant observer gain F_a for ARE control, as well as the time-varying observer gain $F_{a,k}$ for FPRE control, are defined below.

3.2.5.1 ARE Observer-Based Compensator

For ARE control, the constant observer gain F_a is given by

$$F_a = A_a \bar{Q}_a C_a^T (C_a \bar{Q}_a C_a^T + V_2)^{-1}, \quad (3.74)$$

where $\bar{Q} \in \mathbb{R}^{(n+n_{im}) \times (n+n_{im})}$ satisfies

$$\bar{Q}_a = A_a \bar{Q}_a A_a^T - A_a \bar{Q}_a C_a^T (C_a \bar{Q}_a C_a^T + V_2)^{-1} C_a \bar{Q}_a A_a^T + V_1, \quad (3.75)$$

where $V_1 \in \mathbb{R}^{(n+n_{im}) \times (n+n_{im})}$ is positive semidefinite and $V_2 \in \mathbb{R}$ is a positive number.

3.2.5.2 FPRE Observer-Based Compensator

For FPRE control, the time-varying observer gain $F_{a,k}$ is given by

$$F_{a,k} = A_a Q_{a,k} C_a^T (C_a Q_{a,k} C_a^T + V_2)^{-1}, \quad (3.76)$$

where $Q_{a,k} \in \mathbb{R}^{(n+n_{im}) \times (n+n_{im})}$ satisfies

$$Q_{a,k+1} = A_a Q_{a,k} A_a^T - A_a Q_{a,k} C_a^T (C_a Q_{a,k} C_a^T + V_2)^{-1} C_a Q_{a,k} A_a^T + V_1 \quad (3.77)$$

with the positive-semidefinite initial condition $Q_{a,0}$, where $V_1 \in \mathbb{R}^{(n+n_{im}) \times (n+n_{im})}$ is positive semidefinite and $V_2 \in \mathbb{R}^{m \times m}$ is positive definite.

The observer-based compensator (3.72), (3.73) is cascaded with the internal model (3.67), (3.68) to obtain the augmented compensator

$$x_{c,k+1} = A_c x_{c,k} + B_c z_k + \begin{bmatrix} F_a \\ 0_{n_{im} \times (m-1)} \end{bmatrix} \begin{bmatrix} y_k \\ 0_{1 \times 1} \end{bmatrix}, \quad (3.78)$$

$$u_k = C_c x_{c,k}, \quad (3.79)$$

where

$$x_{c,k} \triangleq \begin{bmatrix} \hat{x}_{a,k} \\ x_{im,k} \end{bmatrix} \in \mathbb{R}^{n+2n_{im}}, \quad A_c \triangleq \begin{bmatrix} A_a + B_a K_a - F_a C_a & F_a C_{im} \\ 0_{n_{im} \times (n+n_{im})} & A_{im} \end{bmatrix},$$

$$B_c \triangleq \begin{bmatrix} 0_{(n+n_{im}) \times 1} \\ B_{im} \end{bmatrix}, \quad C_c \triangleq \begin{bmatrix} K_a & 0_{1 \times n_{im}} \end{bmatrix}. \quad (3.80)$$

If the only measurement is y_r , then the last term in (3.78) is absent.

3.2.6 Convergence Analysis

Consider the reformulation of Fig. 3.6 shown in Fig. 3.8, where $G \triangleq \begin{bmatrix} G_{y_r u} & G_{y_r d} \\ G_{y_u} & G_{y_d} \end{bmatrix}$ is the transfer function of the plant (1), (35), where

$$G_{y_r u}(\mathbf{z}) \triangleq H(\mathbf{z}I - A)^{-1}B, \quad G_{y_r d}(\mathbf{z}) \triangleq H(\mathbf{z}I - A)^{-1}D_1,$$

$$G_{y_u}(\mathbf{z}) \triangleq C(\mathbf{z}I - A)^{-1}B, \quad G_{y_d}(\mathbf{z}) \triangleq C(\mathbf{z}I - A)^{-1}D_1, \quad (3.81)$$

and $[y_r \ y]^T = G[u \ d]^T$. Furthermore, $G_c \triangleq [G_{cz} \ G_{cy}]$ is the transfer function of the augmented compensator (45), (46), where $u = G_c[z \ y]^T$ and

$$G_{cz}(\mathbf{z}) \triangleq C_c(\mathbf{z}I - A_c)^{-1}B_c, \quad G_{cy}(\mathbf{z}) \triangleq C_c(\mathbf{z}I - A_c)^{-1} \begin{bmatrix} F_a \\ 0_{n_{im} \times (m-1)} \end{bmatrix}. \quad (3.82)$$

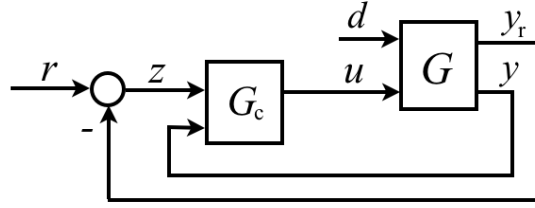


Figure 3.8: Reformulation of Fig. 3.6 for final value theorem analysis.

Since

$$\hat{z} = \hat{r} - \hat{y}_r, \quad \hat{y}_r = G_{y_r u} \hat{u} + G_{y_r d} \hat{d}, \quad (3.83)$$

it follows that

$$\begin{aligned} \hat{z} &= \hat{r} - G_{y_r u} \hat{u} - G_{y_r d} \hat{d} \\ &= \hat{r} - G_{y_r u} G_{c z} \hat{z} - G_{y_r u} G_{c y} \hat{y} - G_{y_r d} \hat{d}. \end{aligned} \quad (3.84)$$

Since

$$\begin{aligned} \hat{y} &= G_{y u} \hat{u} + G_{y d} \hat{d} \\ &= G_{y u} G_{c z} \hat{z} + G_{y u} G_{c y} \hat{y} + G_{y d} \hat{d}, \end{aligned} \quad (3.85)$$

(3.85) implies that

$$\hat{y} = \Phi_{y z} \hat{z} + \Phi_{y d} \hat{d}, \quad (3.86)$$

where

$$\Phi_{y z} \triangleq \frac{G_{y u} G_{c z}}{1 - G_{y u} G_{c y}}, \quad \Phi_{y d} \triangleq \frac{G_{y d}}{1 - G_{y u} G_{c y}}. \quad (3.87)$$

Using (3.86), (3.84) can be written as

$$\hat{z} = \hat{r} - G_{y_r u} (G_{c z} \hat{z} + G_{c y} \Phi_{y z}) \hat{z} - (G_{y_r u} G_{c y} \Phi_{y d} + G_{y_r d}) \hat{d}, \quad (3.88)$$

which implies

$$\hat{z} = \frac{1}{1 + G_{y_r u} (G_{c z} + G_{c y} \Phi_{y z})} \hat{r} - \frac{G_{y_r u} G_{c y} \Phi_{y d} + G_{y_r d}}{1 + G_{y_r u} (G_{c z} + G_{c y} \Phi_{y z})} \hat{d}. \quad (3.89)$$

Let $G_{y_r u} = \frac{N_{y_r u}}{D_{y_r u}}$, $G_{c z} = \frac{N_{c z}}{D_{c z}}$, and $G_{y u} = \frac{N_{y u}}{D_{y u}}$, and note that $G_{y_r d} = \frac{N_{y_r d}}{D_{y_r u}}$, $G_{c y} = \frac{N_{c y}}{D_{c z}}$, and $G_{y d} = \frac{N_{y d}}{D_{y u}}$. Then,

$$\Phi_{y z} = \frac{N_{y u} N_{c z}}{D_{y u} D_{c z} - N_{y u} N_{c y}}, \quad \Phi_{y d} = \frac{N_{y d} D_{c z}}{D_{y u} D_{c z} - N_{y u} N_{c y}}. \quad (3.90)$$

Also, let $\hat{r} = \frac{n_r}{d_r}$ and $\hat{d} = \frac{n_d}{d_d}$. Defining $\Psi \triangleq D_{yu}D_{cz} - N_{yu}N_{cy}$ and $\Gamma \triangleq D_{yru}D_{cz}\Psi + N_{yrd}N_{cz}\Psi + N_{yrd}N_{cy}N_{yu}N_{cz}$, (3.89) can be written as

$$\hat{z} = \frac{D_{yru}D_{cz}\Psi}{\Gamma}\hat{r} - \frac{(N_{yru}N_{cy}N_{yd} + N_{yrd}\Psi)D_{cz}}{\Gamma}\hat{d}. \quad (3.91)$$

Next, since (3.67) is an internal model of r and d , it follows that internal models of the command r and disturbance d are present in the dynamics D_{cz} of G_{cz} . Therefore, $D_{cz} = \tilde{d}_r d_r = \tilde{d}_d d_d$, where \tilde{d}_r , and \tilde{d}_d are polynomials. Hence,

$$\hat{z} = \frac{D_{yru}\Psi\tilde{d}_r n_r}{\Gamma} - \frac{(N_{yru}N_{cy}N_{yd} + N_{yrd}\Psi)\tilde{d}_d n_d}{\Gamma}. \quad (3.92)$$

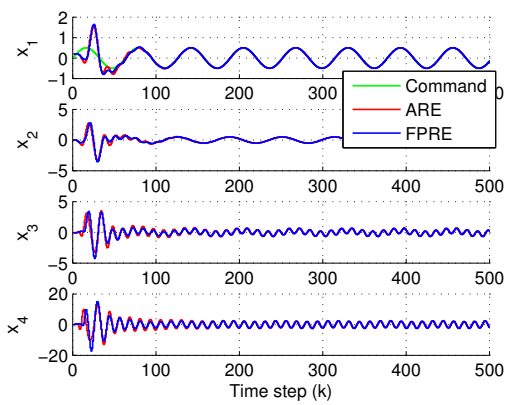
Assuming that Γ is asymptotically stable, the final value theorem implies that

$$\begin{aligned} \lim_{k \rightarrow \infty} z_k &= \lim_{z \rightarrow 1} (z - 1)\hat{z} \\ &= \lim_{z \rightarrow 1} \left[\frac{(z - 1)D_{yru}\Psi\tilde{d}_r n_r}{\Gamma} - \frac{(z - 1)(N_{yru}N_{cy}N_{yd} + N_{yrd}\Psi)\tilde{d}_d n_d}{\Gamma} \right] = 0. \end{aligned} \quad (3.93)$$

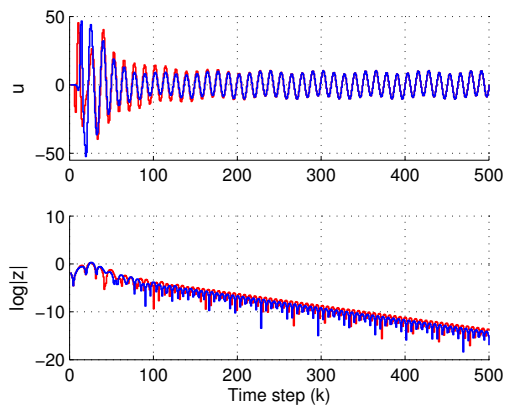
Example 3.2. Output-Feedback Control of the Two-Mass System with Harmonic Command and Harmonic Disturbance.

For output-feedback control of the two-mass system described in Example 3.1 by (3.64), (3.65), let $y_{\text{meas}} = y_r = q_1$, and thus C is omitted.

Consider the same harmonic command and harmonic disturbance as in Example 3.1. The internal model is given by the cascade of two undamped oscillators (3.57) whose frequencies are equal to the frequencies of the command and disturbance. Let $x_0 = [0.2 \text{ m}, 0 \text{ m/sec}, -0.1 \text{ m}, 0 \text{ m/sec}]^T$, and $\hat{x}_{a,0} = 0$. Let $R_1 = I_{n+n_{\text{im}}}$, $R_2 = 1$, $V_1 = R_1$, $V_2 = R_2$. Let $P_{a,0} = I_{n+n_{\text{im}}}$ and $Q_{a,0} = I_{n+n_{\text{im}}}$. Figure 3.9 shows the closed-loop response of the internal-model-based, output-feedback control of the two-mass system.



(a) State trajectories



(b) Control input and command-following error

Figure 3.9: Example 3.2. Closed-loop responses.

CHAPTER 4

FPRE CONTROL FOR LTV SYSTEMS

4.1 FPRE Control for Stabilization of LTV Systems

In many applications the increasing demands on the performance and more rigorous specifications implied over a wide range of operating envelope, diminish the value of LTI models as good approximations of the actual plant. In these cases, LTV models which capture the time dependent characteristics of the plant, can provide a more accurate description of a system. Time dependence may reveal itself as small in magnitude time-varying perturbations of the nominal parameters of a LTI model. In such a case, the control problem can still be approached from a perspective of LTI by designing a control law which is robust with respect to the time-varying parameter perturbations. However, in many nonlinear systems time dependence is quite strong and the linear time-invariant approach is no longer adequate for modeling and control. In these situations a plant can be modeled by a linear ordinary differential equation with time-varying coefficients.

The design of control laws for LTV plants of the form $\dot{x}(t) = A(t)x(t) + B(t)u(t)$ using quadratic optimization criteria yields compensators whose parameters are computed by solving a time-dependent Riccati differential equation [13, 68, 14]. Another study established a compensator design methodology for LTV systems similar to the popular H_∞ robust control approach for LTI plants, where the control objectives are expressed in terms of induced gains of certain closed-loop sensitivity operators [45]. The implementation of these controllers, however, requires great computational effort and becomes less attractive when there are limitations on the time allowed for the

control law computations.

In this section FPRE control is applied for stabilization of LTV systems. Introduced in [121, 28], FPRE control requires a forward-in-time solution of the control Riccati equation, and therefore it does not require advance knowledge of the dynamics $A(t)$, $B(t)$, $C(t)$. Hence, it can be implemented on a time-varying system.

Three benchmark LTV systems are considered. The first system is the classical Mathieu equation, which is a second-order differential equation with a constant-plus-sinusoidal stiffness term. The second example is a two-degree-of-freedom rotating rigid body with force applied to its center of mass in a direction that is fixed in the body frame. The constant rotation of the body gives rise to LTV dynamics with rigid-body instability and with a periodically time-varying input matrix. The last example, which is developed in [26], is an elastic beam with periodic loading and transverse control force. The equations of motion given in [26] have the form of a multi-degree-of-freedom Mathieu equation.

4.1.1 Full-State-Feedback

For an LTV plant

$$\dot{x}(t) = A(t)x(t) + B(t)u(t), \quad x(0) = x_0, \quad (4.1)$$

where $x(t) \in \mathbb{R}^n$, $u(t) \in \mathbb{R}^m$, $A(t) \in \mathbb{R}^{n \times n}$, $B(t) \in \mathbb{R}^{n \times m}$, and (A, B) is stabilizable, the full-state-feedback control law is given by [121]

$$u(t) = K(t)x(t), \quad (4.2)$$

where the controller gain $K(t)$ is given by

$$K(t) = -R_2^{-1}B^T(t)P(t), \quad (4.3)$$

and $P(t)$ is the solution of the forward-in-time differential Riccati equation

$$\dot{P}(t) = A^T(t)P(t) + P(t)A(t) - P(t)B(t)R_2^{-1}B^T(t)P(t) + R_1, \quad (4.4)$$

with a positive-semidefinite initial condition $P(0) = P_0$, and where $R_1 \in \mathbb{R}^{n \times n}$ are positive semidefinite and $R_2 \in \mathbb{R}^{m \times m}$ is positive definite.

Example 4.1. Stabilization of Mathieu equation using full-state feedback.

The Mathieu equation is given by [100]

$$\ddot{q}(t) + (\alpha + \beta \cos(\omega t))q(t) = bu(t), \quad (4.5)$$

where α, β, ω , and b are real numbers. Defining the state vector $x(t) \triangleq [q(t) \quad \dot{q}(t)]^T$ yields the LTV dynamics

$$\dot{x}(t) = A(t)x(t) + Bu(t), \quad (4.6)$$

where

$$A(t) = \begin{bmatrix} 0 & 1 \\ -(\alpha + \beta \cos(\omega t)) & 0 \end{bmatrix}, \quad B = \begin{bmatrix} 0 \\ b \end{bmatrix}. \quad (4.7)$$

Let $\alpha = 1, \beta = 1, b = 1, \omega = 2$, and $x(0) = [2 \quad 2]^T$. Figure 4.1 shows the phase portrait of the uncontrolled Mathieu equation for $x(0) = [2 \quad 2]^T$ and simulation time $t = 20$ sec. The state trajectory diverges as $t \rightarrow \infty$.

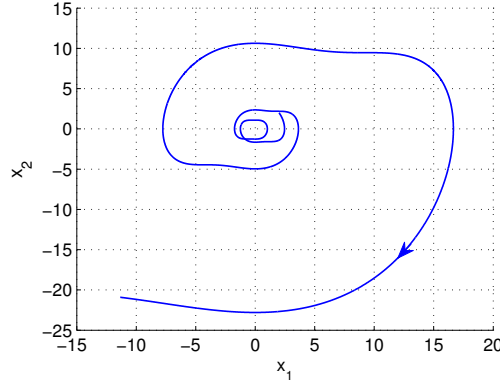


Figure 4.1: Example 4.1. Open-loop phase portrait of Mathieu equation.

Let $R_1 = I, R_2 = 1$ and consider three choices of P_0 , namely, $P_0 = 0, P_0 = I$, and $P_0 = 10I$. Figure 4.2 shows the phase portrait of the closed-loop responses and the control input. Pareto performance curves for FPRE for the Mathieu equation with $P_0 = 0, P_0 = I$, and $P_0 = 10I$ for R_2 ranging from 0.1 to 10 are given in Fig. 4.3.

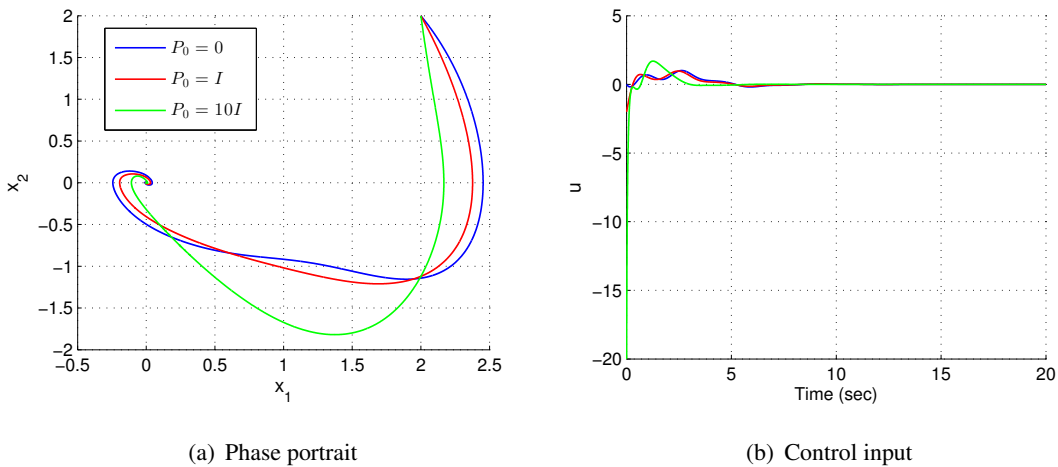


Figure 4.2: Example 4.1. Full-state feedback for Mathieu equation: closed-loop responses.

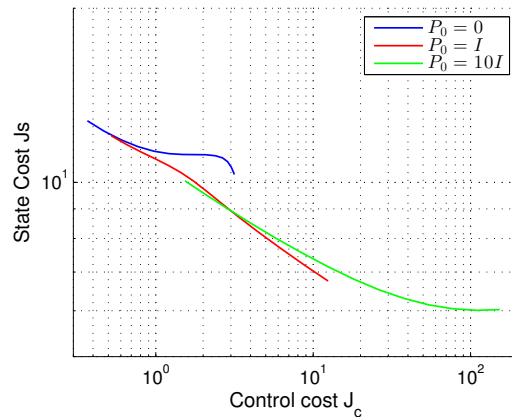


Figure 4.3: Example 4.1. Full-state feedback for Mathieu equation: Pareto performance tradeoff curves.

Example 4.2. Stabilization of a rotating disc using full-state feedback.

In this example, consider a disk that translates on a horizontal plane while rotating at a constant rate ω . Position of the disc on a plane is given by the coordinates $x(t)$ and $y(t)$, whereas $\dot{x}(t)$ and $\dot{y}(t)$ are linear velocities. Control is performed by a thruster, located at the center of mass. The direction of the thrust is fixed with respect to the disk body frame. The goal is to bring the center of mass of the disk to a specified

point. The dynamics are given by

$$x(t) = \begin{bmatrix} x(t) \\ \dot{x}(t) \\ y(t) \\ \dot{y}(t) \end{bmatrix}, \quad A(t) = \begin{bmatrix} 0 & 1 & 0 & 0 \\ 0 & 0 & 0 & 0 \\ 0 & 0 & 0 & 1 \\ 0 & 0 & 0 & 0 \end{bmatrix}, \quad B(t) = \begin{bmatrix} 0 \\ \cos(\omega t) \\ 0 \\ \sin(\omega t) \end{bmatrix}. \quad (4.8)$$

The structure of the state matrix $A(t)$ indicates unstable open-loop dynamics.

Let $R_1 = I$, $R_2 = 10$ and initial position $x(0) = [1 \text{ m}, 0 \text{ m/sec}, 1 \text{ m}, 0 \text{ m/sec}]^T$. Consider three choices of P_0 , namely, $P_0 = 0$, $P_0 = I$, and $P_0 = 10I$. Figure 4.4 shows the phase portrait of the closed-loop responses and the control input. Pareto performance curves for FPRE with $P_0 = 0$, $P_0 = I$, and $P_0 = 10I$ for R_2 ranging from 10 to 100 are given in Fig. 4.5.

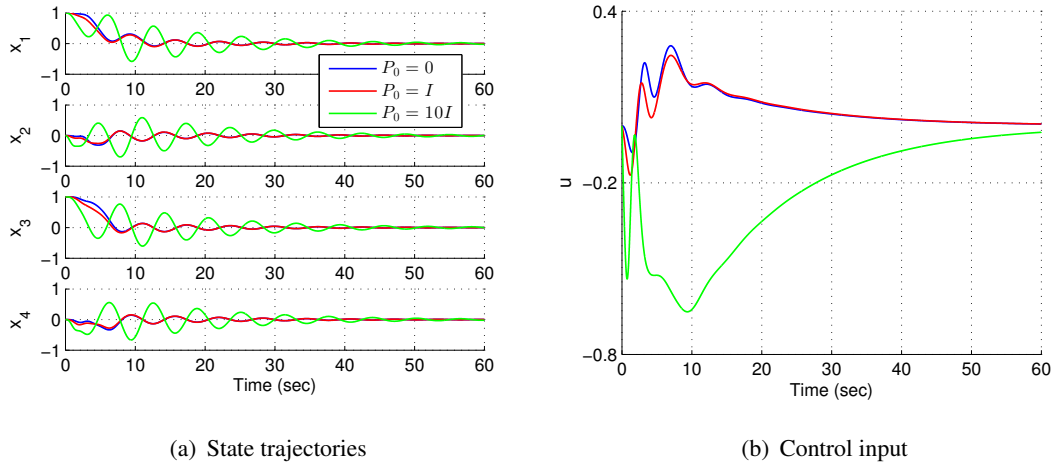


Figure 4.4: Example 4.2. Full-state feedback for the rotating disc: closed-loop responses.

4.1.2 Output-Feedback

Next, consider the case where the full-state measurement is not available, and the output is given by

$$y(t) = C(t)x(t), \quad (4.9)$$

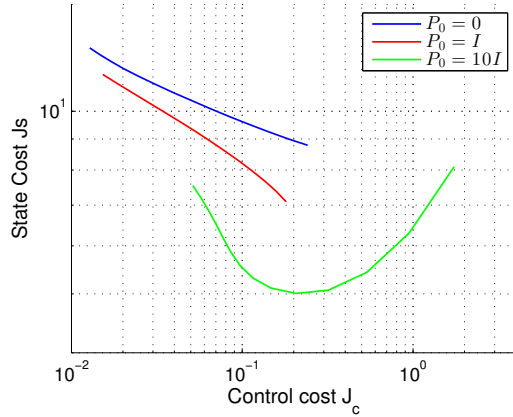


Figure 4.5: Example 4.2. Full-state feedback for the rotating disc: Pareto performance tradeoff curves.

where $y(t) \in \mathbb{R}^l$ and $C(t) \in \mathbb{R}^{n \times l}$. The observer-based compensator is given by [121]

$$\dot{\hat{x}}(t) = A(t)\hat{x}(t) + B(t)u(t) + F(t)(y(t) - C(t)\hat{x}(t)), \quad (4.10)$$

$$u(t) = K(t)\hat{x}(t), \quad (4.11)$$

where $K(t)$ is the full-state-feedback control gain (4.3) observer gain $F(t)$ is given by

$$F(t) = Q(t)C^T(t)V_2^{-1}, \quad (4.12)$$

and $Q(t)$ is the solution of the estimator Riccati equation

$$\dot{Q}(t) = A(t)Q(t) + Q(t)A^T(t) - C(t)C^T(t)V_2^{-1}C(t)Q(t) + V_1, \quad (4.13)$$

with a positive-semidefinite initial condition $Q(0) = Q_0$, and where $V_1 \in \mathbb{R}^{n \times n}$ is positive semidefinite and $V_2 \in \mathbb{R}^{m \times m}$ is positive definite.

The closed-loop system of the LTV plant (4.1) and the observer-based compensator (4.10). (4.11) is given by

$$\begin{bmatrix} \dot{x}(t) \\ \dot{\hat{x}}(t) \end{bmatrix} = \begin{bmatrix} A(t) & B(t)K(t) \\ F(t)C(t) & A(t) + B(t)K(t) - F(t)C(t) \end{bmatrix} \begin{bmatrix} x(t) \\ \hat{x}(t) \end{bmatrix}. \quad (4.14)$$

[121] gives the assumptions, under which the closed-loop system (4.14) is uniformly exponentially stable.

Example 4.3. Stabilization of Mathieu equation using output feedback.

Consider the Mathieu equation (4.7) with the parameters given in Example 4.1. For the output feedback, consider $C = [1 \ 0]$. Let $R_1 = I$, $R_2 = 1$, $V_1 = I$, $V_2 = 1$, $Q_0 = I$, and $\hat{x}(0) = 0$. Consider three choices of P_0 , namely, $P_0 = 0$, $P_0 = I$, and $P_0 = 10I$. Figure 4.6 shows the closed-loop responses, and Pareto performance curves for R_2 ranging from 0.1 to 10 are given in Fig. 4.7.

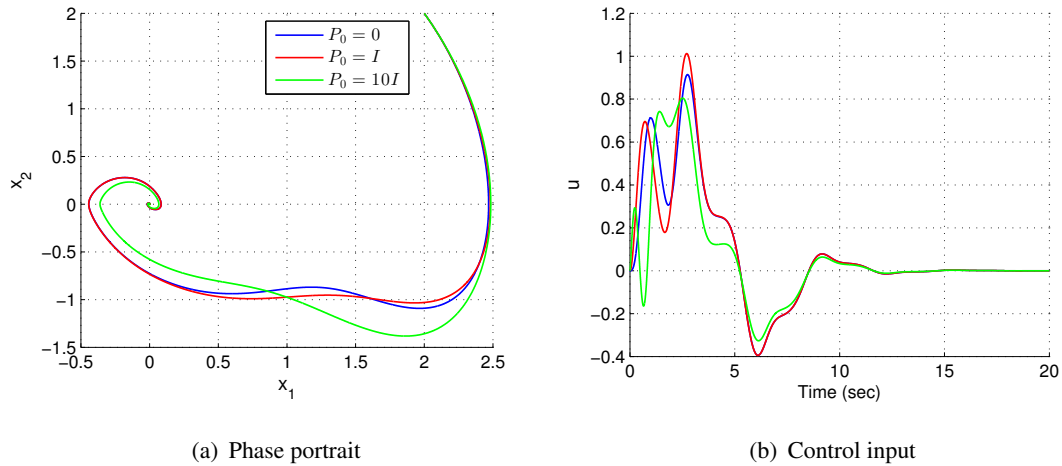


Figure 4.6: Example 4.3. Output feedback for Mathieu equation: closed-loop responses.

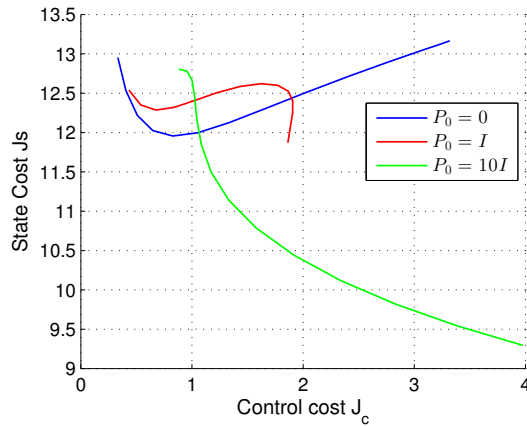


Figure 4.7: Example 4.3. Output feedback for Mathieu equation: Pareto performance tradeoff curves.

Example 4.4. Stabilization of a rotating disc using output feedback.

Consider the problem of stabilization of a rotating disc (4.8) given in Example 4.2. For the output feedback, let $R_1 = I$, $R_2 = 10$, $V_1 = I$, $V_2 = 1$, $Q_0 = 0$, and $\hat{x}(0) = 0$.

Consider three choices of P_0 , namely, $P_0 = 0$, $P_0 = I$, and $P_0 = 10I$. Figure 4.8 shows the closed-loop responses, and Pareto performance curves for R_2 ranging from 10 to 100 are given in Fig. 4.9.

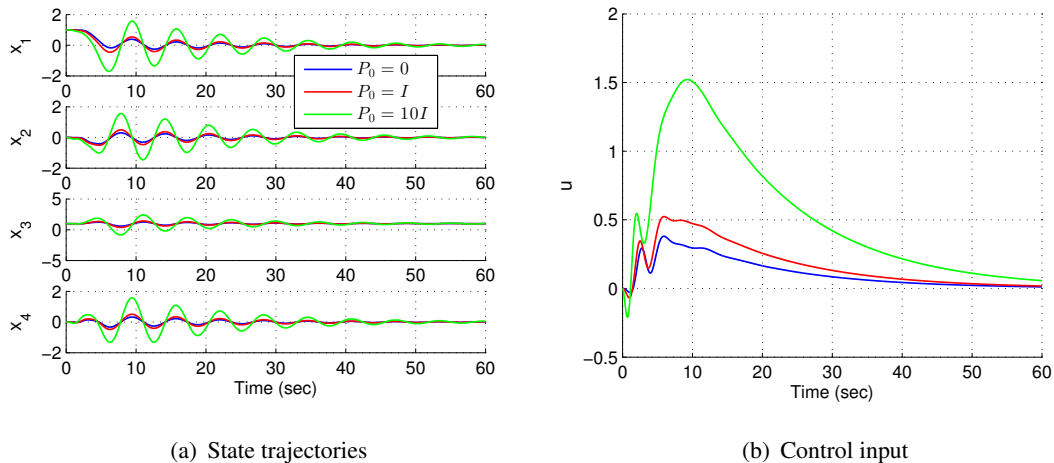


Figure 4.8: Example 4.4. Output feedback for the rotating disc: closed-loop responses.

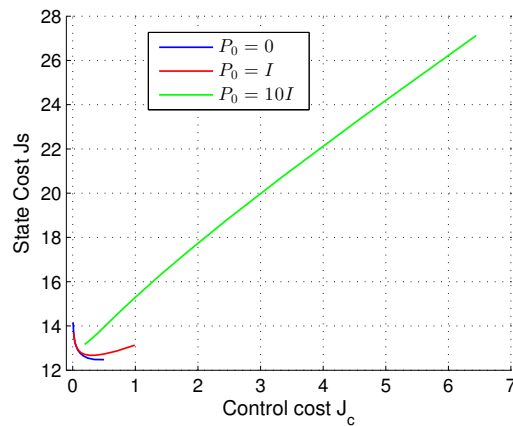


Figure 4.9: Example 4.4. Output feedback for the rotating disc: Pareto performance tradeoff curves.

Example 4.5. Stabilization of elastic beam using output feedback.

Consider the axially loaded simply supported beam [54], shown in Fig. 4.10. The equation of motion is given by

$$EI \frac{\partial^4 v}{\partial x^4} + (P_1 + P_2 \cos \omega t) \frac{\partial^2 v}{\partial x^2} + m \frac{\partial^2 v}{\partial t^2} = 0. \quad (4.15)$$

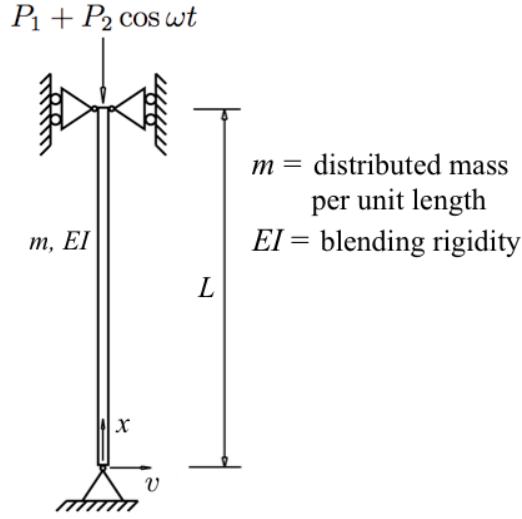


Figure 4.10: Example 4.5. Simply supported beam.

For $i = 1, 2, 3, \dots$ the mode shapes $\phi_i(x)$ and the natural frequencies ω_i are given by

$$\phi_i(x) = \sin\left(\frac{i\pi x}{L}\right), \quad \omega_i = \frac{i^2 \pi^2}{L^2} \sqrt{\frac{EI}{m}}. \quad (4.16)$$

Considering a solution of the form

$$v(x, t) = \sum_{i=1}^r f_i(t) \phi_i(x), \quad (4.17)$$

the differential equation for $f_i(t)$ has the form

$$\frac{\partial^2 f_i}{\partial t^2} + \omega_i^2 \left(1 - \frac{P_1 + P_2 \cos \omega t}{P_i^*}\right) f_i = 0, \quad (4.18)$$

where $i = 1, 2, \dots$ and

$$P_i^* \triangleq i^2 EI \pi^2 / L^2 \quad (4.19)$$

is the i^{th} Euler buckling load. Define

$$\Omega_i \triangleq \omega_i \sqrt{1 - \frac{P_1}{P_i^*}} \quad \mu_i \triangleq \frac{P_2}{2(P_i^* - P_0)}, \quad (4.20)$$

then (4.18) can be written in the form

$$\frac{\partial^2 f_i}{\partial t^2} + \Omega_i^2 (1 - 2\mu_i \cos \omega t) f_i = 0. \quad (4.21)$$

Define the state vector

$$x(t) = \left[f_1(t) \quad \cdots \quad f_r(t) \quad \dot{f}_1(t) \quad \cdots \quad \dot{f}_r(t) \right]^T. \quad (4.22)$$

Assuming a transverse force $u(t)$ concentrated at a single interior point x_a , a measurement is available at a single interior point x_s , and disturbance acts at x_d , yields

$$A(t) = \begin{bmatrix} 0 & I \\ M(t) & 0 \end{bmatrix},$$

$$B(t) = \begin{bmatrix} 0 & \cdots & 0 & \phi_1(x_a) & \cdots & \phi_r(x_a) \end{bmatrix}^T,$$

$$C(t) = \begin{bmatrix} \phi_1(x_s) & \cdots & \phi_r(x_s) & 0 & \cdots & 0 \end{bmatrix},$$

$$D_1(t) = \begin{bmatrix} 0 & \cdots & 0 & \phi_1(x_d) & \cdots & \phi_r(x_d) \end{bmatrix}^T,$$

where

$$M(t) \triangleq \begin{bmatrix} \Omega_1^2(1 - 2\mu_1 \cos \omega t) & \cdots & 0 \\ \vdots & \ddots & \vdots \\ 0 & \cdots & \Omega_r^2(1 - 2\mu_r \cos \omega t) \end{bmatrix}.$$

Consider an aluminum beam, with a length of 1 m, square cross-section of width 5 mm. Let $x_a = L/4$, $x_s = L/3$, $x_d = 3L/4$, $P_1 = 30$ N, $P_2 = 10$ N, and $\omega = 10$ rad/sec. The open-loop response is given in Fig. 4.11.

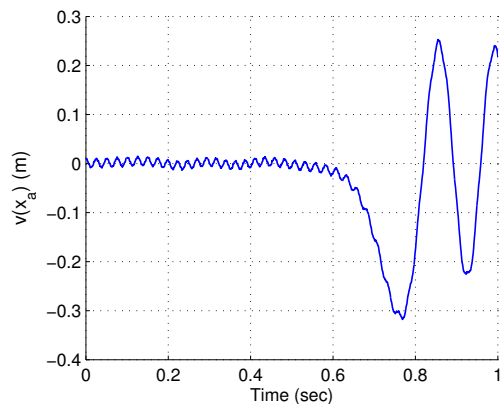


Figure 4.11: Example 4.5. Open-loop response.

Consider two scenarios, namely, stabilization of the flexible beam, and stabilization with a presence of a disturbance, given by a white noise sequence with standard deviation 2 N, which acts at the interior point x_d which differs from x_a , and x_s

For the output feedback, let $R_1 = I$, $R_2 = 0.001$, $V_1 = I$, $V_2 = 0.1$, $Q_0 = 0$, $P_0 = 0$ and $\hat{x}(0) = 0$. Figure 4.12 shows the phase portrait of the closed-loop responses and

the control input. Pareto performance curves for R_2 ranging from 0.001 to 0.1 are given in Fig. 4.13.

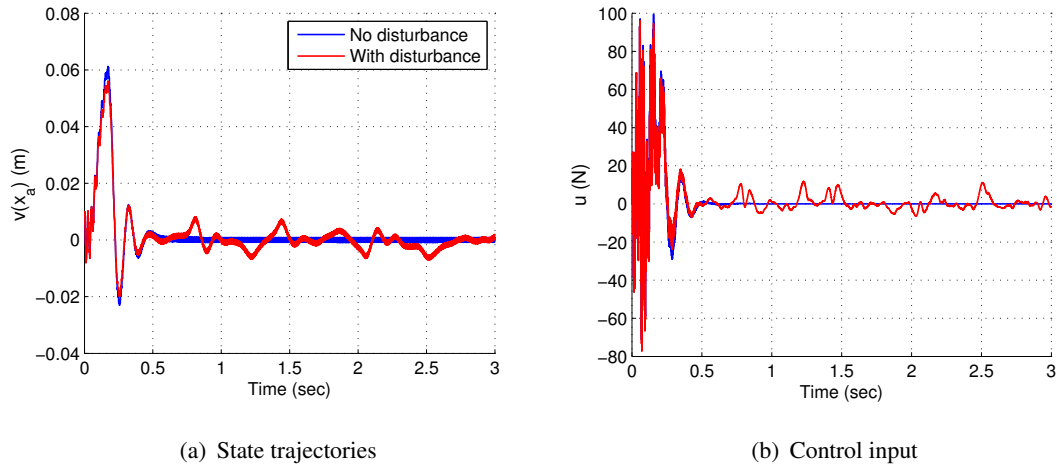


Figure 4.12: Example 4.5. Output feedback for the flexible beam: closed-loop responses.

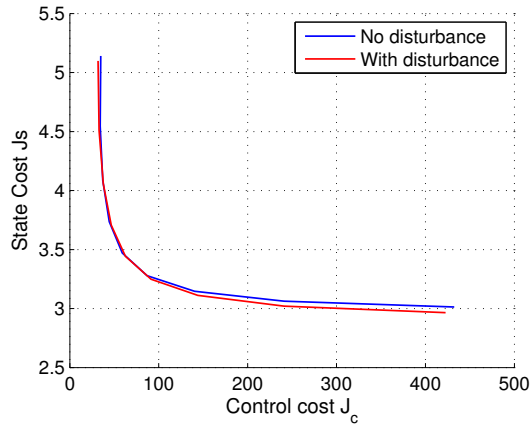


Figure 4.13: Example 4.5. Output feedback for the flexible beam: Pareto performance tradeoff curves.

4.2 FPRE Control for Command Following and Disturbance Rejection

In this section the command following and disturbance rejection methods given in Chapter 3 are applied to LTV plants with replacing the constant matrices A , B , H , C , D_1 by the corresponding time-varying matrices $A(t)$, $B(t)$, $H(t)$, $C(t)$, $D_1(t)$ and utilizing FPRE control.

4.2.1 Tracking FPRE Control

For the command following and disturbance rejection problem, consider a linear quadratic tracking controller, given in Chapter 3, section 3.1.1. Consider an LTV plant in the form (3.1), (3.2), that is

$$\dot{x}(t) = A(t)x(t) + B(t)u(t) + D_1(t)d(t), \quad x(0) = x_0, \quad (4.23)$$

$$y_r(t) = H(t)x(t), \quad (4.24)$$

where $A(t) \in \mathbb{R}^{n \times n}$, $B(t) \in \mathbb{R}^{n \times m}$, $D_1(t) \in \mathbb{R}^{n \times p}$, $H(t) \in \mathbb{R}^{n \times l}$. The tracking error $z(t)$ is given by (3.3), and consider a cost function

$$\mathbf{J}(u) \triangleq \frac{1}{2} \int_0^{t_f} [z^T(t)R_1z(t) + u^T(t)R_2u(t)]dt, \quad (4.25)$$

where $R_1(t) \in \mathbb{R}^{l \times l}$ are positive semidefinite and $R_2(t) \in \mathbb{R}^{m \times m}$ is positive definite.

Assume that the state $x(t)$ is measurable, however, unlike for the linear quadratic optimal control, now it is assumed that the command signal $r(t)$ and disturbance $d(t)$ are not known over the interval $[0, t_f]$. Thus, backward-in-time integration of (3.21) cannot be performed, and therefore, optimal control (3.24) cannot be applied.

For FPRE control, the differential Riccati equation (3.20) is replaced by a forward propagating differential Riccati equation [121] with the time-dependent coefficients

$$\dot{P}(t) = P(t)A(t) + A^T(t)P(t) - P(t)S(t)P(t) + V(t), \quad (4.26)$$

where $S(t) \triangleq B(t)R_2^{-1}B^T(t)$, $V(t) = H^T(t)R_1H(t)$, and a positive-semidefinite initial condition $P(0) = P_0$. Similarly, (3.21) is replaced by a forward propagating differential equation with time-dependent coefficients

$$\dot{g}(t) = [A^T(t) - P(t)S(t)]g(t) + W(t)r(t) - P(t)D_1(t)d(t), \quad (4.27)$$

where $W(t) \triangleq H^T(t)R_1$, and an initial condition $g(0) = g_0$. The control law is given by

$$u(t) = -R_2^{-1}B^T(t)[P(t)x(t) - g(t)] = K(t)x(t) + R_2^{-1}B^T(t)g(t), \quad (4.28)$$

where $K(t) = -R_2^{-1}B^T(t)P(t)$. The weighting matrices R_1, R_2 can be replaced by time-varying weighting matrices $R_1(t), R_2(t)$.

Example 4.6. Tracking FPRE controller for the Mathieu equation

Consider the Mathieu equation in Example 4.1 given by (4.7), with the unmatched disturbance

$$D_{1,\text{cont}}(t) = \begin{bmatrix} 1 & 0 \end{bmatrix}. \quad (4.29)$$

Let $y_r = q$, that is $H = [1 \ 0]$. Let $x_0 = [-1 \ -1]^T$. Let $R_1 = I0^3$, $R_2 = 0.1$, $P_{a,0} = I$, and $g(0) = 0$.

Consider a unit step command at $t = 5$ sec and unit step disturbance at $t = 30$ sec. The closed-loop responses are shown in Fig. 4.14

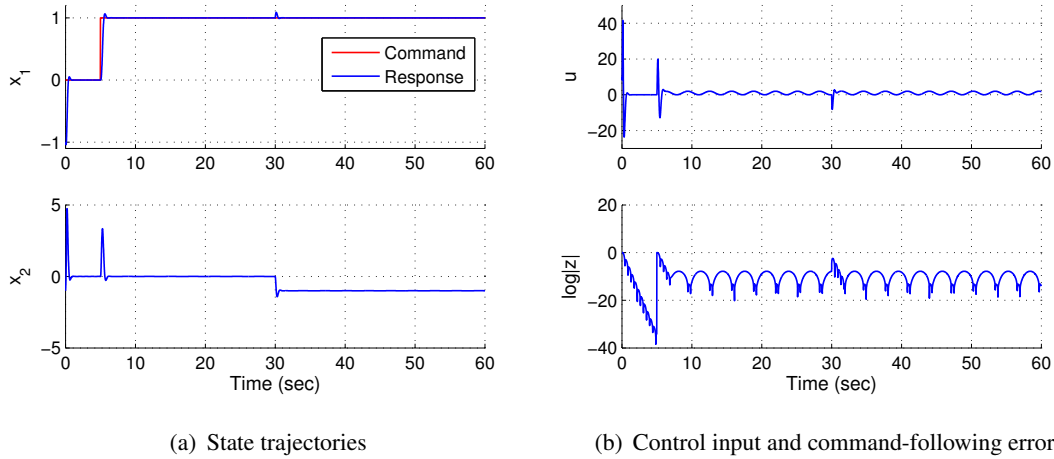


Figure 4.14: Example 4.6. Tracking FPRE control of the Mathieu equation: closed-loop responses.

Next, consider the harmonic command $r(t) = \sin(\Omega_1 t)$ m and the harmonic disturbance $d(t) = 0.1 \cos(\Omega_2 t)$ N, with $\Omega_1 = 0.5$ rad/sec and $\Omega_2 = 0.05$ rad/sec. The closed-loop responses are shown in Fig. 4.15

4.2.2 Internal-Model-Based FPRE Control

For the command following and disturbance rejection problem, consider an internal-model-based full-state-feedback and output-feedback control given in Chapter 3. For LTV systems, the FPRE control law is used. Consider the discrete-time LTV system

$$x_{k+1} = A_k x_k + B_k u_k + D_{1,k} d_k, \quad (4.30)$$

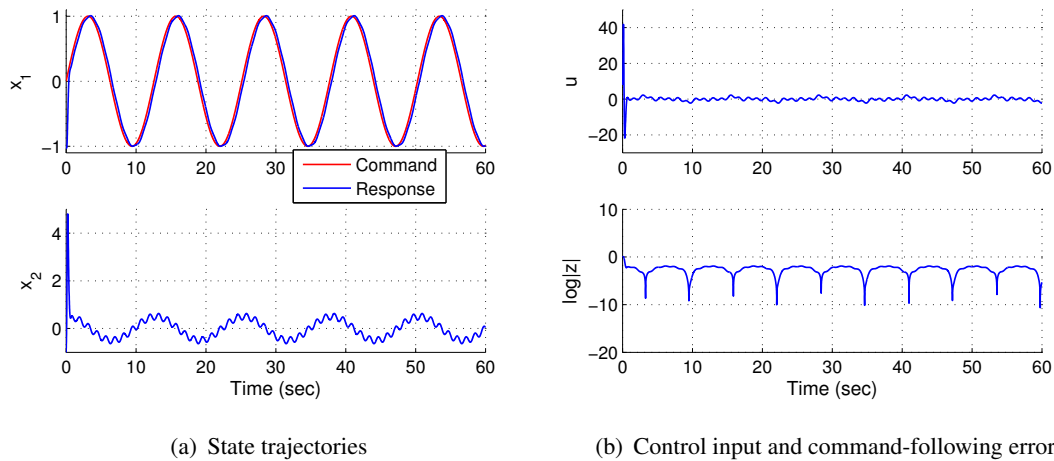


Figure 4.15: Example 4.6. Tracking FPRE control of the Mathieu equation: closed-loop responses.

where $A_k \in \mathbb{R}^{n \times n}$, $B_k \in \mathbb{R}^n$, and $D_{1,k} \in \mathbb{R}^n$. For full-state feedback, the control law is given by (3.40), where the constant feedback gain K_a is replaced by the time-varying feedback gain $K_{a,k}$ given by (3.44), where the constant matrices A , B in the augmented plant (3.38), (3.39) are replaced by the time-varying matrices A_k , B_k , which results in the time-varying matrices $A_{a,k}$, $B_{a,k}$ in place of A_a , B_a in (3.38), (3.39), (3.44), (3.45).

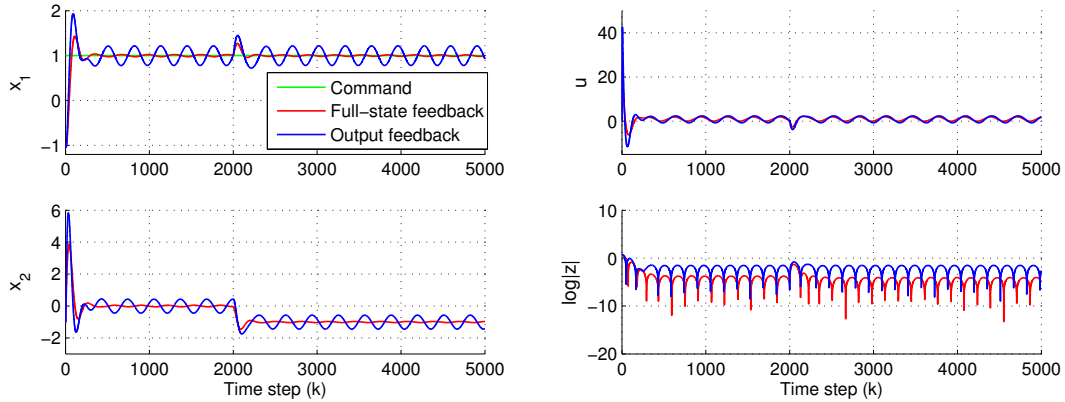
For output feedback, the measurement y_{meas} given by (3.66) is used with the FPRE control given by (3.44), (3.45), and the augmented observer-based compensator (3.76), (3.77). The constant matrices A , B , C in (3.69), (3.70), (3.71) are replaced by the time-varying matrices A_k , B_k , C_k . This results in the time-varying matrices $A_{a,k}$, $B_{a,k}$, $C_{a,k}$ replacing A_a , B_a , C_a in (3.44), (3.45), (3.69), (3.70), (3.71), (3.76), (3.77), and the time-varying matrices $A_{c,k}$, $B_{c,k}$, $C_{c,k}$ replacing A_c , B_c , C_c in (3.78), (3.79), (3.80). The weighting matrices R_1 , R_2 can be replaced by time-varying weighting matrices $R_{1,k}$, $R_{2,k}$.

Example 4.7. Internal-model-based command following and disturbance rejection for the Mathieu equation

Consider the Mathieu equation given in continuous-time by (4.7), (4.29). The discrete-time matrices A_k , B_k , D_k are obtained using (3.62).

For full-state feedback, let $y_r = q$. For output feedback, let $y_{\text{meas}} = y_r = q$, and thus C is omitted. Let $x_0 = [-1 \ -1]^T$, and let $\hat{x}_{a,0} = 0$ for output feedback.

Consider a unit step command and unit step disturbance with the integrator internal model (3.55). Let $R_1 = I$, $R_2 = 10$ for full-state feedback and output feedback, and $V_1 = R_1$, $V_2 = 1$ for output feedback. Let $P_{a,0} = \bar{P}_a$ and $Q_{a,0} = \bar{Q}_a$, where \bar{P}_a and \bar{Q}_a are solutions of (3.43) and (3.75), respectively, with $A_a = A_{a,0}$, $B_a = B_{a,0}$, $C_a = C_{a,0}$, assuming that $(A_{a,0}, B_{a,0})$ is stabilizable, $(A_{a,0}, R_1)$ is detectable, $(A_{a,0}, C_{a,0})$ is detectable, and $(A_{a,0}, V_1)$ is stabilizable. Figure 4.16 shows that residual oscillations at the stiffness frequency are present in the response x_1 for output feedback but not for full-state feedback.



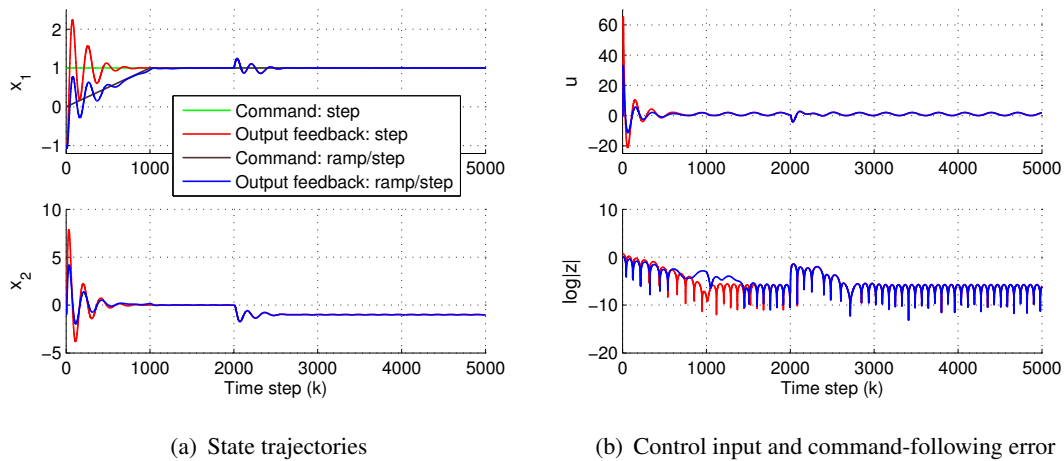
(a) State trajectories

(b) Control input and command-following error

Figure 4.16: Example 4.7. Internal-model-based, full-state-feedback and output-feedback control of the Mathieu equation: closed-loop responses.

To reduce the large transient values of the control input, the step command is replaced with a combination of a ramp and a step. Let $R_1 = I$, $R_2 = 10^8$, $V_1 = R_1$, $V_2 = 1$. Let $P_{a,0} = \bar{P}_a$ and $Q_{a,0} = \bar{Q}_a$. The closed-loop response is shown in Fig. 4.17 for the case of output feedback, where an undamped oscillator is included in the internal model to suppress residual oscillations in the response x_1 due to the time-varying stiffness.

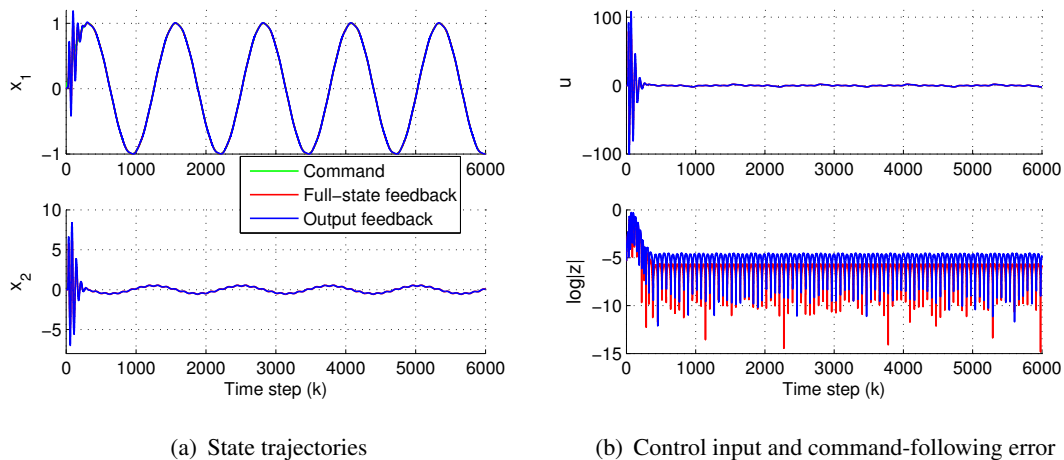
Next, consider the harmonic command $r_k = \sin(\Omega_1 k)$ m and the harmonic disturbance $d_k = 0.1 \cos(\Omega_2 k)$ N, with $\Omega_1 = 0.005$ rad/sample and $\Omega_2 = 0.05$ rad/sample. For $T_s = 0.01$ sec, these discrete-time frequencies correspond to the continuous-time



(a) State trajectories (b) Control input and command-following error
 Figure 4.17: Example 4.7. Internal-model-based, full-state-feedback and output-feedback control of the Mathieu equation: closed-loop responses.

frequencies 0.5 rad/sec and 5 rad/sec, respectively. The internal model is given by the cascade of two undamped oscillators (3.57) whose frequencies are equal to the frequencies of the command and stiffness frequency of Mathieu equation. Since the disturbance frequency is close to the stiffness frequency, only stiffness frequency is included in the internal model.

Let $R_1 = \text{diag}(I_2, 0.1I_4)$, $R_2 = 10^2$ for full-state feedback and output feedback, and $V_1 = R_1$, $V_2 = 0.1$ for output feedback. Let $P_{a,0} = I_6$ and $Q_{a,0} = I_6$. Figure 4.18 shows the closed-loop responses for the full-state feedback and output feedback.



(a) State trajectories (b) Control input and command-following error
 Figure 4.18: Example 4.7. Internal-model-based, full-state-feedback and output-feedback control of the Mathieu equation: closed-loop responses.

CHAPTER 5

REVIEW OF SDRE CONTROL FOR NONLINEAR SYSTEMS

In this section SDRE control for nonlinear systems is considered. SDRE is a systematic approach of designing nonlinear feedback controllers that approximate the solution of the infinite horizon optimal control problem and can be implemented in real-time for a broad class of applications.

The examples considered are the Van der Pol oscillator and the rotational-translational actuator (RTAC) [16, 64]. For each system, full-state feedback and output feedback is applied, and comparisons of the relative accuracy of SDC and Jacobian pseudo-linear models are performed. Next, SDRE control for tracking and disturbance rejection problem is considered. A numerical example is given for the Van der Pol oscillator.

5.1 The SDRE Nonlinear Regulator

Consider the nonlinear plant

$$\dot{x}(t) = f(x(t)) + g(x(t))u(t), \quad x(0) = x_0, \quad (5.1)$$

where $x(t) \in \mathbb{R}^n$, $u(t) \in \mathbb{R}^m$, and, for all $x(t)$ and $u(t)$, $f(x(t)) \in \mathbb{R}^n$, $g(x(t)) \in \mathbb{R}^{n \times m}$, $g(x(t)) \neq 0$. For all $x(t)$, $f(x(t))$ is continuously differentiable function of $x(t)$, that is, $f(x(t)) \in \mathbb{C}^l$, and $f(0) = 0$ [36]. The the finite-horizon cost function is given by

$$\mathbf{J}(u) = \int_0^\infty [x^T(t)R_1(x(t))x(t) + u^T(t)R_2(x(t))u(t)] dt, \quad (5.2)$$

where, for all $x(t)$, $R_1(x(t)) \in \mathbb{R}^{n \times n}$ is positive semidefinite and $R_2(x(t)) \in \mathbb{R}^{m \times m}$ is positive definite.

To simplify the notations, denote $f(x(t)) \triangleq f(x)$, $g(x(t)) \triangleq g(x)$, $R_1(x) \triangleq R_1(x(t))$, and $R_2(x) \triangleq R_2(x(t))$.

5.1.1 State-Dependent-Coefficient Parameterization

As given in [29], extended linearization [53], also known as apparent linearization [122] or SDC parameterization [35, 87], is the process of factorizing a nonlinear system into a linear-like structure which contains SDC matrices.

Under conditions $f(x) \in \mathbb{C}^l$ and $f(0) = 0$, the nonlinear system (5.1) can be written in the SDC form [33]

$$\dot{x}(t) = A(x)x(t) + B(x)u(t), \quad (5.3)$$

where

$$f(x) = A(x)x(t), \quad B(x) = g(x), \quad (5.4)$$

where $A(x) \triangleq A(x(t)) \in \mathbb{R}^{n \times n}$ and $B(x) \triangleq B(x(t)) \in \mathbb{R}^{n \times m}$. For $n > 1$ and under condition that $f(x(t))$ is continuously differentiable function of x , there is infinite number of ways to parameterize the nonlinear system to SDC form [36].

The non-uniqueness of the SDC parameterization brings additional degrees of freedom to the SDRE controller design [33]. Let $A_1(x)$ and $A_2(x)$ be two distinct SDC parameterizations of $f(x)$, that is, $f(x) = A_1(x)x = A_2(x)x$. Then

$$A(x, \alpha(x)) = \alpha(x)A_1(x) + (1 - \alpha(x))A_2(x) \quad (5.5)$$

is an infinite family of SDC parameterizations for the nonlinear function $f(x)$. In general, for $k + 1$ distinct SDC parameterizations, the dimension of $\alpha(x)$ will be k and $A(x, \alpha(x))$ will be of the form

$$A(x, \alpha(x)) = (1 - \alpha_k)A_{k+1}(x) + \sum_{i=1}^k \left(\prod_{j=1}^i \alpha_j \right) (1 - \alpha_{i-1}) A_i(x), \quad (5.6)$$

where $\alpha_0 \triangleq 0$ [35]. If a hyper surface of parameterizations is formed to obtain $A(x, \alpha(x))$, yields the nonlinear feedback controller being parameterized by $\alpha(x)$. The additional degrees of freedom available through $\alpha(x)$ provides design flexibility that can be used to enhance performance or effect tradeoffs between performance, optimality, stability, robustness, and disturbance rejection [33].

5.1.2 Pseudo-Linear Model

Motivated by the extended Kalman filter, which uses a first order Taylor series expansion of $f(x)$, consider the approximation

$$f(x) \approx A_J(x)x(t), \quad (5.7)$$

where

$$A_J(x) \triangleq \left. \frac{\partial f(x)}{\partial x} \right|_{x(t)}. \quad (5.8)$$

Note that the Jacobian $A_J(x)$ of $f(x)$ is not defined at an equilibrium, but rather is updated along the state trajectory.

For full-state feedback with perfect measurements of the state, both $A(x)$ and $A_J(x)$ can be used to update the feedback gain. However, when the state is not measured, $A(x)$ and $A_J(x)$ must be evaluated at an estimate $\hat{x}(t)$ of $x(t)$.

5.1.3 Full-State-Feedback

Assume that, for all $x(t)$, $(A(x), B(x))$ is point-wise stabilizable in a linear sense. The SDRE control law to minimize (5.2) is given by

$$u(t) = K(x)x(t), \quad (5.9)$$

where the feedback gain is

$$K(x) = -R_2^{-1}(x)B^T(x)\bar{P}(x), \quad (5.10)$$

where $\bar{P}(x) \in \mathbb{R}^{n \times n}$ is a unique, symmetric, positive-definite solution of the algebraic state-dependent Riccati equation

$$\bar{P}(x)A(x) + A^T(x)\bar{P}(x) - \bar{P}(x)B(x)R_2^{-1}(x)B^T(x)\bar{P}(x) + R_1(x) = 0. \quad (5.11)$$

The SDRE control (5.9) yields the following closed-loop dynamics

$$\dot{x}(t) = f(x) + B(x)K(x)x(t). \quad (5.12)$$

The structure of SDRE control is the same as the infinite-horizon linear quadratic regulator, where the coefficient matrices are state-dependent.

The selection of the SDC matrix $A(x)$ has a significant effect on the controllability of $(A(x), B(x))$. It should be noted, that, in general, for some arbitrary choice of the SDC matrix $A(x)$, the SDRE control (5.9), (5.10), (5.11) does not recover global optimality with respect to the performance index (5.2) [29].

Issues related to the existence of the solution, local and global stability analysis, also optimality analysis of SDRE control are discussed in [36, 87, 35, 60] and summarized in [29].

5.1.4 Output-Feedback

For the output feedback, the measurement is given by

$$y(t) = C(x)x(t), \quad (5.13)$$

where $y(t) \in \mathbb{R}^l$ and $C(x) \in \mathbb{R}^{n \times l}$. The observer-based compensator, which has the same structure as (4.10), (4.11), is given by

$$\dot{\hat{x}}(t) = A(x)\hat{x}(t) + B(x)u(t) + F(x)(y(t) - C(x)\hat{x}(t)), \quad (5.14)$$

$$u(t) = K(x)\hat{x}(t), \quad (5.15)$$

where $K(x)$ is the full-state-feedback control gain (5.10), and the observer gain $F(x)$ is given by

$$F(x) = \bar{Q}(x)C^T(x)V_2^{-1}(x), \quad (5.16)$$

and $\bar{Q}(x)$ is the solution of the algebraic state-dependent estimator Riccati equation

$$\bar{Q}(x) = A(x)\bar{Q}(x) + \bar{Q}(x)A^T(x) - C(x)C^T(x)V_2^{-1}(x)C(x)\bar{Q}(x) + V_1(x), \quad (5.17)$$

where $V_1(x) \in \mathbb{R}^{n \times n}$ is positive semidefinite and $V_2(x) \in \mathbb{R}^{m \times m}$ is positive definite.

The closed-loop system with the observer-based dynamic compensator (5.14) is given by

$$\dot{x}(t) = f(x) + B(x)K(x)\hat{x}(t), \quad (5.18)$$

$$\dot{\hat{x}}(t) = (A(x) + B(x)K(x) - F(x)C(x))\hat{x}(t) + F(x)C(x)x(t). \quad (5.19)$$

In the output feedback, since the full state is not available, we replace the state x in the SDC matrices by its estimate \hat{x} , resulting in $A(\hat{x})$, $B(\hat{x})$, $C(\hat{x})$. If measurement y includes components of x , then the corresponding components of \hat{x} in the SDC's are replaced by the measurements; the modified state estimate is denoted by \tilde{x} . Then, for use in the observer-based compensator $A(\hat{x})$, $B(\hat{x})$, $C(\hat{x})$ are replaced by $A(\tilde{x})$, $B(\tilde{x})$, $C(\tilde{x})$.

5.2 Discrete-Time SDRE Control Formulation

This section gives formulation of the SDRE control in discrete time. The controller structure is the same as in the continuous time. The difference of the discrete-time control is in the expressions for the feedback control and observer gains, (5.10), (5.16), and also in the algebraic control and estimator Riccati equations (5.11), (5.17).

5.2.1 Discrete-Time Full-State-Feedback

Consider the nonlinear plant (5.1) given in discrete time

$$x_{k+1} = f(x_k) + g(x_k)u_k. \quad (5.20)$$

Then, a discrete-time SDC model of (5.20) is given by

$$x_{k+1} = A_k x_k + B_k u_k. \quad (5.21)$$

where $A_k \triangleq A(x_k)$ and $B_k \triangleq B(x_k)$. The discrete-time full-state-feedback control (5.9) is given in the form

$$u_k = K_k x_k, \quad (5.22)$$

where the feedback gain $K_k \triangleq K(x_k)$ is given by

$$K_k = -(B_k^T \bar{P}_k B_k + R_{2,k})^{-1} B_k^T \bar{P}_k A_k, \quad (5.23)$$

and $\bar{P}_k \triangleq \bar{P}(x_k)$ is the solution of a discrete-time algebraic state-dependent Riccati equation

$$\bar{P}_k = A_k^T \bar{P}_k A_k - A_k^T \bar{P}_k B_k (B_k^T \bar{P}_k B_k + R_{2,k})^{-1} B_k^T \bar{P}_k A_k + R_{1,k}, \quad (5.24)$$

where $R_{1,k} \in \mathbb{R}^{n \times n}$ is positive semidefinite and $R_{2,k} \in \mathbb{R}^{m \times m}$ is positive definite. The closed-loop dynamics is given by

$$x_{k+1} = f(x_k) + B_k K_k x_k. \quad (5.25)$$

Numerical examples below illustrate application of the full-state-feedback SDRE control for stabilization of nonlinear systems. System matrix A_k in (5.23), (5.24) is given by either SDC $A(x_k)$ or a Jacobian $A_J(x_k)$, evaluated at the true state x_k .

Example 5.1. Full-state-feedback SDRE control for stabilization of the Van der Pol oscillator

In this example apply full-state-feedback SDRE control for stabilization of the Van der Pol oscillator given by

$$\ddot{q} - \mu(1 - q^2)\dot{q} + q = bu, \quad (5.26)$$

where $\mu > 0$ and $b \neq 0$. Let the state vector $x \triangleq [q \ \dot{q}]^T$. Equation (5.26) involves one nonlinear term $-\mu x_1^2 x_2$, which can be factored in two ways, namely, $-\mu x_1^2 x_2 = -(\mu x_1^2) x_2 = -(\mu x_1 x_2) x_1$. Consequently, two SDC's can be obtained, namely,

$$A_{1,\text{cont}}(x) = \begin{bmatrix} 0 & 1 \\ -1 & \mu(1 - x_1^2) \end{bmatrix}, \quad (5.27)$$

$$A_{2,\text{cont}}(x) = \begin{bmatrix} 0 & 1 \\ -\mu x_1 x_2 & \mu \end{bmatrix}. \quad (5.28)$$

Note that every affine combination $\alpha A_{1,\text{cont}}(x) + (1 - \alpha) A_{2,\text{cont}}(x)$, where α is a real number, is also an SDC. However, only the cases $\alpha = 1$ and $\alpha = 0$ are considered. The Jacobian is given by

$$A_{J,\text{cont}}(x) = \begin{bmatrix} 0 & 1 \\ -(1 + 2\mu x_1 x_2) & \mu(1 - x_1^2) \end{bmatrix}. \quad (5.29)$$

The input matrix is given by

$$B_{\text{cont}} = [0 \ b]^T. \quad (5.30)$$

Let $T_s = 0.01$ sec, and the discrete-time model of VDP is obtained according to (3.62). Define the corresponding discrete-time pseudo-linear dynamics matrices A_1 , A_2 , A_J . Let $\mu = 0.15$, $b = 1$, and $x_0 = [3 \ 2]^T$.

Let $R_1 = 10I_2$, $R_2 = 0.1$. Figure 5.1 shows the closed-loop responses.

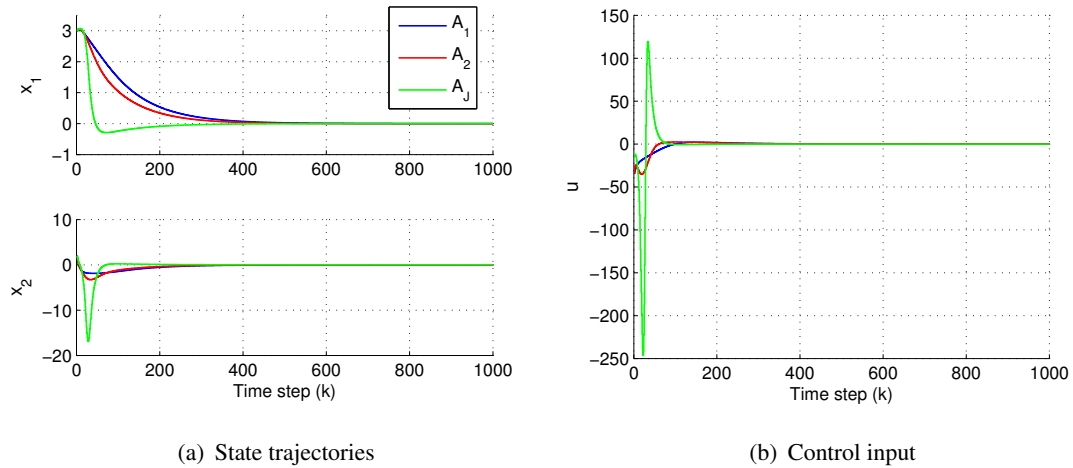


Figure 5.1: Example 5.1. Full-state-feedback SDRE control of the Van der Pol oscillator.

For Pareto plot in Fig. 5.2, $R_1 = 10I_2$, and R_2 ranges from 0.01 to 10.

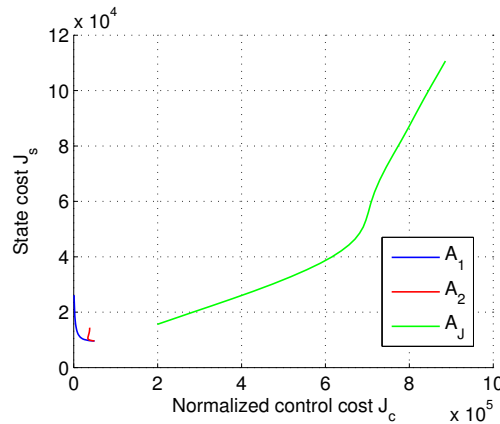


Figure 5.2: Example 5.1. Pareto performance tradeoff curves for full-state-feedback SDRE control of the Van der Pol oscillator.

Example 5.2. Full-state-feedback SDRE control for stabilization of the RTAC

In this example full-state-feedback SDRE control is applied for stabilization of the rotational-translational actuator (RTAC) [16, 64] shown in Fig. 5.3. The equations of

motion are given by

$$(M + m)\ddot{q} + b\dot{q} + kq = -me(\ddot{\theta} \cos \theta - \dot{\theta}^2 \sin \theta) + d, \quad (5.31)$$

$$(J + me^2)\ddot{\theta} = -me\ddot{q} \cos \theta + \tau, \quad (5.32)$$

where q and \dot{q} are the translational position and velocity of the cart, and θ and $\dot{\theta}$ are the angular position and angular velocity of the rotating arm, respectively. M is the mass of the cart, b is the damping coefficient, k is the spring stiffness, m is the mass of the proof-mass, J is the moment of inertia of the arm, e is the length of the arm, τ is the control torque applied to the arm, and d is the disturbance force on the cart. The goal is to command the position of the cart. Parameters for the RTAC configuration are given in Table 5.1.

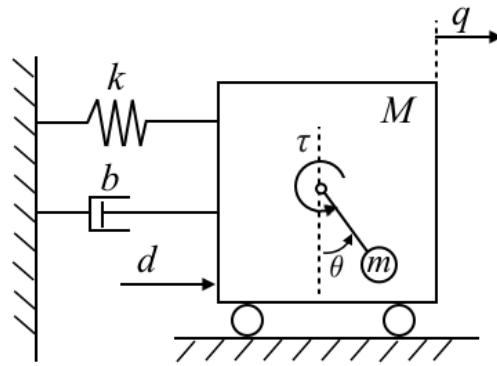


Figure 5.3: Rotational-translational actuator.

Table 5.1: RTAC Parameters

Parameter	Value	Units
Mass of the cart (M)	2	kg
Mass of the arm (m)	0.2	kg
Arm eccentricity (e)	0.1	m
Arm inertia (J)	0.0002	kg-m ²
Spring stiffness (k)	200	N/m
Damping coefficient (b)	0.4	N-sec/m

For the state vector $x = [q \ \dot{q} \ \theta]^T$, the equations of motion have the form

$$\dot{x} = f_{\text{cont}}(x) + B_{\text{cont}}(x)\tau + D_{1,\text{cont}}(x)d, \quad (5.33)$$

where

$$f_{\text{cont}}(x) \triangleq \begin{bmatrix} x_2 \\ -\frac{kx_1}{\delta(M+m)} - \frac{bx_2}{\delta(M+m)} + \frac{mex_4^2 \sin x_3}{\delta(M+m)} \\ x_4 \\ \frac{k\varepsilon^2 x_1 \cos x_3}{\delta me} + \frac{b\varepsilon^2 x_2 \cos x_3}{\delta me} - \frac{\varepsilon^2 x_4^2 \sin x_3 \cos x_3}{\delta} \end{bmatrix}, \quad (5.34)$$

$$B_{\text{cont}}(x) \triangleq \begin{bmatrix} 0 \\ -\frac{\varepsilon^2 \cos x_3}{\delta me} \\ 0 \\ \frac{\varepsilon^2 \cos x_3 + \delta}{\delta(I+me^2)} \end{bmatrix}, \quad D_{1,\text{cont}}(x) \triangleq \begin{bmatrix} 0 \\ \frac{1}{\delta(M+m)} \\ 0 \\ \frac{\varepsilon^2 \cos x_3}{\delta me} \end{bmatrix}, \quad (5.35)$$

where $\varepsilon \triangleq \frac{me}{\sqrt{(J+me^2)(M+m)}}$ and $\delta \triangleq 1 - \varepsilon^2 \cos^2 x_3$.

The vector field (5.34) involves four nonlinear terms that can be factored. Note that $\frac{mex_4^2 \sin x_3}{\delta(M+m)}$ can be factored in two ways, namely, $\frac{mex_4^2 \sin x_3}{\delta(M+m)} = \left(\frac{mex_4 \sin x_3}{\delta(M+m)} \right) x_4 = \left(\frac{mex_4^2 \sin x_3}{\delta(M+m)x_3} \right) x_3$; $\frac{k\varepsilon^2 x_1 \cos x_3}{\delta me}$ can be factored in one way, namely, $\frac{k\varepsilon^2 x_1 \cos x_3}{\delta me} = \left(\frac{k\varepsilon^2 \cos x_3}{\delta me} \right) x_1$; $\frac{b\varepsilon^2 x_2 \cos x_3}{\delta me}$ can be factored in one way, namely, $\frac{b\varepsilon^2 x_2 \cos x_3}{\delta me} = \left(\frac{b\varepsilon^2 \cos x_3}{\delta me} \right) x_2$; and $\frac{\varepsilon^2 x_4^2 \sin x_3 \cos x_3}{\delta}$ can be factored in two ways, namely, $\frac{\varepsilon^2 x_4^2 \sin x_3 \cos x_3}{\delta} = \left(\frac{\varepsilon^2 x_4 \sin x_3 \cos x_3}{\delta} \right) x_4 = \left(\frac{\varepsilon^2 x_4^2 \sin x_3 \cos x_3}{\delta x_3} \right) x_3$. Consequently, four SDC's can be obtained in this way, namely,

$$A_{1,\text{cont}}(x) = \begin{bmatrix} 0 & 1 & 0 & 0 \\ -\frac{k}{\delta(M+m)} & -\frac{b}{\delta(M+m)} & 0 & \frac{mex_4 \sin x_3}{\delta(M+m)} \\ 0 & 0 & 0 & 1 \\ \frac{k\varepsilon^2 \cos x_3}{\delta me} & \frac{b\varepsilon^2 \cos x_3}{\delta me} & 0 & -\frac{\varepsilon^2 x_4 \sin x_3 \cos x_3}{\delta} \end{bmatrix}, \quad (5.36)$$

$$A_{2,\text{cont}}(x) = \begin{bmatrix} 0 & 1 & 0 & 0 \\ -\frac{k}{\delta(M+m)} & -\frac{b}{\delta(M+m)} & 0 & \frac{mex_4 \sin x_3}{\delta(M+m)} \\ 0 & 0 & 0 & 1 \\ \frac{k\varepsilon^2 \cos x_3}{\delta me} & \frac{b\varepsilon^2 \cos x_3}{\delta me} & -\frac{\varepsilon^2 x_4^2 \sin x_3 \cos x_3}{\delta x_3} & 0 \end{bmatrix}, \quad (5.37)$$

$$A_{3,\text{cont}}(x) = \begin{bmatrix} 0 & 1 & 0 & 0 \\ -\frac{k}{\delta(M+m)} & -\frac{b}{\delta(M+m)} & \frac{mex_4^2 \sin x_3}{\delta(M+m)x_3} & 0 \\ 0 & 0 & 0 & 1 \\ \frac{k\varepsilon^2 \cos x_3}{\delta me} & \frac{b\varepsilon^2 \cos x_3}{\delta me} & 0 & -\frac{\varepsilon^2 x_4 \sin x_3 \cos x_3}{\delta} \end{bmatrix}, \quad (5.38)$$

$$A_{4,\text{cont}}(x) = \begin{bmatrix} 0 & 1 & 0 & 0 \\ -\frac{k}{\delta(M+m)} & -\frac{b}{\delta(M+m)} & \frac{m\epsilon x_4^2 \sin x_3}{\delta(M+m)x_3} & 0 \\ 0 & 0 & 0 & 1 \\ \frac{k\epsilon^2 \cos x_3}{\delta m\epsilon} & \frac{b\epsilon^2 \cos x_3}{\delta m\epsilon} & -\frac{\epsilon^2 x_4^2 \sin x_3 \cos x_3}{\delta x_3} & 0 \end{bmatrix}. \quad (5.39)$$

The Jacobian is given by

$$A_{J,\text{cont}}(x) = \begin{bmatrix} 0 & 1 & 0 & 0 \\ A_{21} & A_{22} & A_{23} & A_{24} \\ 0 & 0 & 0 & 1 \\ A_{41} & A_{42} & A_{43} & A_{44} \end{bmatrix}, \quad (5.40)$$

where

$$\begin{aligned} A_{21} &= -\frac{k}{\delta(M+m)}, & A_{22} &= -\frac{b}{\delta(M+m)}, & A_{24} &= \frac{2\epsilon m x_4 \sin x_3}{(M+m)\delta}, \\ A_{23} &= \frac{\epsilon^2 \sin 2x_3 (kx_1 + bx_2)}{(M+m)\delta} + \frac{\epsilon m x_4^2 \cos x_3}{(M+m)\delta} \left(1 - \frac{2\epsilon^2 \sin^2 x_3}{\delta}\right) \\ A_{41} &= \frac{k\epsilon^2 \cos x_3}{m\epsilon\delta}, & A_{42} &= \frac{b\epsilon^2 \cos x_3}{m\epsilon\delta}, & A_{44} &= \frac{\epsilon^2 x_4 \sin 2x_3}{\delta}, \\ A_{43} &= \frac{\epsilon^2 (kx_1 + bx_2) \sin x_3}{\delta^2} (\delta - 2\epsilon^2 \cos^2 x_3) + \frac{\epsilon^2 x_4^2 ((\epsilon^2 - 2) \cos 2x_3 + \epsilon^2)}{2\delta^2} \end{aligned} \quad (5.41)$$

Let $T_s = 0.001$ sec, and define the corresponding discrete-time SDC's by A_1, A_2, A_3, A_4 , which are obtained using (3.62).

Let $x_0 = [0.05 \text{ m}, 0.1 \text{ m/sec}, \pi/6; \text{rad}, 0 \text{ rad/sec}]^T$. Let $R_1 = \text{diag}(10^3 I_2, I_2)$, $R_2 = 1$ for A_1, A_2, A_3, A_4 , and let $R_1 = \text{diag}(100 I_2, I_2)$, $R_2 = 5$ for A_J . Figure 5.4 shows the closed-loop responses.

5.2.2 Discrete-Time Output-Feedback

For a discrete-time nonlinear plant (5.20), given in the SDC form (5.21), consider the measurement in the following form

$$y_k = C(x_k)x_k, \quad (5.42)$$

where $C_k \triangleq C(x_k)$. A discrete-time observer-based compensator is given by

$$\hat{x}_{k+1} = (A_k + B_k K_k - F_k C_k) \hat{x}_k + F_k y_k, \quad (5.43)$$

$$u_k = K_k \hat{x}_k. \quad (5.44)$$

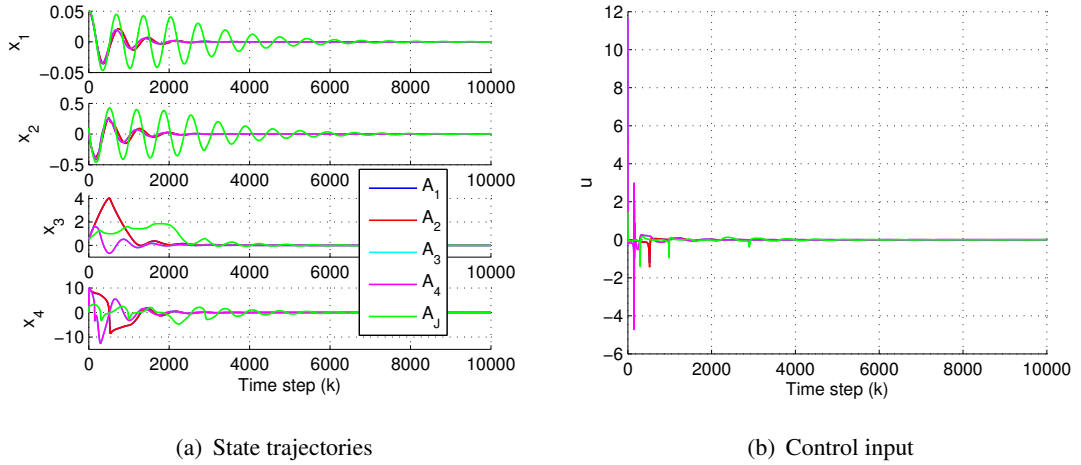


Figure 5.4: Example 5.2. Full-state-feedback SDRE control of the RTAC.

where A_k, B_k, C_k are evaluated at the estimated state \hat{x}_k or \tilde{x}_k . The regulator gain K_k is the full-state-feedback gain (5.23), and the observer gain $F_k \triangleq F(x_k)$ is given by

$$F_k = A_k \bar{Q}_k C_k^T (C_k \bar{Q}_k C_k^T + V_{2,k})^{-1}, \quad (5.45)$$

where $\bar{Q}_k \triangleq \bar{Q}(x_k)$ in (5.45) is a solution of a discrete-time algebraic state-dependent estimator Riccati equation

$$\bar{Q}_k = A_k \bar{Q}_k A_k^T - A_k \bar{Q}_k C_k^T (C_k \bar{Q}_k C_k^T + V_{2,k})^{-1} C_k \bar{Q}_k A_k^T + V_{1,k}, \quad (5.46)$$

where $V_{1,k}$ is positive semidefinite, and $V_{2,k}$ is positive definite. The discrete-time closed-loop system with the observer-based dynamic compensator (5.43) has the form (5.18), (5.19), and is given by

$$x_{k+1} = f(x_k) + B_k K_k \hat{x}_k, \quad (5.47)$$

$$\hat{x}_{k+1} = (A_k + B_k K_k - F_k C_k) \hat{x}_k + F_k C_k x_k. \quad (5.48)$$

Example 5.3. Output-feedback SDRE control for stabilization of the Van der Pol oscillator

In this example output-feedback SDRE control is applied for stabilization of the Van der Pol oscillator (5.26) with the parameters given in Example 5.1. For the output feedback, let $C = [1 \ 0]$. SDC dynamics matrices and the Jacobian are given by (5.27), (5.28), (5.29), and the control matrix is given by (5.30).

Let $\mu = 0.15$, $b = 1$, $x_0 = [3 \ 2]^T$, and $\hat{x}_0 = 0$. Let $R_1 = 10I_2$, $R_2 = 1$, $V_1 = I_2$, and $V_2 = 0.1$. Figure 5.5 shows the closed-loop responses.

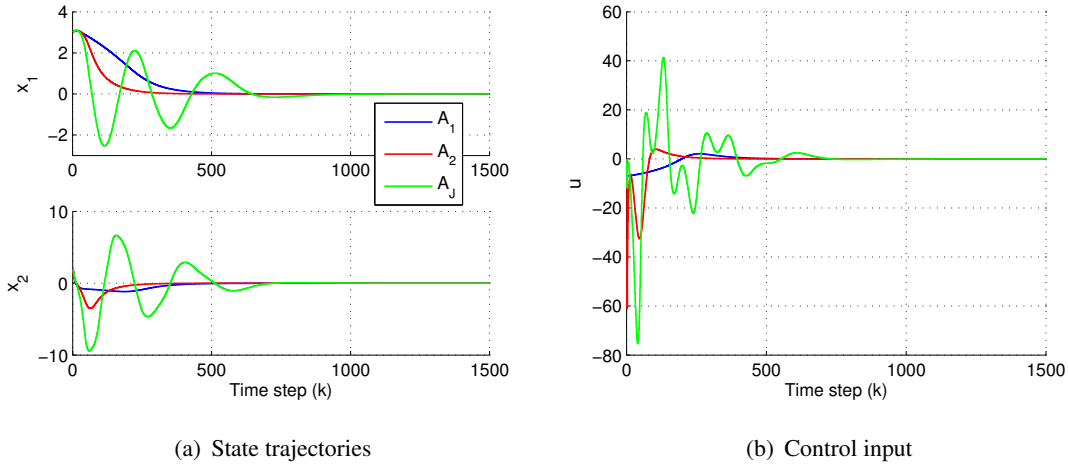


Figure 5.5: Example 5.3. Output-feedback SDRE control of the Van der Pol oscillator.

For Pareto plot in Fig. 5.6, $R_1 = 10I_2$, and R_2 ranges from 0.01 to 10.

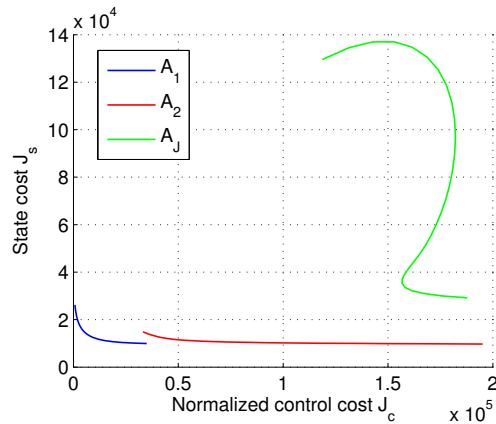


Figure 5.6: Example 5.3. Pareto performance tradeoff curves for output-feedback SDRE control of the Van der Pol oscillator.

Example 5.4. Output-feedback SDRE control for stabilization of the RTAC

In this example output-feedback SDRE control is applied for stabilization of the rotational-translational oscillator (5.31), (5.32) in Example 5.2. The RTAC parameters are given in Table 5.1. SDC dynamics matrices and the Jacobian of the RTAC model (5.33), (5.35) are given by (5.36), (5.37), (5.38), (5.39), and (5.40).

Let $x_0 = [0.05 \text{ m}, 0.1 \text{ m/sec}, \pi/6; \text{rad}, 0 \text{ rad/sec}]^T$. Consider three cases of mea-

measurements that are available, namely, cart position, arm angle, cart position and arm angle. In the first case, where only cart position measurements are available, output-feedback SDRE failed to stabilize the plant for all SDC's A_1, A_2, A_3, A_4 , and Jacobian A_J .

In the second case, where arm angle measurements are available, let $R_1 = \text{diag}(10^2 I_2, I_2)$, $R_2 = 1$ for A_1, A_2, A_3, A_4 , and $R_1 = I_4, R_2 = 1$ for A_J . Let $V_1 = I_4, V_2 = 0.1$ for A_1, A_2, A_3, A_4, A_J . The closed-loop responses are shown in Fig. 5.7.

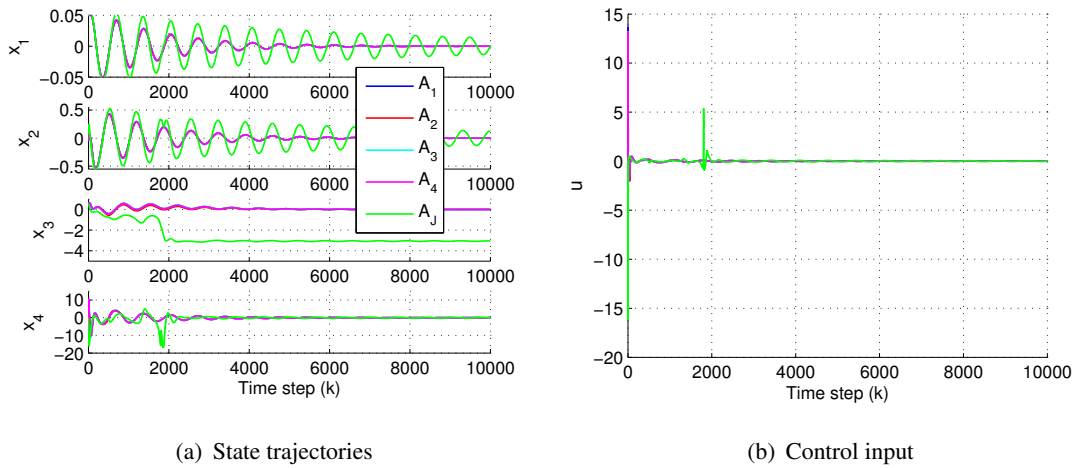


Figure 5.7: Example 5.4. Output-feedback SDRE control of the RTAC with arm angle measurements.

In the third case, where cart position and arm angle measurements are available, let $R_1 = \text{diag}(10^2 I_2, I_2)$, $R_2 = 1$, $V_1 = I_4, V_2 = 0.1 I_2$ for A_1, A_2, A_3, A_4, A_J . The closed-loop responses are shown in Fig. 5.8.

5.3 Tracking SDRE Control

SDRE control for command following and disturbance rejection is based on the infinite-time linear quadratic tracking and disturbance rejection optimal control, given in Section 3 for LTI plants. The same controller structure as it is given for LTI systems is used, with the constant matrices A, B, H replaced by the state-dependent coefficient matrices.

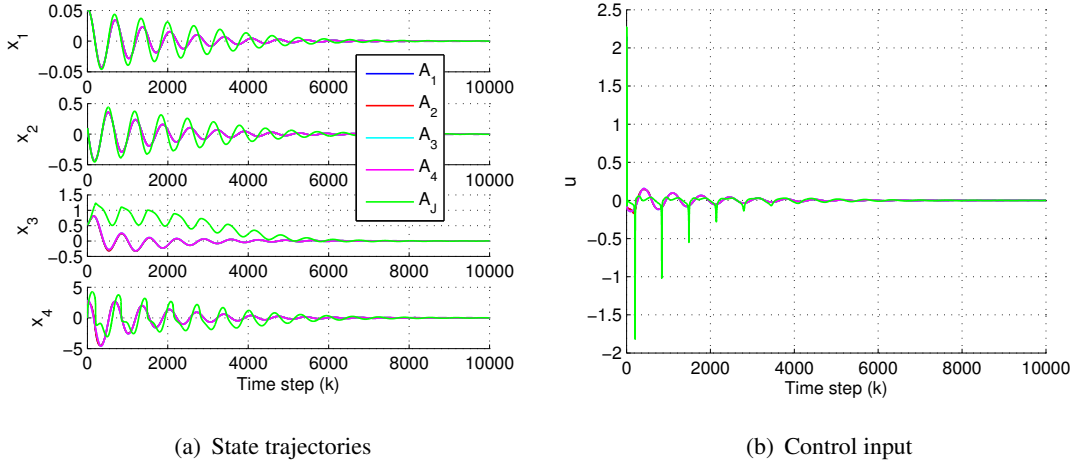


Figure 5.8: Example 5.4. Output-feedback SDRE control of the RTAC with cart position and arm angle measurements.

Consider a nonlinear plant

$$\dot{x}(t) = f(x) + g(x)u(t) + D_1(x)d(t), \quad x(0) = x_0, \quad (5.49)$$

$$y_r(t) = H(x)x(t). \quad (5.50)$$

where $x(t) \in \mathbb{R}^n$, $u(t) \in \mathbb{R}^m$, $d(t) \in \mathbb{R}^p$, $y_r \in \mathbb{R}^l$, and, for all $x(t)$ and $u(t)$, $f(x) \in \mathbb{R}^n$, $g(x) \in \mathbb{R}^{n \times m}$, $H(x) \in \mathbb{R}^{l \times n}$.

Let the SDC form of (5.49), (5.50) be given by

$$\dot{x}(t) = A(x)x(t) + B(x)u(t) + D_1(x)d(t), \quad x(0) = x_0, \quad (5.51)$$

$$y_r(t) = H(x)x(t), \quad (5.52)$$

where it is assumed that $(A(x), B(x))$ is stabilizable. Note that this structure is the same as (3.1), (3.2) but the constant matrices are replaced by the matrices with the state-dependent coefficients. Let $r(t) \in \mathbb{R}^l$ be a command signal, and the control objective is to make the output $y_r(t)$ to track the command signal $r(t)$ and reject a disturbance $d(t)$. It is assumed that the state $x(t)$ is measurable. The tracking error is given by

$$z(t) = r(t) - y_r(t) = r(t) - H(x)x(t), \quad (5.53)$$

and the performance index given by

$$\mathbf{J}(u) \triangleq \frac{1}{2} \int_0^\infty [z^T(t)R_1(x)z(t) + u^T(t)R_2(x)u(t)]dt, \quad (5.54)$$

Note that (5.54) differs from (3.25) by the state-dependent weights $R_1(x)$ and $R_2(x)$. Define

$$S(x) \triangleq B(x)R_2^{-1}(x)B^T(x), \quad (5.55)$$

$$W(x) \triangleq H^T(x)R_1(x), \quad (5.56)$$

$$V(x) \triangleq H^T(x)R_1(x)H(x), \quad (5.57)$$

For slow varying command $r(t)$ and disturbance $d(t)$, the SDRE control for command following and disturbance rejection is given in the form (3.30) with the state-dependent feedback gains

$$u(t) = K(x)x(t) + K_r(x)r(t) + K_d(x)d(t), \quad (5.58)$$

where

$$K(x) = -R_2^{-1}(x)B^T(x)\bar{P}(x), \quad (5.59)$$

$$K_r(x) = -R_2^{-1}(x)B^T(x) \left(A^T(x) - \bar{P}(x)S(x) \right)^{-1} W(x), \quad (5.60)$$

$$K_d(x) = R_2^{-1}(x)B^T(x) \left(A^T(x) - \bar{P}(x)S(x) \right)^{-1} \bar{P}(x)D_1(x), \quad (5.61)$$

where $\bar{P}(x)$ is a unique, symmetric, positive-definite solution of the algebraic State-Dependent Riccati Equation (5.11).

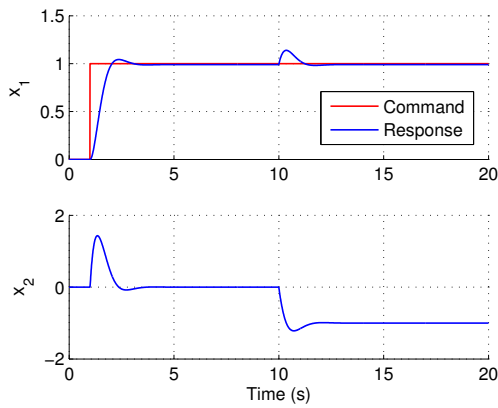
Example 5.5. Command following and disturbance rejection SDRE control of the Van der Pol oscillator

In this example tracking SDRE control is applied. Consider the Van der Pol oscillator (5.26) with the SDC model given by (5.27), (5.30). For an unmatched disturbance, D_1 be given by

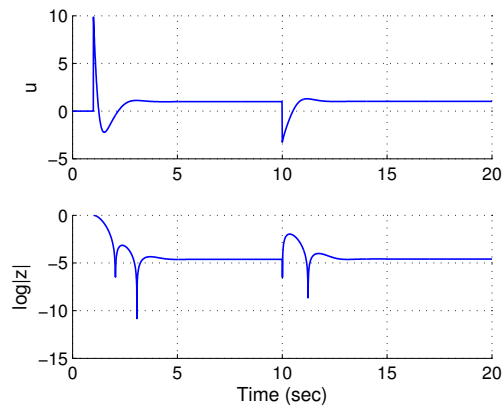
$$D_1 = [1 \ 0]^T, \quad (5.62)$$

Let $\mu = 0.15$, $b = 1$, and $x_0 = [0 \ 0]^T$. For command following, let $H = [1 \ 0]$, that is, $y_r = x_1$.

Consider a unit step command at $t = 1$ sec, and a unit step disturbance at $t = 10$ sec. Let $R_1 = 1$ and $R_2 = 0.01$. Figure 5.9 shows the closed-loop responses. Next, consider a harmonic command $r(t) = \sin(\Omega_1 t)$, and harmonic disturbance

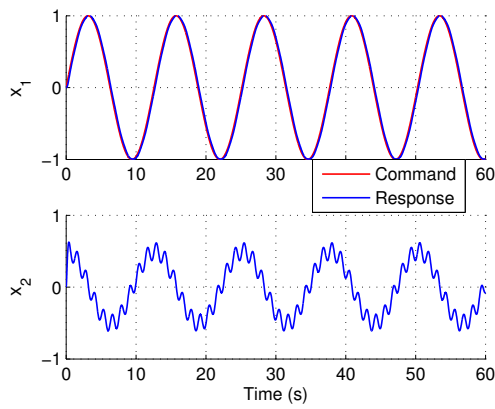


(a) State trajectories

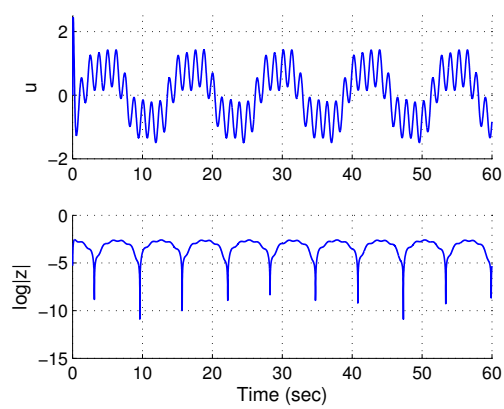


(b) Control input

Figure 5.9: Example 5.5. SDRE control of the Van der Pol oscillator with a step command and step disturbance.



(a) State trajectories



(b) Control input

Figure 5.10: Example 5.5. SDRE control of the Van der Pol oscillator with a harmonic command and harmonic disturbance.

$d(t) = 0.1 \cos(\Omega)2t$, where $\Omega_1 = 0.5$ rad/sec, $\Omega_2 = 5$ rad/sec. Let $R_1 = 100$ and $R_2 = 0.01$. Figure 5.10 shows the closed-loop responses.

CHAPTER 6

FPRE CONTROL FOR NONLINEAR SYSTEMS

FPRE control for nonlinear systems uses analogous approach as FPRE control for LTV systems given in Chapter 4. In this Chapter, full-state-feedback and output-feedback FPRE control is applied for stabilization of nonlinear systems. Next, tracking FPRE and internal-model-based FPRE control for command following and disturbance rejection for nonlinear systems is implemented. Also additional numerical investigation of the performance and robustness of the internal-model-based FPRE control is given in this Chapter.

6.1 FPRE Control for Stabilization of Nonlinear Systems

This section provides discrete-time formulations for the full-state-feedback and output-feedback FPRE control for nonlinear systems.

6.1.1 Full-State-Feedback

Consider the nonlinear discrete-time plant (5.20), given in a SDC form (5.21). The control law is given by

$$u_k = K_k x_k, \quad (6.1)$$

where the feedback gain $K_k \triangleq K(x_k)$ is given by

$$K_k = -(B_k^T P_k B_k + R_{2,k})^{-1} B_k^T P_k A_k, \quad (6.2)$$

and $P_k \triangleq P(x_k)$ is the solution of a state-dependent difference Riccati equation

$$P_{k+1} = A_k^T P_k A_k - A_k^T P_k B_k (B_k^T P_k B_k + R_{2,k})^{-1} B_k^T P_k A_k + R_{1,k}, \quad (6.3)$$

where $R_{1,k} \in \mathbb{R}^{n \times n}$ is positive semidefinite and $R_{2,k} \in \mathbb{R}^{m \times m}$ is positive definite.

Note that FPRE control law (6.1) has the same structure as the control law (5.22) of the SDRE control. The difference is that for SDRE a state-dependent algebraic Riccati equation (5.11) is solved at each instant, assuming that, for all x_k , $(A(x_k), B(x_k))$ is point-wise stabilizable, whereas, for FPRE, stabilizability of $(A(x_k), B(x_k))$ is not required for the forward propagation of the state-dependent difference Riccati equation (6.3).

Example 6.1. Full-state-feedback FPRE control for stabilization of the Van der Pol oscillator

In this example full-state-feedback FPRE control is applied for stabilization of the Van der Pol oscillator (5.26) with the parameters given in Example 5.1. SDC dynamics matrices and the Jacobian are given by (5.27), (5.28), (5.29), and the control matrix is given by (5.30). Let $\mu = 0.15$, $b = 1$, and $x_0 = [3 \ 2]^T$. Let $R_1 = 10I_2$, $R_2 = 0.1$, and initial condition for FPRE is $P_0 = I_2$. Figure 6.1 shows the closed-loop responses.

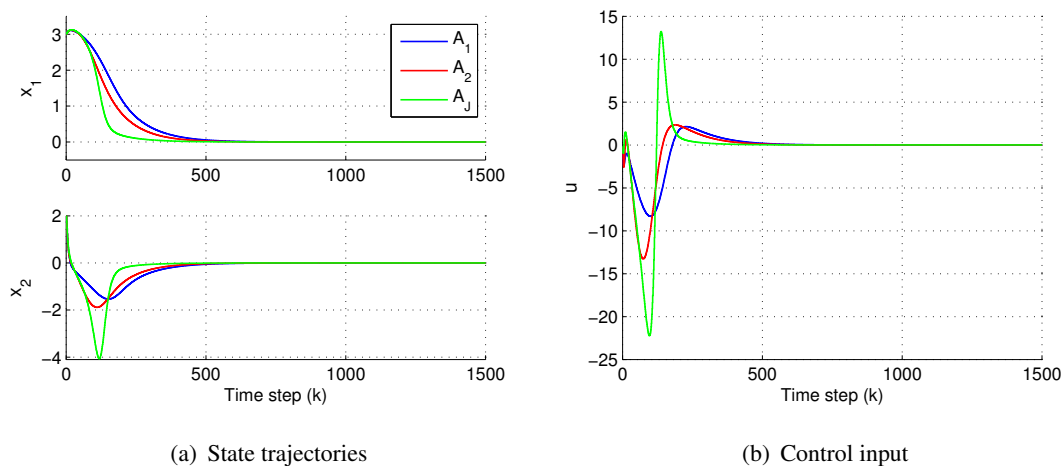


Figure 6.1: Example 6.1. Full-state-feedback FPRE control of the Van der Pol oscillator.

For Pareto plot in Fig. 6.2, $R_1 = 10I_2$, and R_2 ranges from 0.01 to 10.

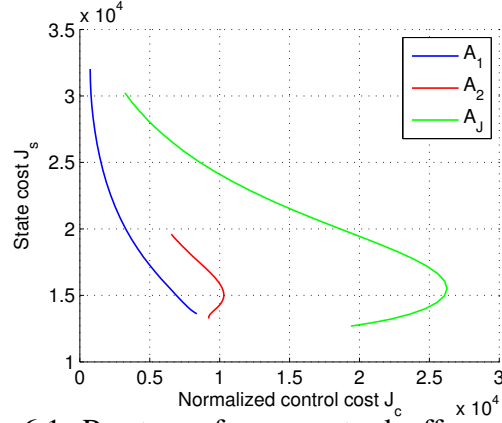
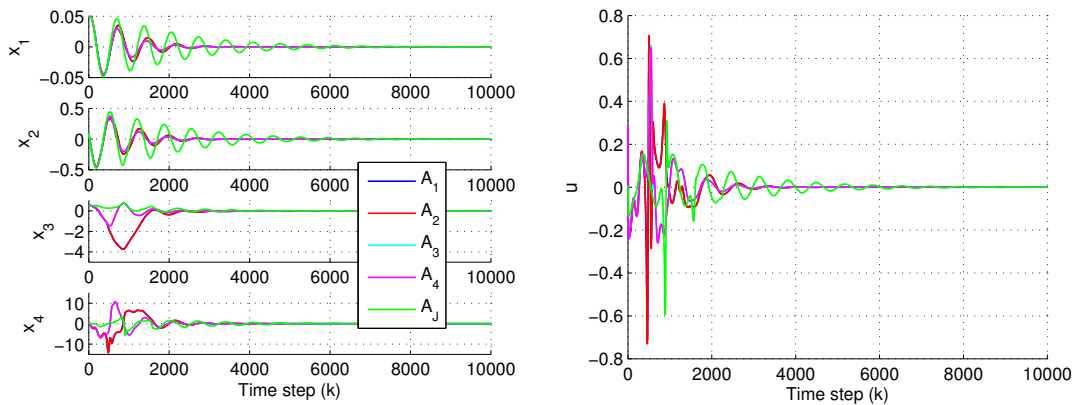


Figure 6.2: Example 6.1. Pareto performance tradeoff curves for full-state-feedback FPRE control of the Van der Pol oscillator.

Example 6.2. Full-state-feedback FPRE control for stabilization of the RTAC

In this example full-state-feedback FPRE control is applied for stabilization of the rotational-translational oscillator (5.31), (5.32), with the parameters given in Example 5.2. SDC dynamics matrices and the Jacobian of the RTAC model (5.33), (5.35) are given by (5.36), (5.37), (5.38), (5.39), (5.40).

Let $x_0 = [0.05 \text{ m}, 0.1 \text{ m/sec}, \pi/6; \text{rad}, 0 \text{ rad/sec}]^T$. Let $R_1 = \text{diag}(10^3 I_2, I_2)$, $R_2 = 1$, for A_1, A_2, A_3, A_4 , and let $R_1 = \text{diag}(10^2 I_2, I_2)$, $R_2 = 1$, for A_J . The initial condition for FPRE is $P_0 = I_4$. The closed-loop responses are shown in Fig. 6.3. .



(a) State trajectories

(b) Control input

Figure 6.3: Example 6.1. Full-state-feedback FPRE control of the RTAC.

6.1.2 Output-Feedback

Consider a discrete-time nonlinear plant (5.20), given in the SDC form (5.21), and the measurement is given by (5.42). For FPRE control, an observer-based compensator has the same structure as in SDRE case (5.43), (5.44), that is

$$\hat{x}_{k+1} = (A_k + B_k K_k - F_k C_k) \hat{x}_k + F_k y_k, \quad (6.4)$$

$$u_k = K_k \hat{x}_k, \quad (6.5)$$

where the regulator gain K_k is the full-state-feedback gain (6.2) computed using (6.3), and the observer gain $F_k \triangleq F(x_k)$ is given by

$$F_k = A_k Q_k C_k^T (C_k Q_k C_k^T + V_{2,k})^{-1}, \quad (6.6)$$

where $Q_k \triangleq Q(x_k)$ in (6.6) is a solution of a discrete-time state-dependent difference estimator Riccati equation

$$Q_{k+1} = A_k Q_k A_k^T - A_k Q_k C_k^T (C_k Q_k C_k^T + V_{2,k})^{-1} C_k Q_k A_k^T + V_{1,k}, \quad (6.7)$$

where $V_{1,k}$ is positive semidefinite, and $V_{2,k}$ is positive definite.

Same as for output-feedback SDRE control, since the full state is not available, the state x_k in the SDC matrices is replaced by its estimate \hat{x}_k , resulting in $A(\hat{x}_k)$, $B(\hat{x}_k)$, $C(\hat{x}_k)$. If measurement y_k includes components of x_k , then the corresponding components of \hat{x}_k are replaced by the measurements; the modified state estimate is denoted by \tilde{x}_k . Then, for use in the observer-based compensator $A(\hat{x}_k)$, $B(\hat{x}_k)$, $C(\hat{x}_k)$ are replaced by $A(\tilde{x}_k)$, $B(\tilde{x}_k)$, $C(\tilde{x}_k)$

Example 6.3. Output-feedback FPRE control for stabilization of the Van der Pol oscillator

In this example output-feedback FPRE control is applied for stabilization of the Van der Pol oscillator (5.26) with the parameters given in Example 5.1. SDC dynamics matrices and the Jacobian are given by (5.27), (5.28), (5.29), and the control matrix is given by (5.30). Let $\mu = 0.15$, $b = 1$, and $x_0 = [3 \ 2]^T$. For the output feedback, assume that measurements of x_1 are available, and thus, $C = [1 \ 0]$. Let $R_1 = 10I_2$, $R_2 = 1$, $V_1 = I_2$, $V_2 = 0.1$. Let $\hat{x}_0 = 0$ and initial conditions for FPRE are $P_0 = I_2$, $Q_0 = I_2$. Figure 6.4 shows the closed-loop responses.

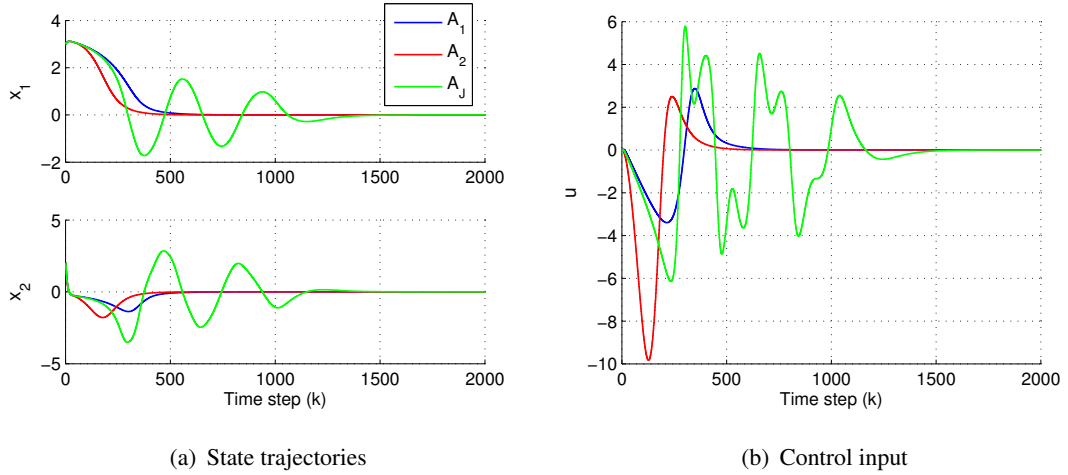


Figure 6.4: Example 6.3. Output-feedback FPRE control of the Van der Pol oscillator.

For Pareto plot in Fig. 6.5, $R_1 = 10I_2$, and R_2 ranges from 0.01 to 10.

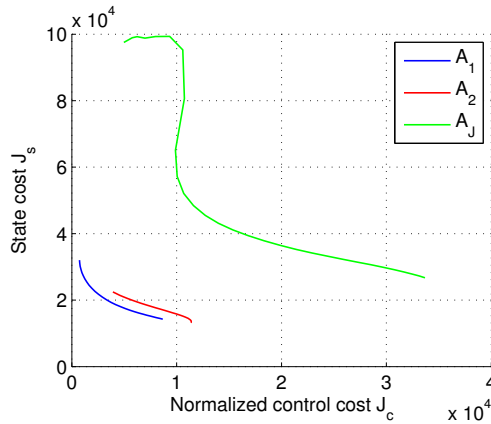


Figure 6.5: Example 6.3. Pareto performance tradeoff curves for output-feedback FPRE control of the Van der Pol oscillator.

Example 6.4. Output-feedback FPRE control for stabilization of the RTAC

In this example output-feedback FPRE control is applied for stabilization of the rotational-translational oscillator (5.31), (5.32), with the parameters given in Example 5.2. SDC dynamics matrices and the Jacobian of the RTAC model (5.33), (5.35) are given by (5.36), (5.37), (5.38), (5.39), (5.40).

Let $x_0 = [0.05 \text{ m}, 0.1 \text{ m/sec}, \pi/6; \text{rad}, 0 \text{ rad/sec}]^T$. Consider three cases of measurements that are available, namely, cart position, arm angle, cart position and arm angle. In the first case, where only cart position measurements are available, let $R_1 = \text{diag}(10^2 I_2, I_2)$, $R_2 = 0.01$, $V_1 = I_4$, $V_2 = 0.01$. Let $\hat{x}_0 = 0$, and initial

conditions for FPRE are $P_0 = I_4, Q_0 = I_4$. The closed-loop responses are shown in Fig. 6.6.

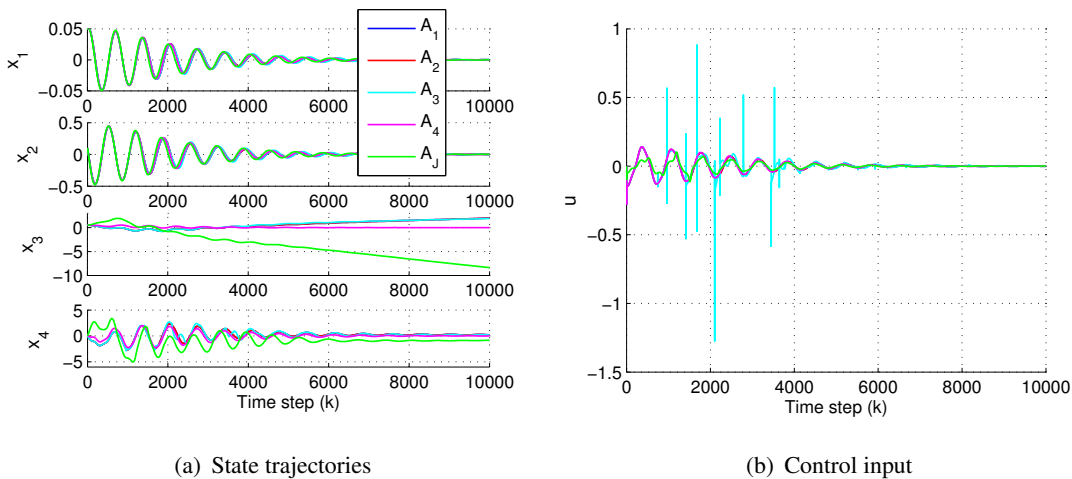


Figure 6.6: Example 6.4. Output-feedback FPRE control of the RTAC with cart position measurements.

In the second case, where arm angle measurements are available, let

$R_1 = \text{diag}(10^2 I_2, I_2)$, $R_2 = 0.1$ for A_1, A_2, A_3, A_4 , and $R_1 = \text{diag}(10 I_2, I_2)$, $R_2 = 1$ for A_J . $V_1 = I_4$, $V_2 = 0.1$ for A_1, A_2, A_3, A_4, A_J . Let $\hat{x}_0 = 0$, and initial conditions for FPRE are $P_0 = I_4, Q_0 = I_4$. The closed-loop responses are shown in Fig. 6.7.

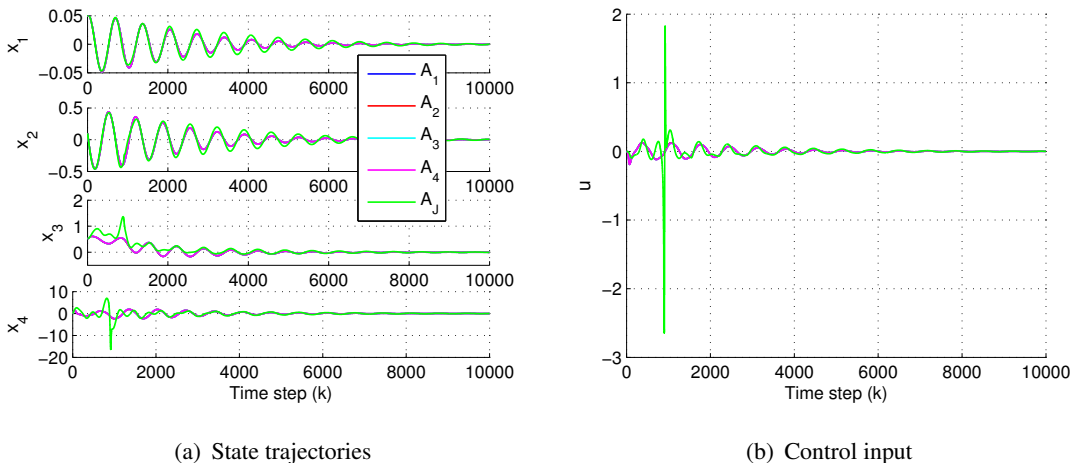


Figure 6.7: Example 6.4. Output-feedback FPRE control of the RTAC with arm angle measurements.

In the third case, where cart position and arm angle measurements are available, let $R_1 = \text{diag}(10^2 I_2, I_2)$, $R_2 = 1$, $V_1 = I_4$, $V_2 = 0.1 I_2$ for A_1, A_2, A_3, A_4, A_J . Let

$\hat{x}_0 = 0$, and initial conditions for FPRE are $P_0 = I_4$, $Q_0 = I_4$. The closed-loop responses are shown in Fig. 6.8, and illustrate that SDRE with A_J executes poor performance in stabilizing the plant.

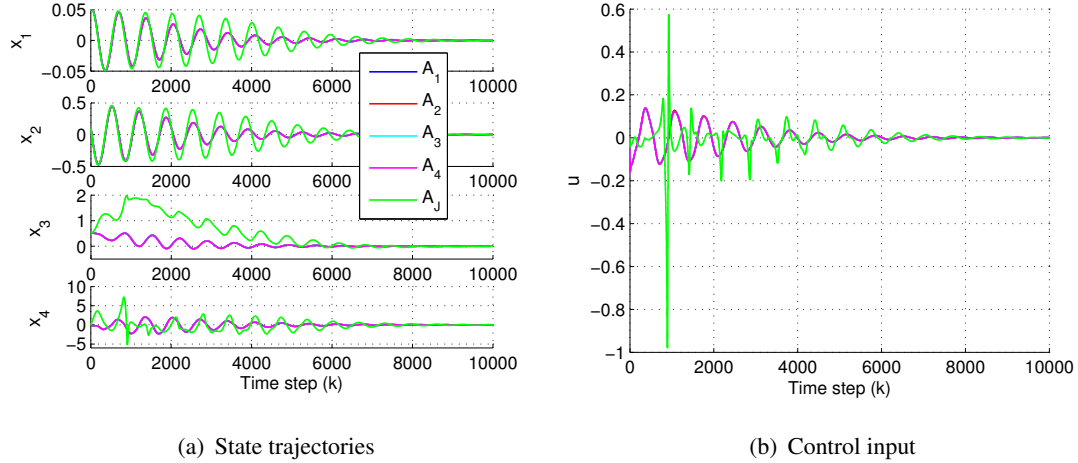


Figure 6.8: Example 6.4. Output-feedback FPRE control of the RTAC with cart position and arm angle measurements.

6.2 FPRE for Command Following and Disturbance Rejection

For FPRE control for command following and disturbance rejection for nonlinear systems, nonlinear dynamics is considered to be given in a state-dependent coefficient form $\dot{x}(t) = A(x)x(t) + B(x)u(t) + D_1(x)d(t)$. Next, the same approach as given in Chapter 4 for LTV systems is applied for tracking FPRE control and internal-model-based FPRE control, but now the time-varying matrices $A(t)$, $B(t)$, $H(t)$, $C(t)$, $D_1(t)$ are replaced by the corresponding SDC matrices $A(x)$, $B(x)$, $H(x)$, $C(x)$, $D_1(x)$.

The detailed procedure is given below.

6.2.1 Tracking FPRE Control

Consider a nonlinear plant (5.49), (5.50), which is given in the SDC form (5.51), (5.52). The control law is given by

$$\begin{aligned} u(t) &= -R_2^{-1}(x)B^T(x)[P(x)x(t) - g(x)] \\ &= K(x)x(t) + R_2^{-1}(x)B^T(x)g(t), \end{aligned} \quad (6.8)$$

where the full-state feedback gain $K(x)$ is given by

$$K(x) = -R_2^{-1}(x)B^T(x)P(x), \quad (6.9)$$

$P(x)$ and $g(x)$ are the solutions of the forward propagating differential equations with state-dependent coefficients

$$\dot{P}(x) = P(x)A(x) + A^T(x)P(x) - P(x)S(x)P(x) + V(x), \quad (6.10)$$

$$\dot{g}(x) = [A^T(x) - P(x)S(x)]g(x) + W(x)r(t) - P(x)D_1(x)d(t), \quad (6.11)$$

with a positive-semidefinite initial condition $P(0) = P_0$ for (6.10), and an initial condition $g(0) = g_0$ for (6.11). Note that, $S(x)$, $W(x)$, $V(x)$ are defined by (5.55), (5.56), (5.57).

Example 6.5. Command following and disturbance rejection FPRE control of the Van der Pol oscillator

Consider the Van der Pol oscillator (5.26) with the SDC model given by (5.27), (5.30). For an unmatched disturbance, D_1 be given by (5.62). Let $\mu = 0.15$, $b = 1$, and $x_0 = [0 \ 0]^T$. For command following, let $H = [1 \ 0]$, that is, $y_r = x_1$.

Consider a unit step command at $t = 1$ sec, and a unit step disturbance at $t = 10$ sec. Let $R_1 = 1$ and $R_2 = 0.01$, and initial conditions for FPRE control are $P(0) = I_2$ and $g(0) = 0$. Figure 6.9 shows the closed-loop responses. Next, consider a harmonic command $r(t) = \sin(\Omega_1 t)$, and harmonic disturbance $d(t) = 0.1 \cos(\Omega_2 2t)$, where $\Omega_1 = 0.5$ rad/sec, $\Omega_2 = 5$ rad/sec. Let $R_1 = 100$ and $R_2 = 0.01$. Figure 6.10 shows the closed-loop responses.

6.2.2 Internal-Model-Based FPRE Control

In this section a discrete-time formulation for the internal-model-based FPRE control for command following and disturbance rejection is presented. This control approach is analogous to the internal-model-based FPRE control for LTV systems, given in Chapter 4.

Consider the discrete-time nonlinear system

$$x_{k+1} = f(x_k, u_k) + D_1(x_k)d_k, \quad x_0 = x_0, \quad (6.12)$$

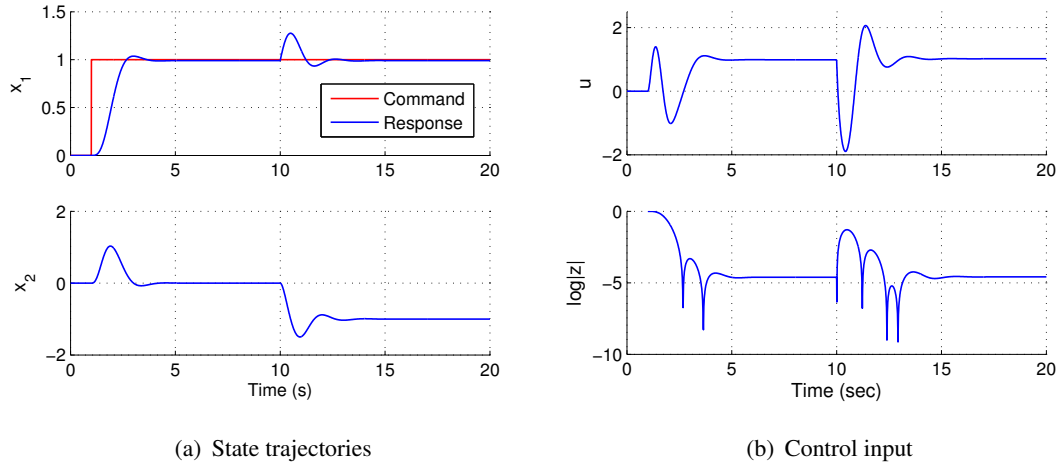


Figure 6.9: Example 6.5. FPRE control of the Van der Pol oscillator with a step command and step disturbance.

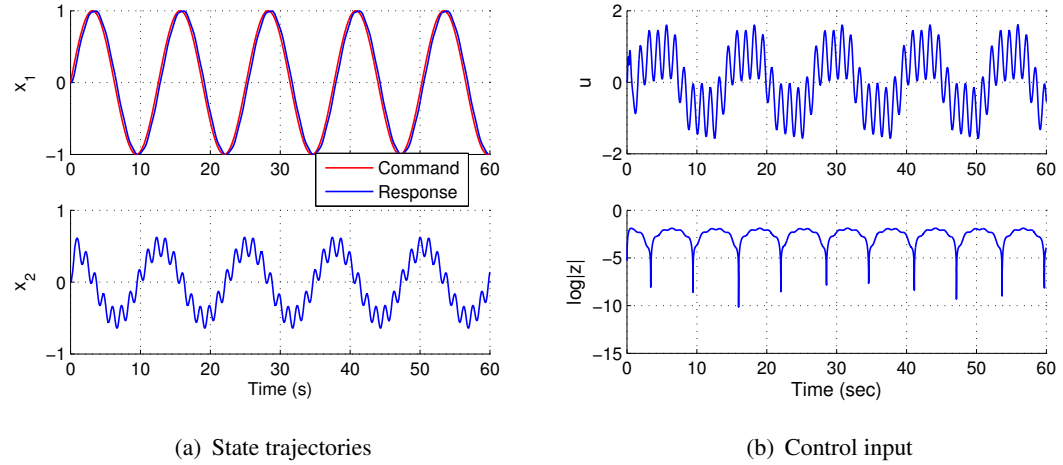


Figure 6.10: Example 6.5. FPRE control of the Van der Pol oscillator with a harmonic command and harmonic disturbance.

where $x_k \in \mathbb{R}^n$, $u_k \in \mathbb{R}$, $d_k \in \mathbb{R}$, and, for all $x_k \in \mathbb{R}^n$ and $u_k \in \mathbb{R}$, $f(x_k, u_k) \in \mathbb{R}^n$. It is assumed that (6.12) can be written in the SDC form

$$x_{k+1} = A(x_k)x_k + B(x_k)u_k + D_1(x_k)d_k, \quad (6.13)$$

where $A(x_k) \in \mathbb{R}^{n \times n}$, $B(x_k) \in \mathbb{R}^n$, and $D_1(x_k) \in \mathbb{R}^n$. Following sections give the full-state-feedback and output-feedback internal-model-based FPRE control.

6.2.2.1 Full-State Feedback

For internal-model-based full-state feedback, consider the nonlinear system (6.12) in SDC form (6.13). For the command r and the output y_r given by (3.35), the command-following error is given by (3.36). For nonlinear systems, replace the constant matrices A , B , D_1 in the augmented plant (3.38), (3.39) by the SDC matrices $A(x_k)$, $B(x_k)$, $D_1(x_k)$, which results in the SDC matrices $A_a(x_k)$, $B_a(x_k)$. Thus, the control law is given by (3.40) and utilizes FPFE control (3.44), (3.45) with the constant matrices A_a , B_a replaced by the SDC matrices $A_a(x_k)$, $B_a(x_k)$. The weighting matrices R_1 , R_2 in (3.44) and (3.45) can be replaced by state-dependent weighting matrices $R_1(x_k)$, $R_2(x_k)$.

6.2.2.2 Output Feedback

In place of (6.12), assume that the measurements have the form

$$y_{\text{meas},k} = h(x_k), \quad (6.14)$$

where $y_{\text{meas},k} \in \mathbb{R}^m$ and $h : \mathbb{R}^n \rightarrow \mathbb{R}^m$. Assume that (6.14) can be written in the form

$$y_{\text{meas},k} = C_{\text{meas}}(x_k)x_k, \quad (6.15)$$

where $C_{\text{meas}}(x_k) \in \mathbb{R}^{m \times n}$. Then, (6.15) can be written in the form of (3.66) as

$$y_{\text{meas},k} = \begin{bmatrix} y_{r,k} \\ y_k \end{bmatrix} = C_{\text{meas}}(x_k)x_k, \quad (6.16)$$

where $C_{\text{meas}}(x_k) = \begin{bmatrix} H \\ C(x_k) \end{bmatrix}$, $H \in \mathbb{R}^{1 \times n}$, and $C(x_k) \in \mathbb{R}^{(m-1) \times n}$.

Note that the state x in the coefficient matrices in (6.13) and (6.16) is replaced by its estimate \hat{x} , resulting in $A(\hat{x})$, $B(\hat{x})$, $C(\hat{x})$, $D_1(\hat{x})$. If y_{meas} includes components of x , then the corresponding components of \hat{x} in the SDC's are replaced by the measurements; the modified state estimate is denoted by \tilde{x} . Then, for use in the observer-based compensator $A(\hat{x})$, $B(\hat{x})$, $C(\hat{x})$, $D_1(\hat{x})$ are replaced by $A(\tilde{x})$, $B(\tilde{x})$, $C(\tilde{x})$, $D_1(\tilde{x})$.

The internal-model-based output-feedback control law for nonlinear systems uses the FPFE control (3.44), (3.45) and the augmented observer-based compensator (3.76),

(3.77), and is obtained using (3.78)-(3.80) with the matrices A, B, C in (3.69), (3.70) replaced by $A(\tilde{x}_k), B(\tilde{x}_k), C(\tilde{x}_k)$, the matrices A_a, B_a, C_a in (3.44), (3.45), (3.69), (3.70), (3.76), (3.77) replaced by $A_a(\tilde{x}_k), B_a(\tilde{x}_k), C_a(\tilde{x}_k)$, and the matrices A_c, B_c, C_c in (3.78), (3.79), (3.80) replaced by $A_c(\tilde{x}_k), B_c(\tilde{x}_k), C_c(\tilde{x}_k)$. The weighting matrices R_1, R_2, V_1, V_2 in (3.44), (3.45), (3.76) and (3.77) can be replaced by state-dependent weighting matrices $R_1(\tilde{x}_k), R_2(\tilde{x}_k), V_1(\tilde{x}_k), V_2(\tilde{x}_k)$.

6.2.2.3 Numerical Investigation of Performance and Robustness

In the absence of theoretical guarantees as in the case of LQG control of LTI plants, the performance of the FPRE full-state-feedback and output-feedback controllers depends strongly on the choice of the weighting matrices R_1, R_2, V_1, V_2 . In particular, the key challenge is to choose R_1, R_2 so that the solution P_k of (3.45) remains bounded.

Another aspect of FPRE control is the choice of the initial condition $P_{a,0}$ in (3.45). The choice $P_{a,0} = \alpha I_{n+n_{im}}$, where $\alpha \geq 0$, typically provides a convergent solution $P_{a,k}$. However, increasing α tends to increase the transient control input u . For nonlinear systems, another "good" choice for $P_{a,0}$ is a solution \bar{P}_a of the ARE, obtained using the SDC matrices $A_a(x_k)$ and $B_a(x_k)$, which are evaluated at the initial state x_0 ; however, this requires that $(A_a(x_0), B_a(x_0))$ be stabilizable. These and related issues are investigated in the following examples.

Example 6.6. Internal-model based FPRE control for command following and disturbance rejection of the Van der Pol oscillator.

Consider the Van der Pol oscillator (5.26), with the SDC parameterizations given by (5.27), (5.28), and the input matrix (5.30). For an unmatched disturbance, let D_1 be given by (4.29). Let $T_s = 0.01$ sec, and define the corresponding discrete-time SDC's by A_1 and A_2 .

For full-state feedback, let $y_r = q$. For output feedback, let $y_{meas} = y_r = q$, and thus C is omitted. Let $\mu = 0.15, b = 1, x_0 = [0.5 \ 0.5]^T$, and $\hat{x}_{a,0} = 0$ for output feedback. Consider a harmonic command $r_k = \sin(\Omega_1 k)$, and harmonic disturbance $d_k = \cos(\Omega_2 k)$, with $\Omega_1 = 0.01$ rad/sample and $\Omega_2 = 0.05$ rad/sample.

Let $R_1 = I_6$, $R_2 = 10^8$ for full-state feedback and output feedback, and let $V_1 = R_1$, $V_2 = 1$ for output feedback. Let $P_{a,0} = \bar{P}_a$ and $Q_{a,0} = \bar{Q}_a$, where \bar{P}_a and \bar{Q}_a are solutions of (3.43) and (3.75) with the coefficients $A_a = A_a(x_0)$, $B_a = B_a(x_0)$, $C_a = C_a(x_0)$. Figures 6.11 and 6.12 show the closed-loop responses for full-state feedback and output feedback, respectively.

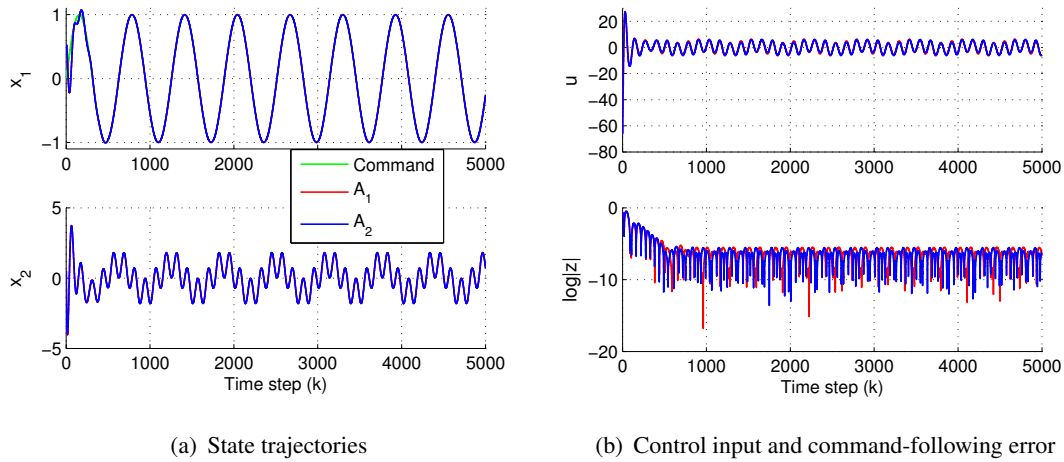


Figure 6.11: Example 6.6. Internal-model-based, full-state-feedback FPRE control of the Van der Pol oscillator.

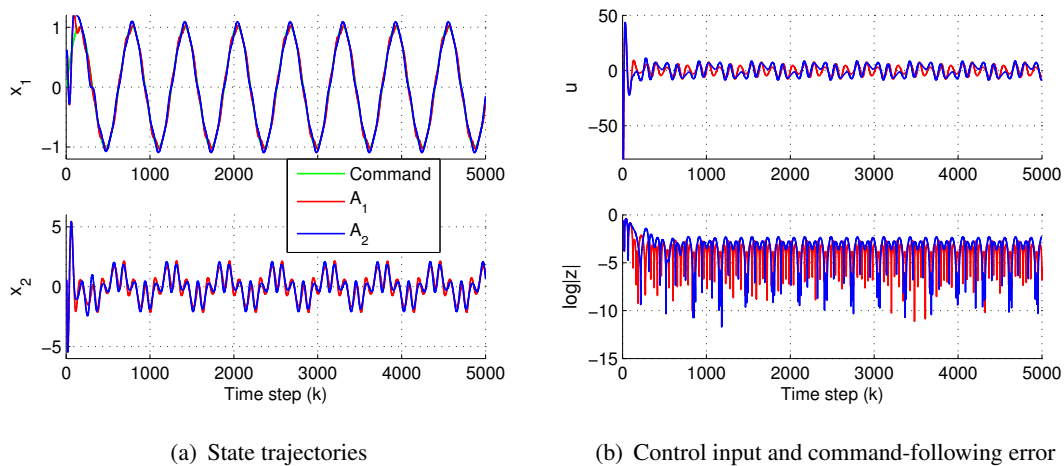


Figure 6.12: Example 6.6. Internal-model-based, output-feedback FPRE control of the Van der Pol oscillator.

Example 6.7. Internal-model based FPRE control for command following and disturbance rejection of the RTAC.

Consider the rotational-translational oscillator actuator given in Example 5.2 (5.31),

(5.32). SDC dynamics of RTAC model (5.33) are given by (5.35), (5.36), (5.37), (5.38), (5.39). Parameters are given in Table 5.1.

The goal is to make the cart follow a harmonic trajectory in the presence of a harmonic disturbance acting on the cart. For full-state feedback and output feedback, let $y_r = q$. For output feedback, the cart position and arm angle are measured, that is, $y_{\text{meas}} = [q \ \theta]^T$, and thus $C = [0 \ 0 \ 1 \ 0]$. Let $x_0 = [0.05 \text{ m}, 0 \text{ m/sec}, \pi/6 \text{ rad}, 0 \text{ rad/sec}]^T$, and let $\hat{x}_{a,0} = 0$ for output feedback.

Consider a harmonic command $r_k = 0.015 \sin(\Omega k)$ m, and harmonic disturbance $d_k = 0.1 \cos(\Omega k)$ N, with the frequency $\Omega = 0.007$ rad/sample, which corresponds to the continuous-time frequency 7 rad/sec. The damped natural frequency of the RTAC is approximately 0.01 rad/sample with a damping ratio of 8%. Let $R_1 = \text{diag}(10^3 I_4, 10^{-3} I_2)$, $R_2 = 1$ for full-state feedback and output feedback, and $V_1 = \text{diag}(I_4, 10^4 I_2)$, $V_2 = I_2$ for output feedback. Let $P_{a,0} = I_{n+n_{\text{im}}}$ and $Q_{a,0} = I_{n+n_{\text{im}}}$. The responses for full-state feedback and output feedback are shown in Figures 6.13 and 6.14, respectively, where all SDC's provide similar state responses. However, the control inputs for A_1 and A_2 exhibit oscillations with larger magnitudes than the control inputs for A_3 and A_4 .

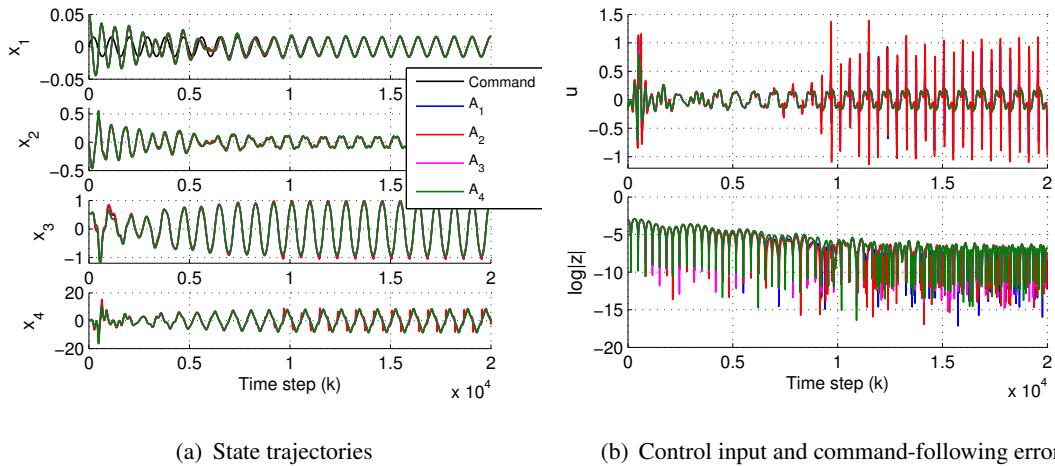


Figure 6.13: Example 6.7. Internal-model-based, full-state-feedback control of the RTAC.

To investigate the range of commendable amplitudes and frequencies in the absence of disturbances, consider harmonic commands with amplitude ranging within $[0.005, 0.12]$ m and frequency ranging within $[0.005, 0.02]$ rad/sample. Figure 6.15

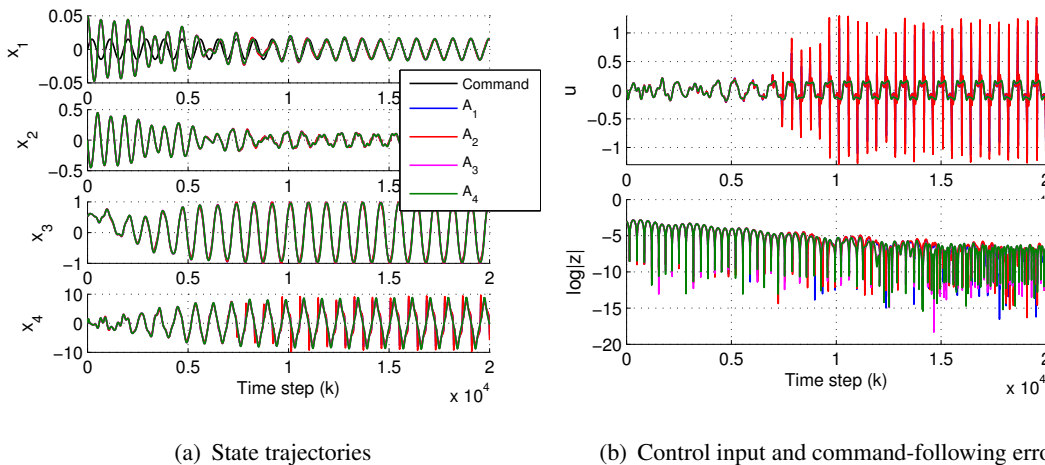


Figure 6.14: Example 6.7. Internal-model-based, output-feedback control of the RTAC.

shows the achievable amplitudes and frequencies for output feedback using SDC A_1 . "x" denotes amplitude/frequency values for which command-following was not achieved. Note that, for command frequencies close to the undamped natural frequency of RTAC, the controller is able to follow commands with larger amplitudes.

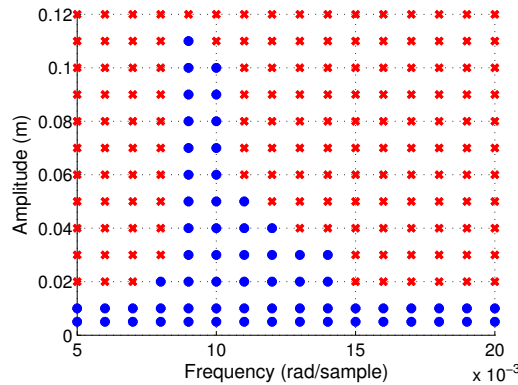


Figure 6.15: Example 6. Amplitude vs frequency for internal-model-based, output-feedback control of the RTAC.

Example 6.8. Internal-model based FPRE control for command following and disturbance rejection for the ball and beam.

The ball and beam, shown in Fig. 6.16, consists of a symmetric beam with inertia J that rotates in a vertical plane by applying a torque τ . A ball of mass M slides without

friction along the beam. The goal is controlling the position q of the ball along the beam.

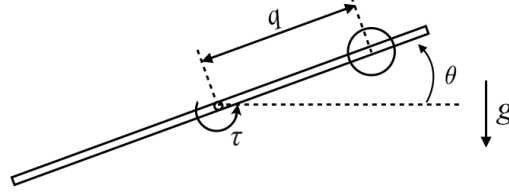


Figure 6.16: Ball and beam system.

Neglecting the inertia of the ball, the equations of motion of the ball and beam are given by [102, 59]

$$\ddot{q} + g \sin \theta - q\dot{\theta}^2 = 0, \quad (6.17)$$

$$(Mq^2 + J)\ddot{\theta} + 2Mq\dot{q}\dot{\theta} + M g q \cos \theta = \tau. \quad (6.18)$$

For the state vector $x \triangleq [q \dot{q} \theta \dot{\theta}]^T$, (6.17), (6.18) can be written as

$$\dot{x}_1 = x_2, \quad (6.19)$$

$$\dot{x}_2 = -g \sin x_3 + x_1 x_4^2, \quad (6.20)$$

$$\dot{x}_3 = x_4, \quad (6.21)$$

$$\dot{x}_4 = -\frac{2M}{Mx_1^2 + J}x_1x_2x_4 - \frac{Mg}{Mx_1^2 + J}x_1 \cos x_3 + \frac{1}{Mx_1^2 + J}\tau. \quad (6.22)$$

The ball and beam equations (6.19)-(6.22) involve four nonlinear terms that can be factored. Note that $\sin x_3$ can be factored in one way, namely, $\sin x_3 = ((\sin x_3)/x_3)x_3$; $x_1x_4^2$ can be factored in two ways, namely, $x_1x_4^2 = (x_1x_4)x_4 = (x_4^2)x_1$; $x_1x_2x_4$ can be factored in three ways, namely, $x_1x_2x_4 = (x_1x_2)x_4 = (x_1x_4)x_2 = (x_2x_4)x_1$; and $x_2 \cos x_3$ can be factored in one way, namely, $x_2 \cos x_3 = (\cos x_3)x_2$. Consequently,

six SDC's can be obtained in this way, namely,

$$\begin{aligned}
A_{1,\text{cont}}(x) &= \begin{bmatrix} 0 & 1 & 0 & 0 \\ x_4^2 & 0 & -\frac{g \sin x_3}{x_3} & 0 \\ 0 & 0 & 0 & 1 \\ -\frac{Mg \cos x_3 + 2Mx_2x_4}{Mx_1^2 + J} & 0 & 0 & 0 \end{bmatrix}, \\
A_{2,\text{cont}}(x) &= \begin{bmatrix} 0 & 1 & 0 & 0 \\ x_4^2 & 0 & -\frac{g \sin x_3}{x_3} & 0 \\ 0 & 0 & 0 & 1 \\ -\frac{Mg \cos x_3}{Mx_1^2 + J} & -\frac{2Mx_1x_4}{Mx_1^2 + J} & 0 & 0 \end{bmatrix}, \\
A_{3,\text{cont}}(x) &= \begin{bmatrix} 0 & 1 & 0 & 0 \\ x_4^2 & 0 & -\frac{g \sin x_3}{x_3} & 0 \\ 0 & 0 & 0 & 1 \\ -\frac{Mg \cos x_3}{Mx_1^2 + J} & 0 & 0 & -\frac{2Mx_1x_2}{Mx_1^2 + J} \end{bmatrix}, \\
A_{4,\text{cont}}(x) &= \begin{bmatrix} 0 & 1 & 0 & 0 \\ 0 & 0 & -\frac{g \sin x_3}{x_3} & x_1x_4 \\ 0 & 0 & 0 & 1 \\ -\frac{Mg \cos x_3 + 2Mx_2x_4}{Mx_1^2 + J} & 0 & 0 & 0 \end{bmatrix}, \\
A_{5,\text{cont}}(x) &= \begin{bmatrix} 0 & 1 & 0 & 0 \\ 0 & 0 & -\frac{g \sin x_3}{x_3} & x_1x_4 \\ 0 & 0 & 0 & 1 \\ -\frac{Mg \cos x_3}{Mx_1^2 + J} & -\frac{2Mx_1x_4}{Mx_1^2 + J} & 0 & 0 \end{bmatrix}, \\
A_{6,\text{cont}}(x) &= \begin{bmatrix} 0 & 1 & 0 & 0 \\ 0 & 0 & -\frac{g \sin x_3}{x_3} & x_1x_4 \\ 0 & 0 & 0 & 1 \\ -\frac{Mg \cos x_3}{Mx_1^2 + J} & 0 & 0 & -\frac{2Mx_1x_2}{Mx_1^2 + J} \end{bmatrix}.
\end{aligned}$$

The control matrix is $B_{\text{cont}}(x) = [0 \ 0 \ 0 \ 1/(Mx_1^2 + J)]^T$, and the unmatched disturbance $D_{1,\text{cont}} = [0 \ 1 \ 0 \ 0]^T$ is applied to the ball. Let $T_s = 0.001$ sec, and define the corresponding discrete-time SDC's by $A_1, A_2, A_3, A_4, A_5, A_6$. Parameters for this system are given in Table 6.1.

For full-state feedback and output feedback, let $y_r = q$. For output feedback, the

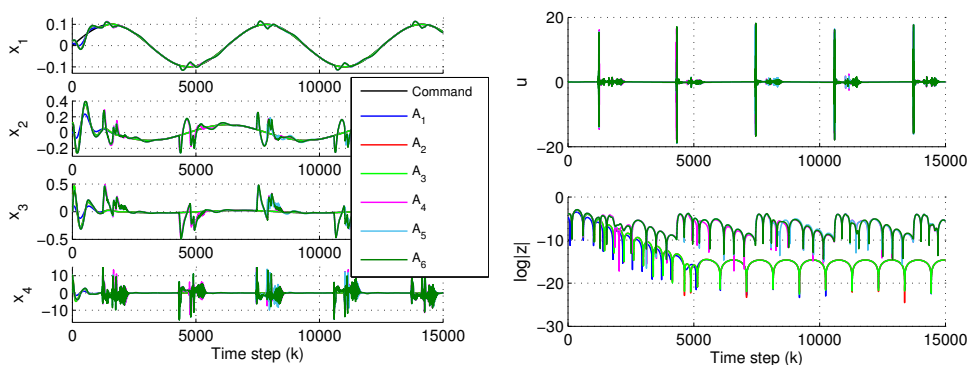
Table 6.1: Ball and Beam Parameters

Parameter	Value	Units
Ball mass (M)	0.1	kg
Ball radius (R)	0.015	m
Beam inertia (J)	10^{-5}	kg-m ²
Gravitational acceleration (g)	9.8	m/sec ²

ball position and the beam angle are measured, that is, $y_{\text{meas}} = [q \ \theta]^T$, and thus $C = [0 \ 0 \ 1 \ 0]$. Let $x_0 = [0.02 \text{ m}, 0.1 \text{ m/sec}, 0 \text{ rad}, 0 \text{ rad/sec}]^T$, and $\hat{x}_{a,0} = 0$ for output feedback. The harmonic command r and harmonic disturbance d are given by $r_k = 0.1 \sin(\Omega k)$ m and $d_k = 0.2 \cos(\Omega k)$ N, with $\Omega = 0.001$ rad/sample.

Let $R_1 = \text{diag}(1, 10^2 I_2, 10^4, 0.1 I_2)$, $R_2 = 10^4$ for full-state feedback and output feedback, and $V_1 = \text{diag}(I_4, 10^4 I_2)$, $V_2 = I_2$ for output feedback. Let $P_{a,0} = \bar{P}_a$ and $Q_{a,0} = \bar{Q}_a$. Figures 6.17 and 6.18 show the responses for the six SDC's for full-state feedback and output feedback. Note that A_1, A_2, A_3 provide similar performance, whereas high-frequency oscillations are present in the responses for A_4, A_5, A_6 .

Let $R_2 = 10^5$, Figures 6.19 and 6.20 show that the high-frequency oscillations are removed, and all six SDC's give similar responses.

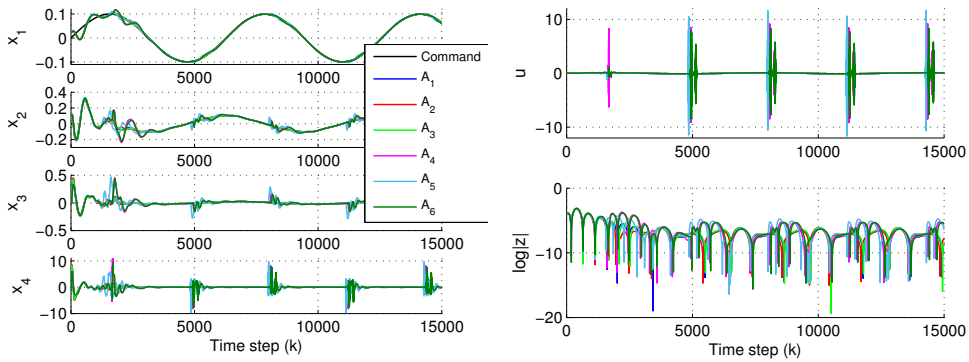


(a) State trajectories

(b) Control input and command-following error

Figure 6.17: Example 6.8. Internal-model-based, full-state-feedback FPRE control of the ball and beam.

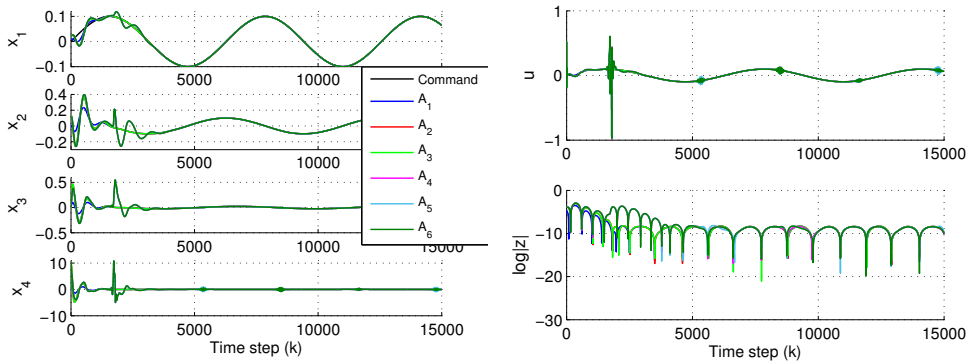
Now, the frequency of the command and disturbance is increased to $\Omega = 0.005$ rad/sample. All six SDC's give similar responses for both full-state feedback and



(a) State trajectories

(b) Control input and command-following error

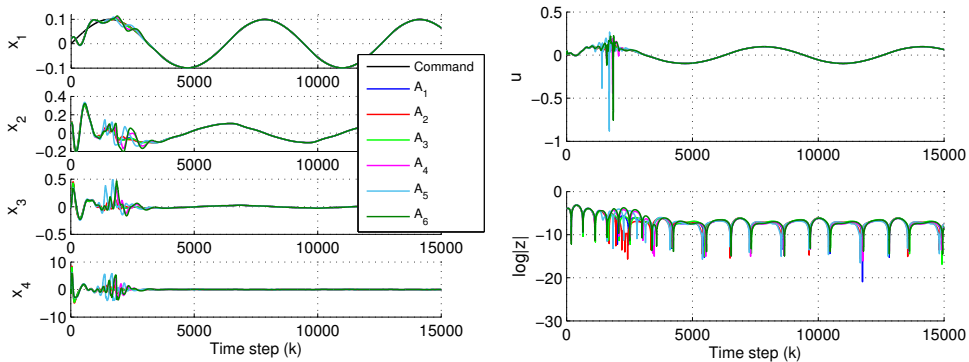
Figure 6.18: Example 6.8. Internal-model-based, output-feedback FPRE control of the ball and beam.



(a) State trajectories

(b) Control input and command-following error

Figure 6.19: Example 6.8. Internal-model-based, full-state-feedback FPRE control of the ball and beam.



(a) State trajectories

(b) Control input and command-following error

Figure 6.20: Example 6.8. Internal-model-based, output-feedback FPRE control of the ball and beam.

output feedback with $R_2 = 1$. The results for output feedback as shown in Fig. 6.21.

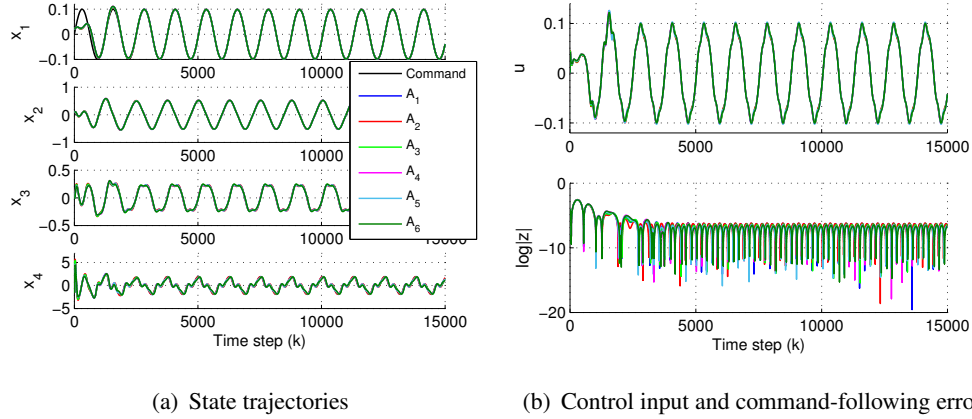


Figure 6.21: Example 6.8. Internal-model-based, output-feedback FPRE control of the ball and beam.

Next, consider a triangular wave command with amplitude 0.1 m, and let $d = 0$. The internal model is the double integrator (3.56), and let $R_1 = \text{diag}(1, 10^2 I_2, 10^4, 0.1 I_2)$, $R_2 = 1$, $V_1 = \text{diag}(I_4, 10^4 I_2)$, $V_2 = I_2$. The response for output feedback with SDC A_1 is shown in Fig. 6.22.

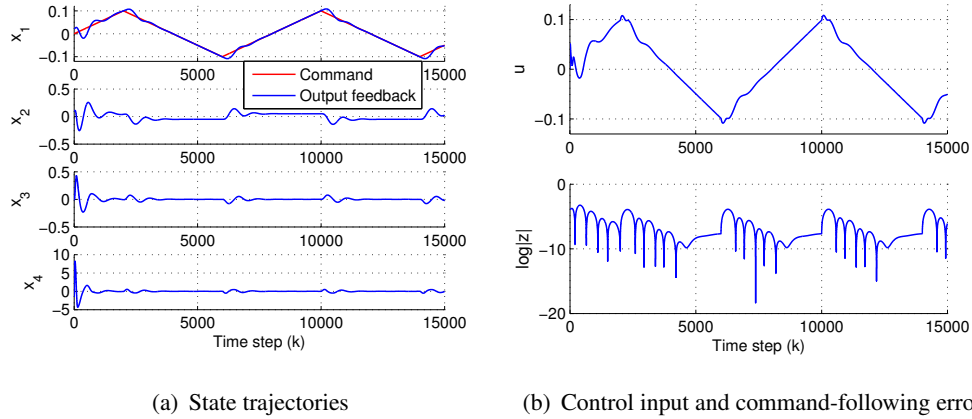
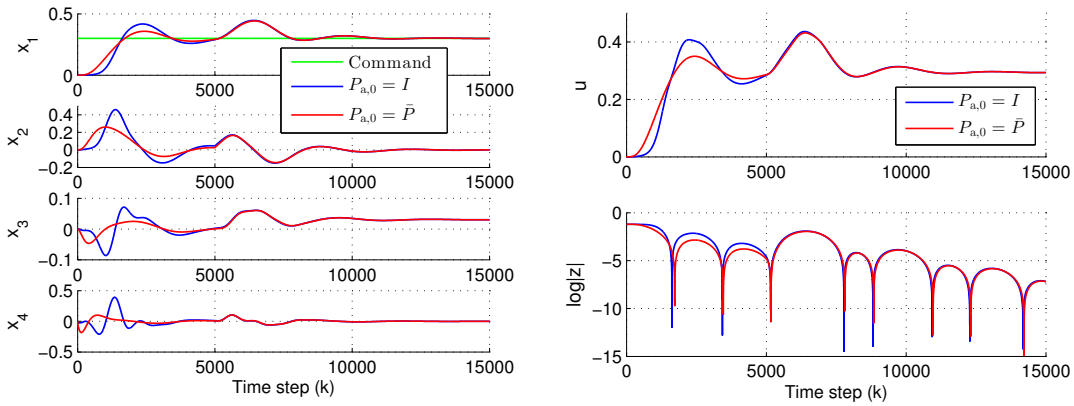


Figure 6.22: Example 6.8. Internal-model-based, output-feedback FPRE control of the ball and beam.

6.2.2.4 Effect of initial condition $P_{a,0}$ for the Ball and Beam

Example 6.9. To investigate the effect of the initial condition $P_{a,0}$ on the performance of FPRE, consider output feedback as in Example 6.8. The goal here is to compare the

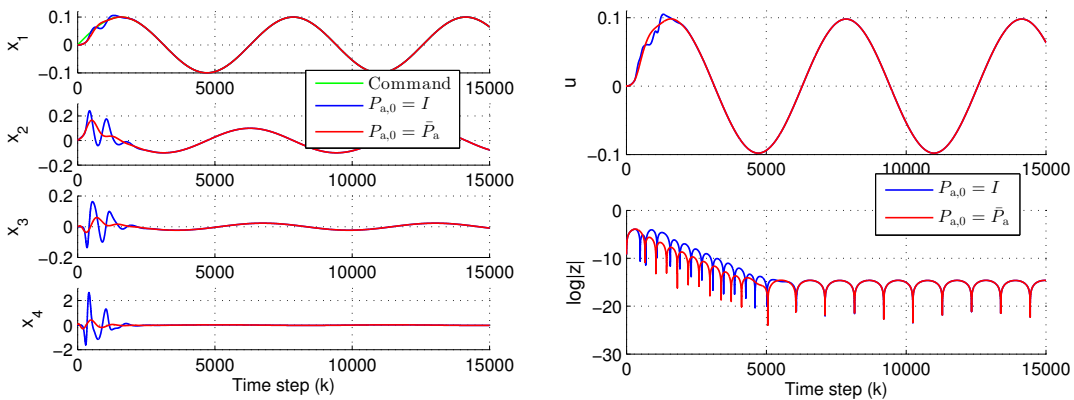
performance for the initial conditions $P_{a,0} = I_{n+n_{im}}$ and $P_{a,0} = \bar{P}_a$, where \bar{P}_a is the solution to (3.43), with the coefficients $A_a = A_a(x_0)$, $B_a = B_a(x_0)$. The weighting matrices R_1, R_2, V_1, V_2 are the same for both choices of $P_{a,0}$. Figures 6.23 and 6.24 show that the transient response with the initial condition $P_{a,0} = \bar{P}_a$ is better than for $P_{a,0} = I_{n+n_{im}}$. However, the rate of convergence is the same for both choices of the initial condition.



(a) State trajectories

(b) Control input and command-following error

Figure 6.23: Example 6.9. Internal-model-based, output-feedback control of the ball and beam.



(a) State trajectories

(b) Control input and command-following error

Figure 6.24: Example 6.9. Internal-model-based, output-feedback control of the ball and beam.

6.2.2.5 Numerical Investigation of the Domain of Attraction for the Van der Pol Oscillator

Example 6.10. In this example the goal is to numerically investigate the domain of attraction of the Van der Pol oscillator under output-feedback control. In particular, consider a step command and step disturbance with the weights R_1 , R_2 , V_1 , V_2 as given in Example 5. Figure 6.25 shows the phase portrait of the state trajectories for several initial conditions x_0 contained in $[-10, 10] \times [-10, 10]$. Figure 6.25 shows that all of the state trajectories converge to $[1 \ 0]^T$, which corresponds to zero asymptotic command-following error.

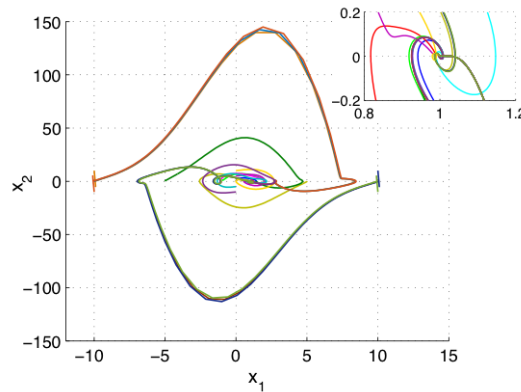


Figure 6.25: Example 6.10. Numerical investigation of the domain of attraction of the Van der Pol oscillator under output-feedback control.

6.2.2.6 Numerical Investigation of the Domain of Attraction for the Ball and Beam

Example 6.11. In this example the goal is to numerically estimate the domain of attraction for the ball and beam under full-state feedback and output feedback. Consider convergence to the equilibrium in the absence of a disturbance, with nonzero initial conditions on the ball position and velocity, and with zero initial conditions on the beam angle and angular velocity.

For output feedback, it is assumed that measurements of the ball position and beam angle are available. For all initial conditions and for both full-state feedback and output feedback, let $R_1 = \text{diag}(10^2, 10^3 I_3)$, $R_2 = 10^3$. For output feedback, let $V_1 = I_4$, $V_2 = 10^2 I_2$ and $\hat{x}_{a,0} = [x_{1,0} \ 0 \ x_{3,0} \ 0]^T$.

Figure 6.26 gives a set of initial conditions with $x_{1,0} \in [0, 60]$ m, $x_{2,0} \in [-15, 5]$ m/sec, $x_{3,0} = 0$ rad, and $x_{4,0} = 0$ rad/sec. These values are illustrative only and are not intended to be physically meaningful. "×" denotes an initial condition from which convergence is not achieved. Only initial conditions with $x_{1,0} > 0$ are considered due to symmetry. For each initial condition, Fig. 6.26 indicates whether or not the state converges. It should be noted that the beam angle θ satisfies $\theta \in (-\pi/2, \pi/2)$ for all cases where the states converge. The phase portraits for selected initial conditions are shown in Fig. 6.27 for full-state feedback, and in Fig. 6.28 for output feedback. In (a) each dot indicates the initial ball position and velocity, while (b) shows the beam angle and angular velocity.

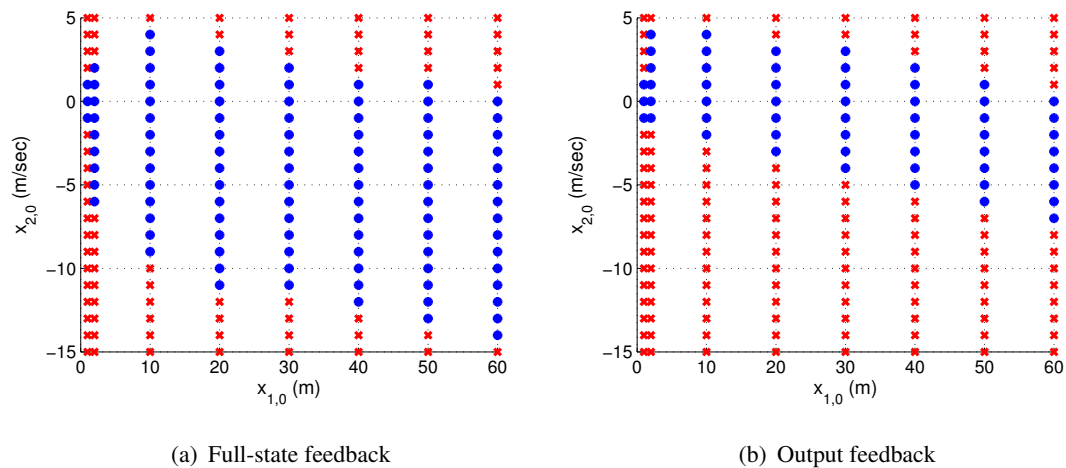
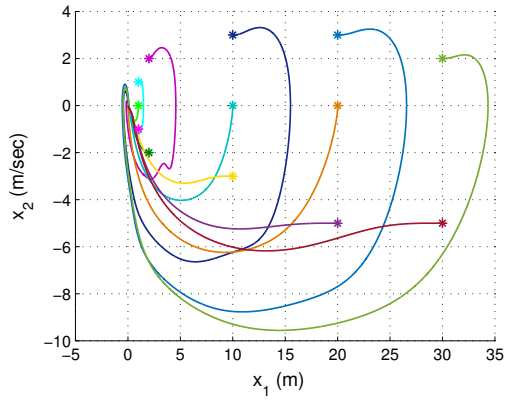
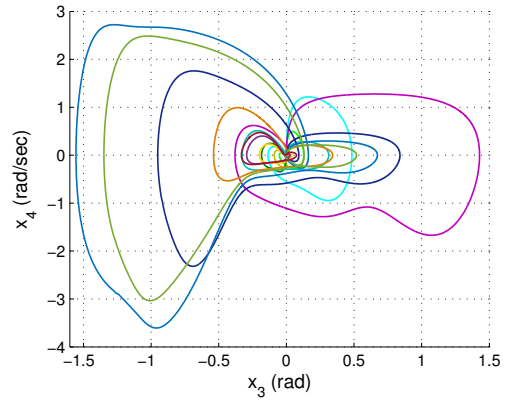


Figure 6.26: Example 6.10. Numerical investigation of the domain of attraction for nonzero $x_{1,0}$ and $x_{2,0}$ for the ball and beam.

Next, consider output feedback for the case where measurements of only the ball position are available for feedback. Let $R_1 = \text{diag}(10^2, 10^3 I_3)$, $R_2 = 10^3$, $V_1 = I_4$, $V_2 = 100$, and $\hat{x}_{a,0} = [x_{1,0} \ 0 \ 0 \ 0]^T$. Consider initial conditions with $x_{1,0} \in [0, 60]$ m, $x_2 = 0$ m/sec, $x_{3,0} = 0$ rad, and $x_{4,0} = 0$ rad/sec. Only initial conditions with $x_{1,0} > 0$ are considered due to symmetry. For all initial conditions within the given range, the state trajectories converge to the zero equilibrium. The phase portraits are shown in Fig. 6.29. In (a) each dot indicates the initial ball position and velocity, while (b) shows the beam angle and angular velocity.

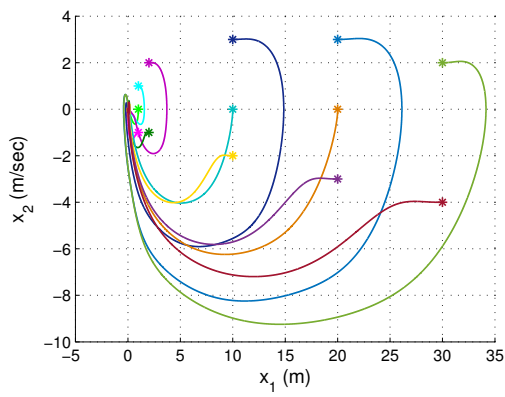


(a) Ball velocity vs position

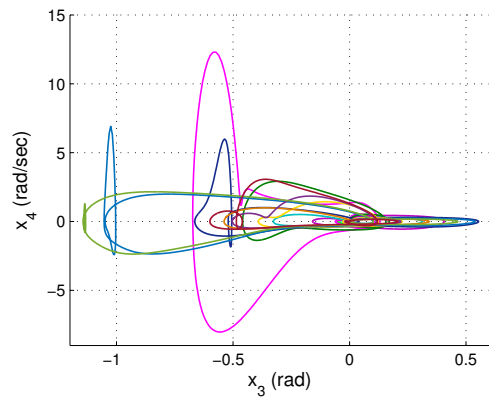


(b) Beam angular velocity vs angle

Figure 6.27: Example 6.10. Numerical investigation of the domain of attraction for full-state-feedback control of the ball and beam using.

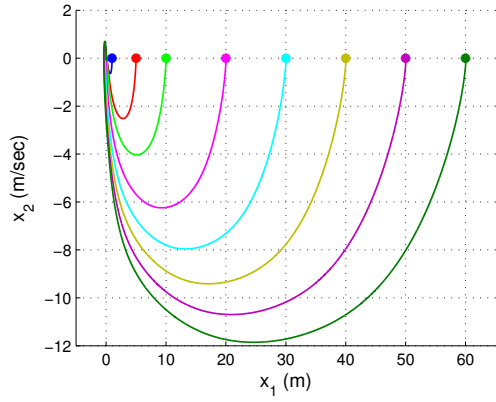


(a) Ball velocity vs position

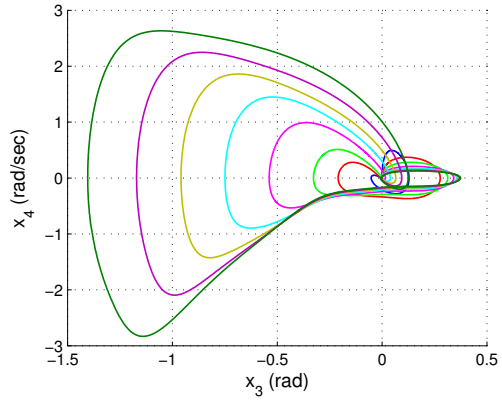


(b) Beam angular velocity vs angle

Figure 6.28: Example 6.10. Numerical investigation of the domain of attraction for output-feedback control of the ball and beam using measurements of ball position and beam angle.



(a) Ball velocity vs position



(b) Beam angular velocity vs angle

Figure 6.29: Example 6.10. Numerical investigation of the domain of attraction for output-feedback control of the ball and beam using measurements of ball position only.

CHAPTER 7

APPLICATION OF FPRE AND SDRE FOR AN AIRCRAFT

This Chapter presents application of the FPRE and SDRE tracking controllers for a fixed-wing aircraft.

7.1 Aircraft Platform

A short range tactical fixed-wing UAV given in Fig. 7.1 is used as a platform [94]. A nonlinear six degrees of freedom model of the UAV was developed and includes aerodynamics, propulsion, mass-inertia, and environment models. Aircraft specification is given in Table 7.1. Mass and inertia parameters are given in Table 7.2.



Figure 7.1: Fixed-wing UAV platform

7.2 Dual-Loop Controller Structure

An SDRE and FPRE tracking controllers are designed to control angular position and altitude of a fixed-wing aircraft. Both SDRE and FPRE controllers have a dual-loop

Table 7.1: UAV Specification

Parameter	Value	Units
Empty mass	90	kg
Maximum payload mass	30	kg
Maximum speed	83	m/sec
Stall speed	18	m/sec
Cruise speed	40	m/sec
Wing span	4.3	m
Length	3	m
Widths of fuselage	0.3	m

Table 7.2: UAV Mass and Inertia Parameters

Parameter	Value	Units
m	105	kg
J_{xx}	37.58	kg-m ²
J_{yy}	34.12	kg-m ²
J_{zz}	67.04	kg-m ²
J_{xz}	-6.91	kg-m ²

structure shown in Fig. 7.2, which is obtained by separating equations of motion of an aircraft into kinematic and dynamic equations. Kinematic equations that relate aircraft velocities to the attitude and position and altitude are used for the outer loop, whereas, dynamic equations that describe the translational and rotational motion of the rigid body aircraft, whereas are treated in the inner loop.

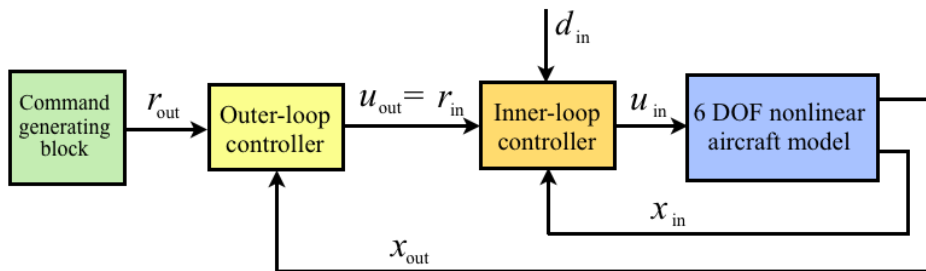


Figure 7.2: Dual-loop controller structure

In Fig.7.2 outer-loop controller and inner-loop controller represent either SDRE or FPRE control. Thus, two SDC models are derived for each control loop. Reference

command vector r_{out} for the outer loop are generated by the command generating block. Output of the outer loop u_{out} represents the reference input r_{in} to the inner loop, whereas, output of the inner loop u_{in} is the control input to the aircraft.

The advantage of the two-loop control structure is the reduction in the dimensions of state vectors, and thus, computational cost associated with the calculation of the feedback gain. It is assumed that full state measurements of the inner and outer loop states are available for feedback. Numerical simulations are performed for a coordinated turn maneuver.

7.3 State-Dependent Model for a Fixed-Wing Aircraft

In the flight control system the outer loop is referred to the control of altitude and attitudes of an aircraft, while the inner loop handles the linear and angular velocities. The control vector for the outer loop represents the state vector for the inner loop, for which the controls combine ailerons, elevator, rudder and thrust.

State-dependent model for a fixed-wing aircraft is developed using the general non-linear 6 degrees-of-freedom equations of motion of an aircraft [49, 101]. Equations of translational motion are given by

$$m(\dot{u} + qw - vr) = X - g \sin \theta, \quad (7.1)$$

$$m(\dot{v} + ru - pw) = Y + mg \cos \theta \sin \phi, \quad (7.2)$$

$$m(\dot{w} + vp - uq) = Z + g \cos \theta \cos \phi, \quad (7.3)$$

and equations of rotational motion are given by

$$J_{xx}\dot{p} - J_{xz}(\dot{r} - pq) + (J_{zz} - J_{yy})qr = L, \quad (7.4)$$

$$J_{yy}\dot{q} + J_{xz}(p^2 - r^2) + pr(J_{xx} - J_{zz}) = M, \quad (7.5)$$

$$J_{zz}\dot{r} - J_{xz}\dot{p} + pq(J_{yy} - J_{zz}) + J_{zz}qr = N, \quad (7.6)$$

Kinematic equations are given by

$$\dot{\phi} = p + \tan \theta (q \sin \phi + r \cos \phi), \quad (7.7)$$

$$\dot{\theta} = q \cos \phi - r \sin \phi, \quad (7.8)$$

$$\dot{\psi} = q \frac{\sin \phi}{\cos \theta} + r \frac{\cos \phi}{\cos \theta}, \quad (7.9)$$

$$\dot{h} = u \sin \theta - v \sin \phi \cos \theta - w \cos \phi \cos \theta. \quad (7.10)$$

The body axis components of the aerodynamic and propulsion forces are given by

$$\begin{aligned} X &= -D \cos \alpha + L \sin \alpha + T, \\ Z &= -D \sin \alpha - L \cos \alpha, \end{aligned} \quad (7.11)$$

Assuming small values of the angle of attack α , (7.11) can be approximated by

$$\begin{aligned} X &\approx -D + L\alpha + T, \\ Z &\approx -D\alpha - L. \end{aligned} \quad (7.12)$$

Aerodynamic forces and moments are expressed in terms of aerodynamic coefficients as follows

$$\begin{aligned} D &= C_D \bar{q} S, \quad L = C_L \bar{q} S, \quad Y = C_Y \bar{q} S, \\ L &= C_l \bar{q} S b, \quad M = C_m \bar{q} S \bar{c}, \quad N = C_n \bar{q} S b, \end{aligned} \quad (7.13)$$

where $\bar{q} = \frac{1}{2} \rho V^2$ is dynamic pressure, S is the wing reference area, \bar{c} is the mean aerodynamic chord, b is the wing span, C_D is the total airplane drag coefficient, C_L is the total airplane lift coefficient, C_Y is the total airplane side force coefficient, C_l is the total airplane aerodynamic rolling moment coefficient, C_m is the total airplane aerodynamic pitching moment coefficient, C_n is the total airplane aerodynamic yawing moment coefficient. The aerodynamic coefficients are expressed in terms of

non-dimensional aerodynamic derivatives [101]

$$\begin{aligned}
C_D &= C_{D_0} + C_{D_\alpha} \alpha + C_{D_{\delta_e}} \delta_e, \\
C_L &= C_{L_0} + C_{L_\alpha} \alpha + C_{L_{\dot{\alpha}}} \frac{\bar{c}}{2u_0} \dot{\alpha} + C_{L_q} \frac{\bar{c}}{2u_0} q + C_{L_{\delta_e}} \delta_e, \\
C_Y &= C_{Y_0} + C_{Y_\beta} \beta + C_{Y_p} \frac{b}{2u_0} p + C_{Y_r} \frac{b}{2u_0} r + C_{Y_{\delta_a}} \delta_a + C_{Y_{\delta_r}} \delta_r, \\
C_l &= C_{l_0} + C_{l_\beta} \beta + C_{l_p} \frac{b}{2u_0} p + C_{l_r} \frac{b}{2u_0} r + C_{l_{\delta_a}} \delta_a + C_{l_{\delta_r}} \delta_r, \\
C_m &= C_{m_0} + C_{m_\alpha} \alpha + C_{m_{\dot{\alpha}}} \frac{\bar{c}}{2u_0} \dot{\alpha} + C_{m_q} \frac{\bar{c}}{2u_0} q + C_{m_{\delta_e}} \delta_e, \\
C_n &= C_{n_0} + C_{n_\beta} \beta + C_{n_p} \frac{b}{2u_0} p + C_{n_r} \frac{b}{2u_0} r + C_{n_{\delta_a}} \delta_a + C_{n_{\delta_r}} \delta_r, \tag{7.14}
\end{aligned}$$

where $C_{D_0} = 0.016$, $C_{L_0} = 0.1$, $C_{m_0} = 0.273$, $C_{Y_0} = C_{l_0} = C_{n_0} = 0$. Longitudinal and lateral non-dimensional aerodynamic derivatives are given in Table 7.3.

Table 7.3: Non-dimensional Aerodynamic Derivatives

	C_D	C_L	C_Y	C_l	C_m	C_n
α	0.8	11.65	–	–	-1.5	–
$\dot{\alpha}$	0	1.46	–	–	-5.2	–
β	–	–	-0.374	-0.135	–	0.6503
p	–	–	-0.03	-0.47	–	-0.027
q	0	3.9	–	–	-13.3	–
r	–	–	0.21	0.07	–	-0.093
δ_a	–	–	0	0.23	–	-0.0055
δ_e	0.0741	0.4275	–	–	-0.75	–
δ_r	–	–	0.11	0.1	–	-0.043

7.3.1 Inner-Loop Model

The inner loop state and control vectors are defined by

$$x_{\text{in}} \triangleq [u \ v \ w \ p \ q \ r]^T, \tag{7.15}$$

$$u_{\text{in}} \triangleq [\delta_a \ \delta_e \ \delta_r \ \delta_T]^T. \tag{7.16}$$

State-dependent model for the inner loop is obtained using the equations of translational and rotational motion (7.1), (7.2), (7.3), (7.4), (7.5), (7.6), with (7.12), (7.13),

(7.14), and is given by

$$\dot{x}_{\text{in}} = A_{\text{in}}x_{\text{in}} + B_{\text{in}}u_{\text{in}} + D_1d_{\text{in}}, \quad (7.17)$$

where

$$A_{\text{in}} = \begin{bmatrix} A_{11} & A_{12} \\ A_{21} & A_{22} \end{bmatrix}, \quad (7.18)$$

where,

$$A_{11} = \begin{bmatrix} \frac{\frac{1}{2}\rho VS(-C_{D0}-C_{D\alpha}\alpha)}{m} & 0 & \frac{\bar{q}S(C_{L\alpha}\alpha+C_{L0})}{mu} \\ 0 & \frac{\bar{q}SC_{Y\beta}}{mu} & 0 \\ \frac{\frac{1}{2}\rho VS(-C_{D0}\alpha-C_{L0})}{m} & 0 & \frac{\bar{q}S(-C_{D\alpha}\alpha-C_{L\alpha})}{mu} \end{bmatrix}, \quad (7.19)$$

$$A_{12} = \begin{bmatrix} 0 & \frac{\bar{q}S\bar{c}(C_{Lq}+C_{L\dot{\alpha}})\alpha}{m} \frac{\bar{c}}{2u_0} - w & v \\ \frac{\bar{q}S\bar{c}^2C_{Yp}}{2mu_0} + w & 0 & \frac{\bar{q}S\bar{c}^2C_{Yr}}{2mu_0} - u \\ -v & \frac{\bar{q}S\bar{c}^2(-C_{Lq}-C_{L\dot{\alpha}})\alpha}{2mu_0} + u & 0 \end{bmatrix}, \quad (7.20)$$

$$A_{21} = \begin{bmatrix} 0 & \frac{\bar{q}Sb(c_3C_{1\beta}+c_4C_{n\beta})}{u} & 0 \\ \frac{\frac{1}{2}\rho VS\bar{c}C_{m0}}{J_{yy}} & 0 & \frac{\bar{q}S\bar{c}C_{m\alpha}}{J_{yy}u} \\ 0 & \frac{\bar{q}Sb(c_4C_{1\beta}+c_9C_{n\beta})}{u} & 0 \end{bmatrix}, \quad (7.21)$$

$$A_{22} = \begin{bmatrix} \frac{\bar{q}Sb^2(c_3C_{1p}+c_4C_{np})}{2u_0} + c_2q & 0 & \frac{\bar{q}Sb^2(c_3C_{1r}+c_4C_{nr})}{2u_0} + c_1q \\ 0 & \frac{\bar{q}S\bar{c}(C_{mq}+C_{m\dot{\alpha}})\bar{c}}{J_{yy}} \frac{\bar{c}}{2V} & 0 \\ \frac{\bar{q}Sb^2(c_4C_{1p}+c_9C_{np})}{2u_0} + c_8q & 0 & \frac{\bar{q}Sb^2(c_4C_{1r}+c_9C_{nr})}{2u_0} - c_2q \end{bmatrix}, \quad (7.22)$$

$$B_{\text{in}} = \begin{bmatrix} 0 & \frac{\bar{q}S(C_{L\delta_e}\alpha-C_{D\delta_e})}{m} & 0 & \frac{C_T}{m} \\ 0 & 0 & \frac{\bar{q}SC_{Y\delta_r}}{m} & 0 \\ 0 & \frac{\bar{q}S(-C_{L\delta_e}-C_{D\delta_e})\alpha}{m} & 0 & 0 \\ \bar{q}Sb(c_3C_{1\delta_a} + c_4C_{n\delta_a}) & 0 & \bar{q}Sb(c_3C_{1\delta_r} + c_4C_{n\delta_r}) & 0 \\ 0 & \frac{\bar{q}S\bar{c}C_{m\delta_e}}{J_{yy}} & 0 & 0 \\ \bar{q}Sb(c_4C_{1\delta_a} + c_9C_{n\delta_a}) & 0 & \bar{q}Sb(c_4C_{1\delta_r} + c_9C_{n\delta_r}) & 0 \end{bmatrix}, \quad (7.23)$$

where

$$\begin{aligned}
c_1 &= \frac{(J_{yy} - J_{zz})J_{zz} - J_{xz}^2}{J_{xx}J_{zz} - J_{xz}^2}, \quad c_2 = \frac{(J_{xx} - J_{yy} + J_{zz})J_{xz}}{J_{xx}J_{zz} - J_{xz}^2}, \quad c_3 = \frac{J_{zz}}{J_{xx}J_{zz} - J_{xz}^2}, \\
c_4 &= \frac{J_{xz}}{J_{xx}J_{zz} - J_{xz}^2}, \quad c_5 = \frac{(J_{zz} - J_{xx})}{J_{yy}}, \quad c_6 = \frac{J_{xz}}{J_{yy}}, \quad c_7 = \frac{1}{J_{yy}}, \\
c_8 &= \frac{(J_{xx} - J_{yy})J_{xx} - J_{xz}^2}{J_{xx}J_{zz} - J_{xz}^2}, \quad c_9 = \frac{J_{xx}}{J_{xx}J_{zz} - J_{xz}^2}.
\end{aligned} \tag{7.24}$$

In (7.17) d_{in} represents a mismatch between the original dynamics and the SDC parametrization, it includes terms that appear due to the gravitational acceleration and is given by

$$d_{\text{in}} = \begin{bmatrix} -g \sin \theta \\ g \cos \theta \sin \phi \\ g \cos \theta \cos \phi \\ 0 \\ 0 \\ 0 \end{bmatrix}. \tag{7.25}$$

Thus, $D_{1,\text{in}} = I_6$. Note that d_{in} depends on the outer-loop states.

7.3.2 Outer-Loop Model

The outer-loop state and control vectors are defined by

$$x_{\text{out}} \triangleq [\phi \ \theta \ \psi \ h]^T, \tag{7.26}$$

$$u_{\text{out}} \triangleq [u \ v \ w \ p \ q \ r]^T. \tag{7.27}$$

Using kinematic equations (7.7), (7.8), (7.9), state-dependent model for the outer loop is given by

$$\dot{x}_{\text{out}} = A_{\text{out}}x_{\text{out}} + B_{\text{out}}u_{\text{out}}, \tag{7.28}$$

where

$$A_{\text{out}} = 0_{4 \times 4}, \tag{7.29}$$

$$B_{\text{out}} = \begin{bmatrix} 0 & 0 & 0 & 1 & \tan \theta \sin \phi & \tan \theta \cos \phi \\ 0 & 0 & 0 & 0 & \cos \phi & -\sin \phi \\ 0 & 0 & 0 & 0 & \sin \phi / \cos \theta & \cos \phi / \cos \theta \\ \sin \theta & -\sin \phi \cos \theta & -\cos \phi \cos \theta & 0 & 0 & 0 \end{bmatrix}. \quad (7.30)$$

7.4 SDRE Controller

Consider tracking SDRE controller, described in Chapter 5, and given by (5.58), (5.59), (5.60), (5.61).

For a dual-loop structure, two separate SDRE controllers are designed for each loop. The SDRE controller for the inner loop utilizes the inner-loop SDC model (7.17) given by (7.18), (7.23), (7.25), whereas, SDRE controller for the outer loop utilizes the outer-loop SDC model (7.28) given by (7.29), (7.30). For both, inner and outer loop, consider full-state feedback, thus, $H_{\text{in}} = I_6$, $H_{\text{out}} = I_4$.

Assuming that, for all x_{in} , $(A_{\text{in}}^T - \bar{P}_{\text{in}}S_{\text{in}})$ is non-singular, the inner-loop SDRE controller is given by

$$u_{\text{in}} = K_{\text{in}}x_{\text{in}} + K_{r,\text{in}}r_{\text{in}} + K_{d,\text{in}}d_{\text{in}}, \quad (7.31)$$

where

$$K_{\text{in}} = -R_{2,\text{in}}^{-1}B_{\text{in}}^T\bar{P}_{\text{in}}, \quad (7.32)$$

$$K_{r,\text{in}} = -R_{2,\text{in}}^{-1}B_{\text{in}}^T(A_{\text{in}}^T - \bar{P}_{\text{in}}S_{\text{in}})^{-1}W_{\text{in}}, \quad (7.33)$$

$$K_{d,\text{in}} = R_{2,\text{in}}^{-1}B_{\text{in}}^T(A_{\text{in}}^T - \bar{P}_{\text{in}}S_{\text{in}})^{-1}\bar{P}_{\text{in}}D_{1,\text{in}}, \quad (7.34)$$

where \bar{P}_{in} is a solution of an algebraic state-dependent Riccati equation

$$\bar{P}_{\text{in}}A_{\text{in}} + A_{\text{in}}^T\bar{P}_{\text{in}} - \bar{P}_{\text{in}}B_{\text{in}}R_{2,\text{in}}^{-1}B_{\text{in}}^T\bar{P}_{\text{in}} + R_{1,\text{in}} = 0., \quad (7.35)$$

and where

$$S_{\text{in}} = B_{\text{in}}R_{2,\text{in}}^{-1}B_{\text{in}}^T, \quad (7.36)$$

$$W_{\text{in}} = H_{\text{in}}^TR_{1,\text{in}}, \quad (7.37)$$

$$V_{\text{in}} = H_{\text{in}}^TR_{1,\text{in}}H_{\text{in}}. \quad (7.38)$$

In a similar way, assuming that, for all x_{out} , $(A_{\text{out}}^{\text{T}} - \bar{P}_{\text{out}}S_{\text{out}})$ is non-singular, and considering $d_{\text{out}} = 0$, the outer-loop SDRE controller is given by

$$u_{\text{out}} = K_{\text{out}}x_{\text{out}} + K_{r,\text{out}}r_{\text{out}}, \quad (7.39)$$

where

$$K_{\text{out}} = -R_{2,\text{out}}^{-1}B_{\text{out}}^{\text{T}}\bar{P}_{\text{out}}, \quad (7.40)$$

$$K_{r,\text{out}} = -R_{2,\text{out}}^{-1}B_{\text{out}}^{\text{T}}(A_{\text{out}}^{\text{T}} - \bar{P}_{\text{out}}S_{\text{out}})^{-1}W_{\text{out}}, \quad (7.41)$$

where \bar{P}_{out} is a solution of an algebraic state-dependent Riccati equation

$$\bar{P}_{\text{out}}A_{\text{out}} + A_{\text{out}}^{\text{T}}\bar{P}_{\text{out}} - \bar{P}_{\text{out}}B_{\text{out}}R_{2,\text{out}}^{-1}B_{\text{out}}^{\text{T}}\bar{P}_{\text{out}} + R_{1,\text{out}} = 0, \quad (7.42)$$

and where

$$S_{\text{out}} \triangleq B_{\text{out}}R_{2,\text{out}}^{-1}B_{\text{out}}^{\text{T}}, \quad (7.43)$$

$$W_{\text{out}} \triangleq H_{\text{out}}^{\text{T}}R_{1,\text{out}}, \quad (7.44)$$

$$V_{\text{out}} \triangleq H_{\text{out}}^{\text{T}}R_{1,\text{out}}H_{\text{out}}. \quad (7.45)$$

Note that, for all x_{in} , x_{out} , the pairs $(A_{\text{in}}, B_{\text{in}})$ and $(A_{\text{out}}, B_{\text{out}})$ must be stabilizable for in order the solutions \bar{P}_{in} and \bar{P}_{out} of (7.35), (7.42) to exist. This condition, however, is not required for FPRE control.

7.4.1 Numerical Simulation Results

In this example, the aircraft is commanded to perform a coordinated turn maneuver with a turn radius 200 m, while keeping the altitude constant at 1000 m, and zero sideslip angle β . A command algorithm is implemented to generate consistent commands for the outer-loop states, that are, ϕ , θ , ψ , and h .

The weighting matrices for the inner and outer loops are given by

$$R_{1,\text{in}} = \text{diag}(10^3, 10^2, 10, 10^5, 2 \times 10^6, 4 \times 10^6), \quad (7.46)$$

$$R_{2,\text{in}} = \text{diag}(10^4, 10^2, 10^4, 10^{-3}), \quad (7.47)$$

$$R_{1,\text{out}} = \text{diag}(3 \times 10^4, 2 \times 10^4, 10^4, 10^4), \quad (7.48)$$

$$R_{2,\text{out}} = \text{diag}(10^2, 10^2, 2 \times 10^3, 1.5 \times 10^{-3}I_3). \quad (7.49)$$

For SDRE control, the controller gains are updated with a frequency $2Hz$.

7.4.1.1 Case 1: Uniform Atmosphere

In the first case, a uniform atmosphere is assumed, that is, no wind and no turbulence. This simulation scenario is not realistic, however it allows to investigate performance of the SDRE controller under ideal conditions.

Figure 7.3 shows the XY -position and altitude of the aircraft; aircraft roll, pitch and yaw angles, also angle of attack and sideslip are shown in Fig. 7.4; linear velocities and angular rates are shown in Fig. 7.5; control-surfaces deflections and thrust are shown in Fig. 7.6. Simulation results show that SDRE controller ensures the aircraft to perform a sequence of coordinates turns with a given radius while holding constant altitude and zero sideslip. Actuators deflections and thrust responses are within the allowable limits.

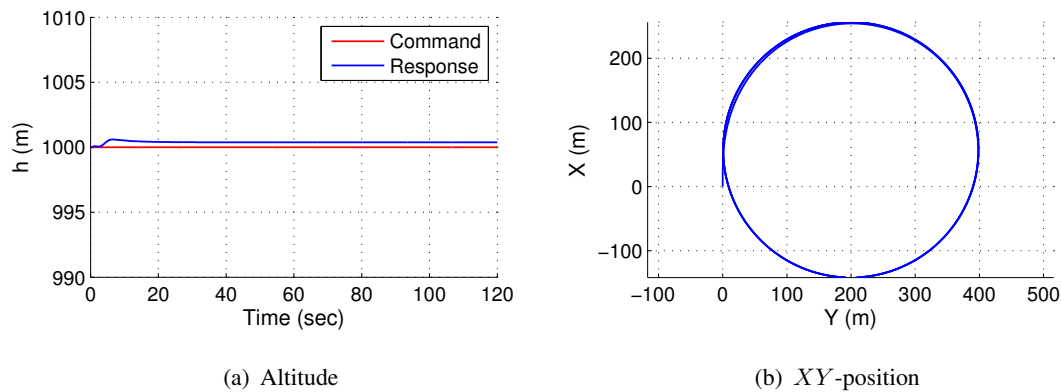


Figure 7.3: SDRE control of the aircraft, case 1: altitude and XY -position.

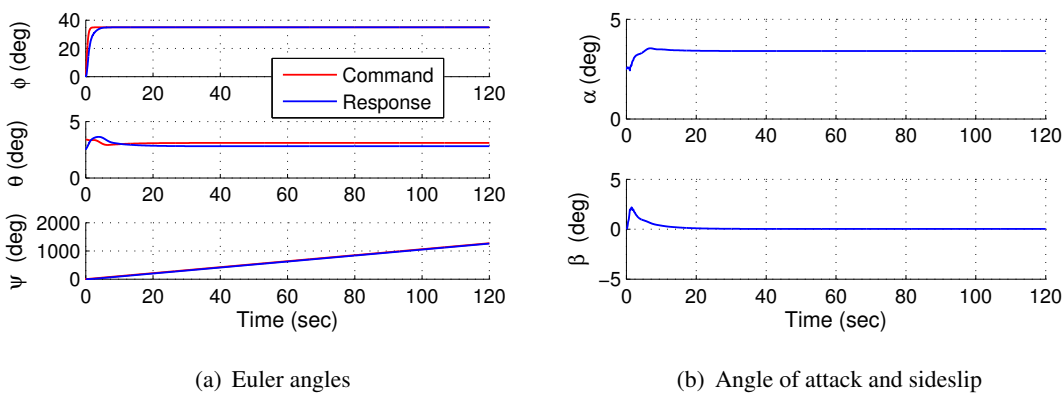


Figure 7.4: SDRE control of the aircraft, case 1: Euler angles, angle of attack and sideslip angle.

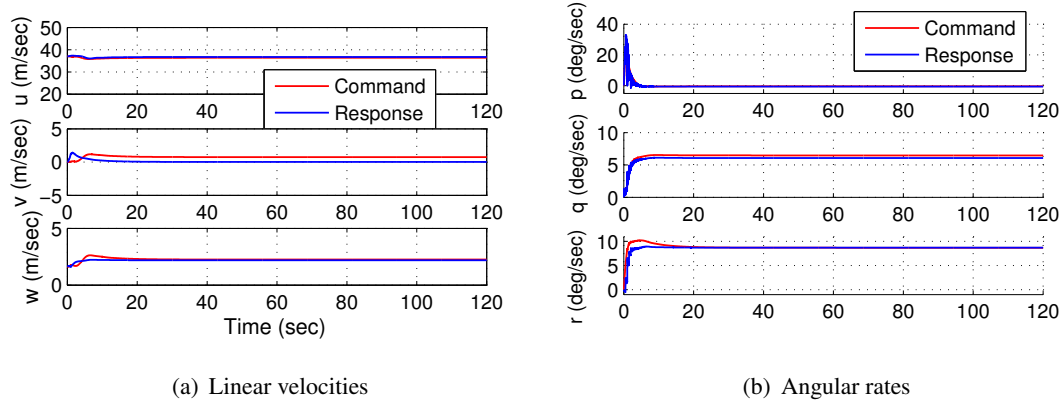


Figure 7.5: SDRE control of the aircraft, case 1: linear and angular velocities.

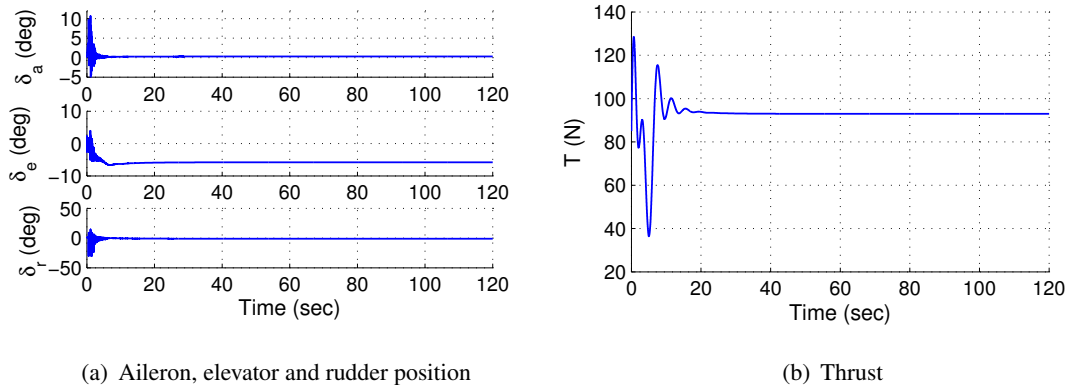


Figure 7.6: SDRE control of the aircraft, case 1: control-surfaces deflections and thrust.

7.4.1.2 Case 2: Light Turbulence

Next, more realistic scenario with a light turbulence is considered. Wind profile is given in Fig. 7.7.

Figure 7.8 shows the XY -position and altitude of the aircraft; aircraft roll, pitch and yaw angles, also angle of attack and sideslip are shown in Fig. 7.9; linear velocities and angular rates are shown in Fig. 7.10; control-surfaces deflections and thrust are shown in Fig. 7.11. Simulation results show that presence of turbulence make the performance of the controller worse. Oscillations are present in the responses. Especially negative effect from the turbulence is observed in the inner loop, where the oscillations are now present in the reference commands, and thrust input reaches saturation values. However, the aircraft is able to perform a coordinated turn, holding the commanded altitude and nearly zero sideslip.

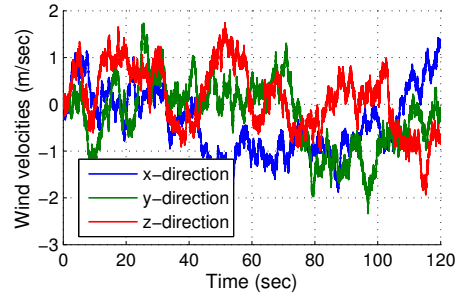


Figure 7.7: Wind profile.

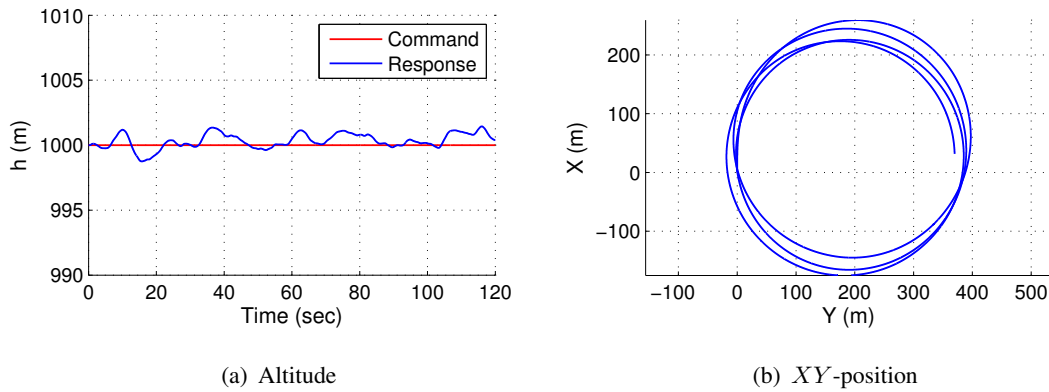


Figure 7.8: SDRE control of the aircraft, case 2: altitude and XY -position.

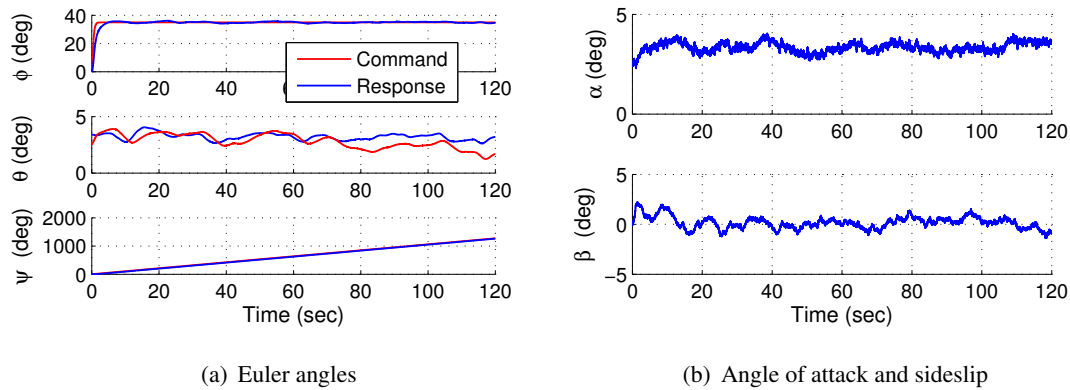


Figure 7.9: SDRE control of the aircraft, case 2: Euler angles, angle of attack and sideslip angle.

7.5 FPRE Controller

Consider tracking FPRE controller, described in Chapter 6, and given by (6.8), (6.9), (6.10), (6.11).

For a dual-loop structure, two separate FPRE controllers are designed for each loop. The FPRE controller for the inner loop utilizes the inner-loop SDC model (7.17)

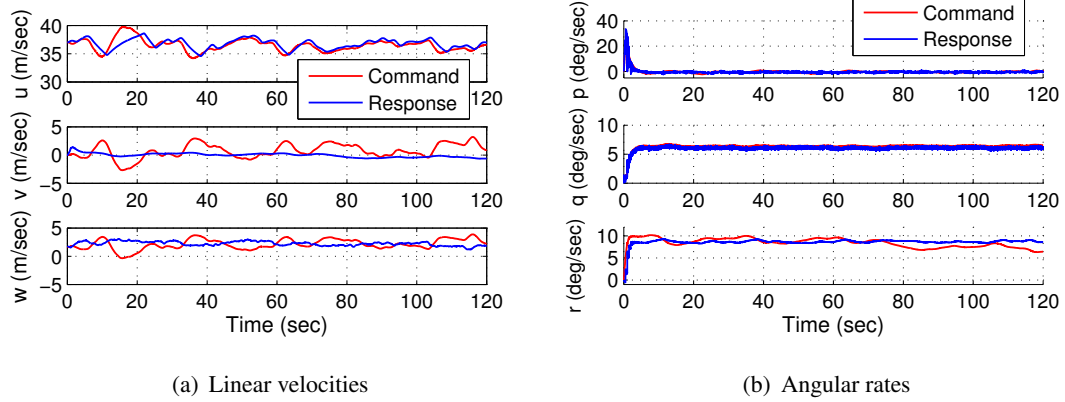


Figure 7.10: SDRE control of the aircraft, case 2: linear and angular velocities.

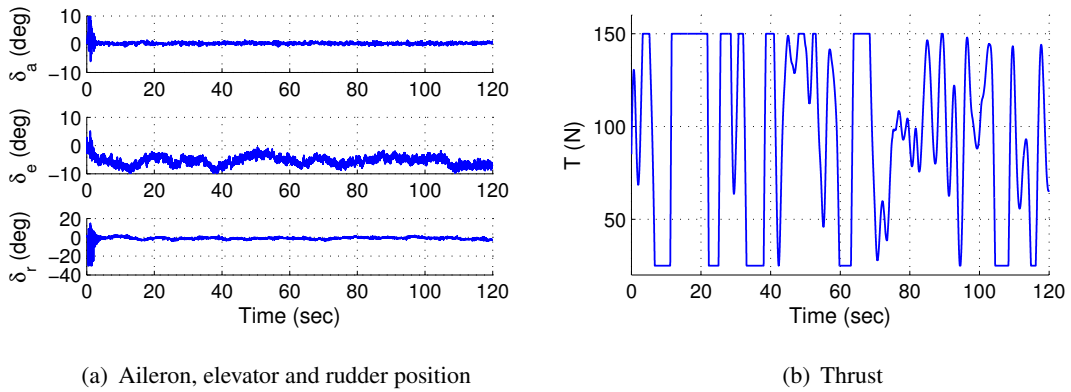


Figure 7.11: SDRE control of the aircraft, case 2: control-surfaces deflections and thrust.

given by (7.18), (7.23), (7.25), whereas, FPRE controller for the outer loop utilizes the outer-loop SDC model (7.28) given by (7.29), (7.30). For both, inner and outer loop, consider full-state feedback, thus, $H_{in} = I_6$, $H_{out} = I_4$.

Thus, the inner-loop FPRE controller is given by

$$u_{in} = K_{in} x_{in} + R_{2,in}^{-1} B_{in}^T g_{in}, \quad (7.50)$$

where K_{in} is given by

$$K_{in} = -R_{2,in}^{-1} B_{in}^T P_{in}, \quad (7.51)$$

where P_{in} and g_{in} satisfy

$$\dot{P}_{in} = P_{in} A_{in} + A_{in}^T P_{in} - P_{in} S_{in} P_{in} + V_{in}, \quad (7.52)$$

$$\dot{g}_{in} = [A_{in}^T - P_{in} S_{in}] g_{in} + W_{in} r_{in} - P_{in} D_{1,in} d_{in}, \quad (7.53)$$

with initial conditions $P_{\text{in}}(0)$, $g_{\text{in}}(0)$, and where S_{in} , W_{in} , V_{in} are given by (7.36), (7.37), (7.38).

In a similar way, considering $d_{\text{out}} = 0$, the outer-loop FPRE controller is given by

$$u_{\text{out}} = K_{\text{out}} x_{\text{out}} + R_{2,\text{out}}^{-1} B_{\text{out}}^{\text{T}} g_{\text{out}}, \quad (7.54)$$

where K_{out} is given by

$$K_{\text{out}} = -R_{2,\text{out}}^{-1} B_{\text{out}}^{\text{T}} P_{\text{out}}, \quad (7.55)$$

where P_{out} and g_{out} satisfy

$$\dot{P}_{\text{out}} = P_{\text{out}} A_{\text{out}} + A_{\text{out}}^{\text{T}} P_{\text{out}} - P_{\text{out}} S_{\text{out}} P_{\text{out}} + V_{\text{out}}, \quad (7.56)$$

$$\dot{g}_{\text{out}} = [A_{\text{out}}^{\text{T}} - P_{\text{out}} S_{\text{out}}] g_{\text{out}} + W_{\text{out}} r_{\text{out}}, \quad (7.57)$$

with initial conditions $P_{\text{out}}(0)$, $g_{\text{out}}(0)$, and where S_{out} , W_{out} , V_{out} are given by (7.43), (7.44), (7.45).

7.5.1 Initial Conditions for FPRE

At $t = 0$, assume that $(A_{\text{in}}, B_{\text{in}})$ and $(A_{\text{out}}, B_{\text{out}})$ are stabilizable, then, the initial conditions $P_{\text{in}}(0)$, $P_{\text{out}}(0)$ for (7.52), (7.56) are $P_{\text{in}}(0) = \bar{P}_{\text{in}}$ and $P_{\text{out}}(0) = \bar{P}_{\text{out}}$, where \bar{P}_{in} and \bar{P}_{out} are the corresponding solutions of (7.35), (7.42) with A_{in} , B_{in} , A_{out} , B_{out} evaluated at $x_{\text{in}}(0)$ and $x_{\text{out}}(0)$.

Next, at $t = 0$, assume that $(A_{\text{in}}^{\text{T}} - \bar{P}_{\text{in}} S_{\text{in}})$ and $(A_{\text{out}}^{\text{T}} - \bar{P}_{\text{out}} S_{\text{out}})$ are non-singular, then the initial conditions $g_{\text{in}}(0)$, $g_{\text{out}}(0)$ for (7.53), (7.57) is given by

$$g_{\text{in}}(0) = -[A_{\text{in}}^{\text{T}} - \bar{P}_{\text{in}} S_{\text{in}}]^{-1} W_{\text{in}} r_{\text{in}}(0) + [A_{\text{in}}^{\text{T}} - \bar{P}_{\text{in}} S_{\text{in}}]^{-1} \bar{P}_{\text{in}} D_{1,\text{in}} d_{\text{in}}(0), \quad (7.58)$$

$$g_{\text{out}}(0) = -[A_{\text{out}}^{\text{T}} - \bar{P}_{\text{out}} S_{\text{out}}]^{-1} W_{\text{out}} r_{\text{out}}(0), \quad (7.59)$$

where A_{in} , B_{in} , $D_{1,\text{in}}$, A_{out} , B_{out} are evaluated at $x_{\text{in}}(0)$ and $x_{\text{out}}(0)$.

7.5.2 Numerical Simulation Results

For FPRE, consider the same coordinated turn maneuver and two simulation cases, as in SDRE case. The weighting matrices for the inner and outer loops are given by (7.46), (7.47), (7.48), (7.49).

7.5.2.1 Case 1: Uniform Atmosphere

This section gives simulation results of the FPRE controller for a case of a uniform atmosphere. Figure 7.12 shows the XY -position and altitude of the aircraft; aircraft roll, pitch and yaw angles, also angle of attack and sideslip are shown in Fig. 7.13; linear velocities and angular rates are shown in Fig. 7.14; control-surfaces deflections and thrust are shown in Fig. 7.15.

The responses show that aircraft performs a desired maneuver, holding constant altitude and zero sideslip. Actuators deflections and thrust are within allowable limits.

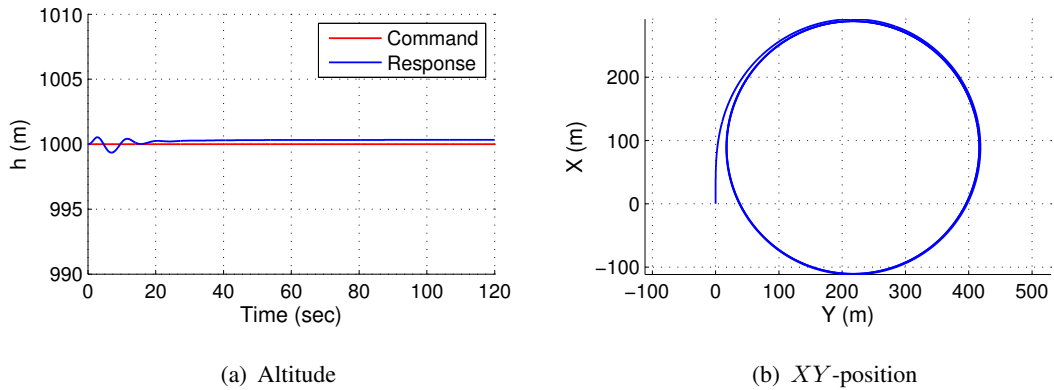


Figure 7.12: FPRE control of the aircraft, case 1: altitude and XY -position.

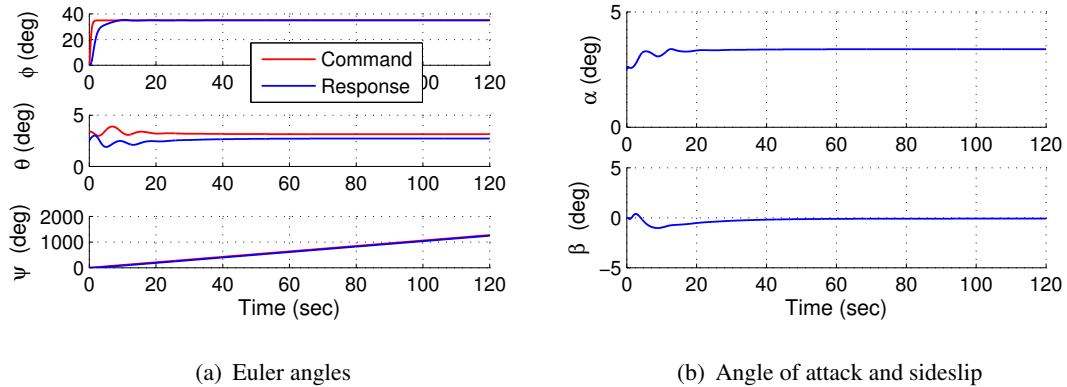
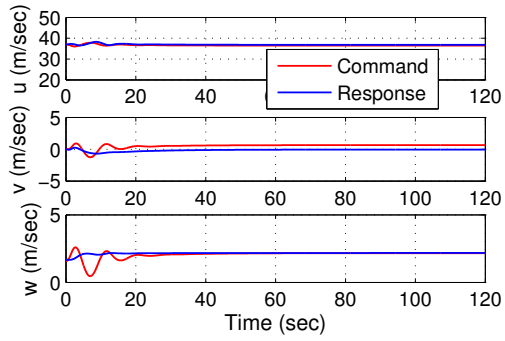
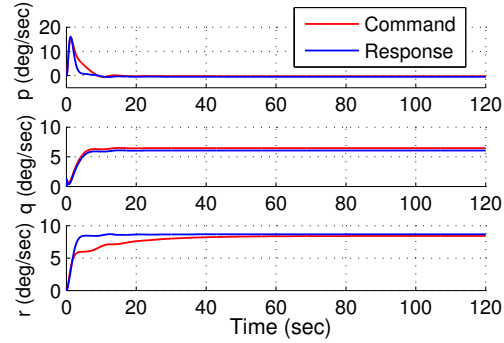


Figure 7.13: FPRE control of the aircraft, case 1: Euler angles, angle of attack and sideslip angle.

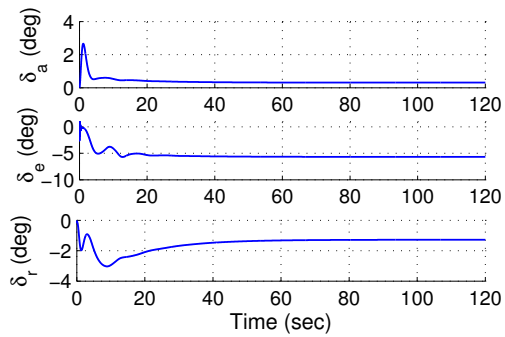


(a) Linear velocities

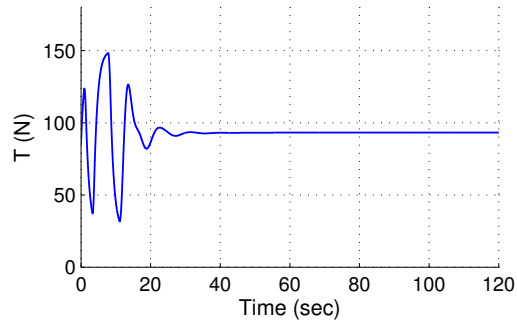


(b) Angular rates

Figure 7.14: FPRE control of the aircraft, case 1: linear and angular velocities.



(a) Aileron, elevator and rudder position



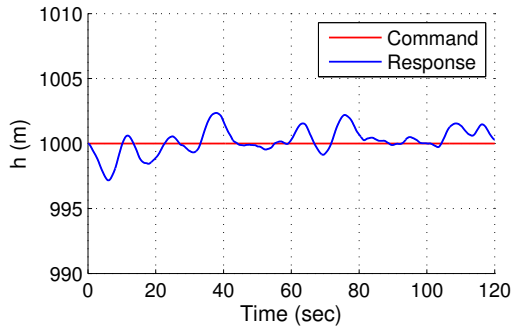
(b) Thrust

Figure 7.15: FPRE control of the aircraft, case 1: control-surfaces deflections and thrust.

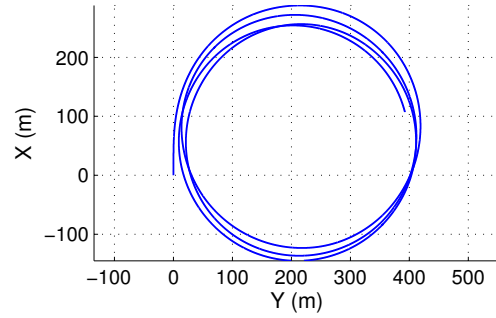
7.5.2.2 Case 2: Light Turbulence

Figure 7.16 shows the XY -position and altitude of the aircraft; aircraft roll, pitch and yaw angles, also angle of attack and sideslip are shown in Fig. 7.17; linear velocities and angular rates are shown in Fig. 7.18; control-surfaces deflections and thrust are shown in Fig. 7.19.

As for SDRE, for FPRE controller presence of turbulence also make the performance worse, which results in oscillatory responses. However, thrust saturation is less than for SDRE controller. Nevertheless, the aircraft performs a desired coordinated turn maneuver at the commanded altitude and nearly zero sideslip.

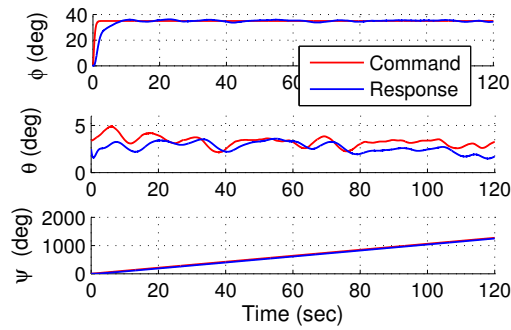


(a) Altitude

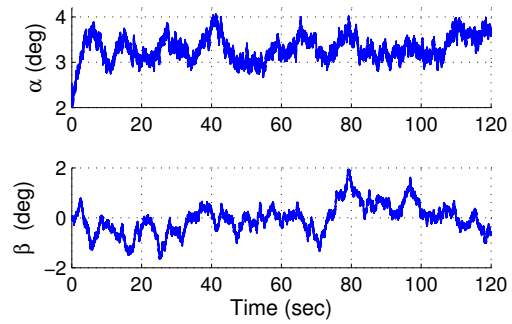


(b) XY-position

Figure 7.16: FPRE control of the aircraft, case 2: altitude and XY-position.

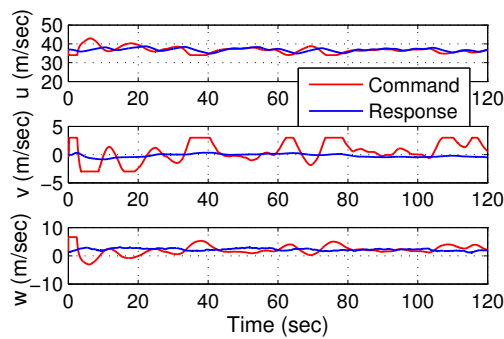


(a) Euler angles

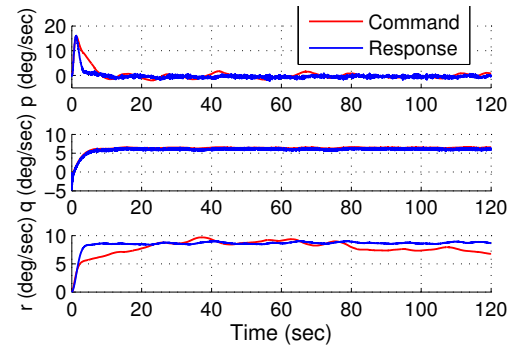


(b) Angle of attack and sideslip

Figure 7.17: FPRE control of the aircraft, case 2: Euler angles, angle of attack and sideslip angle.

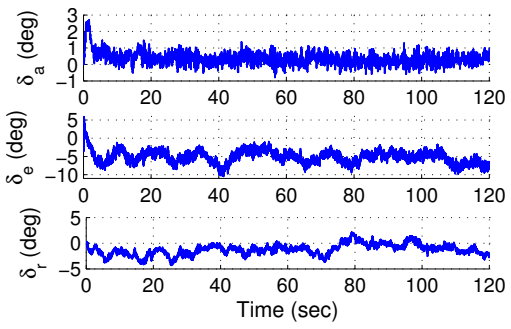


(a) Linear velocities

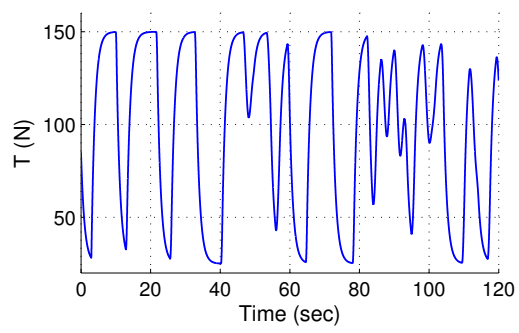


(b) Angular rates

Figure 7.18: FPRE control of the aircraft, case 2: linear and angular velocities.



(a) Aileron, elevator and rudder position



(b) Thrust

Figure 7.19: FPRE control of the aircraft, case 2: control-surfaces deflections and thrust.

CHAPTER 8

CONCLUSIONS

The contribution of this work is a detailed numerical investigation to assess the effectiveness of heuristic techniques for full-state-feedback and output-feedback control of nonlinear and time-varying systems. These techniques combine state-dependent Riccati equation (SDRE) and forward-propagating Riccati equation (FPRE) methods.

In this work emphasis is given to investigation of the FPRE method, which addresses the control problem by reversing the direction of the regulator Riccati equation and, for nonlinear systems, by employing state-dependent coefficients (SDC's) as in the case of SDRE.

For numerical investigation, various plants are considered, including an inverted pendulum on a cart (4th-order LTI), a two-mass system (4th-order LTI), Mathieu equation (2nd-order LTV), a rotating disc (4th-order LTV), a flexible beam (10th-order LTV), the Van der Pol oscillator (2nd order nonlinear), the ball and beam system (4th order nonlinear), RTAC (4th order nonlinear), and a nonlinear model of a fixed-wing UAV.

The first step is the investigation of the properties of the solution of FPRE in the LTI case. In this work analytical expressions for the solutions of the backward propagating and forward propagating Riccati equations are derived. For LTI systems, convergence of the BPRE and FPRE solutions is provided depending on the choice of the final weighting for BPRE and initial condition for FPRE. Lyapunov analysis for LTV systems is used to prove that the FPRE controller provides state convergence. However, this analysis shows that the FPRE controller does not guarantee Lyapunov stability. Numerical examples demonstrate the suboptimality of FPRE relative to

BPRE, which is shown by the Pareto performance tradeoff curves.

Next, FPRE control is applied to stabilization of time-varying systems under full-state and output feedback. For all examples, FPRE works reliably, and Pareto plots illustrate the performance tradeoffs between the control cost and state cost.

For nonlinear systems, FPRE control is compared with either an SDC or the Jacobian of the vector field. These methods are not equally applicable for various reasons. For example, for systems with a non-differentiable vector field, a state-dependent coefficient may exist but the Jacobian may not. Furthermore, while the algebraic Riccati equation requires stabilizability at each step, the forward-propagating Riccati equation does not. Numerical results shows that all methods successfully control the given plants with differences in speed of response and control effort.

The next focus of this work is on output-feedback control of linear time-varying and nonlinear systems, which presents a longstanding challenge to modern control methods. The nonlinear output-feedback compensator is an observer-based compensator with a separation structure. By using this structure, with state estimates used to evaluate the SDC's in the compensator in the case of nonlinear systems, FPRE provides a highly flexible technique for output-feedback control of linear time-varying and nonlinear systems. Like SDRE, FPRE is a heuristic method due to the fact that duality does not hold for time-varying systems. In particular, for linear time-varying plants, the Lyapunov function that guarantees convergence of the state estimate does not provide an analogous Lyapunov function for the regulator.

Analogous applications as for the FPRE control are demonstrated for the SDRE control. Thus, stabilization of nonlinear plants under full-state-feedback and output-feedback SDRE control, using either an SDC or the Jacobian of the vector field, is performed. In all the examples, SDRE with an SDC outperforms SDRE with a Jacobian.

Next, the internal model principle (IMP) is used to achieve command following and disturbance rejection for steps, ramps, and harmonics. The effect of Riccati equation initialization, cost weightings, domain of attraction, and choice of SDC are investigated through simulation. These simulations illustrated the usefulness of FPRE in

controlling these nonlinear systems under measurement constraints that are, in some cases, more restrictive than the prior literature. To illustrate the potential usefulness of the method for problems of practical interest, FPRE is used to determine a set of harmonic commands that can be followed by the RTAC in terms of frequencies and amplitudes.

IMP-based output-feedback FPRE control can be useful for the problems of defining the minimum number of measurements, and, therefore, a number of sensors, needed for the control of nonlinear systems.

Application of the tracking SDRE and FPRE controllers is firstly illustrated for the Van der Pol oscillator. Next, tracking SDRE and FPRE controllers are implemented for a fixed-wing UAV. Controllers for the aircraft are designed with a dual-loop structure and utilize two SDC models for the inner-loop and outer-loop dynamics. A difficult aspect in deriving SDC models for an aircraft is that for SDRE control, for all x , $A^T(x) - \bar{P}(x)S(x)$ must be nonsingular, and, for all x , $(A(x), B(x))$ must be stabilizable. For FPRE these conditions, in general, are not needed, however, they were used in computing the initial conditions $P(0)$ and $g(0)$ for FPRE. To illustrate the performance of tracking SDRE and FPRE controllers, numerical tests are performed using a six-degree-of-freedom nonlinear simulation model of the aircraft. For an ideal case of a uniform atmosphere, both SDRE and FPRE show good command following performance. The second simulation case, which includes a turbulence, shows that the performance of both controllers becomes worse.

The goal of this work is to motivate future research on the search for a rigorous framework for FPRE control, which includes stability proofs and investigation of robustness to modeling uncertainty; to expand application of FPRE to larger classes of systems, and to plants whose linearization is not controllable and that do not satisfy the Brockett necessary condition for continuous time-invariant stabilization. Also, the effect of the state-dependent weighting matrices $R_1(x)$ and $R_2(x)$ on the performance of FPRE needs to be investigated. This will provide more definitive insight into which heuristic technique is the most promising as a foundation for a rigorous faux-Riccati technique for output-feedback control of nonlinear systems.

REFERENCES

- [1] M. Abu-Khalaf and F. L. Lewis. Nearly optimal control laws for nonlinear systems with saturating actuators using a neural network HJB approach. *Automatica*, 41:779–891, 2005.
- [2] B. D. O. Anderson and J. B. Moore. *Linear Optimal Control*. J. Wiley and Sons, New York, N.Y, 1972.
- [3] M. Arcak. Certainty-Equivalence Output-Feedback Design With Circle-Criterion Observers. *IEEE Trans. Autom. Contr.*, 50:905–909, 2005.
- [4] R. Beard, G. Saridis, and J. Wen. Approximate solutions to the Time-Invariant Hamilton-Jacobi-Bellman Equation. *J. Optim. Theory Appl.*, 96(3):589–626, 1998.
- [5] H. Beikzadeh and H. D. Taghirad. Stability Analysis of the Discrete-Time Difference SDRE State Estimator in a Noisy Environment. In *Proc. IEEE Int. Conf. Contr. Automation*, pages 1751–1756, Christchurch, New Zealand, December 2009.
- [6] R. Bellman. *Dynamic Programming*. Princeton University Press, 1957.
- [7] G. Bengtsson. Output Regulation and Internal Models – A Frequency Domain Approach. *Automatica*, 13:333–345, 1977.
- [8] A. Berman, P. Zarchan, and B. Lewis. Comparisons Between the Extended Kalman Filter and the State-Dependent Riccati Estimator. In *AIAA Guid. Nav. Contr. Conf.*, Boston, MA, August 2013.
- [9] D. S. Bernstein. *Matrix Mathematics: Theory, Facts, and Formulas*. Princeton University Press, 2009.
- [10] N. Bhoir and S. N. Singh. Control of Unsteady Aeroelastic System via State-Dependent Riccati Equation Method. *J. Guid. Control Dynam.*, 28:78–84, 2005.
- [11] S. Bittanti and S. Colaneri. *Periodic Systems*. Springer, 2008.
- [12] A. Bogdanov and E. Wan. State-Dependent Riccati Equation Control for Small Autonomous Helicopters. *J. Guid. Control Dynam.*, 30:47–60, 2007.
- [13] R. W. Brockett. *Finite Dimensional Linear Systems*. J. Wiley, 1970.

- [14] A. E. Bryson and Y. C. Ho. *Applied Optimal Control*. Blaisdell Publ. Co., Waltham, MA, 1969.
- [15] D. J. Bugajski, D. F. Enns, and M. R. Elgersma. A Dynamic Inversion Based Control Law with Application to the High Angle of Attack Research Vehicle. In *AIAA Guid. Nav. Contr. Conf.*, Washington, DC, August 1990.
- [16] R. T. Bupp, D. S. Bernstein, and V. Coppola. A Benchmark Problem for Nonlinear Control Design. *Int. J. Robust Nonl. Contr.*, 8:307–310, 1998.
- [17] C. Byrnes and A. Isidori. Limit Sets, Zero Dynamics, and Internal Models in the Problem of Nonlinear Output Regulation. *IEEE Trans. Autom. Contr.*, 48:1712–1723, 2003.
- [18] C. I. Byrnes, A. Isidori, and J. C. Willems. Passivity, Feedback Equivalence, and the Global Stabilization of Minimum Phase Nonlinear Systems. *IEEE Trans. Autom. Contr.*, 36:1228–1240, 1991.
- [19] F. M. Callier and J. L. Willems. Criterion for the Convergence of the Solution of the Riccati Differential Equation. *IEEE Trans. Autom. Contr.*, 26:1232–1242, 1981.
- [20] F. M. Callier, J. Winkin, and J. L. Willems. On the Exponential Convergence of the Time-Invariant Matrix Riccati Differential Equation. In *Proc. Conf. Dec. Contr.*, pages 1536–1537, Tucson, AZ, December 1992.
- [21] F. M. Callier, J. Winkin, and J. L. Willems. Convergence of the Time-Invariant Riccati Differential Equation and LQ-problem: Mechanisms of Attraction. *Int. J. Contr.*, 59:983–1000, 1994.
- [22] P. Carbonell, Z. P. Jiang, and D. W. Repperger. Nonlinear Control of a Pneumatic Muscle Actuator: Backstepping vs. Sliding-mode. In *Proc. IEEE Int. Conf. Contr. Appl.*, pages 167–172, Mexico City, Mexico, September 2001.
- [23] P. Castillo, A. Dzul, and R. Lozano. Real-Time Stabilization and Tracking of a Four-Rotor Mini Rotorcraft. *IEEE Trans. Contr. Syst. Tech.*, 12(4):510–516, 2004.
- [24] J. Chandrasekhar, A. Ridley, and D. S. Bernstein. A SDRE-Based Asymptotic Observer for Nonlinear Discrete-Time Systems. In *Proc. Amer. Contr. Conf.*, pages 3630–3635, Portland, OR, June 2005.
- [25] B. Charlet, J. Levine, and R. Marino. On Dynamic Feedback Linearization. *Syst. Contr. Lett.*, 13:143–151, 1989.
- [26] B. Charlet, J. Levine, and R. Marino. Sufficient Conditions for Dynamic Feedback Linearization. *SIAM J. Control Optim.*, 29:38–57, 1991.

- [27] M. S. Chen and Y. R. Huang. Linear time-varying system control based on the inversion transformation. *Automatica*, 33:683–688, 1997.
- [28] M. S. Chen and C. Y. Kao. Control of Linear Time-Varying Systems Using Forward Riccati Equation. *J. Dyn. Syst., Meas. Contr.*, 119(3):536–540, 1997.
- [29] T. Cimen. State-Dependent Riccati Equation (SDRE) Control: a Survey. In *Proc. 17th IFAC World Congr.*, pages 3761–3771, Seoul, South Korea, July 2008.
- [30] T. Cimen. Systematic and Effective Design of Nonlinear Feedback Controllers via the State-Dependent Riccati Equation (SDRE) method. *Annual Reviews of Control*, 34:32–51, 2010.
- [31] T. Cimen. Survey of State-Dependent Riccati Equation in Nonlinear Optimal Feedback Control Synthesis. *J. Guid. Control Dynam.*, 35:1025–1047, 2012.
- [32] T. Cimen and S. P. Banks. Nonlinear optimal tracking control with application to super-tankers for autopilot design. *Automatica*, 40:1845–1863, 2004.
- [33] J. R. Cloutier. State-Dependent Riccati Equation Techniques: an Overview. In *Proc. Amer. Contr. Conf.*, pages 932–936, Albuquerque, NM, June 1997.
- [34] J. R. Cloutier, C. D’Souza, and C. Mracek. Nonlinear Regulation and Nonlinear H_∞ Control via the State-Dependent Riccati Equation Technique: Part 1, Theory. In *Proc. First Int. Conf. on Nonlinear Problems in Aviation and Aerospace.*, pages 117–141, Daytona Beach, FL, May 1996.
- [35] J. R. Cloutier, C. D’Souza, and C. Mracek. Nonlinear Regulation and Nonlinear H_∞ Control via the State-Dependent Riccati Equation Technique: Part 2, Examples. In *Proc. First Int. Conf. on Nonlinear Problems in Aviation and Aerospace.*, pages 117–141, Daytona Beach, FL, May 1996.
- [36] J. R. Cloutier and D. T. Stansbery. The Capabilities and Art of State-Dependent Riccati Equation-Based Design. In *Proc. Amer. Contr. Conf.*, pages 86–91, Anchorage, AK, May 2002.
- [37] J. R. Cloutier and P. H. Zipfel. Hypersonic Guidance via the State-Dependent Riccati Equation Control Method. In *Proc. IEEE Int. Conf. Contr. Appl.*, pages 219–224, Kohala Coast, HI, August 1999.
- [38] D. A. Copp and J. P. Hespanha. Nonlinear Output-Feedback Model Predictive Control with Moving Horizon Estimation. In *Proc. Conf. Dec. Contr.*, pages 3511–3517, Los Angeles, CA, December 2014.
- [39] J. L. Crassidis and J. L. Junkins. *Optimal Estimation of Dynamic Systems*. CRC Press, 2004.

- [40] E. J. Davison. The Output Control of Linear Time-Invariant Multivariable Systems with Unmeasurable Arbitrary Disturbances. *IEEE Trans. Autom. Contr.*, 17:621–630, 1972.
- [41] E. J. Davison. A Generalization of the Output Control of Linear Multi-Variable Systems with Unmeasurable Arbitrary Disturbances. *IEEE Trans. Autom. Contr.*, 20:788–792, 1975.
- [42] E. J. Davison. The Robust Control of a Servomechanism Problem for Linear Time-Invariant Multivariable Systems. *IEEE Trans. Autom. Contr.*, AC-21:25–34, 1976.
- [43] E. J. Davison and A. Goldenberg. Robust Control of a General Servomechanism Problem: The Servo Compensator. *Automatica*, 11:461–471, 1975.
- [44] E. J. Davison and H. W. Smith. Pole Assignment in Linear Time-Invariant Multivariable Systems with Constant Disturbances. *Automatica*, 7:489–498, 1971.
- [45] C. A. Desoer, R. W. Liu, J. Murray, and R. Saeks. Feedback System Design: The Fractional Representation Approach to Analysis and Synthesis. *IEEE Trans. Autom. Contr.*, 25:399–412, 1980.
- [46] E. B. Erdem and A. Alleyne. Globally Stabilizing Second Order Nonlinear Systems by SDRE Control. In *Proc. Amer. Contr. Conf.*, pages 2501–2505, San Diego, CA, June 1999.
- [47] E. B. Erdem and A. Alleyne. Estimation of Stability Regions of SDRE Controlled Systems Using Vector Norms. In *Proc. Amer. Contr. Conf.*, pages 80–85, Anchorage, AK, May 2002.
- [48] E. B. Erdem and A. Alleyne. Design of a Class of Nonlinear Controllers via State Dependent Riccati Equations. *IEEE Trans. Contr. Syst. Tech.*, 12:2986–2991, 2004.
- [49] B. Etkin. *Dynamics of Atmospheric Flight*. Wiley, 1972.
- [50] R. Findeisen, L. Imsland, F. Allgower, and B. A. Foss. State and Output Feedback Nonlinear Model Predictive Control: An Overview. *Eur. J. Contr.*, 9:190–206, 2003.
- [51] B. A. Francis, A. Sebakhy, and W. M. Wonham. Synthesis of Multivariable Regulators: The Internal Model Principle. *J. Appl. Math. Optim*, 1:64–86, 1974.
- [52] B. A. Francis and W. M. Wonham. The Internal Model Principle for Linear Multivariable Regulators. *J. Appl. Math. Optim*, 2:170–194, 1975.

- [53] B. Friedland. *Advanced Control System Design*. Prentice Hall, Englewood Cliffs, NJ, 1996.
- [54] P. Friedmann, C. E. Hammond, and T.-H. Woo. Efficient Numerical Treatment of Periodic Systems with Application to Stability Problems. *Int. J. Numer. Meth. Eng.*, 11:1117–1136, 1977.
- [55] W. L. Garrard. Suboptimal feedback control for nonlinear systems. *Automatica*, 8:219–221, 1972.
- [56] J. W. Grizzle and Y. Song. The Extended Kalman Filter as a Local Asymptotic Observer for Nonlinear Discrete-Time Systems. *Proc. Amer. Contr. Conf.*, pages 3365–3369, June 1992.
- [57] W. M. Haddad and V. Chellaboina. *Nonlinear Dynamical Systems and Control: A Lyapunov-Based Approach*. Princeton University Press, 2011.
- [58] D. Haessig and B. Friedland. A Method for Simultaneous State and Parameter Estimation in Nonlinear Systems. In *Proc. Amer. Contr. Conf.*, pages 947–951, Albuquerque, New Mexico, June 1997.
- [59] J. Hauser, S. Sastry, and P. Kokotovic. Nonlinear Control via Approximate Input-Output Linearization: The Ball and Beam Example. *IEEE Trans. Autom. Contr.*, 3:392–398, 1992.
- [60] Y. Huang and W. Lu. Nonlinear Optimal Control: Alternatives to Hamilton-Jacobi Equation. In *Proc. Conf. Dec. Contr.*, pages 3942–3947, Kobe, Japan, December 1996.
- [61] R. A. Hyde and K. Glover. The application of scheduled H_∞ controllers to a VSTOL aircraft. *IEEE Trans. Autom. Contr.*, 38:1021–1039, 1993.
- [62] A. Isidori. *Nonlinear Control Systems*. Springer-Verlag, London, 1995.
- [63] A. Isidori, L. Marconi, and A. Serrani. *Robust Autonomous Guidance: An Internal Model Approach*. Springer, 2003.
- [64] M. Jankovic, D. Fontaine, and P. V. Kokotovic. TORA Example: Cascade- and Passivity-Based Control Designs. *IEEE Trans. Contr. Syst. Tech.*, 4(3):292–297, 1996.
- [65] C. D. Johnson. Accommodation of External Disturbances in Linear Regulator and Servomechanism Problems. *IEEE Trans. Autom. Contr.*, 16:635–644, 1971.
- [66] S. C. Julier and J. K. Uhlmann. Unscented Filtering and Nonlinear Estimation. *Proc. IEEE*, 92:401–422, 2002.

- [67] J. L. Junkins and J. D. Turner. *Optimal Spacecraft Rotational Maneuvers*. Elsevier, 1986.
- [68] T. Kailath. *Linear Systems*. Prentice Hall, Englewood Cliffs, NJ, 1980.
- [69] R. E. Kalman. When Is a Linear Control System Optimal. *J. Basic Eng.-T. ASME*, 86:51–60, 1964.
- [70] R. Kamalapurkar, H. Dinh, S. Bhasin, and W. E. Dixon. Approximate optimal trajectory tracking for continuous-time nonlinear systems. *Automatica*, 51:40–48, 2015.
- [71] O. Kato and L. Sugiura. An Interpretation of Airplane General Motion and Control as an Inverse Problem. *J. Guid. Control Dynam.*, 9(2):198–204, 1986.
- [72] S. S. Kerthi and E. G. Gilbert. Optimal Infinite-Horizon Feedback Laws for a General Class of Constrained Discrete-Time Systems: Stability and Moving-Horizon Approximations. *J. Optim. Theory Appl.*, 57:265–293, 1988.
- [73] H. Khalil. *Nonlinear Systems*. Prentice Hall, 2001.
- [74] A. Khamis and D. S. Naidu. Nonlinear Optimal Tracking Using Finite Horizon State Dependent Riccati Equation (SDRE). In *Proc. 4th Int. Conf. Circ., Syst., Contr., Sign.*, pages 37–42, Valencia, Spain, August 2013.
- [75] A. Khamis and D. S. Naidu. Nonlinear Optimal Tracking With Incomplete State Information Using Finite-Horizon State Dependent Riccati Equation (SDRE). In *Proc. Amer. Contr. Conf.*, pages 2420–2425, Portland, OR, June 2014.
- [76] A. Khamis, D. S. Naidu, and A. M. Kamel. Nonlinear Finite-Horizon Regulation and Tracking for Systems with Incomplete State Information Using Differential State Dependent Riccati Equation. *Int. J. Aerospace Eng.*, 2014, 2014.
- [77] Y. Kim, F. Lewis, and D. Dawson. Intelligent optimal control of robotic manipulators using neural networks. *Automatica*, 36:1355–1364, 2000.
- [78] A. J. Krener. On the Equivalence of Control Systems and the Linearization of Nonlinear Systems. *SIAM J. Control Optim.*, 11:670–676, 1973.
- [79] M. Krstic, I. Kanellakopoulos, and P. V. Kokotovic. *Nonlinear and Adaptive Control Design*. Wiley, 1995.
- [80] V. Kucera. A Review of the Matrix Riccati Equation. *Kybernetika*, 9:42–61, 1973.
- [81] H. Kwakernaak and R. Sivan. *Linear Optimal Control Systems*. J. Wiley and Sons, New York, N.Y, 1972.

- [82] S. Lane and R. F. Stengel. Flight Control Design Using Non-Linear Inverse Dynamics. *Automatica*, 24:471–483, 1988.
- [83] F. L. Lewis, D. Vrabie, and K. G. Vamvoudakis. Reinforcement Learning and Feedback Control: Using Natural Decision Methods to Design Optimal Adaptive Controllers. *Contr. Sys. Mag.*, 32:76–105, 2012.
- [84] D. Mayne, S. Rakovic, R. Findeisen, and F. Allgower. Robust Output Feedback Model Predictive Control of Constrained Linear Systems. *Automatica*, 42:1217–1222, 2006.
- [85] D. Q. Mayne and H. Michalska. Receding Horizon Control of Nonlinear Systems. *IEEE Trans. Autom. Contr.*, 35:814–824, 1990.
- [86] D. Q. Mayne, J. B. Rawlings, C. V. Rao, and P. O. M. Scokaert. Constrained Model Predictive Control: Stability and Optimality. *Automatica*, 36:789–814, 2000.
- [87] C. P. Mracek and J. R. Cloutier. Control Designs for the Nonlinear Benchmark Problem via the State-Dependent Riccati Equation Method. *Int. J. Robust Non-linear. Contr.*, 8:401–433, 1998.
- [88] C. P. Mracek, J. R. Cloutier, and C. A. D’Souza. A New Technique for Nonlinear Estimation. In *Proc. Conf. Contr. Appl.*, pages 338–343, Dearborn, MI, September 1996.
- [89] D. S. Naidu. *Optimal Control Systems*. CRC Press, 2002.
- [90] R. A. Nichols, R. T. Reichert, and W. J. Rugh. Gain Scheduling for H-Infinity Controllers: A Flight Control Example. *IEEE Trans. Contr. Syst. Tech.*, 1(2):69–79, 1993.
- [91] H. Nijmeijer and T. I. Fossen. *New Directions in Nonlinear Observer Design*. Springer, 1999.
- [92] D. K. Parrish and D. R. Ridgely. Attitude Control of a Satellite Using the SDRE Method. In *Proc. Amer. Contr. Conf.*, pages 942–946, Albuquerque, NM, June 1997.
- [93] J. D. Pearson. Approximation Methods in Optimal Control. *J. Electronics and Control*, 13:453–469, 1962.
- [94] A. Prach. *Robust Controller Design for a Fixed Wing UAV*. M. S. Thesis, METU, 2009.
- [95] A. Prach, O. Tekinalp, and D. S. Bernstein. A Numerical Comparison of Frozen-Time and Forward-Propagating Riccati Equations for Stabilization of Periodically Time-Varying Systems. In *Proc. Amer. Contr. Conf.*, pages 5633–5638, Portland, OR, June 2014.

- [96] A. Prach, O. Tekinalp, and D. S. Bernstein. Faux-Riccati Synthesis of Nonlinear Observer-Based Compensators for Discrete-Time Nonlinear Systems. In *Proc. Conf. Dec. Contr.*, pages 854–859, Los Angeles, CA, December 2014.
- [97] A. Prach, O. Tekinalp, and D. S. Bernstein. Infinite-Horizon Linear-Quadratic Control by Forward Propagation of the Differential Riccati Equation. *IEEE Contr. Sys. Mag.*, 35, April 2015.
- [98] A. Ratnoo and D. Ghose. State-Dependent Riccati-Equation-Based Guidance Law for Impact-Angle-Constrained Trajectories. *J. Guid. Control Dynam.*, 32:320–326, 2009.
- [99] J. B. Rawlings and K. R. Muske. The Stability of Constrained Receding Horizon Control. *IEEE Trans. Autom. Contr.*, 38:1512–1516, 1993.
- [100] J. A. Richards. *Analysis of Periodically Time-Varying Systems*. Springer, 1983.
- [101] J. Roskam. *Airplane Flight Dynamics and Automatic Flight Controls. Part 1*. Darcorporation, 2001.
- [102] S. Sastry. *Nonlinear Systems: Analysis, Stability, and Control*. Springer, 1999.
- [103] C. Scherer. LPV Control and Full Block Multipliers. *Automatica*, 37:361–375, 2001.
- [104] C. B. R. Sepulchre, L. Wei, and P. V. Kokotovic. Global Asymptotic Stabilization of the Ball-and-Beam System. In *Proc. Conf. Dec. Contr.*, pages 2351–2355, San Diego, CA, December 1997.
- [105] J. S. Shamma and M. Athans. Gain Scheduling: Potential Hazards and Possible Remedies. *Control Syst. IEEE*, 12:101–107, 1992.
- [106] J. S. Shamma and J. R. Cloutier. Existence of SDRE Stabilizing Feedback. *IEEE Trans. Autom. Contr.*, 48(3):513–517, 2003.
- [107] J. Slotine and W. Li. *Applied nonlinear control*. Englewood Cliffs, New York, N.Y, 1991.
- [108] S. A. Snell, D. F. Enns, and W. L. Garrard. Nonlinear Inversion Flight Control for a Supermaneuverable Aircraft. *J. Guid. Control Dynam.*, 15(4):976–984, 1992.
- [109] M. Sorine and P. Winternitz. Superposition laws for solutions of differential matrix riccati equations arising in control theory. *IEEE Trans. Autom. Contr.*, 30:266–272, 1985.
- [110] J. L. Speyer and D. H. Jacobson. *Primer on Optimal Control Theory*. SIAM, 2010.

- [111] D. T. Stansbery and J. R. Cloutier. Position and Attitude Control of a Spacecraft Using the State-Dependent Riccati Equation Technique. In *Proc. Amer. Contr. Conf.*, pages 1867–1871, Chicago, IL, May 2000.
- [112] G. Tadmor. Receding Horizon Revisited: An Easy Way to Robustly Stabilize an LTV system. *Syst. Control Lett.*, 18:285–294, 1991.
- [113] G. Tadmor. Dissipative Design, Lossless Dynamics, and the Nonlinear TORA Benchmark Example. *IEEE Trans. Contr. Syst. Tech.*, 9(2):391–398, 2004.
- [114] A. R. Teel. Beyond Linear Feedback for the Nonlinear Regulator. In *Proc. Conf. Dec. Contr.*, pages 757–758, Tucson, AZ, December 1992.
- [115] A. R. Teel. Global Stabilization and Restricted tracking for Multiple Integrators with Bounded Controls. *Syst. Contr. Lett.*, 18:165–171, 1992.
- [116] A. R. Teel. Semi-Global Stabilization of the ‘Ball and Beam’ using ‘Output’ Feedback. In *Proc. Amer. Contr. Conf.*, pages 2577–2581, San Francisco, CA, June 1993.
- [117] A. R. Teel. A Nonlinear Small Gain Theorem for the Analysis of Control Systems with Saturation. *IEEE Trans. Autom. Contr.*, 41:1256–1270, 1996.
- [118] V. I. Utkin. *Sliding Models in Control and Optimization*. Springer-Verlag, Berlin, 1991.
- [119] J. van den Berg. Iterated LQR Smoothing for Locally-Optimal Feedback Control of Systems with Non-Linear Dynamics and Non-Quadratic Cost, June 2014.
- [120] M. van Nieuwstadt, M. Rathinam, and R. M. Murray. Differential Flatness and Absolute Equivalence of Nonlinear Control Systems. *SIAM J. Control Optim.*, 36:1225–1239, 1998.
- [121] A. Weiss, I. Kolmanovsky, and D. S. Bernstein. Forward-Integration Riccati-Based Output-Feedback Control of Linear Time-Varying Systems. In *Proc. Amer. Contr. Conf.*, pages 6708–6714, Montreal, Canada, June 2012.
- [122] A. Wernli and G. Cook. Suboptimal control for the nonlinear quadratic regulator problem. *Automatica*, 11:75–84, 1975.
- [123] W. M. Wonham. *Linear Multivariable Control: A Geometric Approach*. New York: Academic, 1974.
- [124] P. C. Young and J. C. Willems. An Approach to the Multivariable Servomechanism Problem. *Int. J. Contr.*, 15:961–979, 1972.
- [125] T. Yucelen, A. S. Sadahalli, and F. Pourboghra. Online Solution of State Dependent Riccati Equation for Nonlinear System Stabilization. In *Proc. Amer. Contr. Conf.*, pages 6336–6341, Baltimore, MD, June 30 – July 2 2010.

CURRICULUM VITAE

PERSONAL INFORMATION

Surname, Name: Prach, Anna

Nationality: Ukrainian

Date and Place of Birth: 23.10.1984, Ukraine

Email: annprach@gmail.com

EDUCATION

Degree	Institution	Year of Graduation
M.S.	National Technical University of Ukraine "Kyiv Polytechnic Institute"	2010
M.S.	Middle East Technical University	2009
B.S.	National Technical University of Ukraine "Kyiv Polytechnic Institute"	2006

PUBLICATIONS

1. A. Prach, O. Tekinalp, D. S. Bernstein, "A Numerical Investigation of Output-Feedback Control of Linear Time-Varying and Nonlinear Systems Using the Forward Propagating Riccati Equation", International Journal of Control, submitted in Feb 2015, in review.
2. A. Prach, O. Tekinalp, D. S. Bernstein, "Infinite-Horizon Linear-Quadratic Control by Forward Propagation of the Differential Riccati Equation", IEEE Control Systems Magazine, vol. 35, pp. 78–93, April 2015.

International Conference Publications

1. A. Prach, O. Tekinalp, D. S. Bernstein, "Faux-Riccati Synthesis of Nonlinear Observer-Based Compensators for Discrete-Time Nonlinear Systems", IEEE 53rd Conference on Decision and Control, December 15-17, 2014, Los Angeles, CA.
2. A. Prach, O. Tekinalp, D. S. Bernstein, "A Numerical Comparison of Frozen-Time and Forward- Propagating Riccati Equations for Stabilization of Periodically Time-Varying Systems", American Control Conference, June 2-4, 2014, Portland, OR.
3. A. Prach, O. Tekinalp, "Design of a Full State SDRE Tracking Controller for an Unmanned Aircraft", SciTech 2014, January 13-17, 2014, Maryland, Washington DC.
4. A. Prach, O. Tekinalp, "A Multiple-Loop Aircraft Flight Controller Using SDRE Technique", 7. Ankara International Aerospace Conference, September 11-13, 2013, Ankara, Turkey.
5. A. Prach, O. Tekinalp, "Development of a State Dependent Riccati Equation Based Tracking Flight Controller for an Unmanned Aircraft", AIAA Guidance, Navigation, and Control (GNC) Conference August 19-22, 2013, Boston, MA.
6. G. Gursoy, A. Prach, I. Yavrucuk, "Design of a Waypoint Tracking Control Algorithm for Parachute- Payload Systems", 2nd CEAS Specialist Conference on Guidance, Navigation and Control, DELFT, Netherlands, 2013.